

Harper Adams University.

**Investigation of the Potential for Precision Soil and Crop Growth Mapping to Improve
Potato (*Solanum tuberosum L.*) Tuber Size Distribution at Harvest.**

**A thesis submitted in partial fulfilment of the requirements of
Harper Adams University for the degree of Doctor of Philosophy.**

By

Kanthu Joseph Mhango.

BSc Agronomy (University of Malawi).

MSc Soil Science (Egerton University).

February 2022.

Contents

List of Figures	x
List of Tables	xvi
Publications.....	xx
Declarations	xx
Acknowledgements.....	xxi
Abstract.....	1
CHAPTER 1 - Introduction	2
1.1 Thesis Map	5
CHAPTER 2 – Literature Review	7
2.1 Overview	7
2.2 Introduction	10
2.3 Phenology of the Potato Crop	11
2.3.1 Breaking Seed Tuber Dormancy and Pre-sprouting	12
2.3.2 Land Preparation and Planting	14
2.3.3 Post-Emergence Development and Apical Dominance	15

2.3.4 Tuber Induction and initiation	17
2.3.5 Tuber Set and Size Distribution	19
2.4 The Influence of Edaphic Factors on Tuber Size Distribution	25
2.4.1 Fertilizer Practices in Potato Production	25
2.4.2 Effect of Soil Nutrients on Tuber Development and Size Distribution	26
2.4.2.1 Nitrogen	26
2.4.2.2 Effect of Potassium and Sulphur Fertilization on TSD	36
2.4.2.3 Effect of Phosphorus on TSD	39
2.4.2.4 Secondary Macronutrients	42
2.4.3 The Influence of Soil Physical Properties on TSD.....	44
2.4.4 Apparent Electrical Conductivity (ECa)	45
2.5 Remote Sensing in Precision Agriculture	49
2.5.1 Data Acquisition and Spectral Analysis Techniques	51
2.5.2 Vegetation Indices and their Applications in Potato Production	52
2.5.3 Application of the NDVI in Potato Studies.....	54
2.5.4 Other vegetation indices	56

2.5.5 Practical Use of Imagery in UAV-based Remote Sensing in Potatoes	57
2.6 Geospatial Modelling for Precision Agriculture.....	60
2.6.1 Collection of Geospatial Data	61
2.6.2 Geospatial Analysis Techniques.....	63
2.6.2.1 Spatial Interpolation	63
2.6.2.2 Inverse Distance Weighting (IDW).....	65
2.6.2.3 Kriging and Covariance Structures.....	66
2.7 Literature Review Conclusion	69
CHAPTER 3 – Relationships between Soil Variability and Tuber Size Distribution.....	71
3.1 Comparison of Potato Tuber Size Distribution Fitting Methods and Evaluation of the Relationship between Soil Properties and Estimated Distribution Parameters.....	71
3.1.1 Introduction	72
3.1.2 Methodology.....	74
3.1.2.1 Site Characterisation.....	74
3.1.2.2 Sampling Design.....	75
3.1.2.3 Soil and Nutrient Analysis	77
3.1.2.4 Yield Data Collection.....	77

3.1.2.5 Data Analysis.....	78
3.1.3 Results.....	83
3.1.3.1 Summary Statistics.....	83
3.1.3.2 Comparison of TSD functions	85
3.1.3.3 Linear Modelling.....	92
3.1.4 Discussion	95
3.1.4.1 Tuber Size Distribution Model	95
3.1.4.2 Effect of Soil Factors on Tuber Size Distribution	98
3.1.5 Conclusion.....	100
3.2 Examination of the Relationship between Apparent Electrical Conductivity and Soil Physical and Chemical Properties.....	101
3.2.1 Introduction	101
3.2.2 Data and Methods	102
3.2.2.1 Site Characterisation.....	102
3.2.2.2 Soil Sampling and Analysis.....	102
3.2.2.3 Apparent Electrical Conductivity	103
3.2.2.4 Geostatistical Interpolation and Data Analysis.....	103

3.2.3 Results.....	103
3.2.3.1 General Ranges of Data	103
3.2.3.2 Variography.....	104
3.2.3.3 Correlation between ECa and Soil Properties	107
3.2.4 Discussion	108
3.2.5 Conclusion.....	109
CHAPTER 4 - Applying Colour-Based Feature Extraction and Transfer Learning to Develop a High Throughput System for detecting Potato (<i>Solanum tuberosum L.</i>) Stems with Images from Unmanned Aerial Vehicles after Canopy Consolidation.....	110
4.1 Introduction	111
4.2 Materials and Methods.....	113
4.2.1 Feature Engineering: Development of Colour Indices.....	113
4.2.1.1 Data Acquisition.....	113
4.2.1.2 Visible Light Colour Index Selection.....	115
4.2.2 Image Segmentation using k-Means Clustering	120
4.2.3 Noise Reduction and Final Bounding Box Generation.....	120
4.2.4 Development of a Transfer Learning Model.....	121

4.2.5 Model Testing	124
4.2.5.1 Data Acquisition.....	124
4.2.5.2 Image Processing and Data analysis	125
4.3 Results.....	126
4.3.1 Feature Engineering and Selection of Appropriate Indices.....	126
4.3.2 Model Testing	131
4.3.2.1 Mean Stem Counts	131
4.3.2.2 Localization Accuracy.....	135
4.4 Discussion.....	136
4.4.1 Feature Engineering and Development of Colour Indices.....	136
4.4.2 Model Testing	137
4.5 Conclusion.....	142
CHAPTER 5 - Mapping Potato Plant Density Variation Using Deep Learning and Unmanned Aerial	
Vehicles for Accurate Predictions of Yield	143
5.1 Introduction	144
5.2 Methods.....	148
5.2.1 Data capture and Modelling	148

5.2.2 Model Testing	152
5.3 Results.....	155
5.4 Discussion.....	163
5.5 Conclusion.....	166
CHAPTER 6 - Use of Spatio-Temporal Variation in Sentinel-2 Data to Develop Indices of Fine	
Scale Canopy Variations for Potato Yield and Stem Density	168
6.1. Introduction	169
6.2. Materials and Methods.....	174
6.2.1. Site Characterisation.....	174
6.2.2. Sampling Design.....	176
6.2.3. Collection and Processing of Satellite Imagery.....	178
6.2.4. Principal Component Analysis	178
6.2.5. Rates of Change in Reflectance	179
6.2.6. Estimation of Red-Edge Inflection Points	181
6.2.7. Yield Data Collection	182
6.2.8. Statistical Analysis.....	183
6.3. Results.....	184

6.3.1. Summary of Spectral Reflectance and Intrinsic Indices.....	184
6.3.2. Summary of Temporal Variables	188
6.3.2.1. Principal Components of Reflectance at Different Time Points.....	188
6.3.2.2. Temporal Change in the Spectral Signature and Position of the Red-Edge Inflection Point	190
6.3.3. Summary Statistics of In-Situ Potato data	192
6.3.4. Linear Model for Marketable Yield	192
6.3.5. Modelling Stem Density.....	194
6.4. Discussion.....	196
6.5. Conclusions	199
CHAPTER 7 - General Discussion.....	201
7.1 Conclusion.....	206
7.2 Recommendations	207
8. References	209
9. Appendices.....	251

List of Figures

Figure 1: A flow chart of the main themes of the thesis	6
Figure 2: A labelled image of a typical potato plant showing the location of primary and secondary stems	12
Figure 3: An adaptation of the observed effects of in-row seed piece spacing on yield of tubers Frontier Russet, Ranger Russet and Russet Burbank varieties. Simulated from Love & Thompson (1998) data using a Weibull distribution by varying shape and scale parameters.	21
Figure 4: Effect of nitrogen rates (0-270 kg/ha) on the proportion of small, medium and large tubers in the yield. Adapted from Porter and Sisson (1991).....	29
Figure 5: Effect of nitrogen rate (0-100 kg/ha) on the percentage of culled, small, medium and large potato tubers in the final yield. Adapted from Gao et al. (2018).....	30
Figure 6: Effect of nitrogen (N) rate (0-200 kg/ha) on the percentage of small, medium and large potato tubers in the final yield. Adapted from Cambouris et al. (2007).	32
Figure 7: Effect of nitrogen (N) timing on the percentage of small, medium and large potato tubers in the final yield. Adapted from Cambouris et al. (2007).....	35
Figure 8: Effect of split nitrogen application on the percentage of culled, small, medium and large potato tubers in the final yield. Adapted from Gao et al. (2018).....	36
Figure 9: Effect of Potassium (K) fertilizer type and rate on the percentage of large potato tubers in the final yield. Adapted from Dickins et al. (1962).	38

Figure 10: Effect of inherent soil phosphorus (P) concentration on potato tuber size distribution. Adapted from Fernandes et al. (2016).40

Figure 11: Effect of Phosphorus (P) rates (0-74 kg/ha) on the percentage of various tuber weight classes in the final yield. Adapted from Rosen and Bierman (2008).41

Figure 12: Schematic diagram of a semivariogram of a soil phosphorus test in ppm (Mulla, 2015).66

Figure 13: The effect of changing the shape parameter on a conceptual Weibull probability density curve..... 79

Figure 14: The Gaussian, Gamma and Weibull distribution functions fitted to the average proportional tuber weights at HF7 (A), Buttery Hill (B), Crabtree Leasow (C), Deaton 6 (D) and Horse Foxhole (E)86

Figure 15: The Gaussian, Gamma and Weibull distribution functions fitted to the average proportional tuber numbers at HF7 (A), Buttery Hill (B), Crabtree Leasow (C), Deaton 6 (D) and Horse Foxhole (E)87

Figure 16: Illustration of the effect of Phosphorus concentration on the tuber size distribution at Deaton 6 (A), Buttery Hill (B), HF7 (C), and Horse Foxhole (D).93

Figure 17: Experimental variogram of apparent electrical conductivity of soil at Buttery Hill in the first 75 cm depth105

Figure 18: Experimental variogram of apparent electrical conductivity of soil at Buttery Hill between 75 cm and 150 cm depth105

Figure 19: Experimental variogram of apparent electrical conductivity of soil at Deaton 6 in the first 75 cm depth.....106

Figure 20: Experimental variogram of apparent electrical conductivity of soil at Deaton 6 between 75 cm and 150 cm depth106

Figure 21: An aerial view of a typical potato plant (left) with labelled locations of stem growing tips that a vegetation index or object detection model are expected to elucidate (right)...116

Figure 22: Flow chart of the image analysis algorithm for generating meristem objects and inferring stem number119

Figure 23: Flow chart of the Faster R-CNN algorithm for training a potato meristem object detector.....123

Figure 24: Aerial image of the testing site for the image analysis and convolutional neural network algorithms.....124

Figure 25: The difference between Green and Blue colour plotted against the difference between Red and Blue colour in pixels selected from four prevalent features in a potato canopy.....127

Figure 26: Examples of the blue difference normalized index (middle) and the cumulative blue difference index (right) applied to an aerial image of a growing potato crop (left)128

Figure 27: Index values of Meristems, Leaves, Dry soil and Wet soil using eight colour indices, from images taken before canopy consolidation of partially irrigated Sandy Loam soil. a - Blue Difference Normalized Index, b - Cumulative Blue Difference Index, c - Excess Green

minus Excess Red Index, f - Normalized Difference Green Redness Index, g - Excess Red, h - Excess Blue Index129

Figure 28: Observed vs Predicted of the number of meristems in potato canopies when predictions were made using the traditional image analysis approach132

Figure 29: Observed vs Predicted number of meristems when predictions were made using a Convolutional Neural Network-based object detector133

Figure 30: Observed number of stems vs Predicted number of meristems when predictions were made using a Convolutional Neural Network.....134

Figure 31: Observed number of stems vs Predicted number of meristems when predictions were made using the traditional image analysis approach134

Figure 32: Flow chart of the Faster-RCNN-based transfer learning process for producing a Potato plant detection model151

Figure 33: Flow chart for the production of a plant density plot from a transfer-learning model154

Figure 34: Actual vs Predicted potato plant numbers in a test dataset of potato plants using predictions from a Faster-RCNN transfer learning model.....156

Figure 35: Visualisation of the bounding-box predictions from a Faster-RCNN transfer-learning model (red colour) against manually labelled bounding boxes (yellow colour) at Horse Foxhole Field (image width = 1.5 m).....157

Figure 36: An interpolated predicted plant density plot of Horse Foxhole field, predicted using the Faster-RCNN transfer learning model158

Figure 37: An interpolated plot of early-season NDVI in the Horse Foxhole field constructed from a Sentinel-2 (10 m spatial resolution) satellite image159

Figure 38: Actual plant density at Buttery Hill and Horse Foxhole vs predicted densities from the Faster-RCNN transfer learning model.....160

Figure 39: Map of the United Kingdom territory showing the locations of the 5 study sites (Crabtree Leasow, Horse Foxhole Buttery Hill, Deaton 6, and Branston Booths).....175

Figure 40: An illustrative graph showing how spectral index values like the Normalized Difference Vegetation Index (NDVI) were plotted in time and their peak and rate parameters derived.....180

Figure 41: Illustration of the observed spread of the peak reflectance values of the nine Sentinel-2 wavelengths observed during the growing period at five study sites.185

Figure 42: Illustration of the spread of the observed number of days between planting day and the peak value of Normalized Difference Vegetation Index, Specific Leaf Area Vegetation Index, Normalized Difference Moisture Index, and the Red Edge Inflection Point.187

Figure 43: Illustration of the spread of the observed number of days between planting day and the peak value of each of the Sentinel-2 satellite wavebands.....188

Figure 44: The spectral signature of the standardized first principal components of each Sentinel-2 waveband’s temporal variation in the potato canopies at 5 different study sites190

Figure 45: Smoothed (using the Savitzky-Golay filter) spectral signatures of the potato canopy at the 3 different times of the season at Buttery Hill (A), HF7 (B), Deaton 6 (C), Horse Foxhole (D), and Crabtree Leasow (E).191

Figure 46: A Choropleth map of the field's variation in Soil Brightness and approximate soil sampling locations. Soil brightness was re-scaled to range between 0 and 10, where 0 represents a dark soil and 10 represents a light soil.252

List of Tables

Table 1: Summary of the main literature review sub-sections and main keywords used to perform literature search	8
Table 2: Correlation coefficients between ECa and a selection of edaphic factors from 3 different studies.....	48
Table 3: A summary of the most popular vegetation indices based on R, G, B and NIR in the units of remote-sensing reflectance ratio.	57
Table 4: Summarized information of the study sites.....	75
Table 5: Summary statistics of key soil and plant variables measured at each study site.....	83
Table 6: summary statistics of the tuber size distribution (TSD) parameters at five different sites	85
Table 7: Average log relative likelihood estimate and confidence intervals of fitted Gaussian, Weibull, Gamma and Weibull Percentiles curves to potato tuber size distributions at five, relative to the likelihood of the observed discrete distribution	88
Table 8: Average log relative likelihood estimate and confidence intervals of fitted Gaussian, Weibull, Gamma and Weibull Percentiles curves to the 45 mm to 65 mm size band of potato tuber size distributions at five, relative to the likelihood of the observed discrete distribution	90

Table 9: Root Mean Square Error (RMSE) of estimates from the Gaussian, Gamma and Weibull (Percentiles approach) benchmarked against the Weibull model with Maximum Likelihood Estimation (MLE).....	91
Table 10: Linear modelling results for the relationships between soil nutrients (and stem density) and TSD parameters with respect to tuber number	92
Table 11: Linear modelling results for the relationships between soil nutrients (and stem density) and TSD parameters with respect to tuber weight	95
Table 12: Summary statistics of major variables considered for analysis.....	104
Table 13: Correlation coefficients between Apparent Electrical Conductivity and edaphic factors at Buttery Hill and Deaton 6	107
Table 14: Specifications of Unmanned Aerial Vehicle cameras and crop stage used in the study	114
Table 15: Descriptions and functions of popularly cited and custom colour indices based on standard Red, Green and Blue bands.	117
Table 16: Mean (and standard deviations) of indices calculated from the pixels of Leaves, Meristems, Wet soil and Dry soil using four cameras	130
Table 17: Performance of image analysis and Convolutional Neural Network approaches in the enumeration of meristems in all the varieties. The varieties are grouped into determinancy types for presentation purposes and “Actual Stem Number” information is included to illustrate the difference between meristem and stem counts.....	131

Table 18: Means and standard deviations (in parentheses) of detection and localization performance metrics of the image analysis and Convolutional Neural Network against manually labelled meristem data	135
Table 19: Summary of the locations, ground sampling distances (GSD) and crop stage of the images used in the study. In all instances, the cropped variety was Amora.....	148
Table 20: Summary statistics of the plant density and Potato yield components at Buttery Hill and Horse Foxhole fields.....	161
Table 21: Correlation coefficients showing the relationship between actual plant density, potato yield components and plant density predicted from the Faster-RCNN transfer learning model at Buttery Hill and Horse Foxhole fields	162
Table 22: Summary of the location and key production information of the study sites	175
Table 23: Summary of the vegetation indices used in the study.	181
Table 24: Means and standard deviations (in parentheses) of the peak values of vegetation indices during the potato production season.....	186
Table 25: The mean and standard deviations (in parentheses) of the percentage of variance are explained by the first three principal components of the satellite imagery time series at each sampling point at five locations.....	189
Table 26: Summary statistics (mean with standard deviation in parentheses) of the potato yield sampling results at five different study sites.....	192

Table 27: Estimated coefficients for explanatory variables of marketable yield and the estimated spatial autocorrelation structure.....193

Table 28: Estimated coefficients for explanatory variables of potato stem density and the estimated spatial autocorrelation structure.195

Publications

Mhango, J.K., W. Harris, E., and Monaghan, J.M. (2021). Relationships between the Spatio-Temporal Variation in Reflectance Data from the Sentinel-2 Satellite and Potato (*Solanum tuberosum* L.) Yield and Stem Density. *Remote Sensing* 13(21).
<https://doi.org/10.3390/rs13214371>

Mhango, J.K., Grove, I.G., Hartley, W. Harris, E., and Monaghan, J.M. (2021). Applying colour-based feature extraction and transfer learning to develop a high throughput inference system for potato (*Solanum tuberosum* L.) stems with images from unmanned aerial vehicles after canopy consolidation. *Precision Agric.*
<https://doi.org/10.1007/s11119-021-09853-4>

Mhango, J.K., W. Harris, E., Green, R., and Monaghan, J.M. Monaghan (2021). Mapping Potato Plant Density Variation Using Aerial Imagery and Deep Learning Techniques for Precision Agriculture. *Remote Sensing* 13(14). <https://doi.org/10.3390/rs13142705>

Mhango, J.K., W. Harris, E., and Monaghan, J.M. (2021). Comparison of potato (*Solanum tuberosum* L.) tuber size distribution fitting methods and evaluation of the relationship between soil properties and estimated distribution parameters. *The Journal of Agricultural Science*, 1-15. <https://doi.org/10.1017/S0021859621000952>

Declarations

I declare that the following thesis is the work of myself and as not been submitted or accepted for the award of any degree at any other academic institute. The research undertaken in this thesis was conducted primarily at Harper Adams University with the support of the Agriculture and Horticulture Development Board and Branston Limited

Joseph Mhango.



21st February 2022.

Acknowledgements

I would like to thank Prof Jim Monaghan for his never-ending support, encouragement, guidance and pulling me out of a thousand rabbit holes. As a global pandemic rapidly destroyed “the old normal”, you often had to forgo your precious time to steer the ship and make sure I never fell behind. I am really grateful for your support throughout the three years. To Dr Ed Harris, I am truly appreciative for your guidance, encouragement and constructive criticism. You pushed me from a novice to the high level of capabilities in R that was required for the work in this thesis. For that I am grateful. To Dr Will Hartley, I am very grateful for your guidance on all things soil. I really appreciate your guidance on methodologies, which ensured I never veered off-course in my soils work. A special mention to Dr Ivan Grove who never doubted my capabilities, even when I had the dreaded “impostor syndrome” as a new student in the United Kingdom. I thank you for your selfless support, advice and leadership. I hold every advice that you’ve ever given me very dearly.

I would like to acknowledge the Crops and Environment Research Centre of Harper Adams University and the Agriculture and Horticulture Development Board’s Potatoes Division for providing the experimental sites for this study and the National Centre for Precision Farming at Harper Adams University for the operation of UAVs during image acquisition.

To my family, I thank you for giving me the opportunity to undertake this three year journey. To my daughter Ivy Nyambura Mhango, this work, in its entirety, was done for you and is dedicated to you. Thank you for being the light of my life.

Abstract

Control of tuber size distribution (TSD) in potatoes (*Solanum tuberosum* L) is desired for farmers seeking to maximize profit in a market environment that is sensitive to tuber size. The TSD and its spatial variability are related to stem density variation. Throughput improvements in the methods of quantifying stem density will unlock adoption of more precise methods of managing TSD. Understanding the variability of soil nutrients and their effects on TSD can also help in the delineation of management zones for precision applications like variable rate fertilization. In this study, a method for quantifying TSD based on the Weibull distribution was proposed, with consistently lower Root Mean Square Error than currently prevalent methods. With this method, negative relationships between TSD and excess soil nutrients were uncovered. In above-ground canopy studies, a novel potato stem detector was developed using deep convolutional neural network (CNN) and aerial imagery. Novel colour indices were also developed for elucidating the locations of potato stems from aerial imagery. For the first time, this study demonstrated the potential to map stem density (a key determinant of TSD) in a field using high throughput methods. The potential of satellite image time series in modelling stem density and yield was also examined. Sentinel-2 satellite data was used to create spectral signatures of potato plants and their temporal evolution. Features engineered from this data were able to model potato Marketable yield and stem density. Temporal evolution of specific wavelengths (e.g. 559nm), integrated with manually determined stem density, was found to have highly significant relationships with marketable yield. As a conclusion, the study uncovered high potential for crop growth mapping to predict TSD and aid in decision-support systems. Furthermore, the study proposed a unitless Weibull shape parameter as a means of quantifying TSD to enable inter-study comparisons in TSD work.

CHAPTER 1 - Introduction

Potatoes (*Solanum tuberosum* L.) are the world's third most important food crop after wheat and rice (De Jong, 2016), with global production increasing by 26% over the past decade FAOSTAT (2021). Grown predominantly in temperate regions, potato production systems are input-intensive with high yields and margins due to well developed, technologically advanced markets that depend on the consistent supply of high quality potato raw material. The potato processing industry in the developed world is a mature industry that is efficient in maintaining continuous control of processing quality and quantity to satisfy consumer demands, therefore, apart from the diversification of current potato products and the unlocking of new sources of demand, improvements in the value chain are likely to come from reduced post-harvest losses due to improved tuber quality (Keijbets, 2008). For potato growers, this means that high productivity does not necessarily translate into high returns due to increasing selectivity of processors for tuber size grades (Machakaire et al., 2016), dry matter content, tuber shape and other "tuber quality" factors, especially in the pre-fried potato processing sector, which accounts for 62% of the global processed potato market (Keijbets, 2008). It is therefore imperative for growers to improve the quality of their crop to realise greater value.

Conventional potato production management is mostly spatially invariable within a field, with uniform management of seed rates, irrigation and fertilisation at an individual field scale, though significant spatial variation has been reported in potato yield and size distribution (Taylor et al., 2018). The partitioning of photosynthetic products to potato tubers and subsequent tuber bulking is a highly plastic process that is continuous until senescence (Kooman & Haverkort, 1995) and can be temporally influenced by predictable environmental factors such as soil temperature and nitrogen (N) (Ewing & Struik, 2010). This means that potato tuber sizes can be predicted as a function of spatially variable environmental factors and maps of tuber size variation can be produced. Such maps could be for decision-support on variable harvest timing, where areas with small tubers can be desiccated later than other areas to allow tubers to grow to the required sizes. Cambouris et al. (2006) report that variability of tuber sizes in a field can be addressed through delineation of field management zones based on the Electromagnetic Induction (EMI)

properties of the soil, particularly the Apparent Electrical Conductivity (ECa) of the soil. The ECa is a proxy to understanding soil composition because its value is an expression of the collective effect of the soils mineralogical and hydrological composition (Peralta et al., 2013). In experiments by Cambouris et al. (2006), EMI-based delineated zones received variable nitrogen application, leading to a more uniform tuber yield. Promising results have also been achieved in tuber size prediction through the manipulation of apical dominance and canopy densities through seed ageing techniques (Iritani et al., 1983; Knowles & Knowles, 2016; Struik, 2007). Love and Thompson-Johns (1999) report that tuber size has a positive correlation with intra-row seed spacing, corroborated by Shayanowako et al. (2015) and Bussan et al. (2007). Additionally, Bussan et al. (2007) found that stem density was a better predictor of potato tuber size than general plant density. However, most of the purported edaphic factors affecting TSD are derived from controlled experiments where larger variations in soil nutrient concentrations are induced than can be expected in typical production conditions. The on-farm experimentation approach is becoming increasingly important in the development of predictive models that are Consistent across a range of underlying sources of variation available in a field (Taylor et al., 2018).

These findings show that early-season prediction of potato tuber number and size distribution may be possible where above-ground factors like stem number are determined. Agronomists routinely collect manually plant and stem density data to predict tuber number and commercial solutions have been developed to model tuber yield and size distribution using this data aggregated at farm level. There is an interest to add a spatial dimension to these models, to account for variation in plant population density and subsequent stem density due to inefficiencies in plant spacing and other factors (Allen & Wurr, 1992). Spatial variability in plant and stem population can potentially be used to predict spatial variation in yield and tuber size distribution and enable delineation of management zones for precision agriculture.

Advances in remote sensing have enabled an improved assessment of potato canopy development for yield prediction at a regional level, but field level studies are rare. The normalized difference vegetation index (NDVI), derived from satellite imagery, has been used to model potato yield at the sub-country regional level in several studies (Al-Gaadi et

al., 2016). The coarse resolutions of satellite imagery and limited reporting of the use of spectral un-mixing and spatial interpolation in this domain means that these models offer little applicability at the farm level where localised decision-support application is required for precision agriculture. Although satellite imagery is publicly available with weekly revisit times globally, there are few published studies on the extent to which individual spectral reflectance data from satellite imagery, and their temporal evolution, can be used to predict yield or canopy development in the potato crop. Unmanned Aerial Vehicles (UAVs) solve the problem of spatial resolution, making it possible for data scientists to focus on other bottlenecks to accurate model development. Consequently, there have been rapid advances in the literature regarding the development of plant-counting algorithms in potatoes using computer vision machine learning approaches with various degrees of accuracy (Li et al., 2019; Machefer et al., 2020; Sankaran et al., 2017). Asynchrony in potato emergence dates in the field is a major limitation to the accuracy of early-season plant counts, which necessitates delayed UAV imaging to increase the probability of capturing all viable plant units. Unfortunately, delayed imaging introduces the problem of overlapping plants, which all previous studies on potatoes have not been able to solve, cognizant of the challenges associated with traditional methods of separating overlapping objects in images (e.g. watershed segmentation). Additionally, potatoes form a cluster of stems per planted tuber and the stem is recognized as the true unit of plant density that related to yield components (Allen & Wurr, 1992). No previous studies in the literature have attempted the approach reported in this thesis to predict the number of stems in a potato canopy from UAV imagery.

An interdisciplinary approach is required in order to bring together the edaphic and above-ground sources of variation that contribute to spatial variation in TSD and produce predictive models. Key knowledge gaps in this domain include the establishment of an appropriate index for TSD and its linkage to key edaphic factors. There is also a need to improve current methods for UAV-based plant-counting to detect individual potato stems as well as test whether techniques in geospatial analysis can be used to create reliable maps of the spatial variation in plant density, which is pertinent to decision-support in precision agriculture applications.

The overall aim of this work was to contribute to the knowledge of the appropriate methods for spatial mapping and prediction of potato yield and TSD. The studies focused on mapping spatial variability in soil nutrients, as indicators of crop nutrition, and canopy reflectance as indicators of plant population and biomass. Specifically, the overall goal was pursued using the following key sub-objectives:

1. Examine the relationships between soil properties and TSD at harvest, indexed using the Weibull distribution shape parameter
2. Examine if a significant relationship between soil properties and ECa exists
3. Develop algorithms for individual stem detection in potatoes at an advanced canopy development stage using UAV imagery
4. Investigate the usefulness of spatio-temporal variation of satellite imagery in the prediction of potato yield variation in a field
5. Evaluate the usefulness of plant density maps produced from UAV images and potato yield components

This work integrated agronomy with biosystems engineering, geospatial analytical methods were used to model dependent variables from edaphic factors, while above ground studies mainly integrated remote sensing, computer vision, machine learning and geospatial analysis to model potato canopy metrics that are related to yield and TSD.

1.1 Thesis Map

After a literature review chapter discussing the published research record of all the key research themes, this thesis has been organised into chapters that are formatted as journal papers. The chapters will be extracted and submitted for publication in peer reviewed

journals. The thesis has been organised as follows:

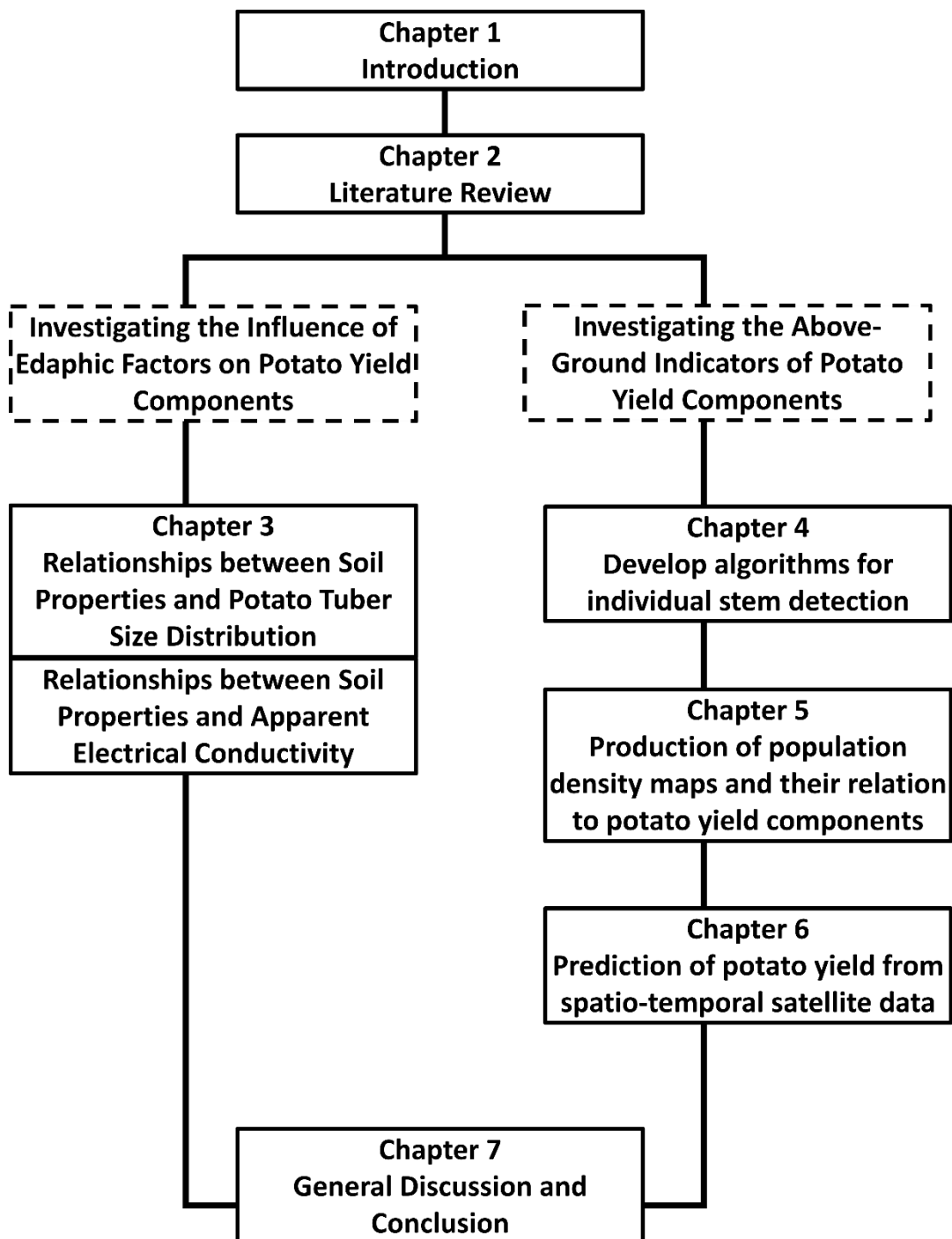


Figure 1: A flow chart of the main themes of the thesis

CHAPTER 2 – Literature Review

2.1 Overview

This literature review was based on peer-reviewed journal articles with original research or reviews papers accessible using the Harper-Adams University’s electronic library system, with access to the Web of Science core collection. Google Scholar was also used to search for articles and relevant non-peer reviewed (grey) literature that could not be found on the university library system. The purpose of the literature review was to determine the status of research on potato tuber size distribution (TSD) in relation to spatially variable soil nutrients and above-ground measurements that can be predicted to inform decisions for precision agriculture. The literature review therefore informed decisions on research questions pertaining to precision agriculture in subsequent investigations. Low-intensity soil sampling for nutrient analysis was discovered to require interpolation to create field-scale maps that are relevant for the spatially variable management that is inherent to precision agriculture. This entailed the review of research and methods for geospatial analysis in order to create valid interpolations of point-sampled data during the investigations. Through this review, it was envisaged that key links between well-known potato physiology phenomena and TSD would be established then potential “points of manipulation” relevant to spatially variable precision agriculture would be identified. After an introductory section, the literature review comprises of the sections summarized in table 1.

Phenology of the Potato Crop: The literature search was done using the Web of Science core collection. This section starts with an introductory overview of the potato crop in Section 2.2, then isolates the key stages within a typical potato production cycle that contribute to tuber variation at harvest in Section 2.3. The growth stages emphasized in this review include tuber sprouting and breaking of dormancy, soil conditioning and land preparation, plant population establishment, post-emergence development, tuber induction and initiation and tuber bulking, all of which culminate in a context-specific TSD at harvest.

Table 1: Summary of the main literature review sub-sections and main keywords used to perform literature search

Section	Title	Main Keywords
2.1	Phenology of the Potato Crop	Potato physiology Potato agronomy practices Apical Dominance Induced Dormancy Tuber Size Distribution Potato phenology Tuber induction
2.2	Influence of Edaphic Factors on Tuber Size Distribution	Apparent Electrical Conductivity Potato Soil Nitrogen Potato Phosphorus Potato Potassium Demand Potato soil requirements
2.3	Remote Sensing for Precision Agriculture:	Remote Sensing Spatial Variability Vegetation Indices Supervised and Unsupervised Classification Potato Precision Farming
2.4	Spatial Analysis for Precision Agriculture:	Spatial Modelling Kriging CoKriging Spatial Interpolation Gaussian process spatial modelling Matern covariance

Influence of Edaphic Factors on Tuber Size Distribution: Literature was searched to identify key edaphic factors that affect TSD with the aim of evaluating their forms of action and efficacy as reported in literature. This was done to identify and potentially justify the

inclusion of any edaphic variable in field surveys and experiments. The review therefore identified nitrogen, phosphorus, potassium, calcium and sulphur as key edaphic factors that have been studied in relation to TSD. Soil sampling for nutrient analysis is currently a predominantly manual and low intensity operation that is aimed at generating a general field-level recommendation for fertilizer application. Interpolation of results to produce spatially variable density maps is important towards the adoption of variable management decisions based on soil variability. The review therefore discusses the potential for using apparent electrical conductivity (ECa) – a soil attribute for which high resolution maps are readily producible – as a proxy for soil nutrient concentration. Section 2.4 is therefore dedicated to a thorough discussion of literary discourse on these soil phenomena in relation to potato tuber development.

Remote Sensing for Precision Agriculture: Section 2.5 explores the advances in remote sensing for precision farming. Calling back to earlier discussions on the correlation between stem density and tuber size distribution, the review is done to identify remote sensing techniques that can potentially be used to create predictive models for tuber size distribution. The review therefore focused on vegetation indices and their potential for description and analysis of spatial variability in the field with the goal of utilizing identifying potential areas for spatial modelling of TSD. ScienceDirect and Google Scholar were mainly used for the literature search. Apart from the use of vegetation indices for mapping spatial variation, the review discusses the relatively new field of computer vision and machine learning, in relation to detection of objects of interest from plant canopy imagery collected using unmanned aerial vehicles (UAV). The purpose of this section is to identify the potential for using UAVs to detect and map potato plant density and stem density and produce 2D density maps (heat maps) of their variation. Such maps can then be used to model the spatial variation in TSD.

Spatial Analysis for Precision Agriculture: In Section 2.6, the review discusses the currently available techniques for spatial modelling of edaphic and above-ground factors at the field level. A review of spatial analysis techniques follows gradually developing from deterministic inverse distance weighting to geo-statistical kriging and Gaussian process modelling.

Conclusion: The literature review concludes with a summary of the research gaps identified in the literature and recommendations for further investigation.

2.2 Introduction

The potato (*Solanum tuberosum L.*) crop is the world's third most important crop primarily grown for human consumption after wheat and rice (De Jong, 2016). According to the latest data from FAOSTAT (2019), global production of potatoes increased by 26% from 297 million to 376 million Metric Tonnes (MT) between 2006 and 2016. The potato crop is popular partly due to its harvest index of 0.81 (Bradshaw & Ramsay, 2009), which is higher than that of all the world's major cereals and grain crops (Unkovich et al., 2010).

The United Kingdom of Great Britain (GB) has enjoyed a period of sustained increase in farm productivity over the past 50 years with yields rising from an average 20 t/ha in 1960 to a peak of 48 t/ha in 2011 (Potato Council, 2012), attributed to improved crop protection, fertilizer regimes, varieties, and irrigation. Within the same period, the Potato Council (2012) reports that the registered number of hectares has dropped by 58%, with a sharp 97% decrease in the number of registered growers from around 86000 in 1960 to less than 2000 in 2016. This further puts into context the increase in productivity through improved management, capitalisation and specialisation evidenced by the growth in area planted per grower from an average 5.5 ha in 1970 to over 50 ha in 2016 (FAOSTAT, 2019). The east of England is historically the main potato producing area of GB with 27% of the potato planted area followed by Scotland then East Midlands at 21% and 14% respectively (AHDB, 2018). Furthermore according to the AHBD (2018), the most common variety is the Maris Piper with its production area fluctuating around 14% of the country's total potato production area while the closest competitor covered only 5%. The majority of potatoes are sold as either fresh potatoes or chips, however, there is also a significant share of market for frozen potato products

Potato growers mechanically grade their seed into discreet size grades to meet market requirements for ware potatoes, defined as potatoes which are destined for human consumption (Witney & McRae, 1992). The ware-grade size range reported in literature has shifted from 35 mm-80 mm range (Allen & Wurr, 1992; Witney & McRae, 1992) to the current most widely quoted commercial range of 45 mm-85 mm (Yara, 2018; AFBI, 2018). Consequently, it is in the interest of every farmer to maximize the percentage of their yield falling within this range for maximum returns, which raises the interest in developing the

ability to predict and control Tuber Size Distribution (TSD) at harvest (Machakaire et al., 2016).

2.3 Phenology of the Potato Crop

The potato plant belongs to the Solanaceae family and was domesticated in South America in the pre-Columbian period (Camire et al., 2009). It is a herbaceous dicotyledonous plant with one or more primary stems that anchors compound leaves with three to four pairs of primary and secondary leaflets (Kirk & Marshall, 1992) as illustrated in Figure 2. Potatoes flower and set true seed in berries through insect pollination, however, due to gradual selection for high yielding varieties by farmers, the currently cultivated varieties of potatoes are self-pollinating but mostly self-incompatible polyploids (Spooner & Bamberg, 1994). Propagation of potatoes is therefore mainly vegetative through the tuber to enable maintenance of varietal purity (Spooner & Bamberg, 1994). The growth stages of the potato crop overlap from the time a tuber sprouts up to senescence and skin set, therefore there is no definitive chronological key for describing the growth of the potato (Jefferies & Lawson, 1991). However, drawing from earlier unconsolidated descriptions by other authors, Jefferies and Lawson (1991) proposed a growth-stage based key for scientific data recording and commercial production purposes namely Tuber dormancy, Tuber sprouting, Emergence and shoot expansion, Flowering, Tuber Development and Senescence.

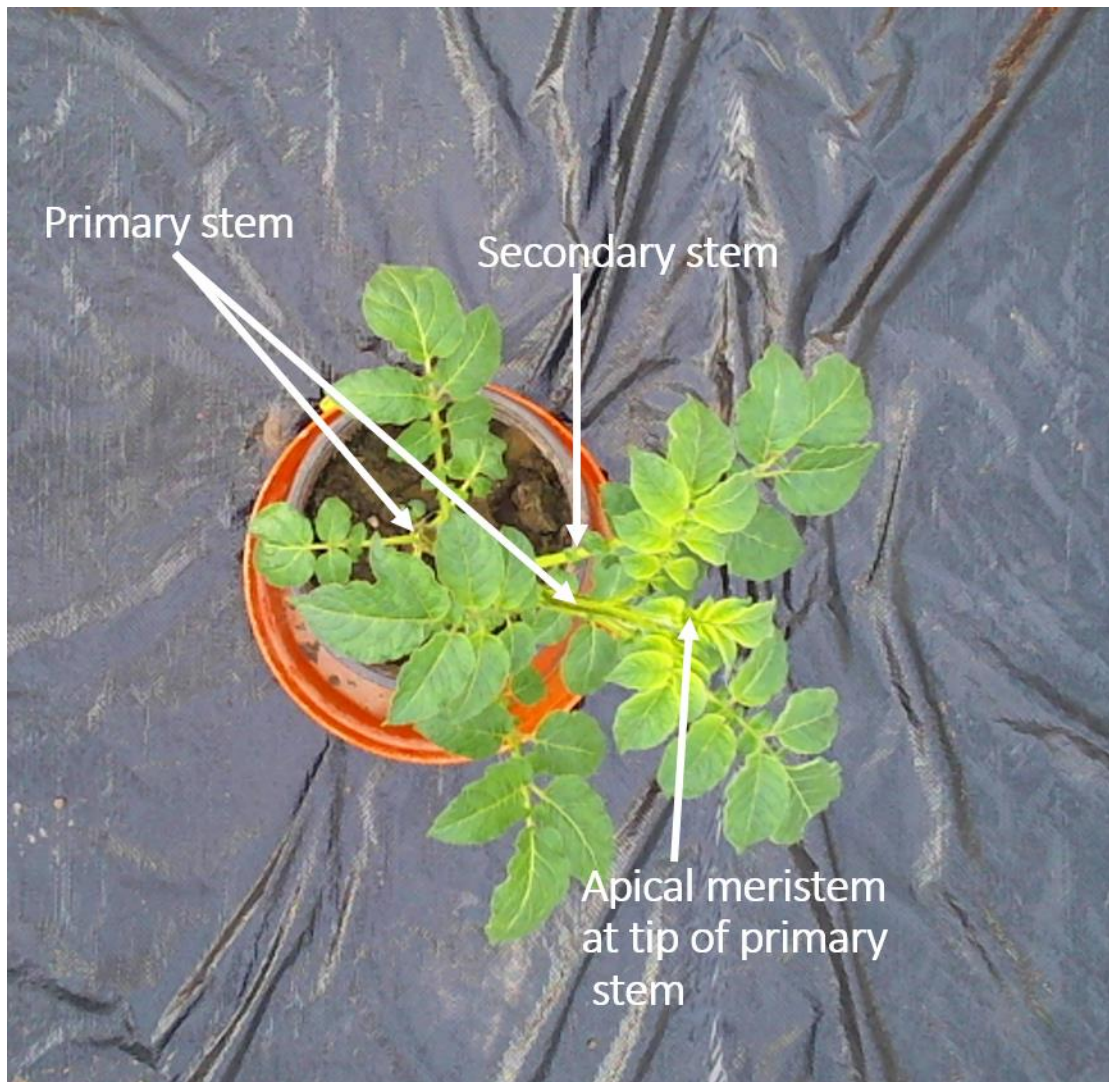


Figure 2: A labelled image of a typical potato plant showing the location of primary and secondary stems

Practical production of potatoes involves the manipulation of the environment to affect the rate of these phases with the ultimate goal of improving the harvest index. The following sections discuss the critical stages of the cycle which have impact on tuber quality and size distribution.

2.3.1 Breaking Seed Tuber Dormancy and Pre-sprouting

Potato tuber dormancy is described as an initial period after tuber formation when the tuber will not initiate sprouts under ideal natural conditions (Reust et al., 2001). While there is a debate over when dormancy starts, it is generally agreed that potatoes exhibit the two typical forms of dormancy common in seed producing crops namely deep dormancy

(obligate rest period) and induced dormancy due to environmental factors (Caldiz et al., 2001; Jefferies & Lawson, 1991). Obligate deep dormancy is cultivar dependent and hormonally controlled (Suttle, 2004), followed by a period of induced dormancy starts which can be usually broken by growth stimulating hormones like Gibberellic Acid (GA) (Knowles & Knowles, 2006). Dormancy is naturally broken in dark conditions at temperatures of 15-20°C and relative humidity over 90% to initiate sprouting (Jefferies & Lawson, 1991). Some farmers deliberately break dormancy and pre-sprout their potatoes before planting in order to ascertain that planted potatoes have viable stems and to exercise a control on stem numbers per tuber where possible (Allen & Wurr, 1992). This stage, combined with physiological aging provides one of the first points in the production cycle at which a farmer can influence the stem density of his crop to ultimately affect tuber number and TSD (Knowles & Knowles, 2006).

The final number of stems developed from a single tuber depends on several factors including the variety, tuber size, number of eyes on the tuber and the physiological age of the tuber at planting (Jefferies & Lawson, 1991; Knowles & Knowles, 2006). The physiological age of a potato tuber is defined by Allen et al. (1979) as the sum of the average daily temperatures above 4°C after the release of deep dormancy. In physiologically old seed (subjected to growth conditions relatively earlier), the apical bud exerts enough dominance to suppress the growth of other buds, leading to fewer sprouts per tuber (Allen et al., 1979), while in seeds which have been subjected to prolonged low temperatures (physiologically young) exhibit less apical dominance, leading to more sprouts per tuber (Allen et al., 1979). Knowles and Knowles (2006) observed an increase in stem numbers with advanced physiological age, however, the ageing process was based on accumulation of heat units by altering storage temperatures above 4°C. However, similar to the drivers of apical dominance, the nature of physiological aging and how it affects stem numbers remains poorly understood and may be cultivar-dependent, as asserted by (Struik et al., 2006). Ultimately, variation in stem numbers on account of differences in physiological age in different seed batches can be expected, translating to potential spatial variations where more than one batch is planted a field.

2.3.2 Land Preparation and Planting

Land preparation in potatoes is tailored towards maintaining a well aggregated, stable, aerated, free-draining and biologically active soil (Harris, 1992). Field operations to achieve this are site-dependent to remediate the effects of prior land use practices. Soils are often assessed in late summer or autumn for structure and texture problems as well as potential water run-off in the first 500 mm (Witney & McRae, 1992). Depending on the findings, subsoiling can be done to break compaction pans. Ploughing is recommended up to 30 cm depth to loosen the soil, bury weed seeds and ensure good tilth (Harris, 1992) followed by seed bed (rows) formation at 80-90 cm apart. The depth of the beds matches the plough layer (Harris, 1992). After bed formation, de-stoning is done to reduce the risk of eventual tuber bruising at harvest at 30-38 cm for ware potatoes and 25-30 cm for seeds and salads, though it has been reported that no advantage in productivity (yields) is gained when soils are destoned deeper than 25 cm for any potato grade (Stalham et al., 2007). De-stoning is often combined with planting in a single operation; windrowers are mounted with a planter to combine the operations (Harris, 1992). Fertilizer application is also done at planting, often combined with the planting operation while ensuring that placement is done on the side and below the seed pieces (Harris, 1992). This is done to reduce direct contact between the seed pieces and concentrated fertilizer pellets which may be injurious to emerging seedlings.

The most commonly used measure of plant density in potatoes is the seed rate, which is defined as the weight of seed planted per unit area (Allen & Wurr, 1992). This is affected by the size of seed tubers, therefore a desired plant population for each particular seed size is selected based on seed supplier information on emergence rates of the tubers after which the seed rate is calculated backwards (Allen & Wurr, 1992). Within-row spacing is therefore dependent upon the desired plant population as a function of seed size. Two types of potato planters in common use in the UK are the cup planter and belt planter (Witney & McRae, 1992). Cup planters deliver seed to the soil using evenly spaced cups which scoop up the seed from a reservoir. The accurate spacing of the cups means that a high degree of accuracy is achieved in plant spacing, however, the fixed size of the cup causes problems in handling of large seed. The scooping action also causes damage to sprouts where pre-sprouted seed is used. The belt planter delivers the seed to the soil via a conveyor belt on

which seeds are arranged in a stream. This minimizes damage to pre-sprouted seeds, however, the seed is delivered with a forward trajectory which causes inaccuracies in spacing (Allen & Wurr, 1992). Plant spacing is one of the key determinant of tuber number and size. Increasing plant spacing significantly affects the population of tuber-bearing units per unit area and in turn decreases the total and marketable yield (Bohl et al., 2011). Several studies have also reported an increase in small-sized tubers in densely planted plots, establishing a negative relationship with tuber size due to increased competition to bulk a larger number of tubers from a finite source of intercepted radiation at full canopy (Allen & Wurr, 1992; Arsenault et al., 2001; N. R. Knowles & Knowles, 2006; Love & Thompson-Johns, 1999). The problems with plant spacing caused by inconsistent seed sizes and inefficient planters call for better standardization of seed sizes and more research in seed delivery mechanisms in planters respectively. From a precision agriculture perspective, it is also pertinent to do an ex-post determination of any apparent spatial variation in plant density after emergence so that yield expectations can be adjusted and zones for variable management (e.g. variable harvest timing) can be delineated.

2.3.3 Post-Emergence Development and Apical Dominance

After emergence, a potato plant is anchored by a main stem which determines the plant's height, canopy spread and density through axillary branches and leaves (Almekinders & Struik, 1996). The leaves of potatoes start out as undivided whole leaves on the first 4 buds from the soil surface, however, from the 5th bud upwards, compound leaves are formed consisting of several pairs of lateral leaflets and a terminal leaflet (Jefferies & Lawson, 1991).

The main stem's apical dominance is broken by the development of flowers which terminates vertical growth, however in indeterminate varieties, this paves way for the development of secondary stems through sympodial and axillary buds (Almekinders & Struik, 1996; Jefferies & Lawson, 1991). The degree of apical dominance therefore determines the stem and branch density in a plant. Prediction and control of stem density is of interest in potato production because it has been reported to have an influence on tuber size distribution (Bussan *et al.*, 2007). Apical dominance is hormonally controlled by Auxins and Cytokinins, and their interactions (Hall & Hillman, 1975). Historically, three theories around production of the auxin indole-3-acetic acid (IAA) in apical meristems have been used to explain apical dominance (Kebrom, 2017; Mason et al., 2014);

1. Direct Inhibition: Excess auxin production in the apical meristem enters the phloem and is transported into axillary buds where it concentrates, and inhibits auxin synthesis which is necessary for bud growth.
2. Canalization: Excess auxin production in the apical meristem is moved down the stem where it inhibits the biosynthesis of cytokinins and other plant hormones which are necessary for axillary bud initiation.
3. Indirect Inhibition: Auxins in the apical meristem induce stem elongation at the apex thereby increasing the demand for sucrose and other growth factors. This essentially maintains a sharp sugar gradient which deprives the buds of nutrition hence controlling growth and maintaining apical dominance.

The direct inhibition theory was originally disproved by Hall and Hillman, (1975), who observed that apical dominance was broken before the concentration of auxins dropped in the stems when apical meristems of *Phaseolus vulgaris* were decapitated. This proved the existence of a secondary signal from the apical meristem which inhibits bud outgrowth and acts faster than the auxin gradient. Although there is no consensus on the nature of the second signal, it is widely accepted that cytokinins and strigolactones are central to bud activation (Domagalska & Leyser, 2011). As a result, the canalization theory is the most widely adopted and utilized in mechanistic models.

The indirect inhibition theory has recently gained traction after Mason et al. (2014) observed that sugar accumulation in stems follows immediately after apical meristem excision in Peas (*Pisum Sativa*). Additionally, infusion of sugar into dormant buds of peas significantly induced bud growth. These findings suggest that sucrose may also act as a signalling molecule for apical dominance. It can be theorized that stem elongation at the meristems suppresses branching in dicots by acting as an active sink for photosynthetic products which deprives the axillary buds of carbohydrates needed for growth (Kebrom, 2017). As stolons are part of the stem system, low apical dominance at the stolon apex should also hypothetically lead to more equitable sugar distribution in the primary and lateral apices from which tubers are formed. Potato tubers are formed from either primary or secondary stolons, which also exhibit apical dominance; primary stolons are more likely to form tubers than secondary stolons (O'Brien et al., 1998). Apart from apical dominance,

stolons also exhibit variations in apical control and sink strength, causing large variations in tuber sizes among tubers falling on the same main stem (O'Brien *et al.*, 1998).

Ultimately the determination of above-ground apical dominance may provide a proxy for understanding the variation in tuber sizes and stolon numbers below-ground if their realizations are controlled by the same signal. A correlation of these two variables has not been identified in literature but it might aid in explaining a portion of the variation in tuber sizes at harvest. Furthermore, the correlation between stem density and TSD has been reported by various authors, with a general consensus that higher stem density per unit area leads to a proliferation of more tubers but with a smaller average size due to competition for a finite source of resources for tuber bulking (Bleasdale, 1965; Gray, 1972; Knowles & Knowles, 2006; Love & Thompson-Johns, 1999). However, at the plant level, the possible natural propensity of mother tubers with low apical dominance to produce smaller tubers due to auxin-regulated sugar distribution over more stolons has not been investigated in the literature and remains a key knowledge gap. From a precision agriculture perspective, development of reliable methods for the determination of stem density and its spatial variation would constitute a significant progression in this field. This is because stem density is considered to be the true unit of plant density for predicting yield and TSD but its accurate prediction across a field has so far eluded agronomists (Allen & Wurr, 1992).

2.3.4 Tuber Induction and initiation

The term Tuber Induction in potatoes refers to the hormone-controlled processes that result in the halting of stolon tip elongation to favour of lateral growth culminating in tuber initiation, which is the swelling of the stolon tip to form a tuber (Claassens & Vreugdenhil, 2000). A literature review of this stage and tuber initiation is warranted as its timing ultimately affects decisions on planting date and harvest date. Management decisions of vine desiccation and harvesting are based on the maximization of groundcover between tuber initiation and harvest, as well as the monitoring of tuber bulking towards the preferred tuber size profile. It is therefore necessary to understand the signals that control tuber initiation for possible manipulation of tuber numbers and hence biomass partitioning towards a desired tuber size profile.

Xu *et al.* (1998) reported that a switch occurs from transversal to longitudinal cell division during tuber induction, associated with the activity of auxins, analogous to above-ground axial branching. Roumeliotis *et al.* (2012) found that the expression of the StYUC-like1 gene which controls auxin biosynthesis in stolons increases in a direct relationship with stolon auxin concentration when short day conditions are induced. To locate dominant sites of auxin production and distribution, Roumeliotis *et al.* (2012) tracked the direction of auxins movement in the stolon using ^{14}C labelled IAA and the direction was found to be basipetal. This suggests that stolon tips display apical dominance and control tuber induction through auxin activity using similar mechanisms to those that main stems use to control above-ground lateral branching. Endogenous GA concentration was also identified as the dominant regulator of tuber formation, having an inverse relationship to tuber induction. This corroborated widely reported results that the exogenous application of GA inhibits tuber induction while its declining concentration induces tuberization (Ewing & Struik, 2010; Kumar & Wareing, 1972; Railton & Wareing, 1973). Xu *et al.* (1998) also identify abscisic acid as an induction promoter which may have an antagonistic relationship with GA on tuber induction.

Potatoes are qualitative short day plants and tuberize at day lengths shorter than 12 hours (Ewing & Struik, 2010). The photoperiodic response is perceived in the leaves but the signal is transmitted into the stolons and regulates induction through the action of GA (Jackson *et al.*, 2000). As a result, planting date is very important in potato production in order to ensure that tuber induction occurs when the above-ground canopy has developed adequately for maximum photosynthetic efficiency and tuber bulking. High temperatures are also known to inhibit tuberization by encouraging the growth of stolons and the partitioning of more photosynthetic products to the shoot by stimulating bud activity to favour stolon and branch development (Jackson, 1999). Even on already bulking tubers, increased soil temperatures have been reported to result in the reactivation of stolon growth towards the soil surface at the apical bud until this is halted by decreased temperature (Ewing & Struik, 2010). It is further suggested that alternating soil temperature regimes can lead to multiple tuber initiations and intermittent stolon growths leading to the formation of chain tubers (Jackson, 1999). Additionally, Jackson (1999) report that high concentration of nitrogen ions supplied as ammonium or nitrates has a similar inhibitory

effect and temporal dips and rises in nitrogen ion concentration in the rhizosphere equally leads to the formation of a chain of tubers.

The inhibitory effect of GA on tuberization brings up a question of whether GA application at a critical stage can limit tuber number and thereby enable more biomass partition to a controlled number of tubers. GA inhibitors can also potentially be used to induce early tuberization. These potential applications have not been reported extensively in literature, warranting their possible investigation.

2.3.5 Tuber Set and Size Distribution

The term tuber set is used to describe the total number of tubers produced per planting station/hill (Knowles & Knowles, 2006; Rosen & Bierman, 2008). It is reported to be cultivar dependent (Love & Thompson, 1999) but also environmentally controlled (Freeman, Franz, & Jong, 1998; Knowles & Knowles, 2006; Wurr et al., 1993). For example, Rosen and Bierman (2008) report of a positive correlation between soil P test and tuber set, however the increase in tuber number came from small (unmarketable) tubers (less than 85g) while the number of marketable tubers decreased. Several studies have also established GA as a determinant of tuber set. Dean et al. (2018a) suggested a combination of GA and Naphthaleneacetic acid to decrease the average tuber size and stem number respectively, a combinatory strategy that has the effect of standardizing tuber size in varieties that exhibit low apical dominance. An inverse relationship also exists between plant spacing and tuber set as observed in experiments by Wurr *et al.* (1993). Additionally, Allen and Wurr (1992) report that increase in the number of stems per plant is associated with increase in the number of tubers per plant. However edaphic factors and plant nutrition are the main determinant of the final number of tubers and their sizes. Their influence has therefore been discussed in detail in Section 2.4.

Attempts have been made to mathematically model tuber development in potatoes using crop models like the LINTUL-POTATO (Kooman & Haverkort, 1995), which is reported to accurately predict yields several weeks in advance of harvest but without the provision to predict TSD at harvest. The term TSD refers to a measure of the proportions of different discreet tuber size (Wurr et al., 1993) or weight (Marshall et al., 1993) grades in a harvest sample. There is high tuber size variability in potatoes – even those harvested from a single

stem – due to stolon characteristics, hormone and enzyme activity as well as environmental factors (Struik et al., 1991). There have been many attempts to control these factors to achieve a degree of predictability of TSD to maximize size uniformity in harvested tubers (Wurr, *et al.*, 1993; Bussan *et al.*, 2007; Struik *et al.*, 1991). The ability to predict and manipulate TSD depends on its accurate description and choice of parameters to measure it. Travis (1987) used the mean tuber weight and the standard deviation, assuming a Gaussian distribution of tuber weights falling under predetermined weight grades, a model later adopted by Struik et al. (1991) and Wurr et al. (1993). However, later literature including Bussan *et al.* (2007), Hide and Welham (1992) and Nemecek et al. (1996) contend that TSD rarely follows a Gaussian distribution. After long term observations of potato bulking rates and tuber development between 1965 and 1974, Hide & Welham (1992) found that a potato plant produces two populations of tubers with different means and variances during the season and the TSD is best modelled using a combination of two normal distributions. However, this model has not been widely adopted due to the fine riddle sizes required to collect data that the model can adequately fit and the occasional prediction of negative tuber sizes, classified as resorbed tubers by the authors. The use of a flexible distribution is strengthened by evidence from Love and Thompson-Johns (1999), where TSD was shown to shift from predominantly small tubers to predominantly large tubers as in-row plant spacing is increased (Figure 3).

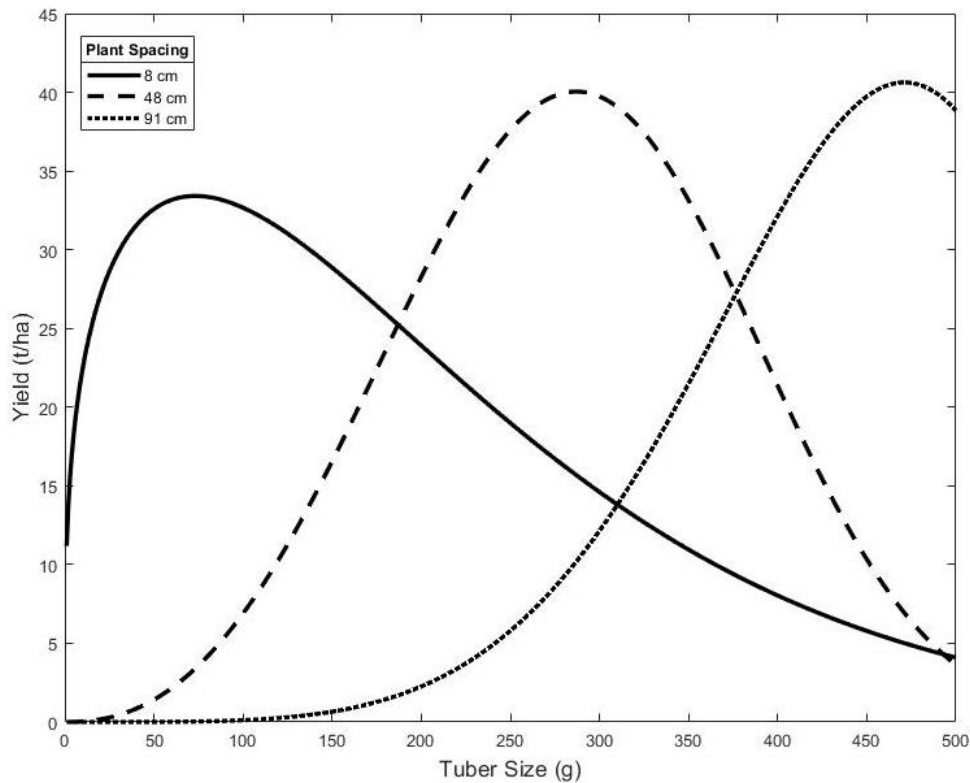


Figure 3: An adaptation of the observed effects of in-row seed piece spacing on yield of tubers Frontier Russet, Ranger Russet and Russet Burbank varieties. Simulated from Love & Thompson (1998) data using a Weibull distribution by varying shape and scale parameters.

A less widely adopted model which eliminates the prediction of negative tuber sizes and offers a flexible shape depending on sample characteristics is the Weibull function adopted by Nemecek et al. (1996) and Bussan et al. (2007) among others. The Weibull distribution, as described by Nemecek et al (1996), is a continuous distribution mainly used in survival analysis, due to its flexible shape parameter that determines a rate of failure of the modelled process over time. The flexibility of the shape parameter allows for modelling both left and right skewed distributions as well as symmetrical distributions, as illustrated in Figure 3. Nemecek *et al.* (1996) and Bussan *et al.* (2007) were able to predict the tuber size variation by fitting a Weibull distribution to their data due to the flexibility of the curve to shape changes. If a sample tuber set is partitioned into quantiles based on tuber size, the shape parameter of a fitted Weibull distribution can potentially be used as an estimate of the shape of the TSD. However, Nemecek *et al.* (1996) suggest that the shape parameter remained constant at 2.3 while only the scale parameter shifted, and therefore enabled them to model TSD using the probability density function of the Weibull distribution. Bussan

et al. (2007) opted to estimate the Weibull parameters as functions of other measured variables, for example, the scale variable was modelled as a function of stem number. Aliche *et al.* (2019) also used the Gamma function to model TSD, which closely relates to a Weibull distribution with a small shape parameter as adopted by Nemeček *et al.* (1996). These different approaches show that the description and measurement of TSD is currently non-standardized, making it difficult to compare studies where different treatments have been used to purportedly influence TSD.

Several studies describe TSD either as the coefficient of variation assuming a Gaussian distribution (Wurr *et al.*, 1993), sometimes only described qualitatively, comparing different treatments using polygonal charts (Knowles & Knowles, 2006), or as the yield proportion of a “desired” tuber size range (Arsenault *et al.*, 2001). There is a huge variation in “desired” TSD in different countries and markets (i.e. table potato vs seed potato), which complicates the choice of parameter to describe TSD and target its manipulation. Generally, tubers are graded into marketable and unmarketable subsets based on a size threshold, then the marketable subset is further graded into small, medium and large tubers which have different market values (Cambouris *et al.*, 2015). The thresholds for marketable tubers and their further grading into different size ranges varies in different markets. While some countries (e.g. USA and Canada) have pre-defined tuber classification systems which conveniently create fixed bins for modelling TSD, thresholds for marketable tuber size in GB are generally decided by the outlet market (Taylor *et al.*, 2018) and may be re-negotiated during the season depending on crop performance. Though classification of tubers into weight grades is common across the globe, tubers are normally graded according to their diameter using a square mesh (Nemeček *et al.*, 1996), then the subsequent yield of each size grade per hectare ultimately decides the commercial value of the produce. Therefore, there is more direct benefit in developing TSD models based on linear measurement grades (i.e. mm, in or cm) then utilize size to weight conversion functions such as provided by Travis (1987) to predict and extrapolate yields. However, both size and weight-based classification systems are used in several different countries with no standardization hence the effect of independent variables on TSD as reported in literature are contingent upon the grading system used, making it difficult to compare different studies.

A cursory search on peer reviewed publications over the past 50 years (1970-2020) shows increased interest in optimization of potato tuber size and its distribution using appropriate rates and application strategies of primary and secondary macronutrients since the 1990s. For example, using the “tuber yield” keyword refined to Potato-related papers in the “Web of Science” (WoS) database yields results mainly composed of genetic crop improvement and manipulation of metabolic pathways using plant growth regulators, reflecting the domination of plant breeding in yield gap reduction research. However, soil amendment with primary and secondary macronutrients for optimization of tuber yield has been studied in up to 20% of published potato research per decade since 1970. The optimization of potato tuber sizes has become important for maximizing marketable yields and minimizing post-harvest losses in crop value. While crop improvement also dominates research on tuber size optimization, the past 50 years have seen an increase in the percentage of studies investigating the effect of primary and secondary macronutrient soil amendments from 12% in the 1970’s to 24% between 2010 and 2020. Consequently, the use of the keyword “tuber size distribution” in publications has increased exponentially since 1970 and macronutrient-related research on TSD has increased from virtual non-existence in the 1970’s to 17% of all indexed papers on TSD between 2010 and 2020. This provides an opportunity for the current study to contribute towards defining an objective measure of TSD that can be across different studies. The Weibull distribution shape parameter provides such a unit-less index.

In a bid to understand production factors that affect TSD, Bleasdale (1965) first reported a positive correlation between stem density and yield within each tuber size fraction. This was subsequently corroborated by several authors (Gray, 1972; Wurr, 1974) leading to widespread adoption of stem density as a proxy for predicting/manipulating expected tuber size fractions. Bussan *et al.* (2007) was able to predict increases in the proportion of small tubers with increased stem density at the expense of the proportion of large tubers. The model was able to predict the relative stability of proportions of mid-grade seed sizes with shifting stem densities. This agrees with findings by Struik *et al.* (1991) that the number of tubers that will reach marketable size is usually fixed before tuber bulking, partly by the stem density. Subsequently, tuber bulking favours the larger tubers to the smaller tubers, leading to non-symmetric TSD for late harvested potatoes. From these findings, it can be hypothesized that combining the tuber size prediction power of stem density and the ability

to choose a time of harvest could offer a practical management option for optimizing tuber size at harvest.

Apart from stem density, many other techniques for manipulating TSD have been proposed. (Dean, Knowles, & Knowles, 2018b) were able to achieve this using 2mg^{-1} seed dips in GA which resulted in a proportional increase in undersized ($<113\text{g}$) tubers and a reduction in oversized ($>397\text{g}$) tubers. This however also depressed the average tuber weight by 20% in comparison with non-treated controls. GA favours stolon elongation to tuber formation (Xu *et al.*, 1998), therefore it is expected that it would slow tuber bulking rates and depress yields as observed in this study. In experiments with Russet Burbank and Ranger Russet varieties, Love and Thompson (1999) found positive correlation between seed spacing and large ($>452\text{g}$) tuber size proportion in the TSD, ranging from 0% at 8cm intra-row spacing to 37% and 49% at 91cm spacing respectively for the two varieties.

In order to predict TSD and its spatial variation at harvest in a precision agriculture context, there is need to model it as a function of stem density, soil variation or their proxies. The effect of stem number on TSD has mostly been evaluated in stem density experiments in controlled environments. It is necessary to test this relationship at a field scale in typical commercial production settings by means of field surveys. This necessitates the development of a rapid way of evaluating TSD using a parameter that can be used to model the relationship with stem densities which has not been done in literature. While the effects of above-ground plant canopy factors on TSD have been widely studied, the effect of the primary soil nutrients is not elucidated and examined in a coherent way. Wurr *et al.* (1993) and Struik *et al.* (1991) reviewed the agronomic manipulation of plant processes that determine TSD. With many studies collecting graded tuber yield data in relation to macronutrient amendment rates and timings, a review of the overall trends in responses and the current status of the research questions surrounding TSD and soil nutrition is not available. It is therefore important to review the body of literature that links soil factors to TSD for the purpose of selecting appropriate nutrients to incorporate is a potential predictive model for TSD.

2.4 The Influence of Edaphic Factors on Tuber Size Distribution

The purpose of this section is to evaluate research work on the influence of soil physical and chemical properties on Potato Tuber Size Distribution (TSD), with a focus on properties that have a potential for use in precision agriculture as decision support information for variable rate fertilizer application or management zone delineation for improved productivity. The review identifies knowledge gaps in the edaphic factors that control TSD at the agronomic management level with the aim of formulating research questions to direct subsequent field experiments. As such, the review starts with an evaluation of the current fertilizer management practices in potato production in GB then goes into the discussion of some of the key soil variables with potential for efficacy in the control of TSD in a precision agriculture context.

2.4.1 Fertilizer Practices in Potato Production

Current fertilizer recommendations in potatoes for phosphorus, potassium and magnesium in the UK are based on achieving and maintaining target soil Indices for each nutrient in the soil. The fertilizer recommendation guide AHDB (2021) is currently recommended for decisions on fertilizer application. According to AHDB (2021), historical experimentation has led to the current recommendation to maintain a target of at least 16 mg/kg, 121 mg/kg and 51 mg/kg of P, K and Mg respectively in the soil across the UK. Consequently, fertilizer requirements are based on remediating deviations in soil tests to achieve these concentrations. Recommended application times for the three elements is in spring, however, where the recommended rate of potassium exceeds 300 kg/ha, a split application is done by applying half of the requirement in winter. Due to this potential advance requirement, soil analysis is usually done in the summer or immediately after harvest. Sulphur application is generally not recommended in the UK, however, a flat rate of 25 kg/ha SO_3 is recommended where deficiencies are noted.

Nitrogen application requirements are calculated annually by measurement of Soil Nitrogen Supply (SNS) and Soil Mineral Nitrogen (SMN) levels (AHDB, 2021). The SNS is based on the analysis of nitrate and ammonium concentrations in the soil in kg/ha. It is recommended to estimate and sum the SNS at 0-90 cm depth or to a known rooting depth. The SMN is subjectively estimated based on any planned organic matter incorporations to the soil after soil sampling. Drawing from prior research by Cambridge University Farm and Harris (1992),

AHDB (2021) reports that indeterminate varieties generally require less nitrogen than determinate ones, and nitrogen mainly affects the crop by prolonging the period of green haulms. This means the efficacy of nitrogen application is closely tied to the date of harvest. With these findings, all commonly grown varieties in the UK have been classified into four groups based on their determinacy and production seasons have been classified into 4 groups of 30 days each. Using these calculations, soil nitrogen requirements are therefore calculated as a function of SNS, crop determinacy and length of growing season. All nitrogen applications are done in the seedbed before planting, however, a split application is recommended where top dressing is preferred by applying two thirds in the seedbeds and one third after 50% emergence. The SMN index allows for estimating nitrogen requirements based on previous crop, soil type and general rainfall pattern of the production area, however, this may not allow for the establishment of in-field variability necessary for precision farming therefore has not been reviewed here.

2.4.2 Effect of Soil Nutrients on Tuber Development and Size Distribution

2.4.2.1 Nitrogen

A positive relationship between potato yield and nitrogen fertilization rate has been well documented in literature (Long et al., 2004; Porter & Sisson, 1991; Schippers, 1968a; R. K. Scott, 1980), enabling the development of N management models for yield optimization. N availability is one of the most important yield limiting aspects in agricultural production and potato yields are known to respond positively to its accumulation in the soil up to an optimal value.

Schippers (1968) found that potato yields respond positively to incremental doses of soil-applied N between 0-80 N kg/ha, reaching an asymptote at N rates in excess of 80 kg/ha in sandy soils with spatially variable water retention. Porter & Sisson (1991) reported similar quadratic regression curves whereby Russet Burbank and Shepody potato optimized tuber yield at 196 N kg/ha and 211 N kg/ha respectively when preceded by a cereal in rotation and 126 N kg/ha and 136 N kg/ha respectively in a legume rotation. These quadratic responses have been consistently reported over the last 5 decades and help formulate the basis of fertilizer recommendations for potato production. In a widely accepted conclusion, Scott (1980) discuss that although incremental soil-applied N rates correlate positively with the

actual amounts of N taken up by the crop, resultant plant growth response is observed in leaf expansion rather than tuber growth, with luxury N-uptake observed at 400 N kg/ha and tuber bulking delayed by an average 8.5 days. Additionally, temporal (Scott, 1980) and spatial (Cambouris et al., 2007) autocorrelation of yield is partially dependent on in-field N variability, which highlights the site-specific nature of nitrogen effects on potato yield.

The positive influence of N on average tuber size has been reported by several authors but its effect on the overall TSD and its central tendency has not been consistently demonstrated. This is partly due to the loose application of the term “TSD” by authors and the lack of a standardized and generally accepted method of its quantification (Wurr et al., 1993). As earlier discussed, potato growers target different tuber sizes at harvest depending on their outlet market (Taylor et al., 2018; Wurr et al., 1993), which makes it difficult to standardize the size classes and objectively compare TSD from different studies. Studies on how N variation translates to variation in TSD often focus on the effect of rate on yield or proportion of a specific desired “marketable” weight or diameter range in the yield. Most of the studies considered in this review had TSD as a secondary hypothesis to the effect of N rate on average yield, desired to minimize post-harvest/grading losses and maximize the market value of production. Ammonium Nitrate is the predominant form used in N studies. While there is limited use of ammonium sulphate (Fontes et al., 2010) and UREA (Boydston et al., 2017; Gao et al., 2018) and polymer coated UREA for controlled N release (Gao et al., 2018), the effect of N form on TSD is either insignificant (Gao et al., 2018) or has not been evaluated in most studies. Therefore, the most probable way in which targeted N delivery will be achieved for TSD and yield improvement will be through applying the right rates of fast-release N sources like UREA and Ammonium Nitrate at critical times. The critical need – which is the subject of this section of the review – is to accurately determine the critical times of N application and their corresponding N rates that optimize TSD.

Responses of TSD to N rates

TSD Graded by Weight

Multiple researchers over the past 5 decades have consistently reported observing a positive influence of N on TSD at harvest, mostly when it is measured as the proportion or

absolute quantity of yield above a weight or diameter threshold (Arsenault et al., 2001; Gao et al., 2018; Porter & Sisson, 1991; Schippers, 1968a). Adopting the Travis (1987) model, Wurr et al. (1993) studied the effect of N on TSD from 9 potato experiments spanning 3 years in Cambridge, England where TSD was described as the coefficient of variation (CV) in tuber diameters for each plot. The authors observed that increasing N rates also increased and explained 68% of the CV in combined 3-year data, which suggests that increasing N leads to more uniform proportions of tubers in variable grade sizes across the range. In contrast, Porter and Sisson (1991) reported significant positive quadratic relationships between N rates and TSD, calculated as the percentage of large (> 0.23 kg) tubers, where proportion of marketable tubers increased linearly or in a quadratic polynomial by between 8 and 24% in comparison to the control when subjected to a rate of 90 N kg/ha over 3 years. The percentage of yield in the > 0.23 kg size class further increased at the expense of smaller size classes with increasing N rate (Figure 4) and optimized either at 180 N kg/ha or 135 N kg/ha depending on whether a nitrogen-fixing legume crop preceded the experiment or not. Bélanger et al. (2000) corroborated the positive asymptotic relationship between fertilizer N rate and marketable tuber yield and found that the absolute marketable yield optimized at 175 N kg/ha and 240 N kg/ha in 1999 and 2000 respectively though their threshold weight of marketable tubers against small unmarketable tubers was not disclosed.

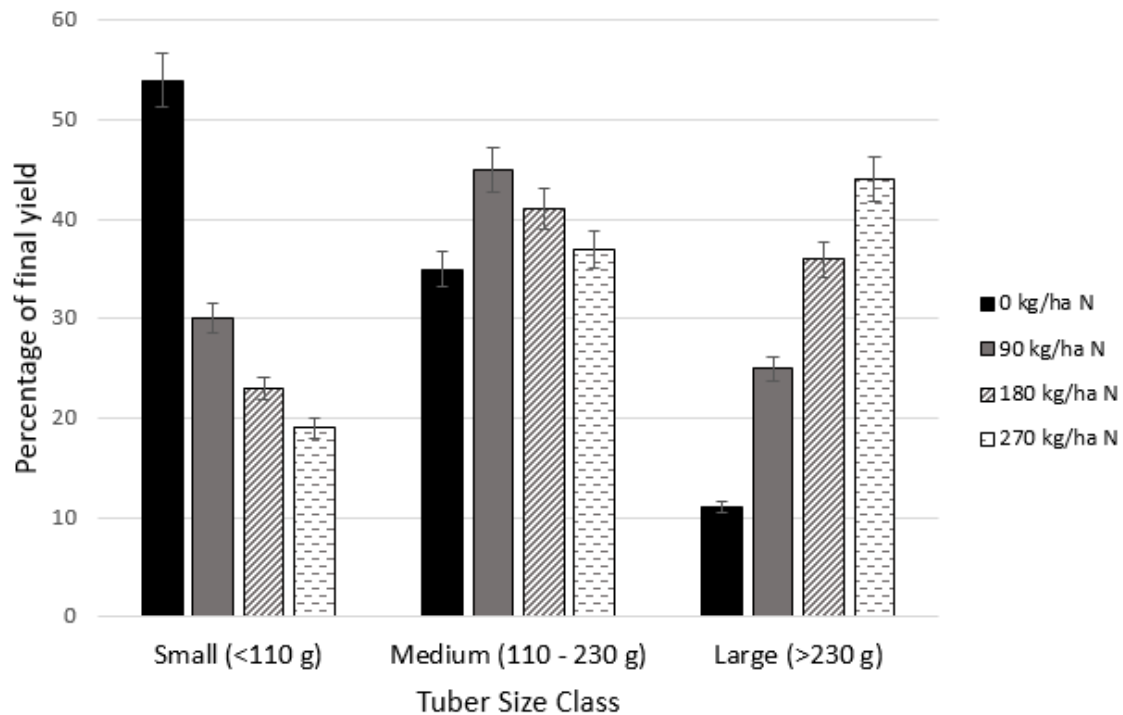


Figure 4: Effect of nitrogen rates (0-270 kg/ha) on the proportion of small, medium and large tubers in the yield. Adapted from Porter and Sisson (1991).

To assess TSD and how it shifts with any treatments, it makes more sense to compare treatments in terms of their effect on the probability density of a desired class of tubers (preferably the modal class) than absolute yield values, which are confounded by variation in tuber numbers per plot and other less-understood phenomena like tuber bulking rates. Gao et al. (2018) conducted a 3 year N trial with 0 or 100 kg/ha N applied on the Russet Burbank potato variety and classified tubers into undersize (<85 g), small (85–170 g), medium (170–340 g), and bonus (>340 g) size classes, considering all tubers weighing over 85 g as “marketable”. Regardless of the application method, N increased the ratio of marketable to total yield by 6% from 0.87 to 0.93. While this is lower than the results from the earlier study by Porter & Sisson (1991), it corresponds with the lower maximum rate of nitrogen used. Additionally, the huge difference in the threshold weight for marketable tuber classification between the Porter & Sisson (1991) and Gao et al. (2018) study (230 g and 85 g respectively) confounds the interpretation of the differences. Figure 4 and Figure 5 illustrate the variability in TSD in the two studies.

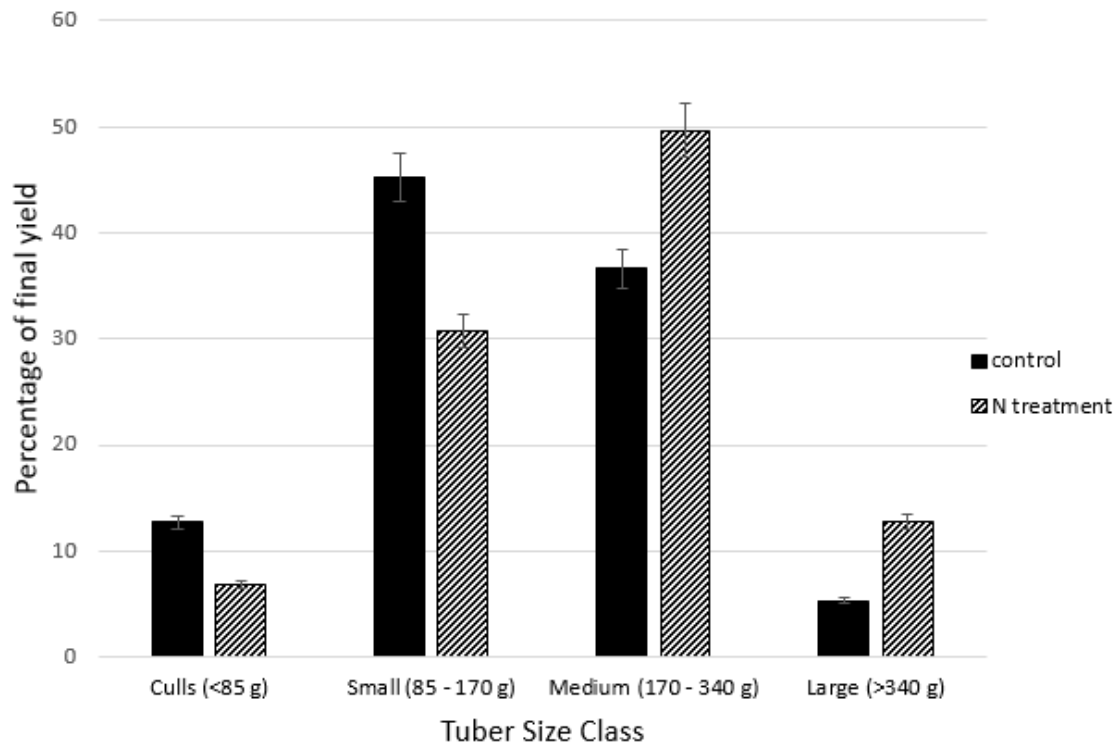


Figure 5: Effect of nitrogen rate (0-100 kg/ha) on the percentage of culled, small, medium and large potato tubers in the final yield. Adapted from Gao et al. (2018)

The results from Gao et al. (2018) show that TSD followed a Gaussian distribution in both the non-fertilized and 100 N kg/ha fertilized treatment, with a considerable gain in medium and large tubers in the fertilized treatment. In contrast, the results from Porter and Sisson (1991) show linearly decreasing proportions in the non-fertilized treatment, followed by a Gaussian distribution at 90 N kg/ha then linearly increasing proportions at 180 N kg/ha and 270 N kg/ha. In both studies, N addition favoured the production of tubers of higher weight but there was significant evidence ($P < 0.05$) of a decrease in specific gravity of tubers with increasing N rate in the Porter and Sisson (1991) study. This has been historically corroborated by several authors including Schippers (1968), White and Sanderson (1983), and more recently by Caldiz et al. (2018), suggesting the accumulation of more water per unit dry matter in larger tubers. Under this premise, it can be hypothesized that factors which increase the dry matter content of tubers potentially correlate negatively with the tuber size in units of linear measurements (i.e. diameter and length). Due to the common practice of grading tubers through square meshes of predetermined diameters desired for

downstream processing (Taylor et al., 2018), it is important to examine the effect of soil nutrients on TSD with tubers classed by their diameter.

TSD Graded by Diameter

Arsenault et al. (2001) studied the yield response curves of 8 potato varieties to 0 to 224 N kg/ha in Harrington, Prince Edward Island, Canada, quantifying TSD as the ratio of *Canada Number 1* (51-89 mm) size grade yield to the total yield. Since the Canada Number 1 size grade represented the medium grade in the range of tuber sizes observed (0 to over 114 mm diameters), a high TSD ratio meant a stronger central tendency in the distribution. A consistent positive increase in the ratio from 0.65 to 0.8 was observed as fertilizer rate increased from 0 to the lowest rate of N applied (~150 kg/ha) respectively across 7 studied varieties. Any further positive responses to incremental N doses were highly dependent on variety and plant spacing. While this suggests a general positive relationship between N rate and TSD, recent results from Boydston et al. (2017) showed no significant effect of N rate (range 34 – 101 N kg/ha) on the proportion of marketable tuber yield (0.62 in Bintje variety and 0.53 in Ciklamen variety) in early harvested potatoes when TSD was measured as the proportion of a modal (marketable) tuber size grade in the total yield. In this study, tubers were classified as undersized (< 25 mm diameter), marketable (25 to 38 mm diameter) and oversized (> 38 mm diameter). As an early-harvested crop, TSD was largely dependent on the tuber bulking hierarchy at the time of the desiccation as the tubers were still bulking, therefore the study illustrates the inadequacies of using N to improve TSD in specialty early-harvested potato markets.

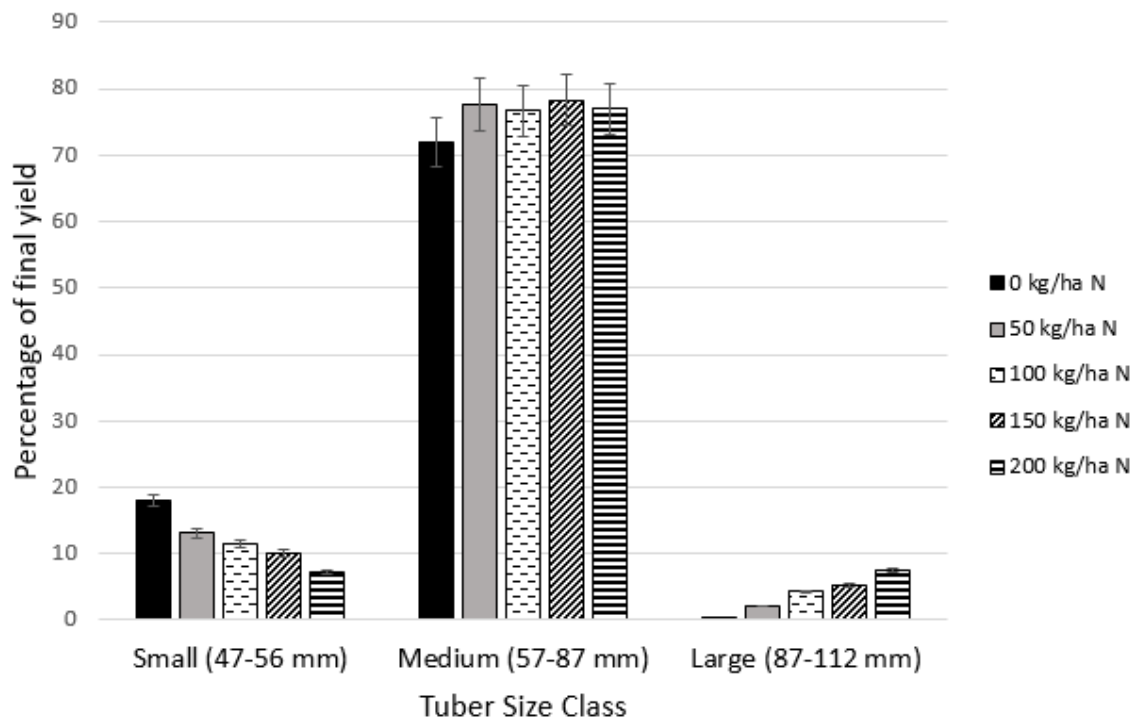


Figure 6: Effect of nitrogen (N) rate (0-200 kg/ha) on the percentage of small, medium and large potato tubers in the final yield. Adapted from Cambouris et al. (2007).

To test the practical application of variable N rates for TSD optimization in a precision agriculture context, Cambouris et al. (2007) tested the effect of five ammonium nitrate rates (0–240 N kg/ha over three years) and application timings on TSD three years in Quebec, Canada. Tubers were classified as culls (<47 mm), small (47 ≤ diameter ≤ 56 mm), medium (57 mm ≤ diameter ≤ 87 mm) or large (88 mm ≤ diameter ≤ 112 mm). In all three years, increasing N rate increased the proportion of large tubers and decreased the proportion of small tubers (Figure 6). Increasing N rate also increased the percentage of medium tubers from 0.71 to 0.77, however, this increase was observed at 50 N kg/ha and no further consistent trend was observed above that rate, suggesting that the desired TSD was optimized at the low N rate. Similar results were reported by Fontes et al. (2010) who assessed TSD as the proportion of a modal tuber size class (33 mm < diameter < 85 mm) on a distribution with a range truncated at 85 mm due to non-observance of large tubers.

In a recent main-crop field study, Maltas et al. (2018) studied the effect of five doses of ammonium nitrate (0, 80, 120, 160 and 200 N kg/ha) on the central tendency of the TSD measured as the proportion of medium sized (42.5–70 mm) marketable tubers. Compared

to the non-fertilized treatments, the proportion of marketable tubers increased by up to 11% with the addition of N at 80 kg/ha in the first year and 120 kg N in a subsequent year then plateaued. Since the non-fertilized and 200 N kg/ha treatments had a negative effect on the percentage of marketable tubers this study represents a recent addition to the generally established trend of a positive quadratic effect of N of the proportion of marketable tubers, optimizing between 100 and 200 kg/ha N as reported by other authors.

Many studies over the past 10 years back up the hypothesis that the total tuber yield increases with the rate of N. However, only a few studies, most of which have been reviewed here, discuss the increase in terms of proportions of marketable yield, which is more important to farmers. Indeed, if the yield gains realized by addition of N occur mostly in unmarketable tubers or less profitable size classes within the marketable range, the advantage is lost or reduced at the grading stage. Fertilizer strategies for maximizing the proportion of marketable tubers of the highest market value are therefore a key area of interest, which spurs interest in researchers to collect TSD data though it is rarely effectively utilized. The weight of evidence from published peer-reviewed research shows that increasing N rate optimizes TSD towards higher probability densities of large marketable tubers. A single inconsistency to this consensus was reported by White and Sanderson (1983), who found that increasing N rate from 67 N kg/ha to 201 N kg/ha only increased Russet Burbank and reduced Kennebec marketable tuber proportions by one percentage point. Long et al. (2004) also found no effect of N rate above 200 kg/ha on the proportion of marketable tubers as per the US classification system, though the high rates of N used mean the results might be in general agreement with most studies that found that TSD is optimized at N rates below 200 kg/ha. This review shows that wherever marketable tubers are classified as all tubers above a size threshold, N generally improves the proportion of the marketable component of yield and is generally optimized below 200 N kg/ha in field experiments. As reported by Fontes et al. (2010), the trajectories of the response curves of marketable yield seem to mirror those of total yield, and over-fertilization beyond 300 N kg/ha has a detrimental effect on yield (Long et al., 2004) and specific gravity (Porter & Sisson, 1991). Adopting the findings that yield and proportion of marketable yield optimize at similar N rates, finding a critical delivery method for maximizing the proportion of marketable yield at or below the optimized N rates seems to be the most direct way of

minimizing grading-related yield losses. This can potentially be done by determining the critical time for N delivery that maximizes the left skewness of a TSD, though there is limited availability of definitive studies in this regard.

Nitrogen Timing

Some farmers strategically grow potatoes in sandy acidic soils for easier tuber growth and to minimize the chances of Scab (Hawkins, 1954; Houghland, 1960). Poor water holding capacities of sandy soil comes with the risk of nitrate leaching which causes problems in maintaining an adequate supply of nitrogen at the peak of its demand during tuberization and bulking (Prunty & Greenland, 1997) in management programs where nitrogen is applied before or at planting. As a result, there are many studies concerning the optimization of fertilizer N delivery through split applications between planting and projected time of peak demand (tuber initiation or tuber bulking stage). However, most of the studies over the past decade have focused on the effect of fertilizer timing on total and marketable yields but stop short of evaluating the effects of the treatments on the overall TSD due to experimental design limitations. The primary designs of many fertilizer timing studies enable the evaluation of the effect of the interaction between timing and rate with respect to yield only. To evaluate the effect of splitting applications, a single rate of N needs to be tested in two or more treatments, one including the full rate at pre-plant then others with the desired splitting levels. With such a design, Cambouris et al. (2007) showed that splitting N applications between planting and hilling generally increases tuber yield as corroborated by Ojala et al. (1990) and other studies. However, the authors caution that the treatment effect ultimately depends on downstream stages of the nitrogen cycle as influenced by localized soil physicochemical properties and the form of N applied. In the Gleysols and Podzols with 4-5% nitrate N tested by the authors, there is a trend towards increasing the proportion of medium-sized tubers at the expense of large sized tubers. TSD was measured by diameter but the visual evidence (Figure 7) shows that the effect size is very small (~4% increase in medium sized tubers) within the tested range.

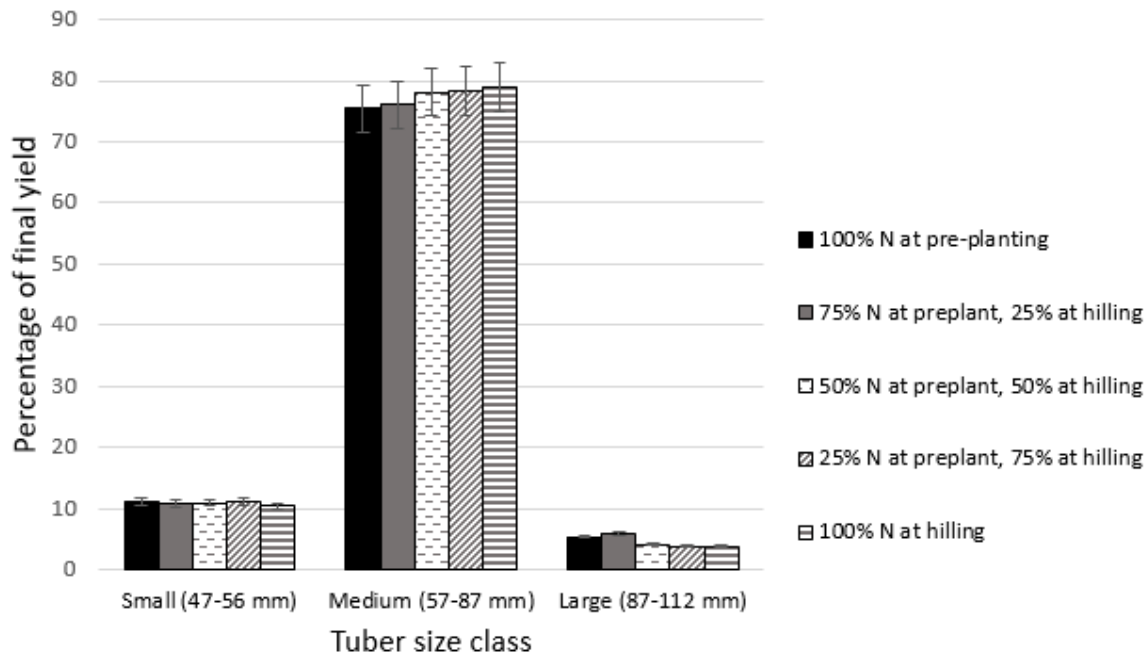


Figure 7: Effect of nitrogen (N) timing on the percentage of small, medium and large potato tubers in the final yield. Adapted from Cambouris et al. (2007).

Similarly in TSD measured by weight, the merits of splitting nitrogen application between planting and hilling (40% UREA at planting, 60% at hilling) are supported by evidence from Gao et al. (2018) where splitting provided the best option for minimizing the proportion of small tubers and maximizing the proportion of medium-sized tubers (Figure 8) with small margins. Furthermore, Kelling et al. (2015) tested split applications of nitrogen between emergence, tuberization and 20 days after tuberization (DAT) and reported that the effect of N splitting was more prevalent on TSD than yield. When the tubers were separated into <113, 114 to 170, 171 to 284, 285 to 370, 371 to 454, and >454 g size categories, the authors report observing significantly fewer tubers in the <113g and 114 to 170 g size categories, and more in the 171 to 284 g category when the N was split into three applications (i.e. Emergence, tuberization and 20 DAT) compared to two and four applications. These studies open up the possibility of optimizing medium tuber size using N at tuber initiation and presents a research question warranting more controlled trials to potentially elucidate the effects that were confounded by nitrogen rates in Cambouris et al. (2007).

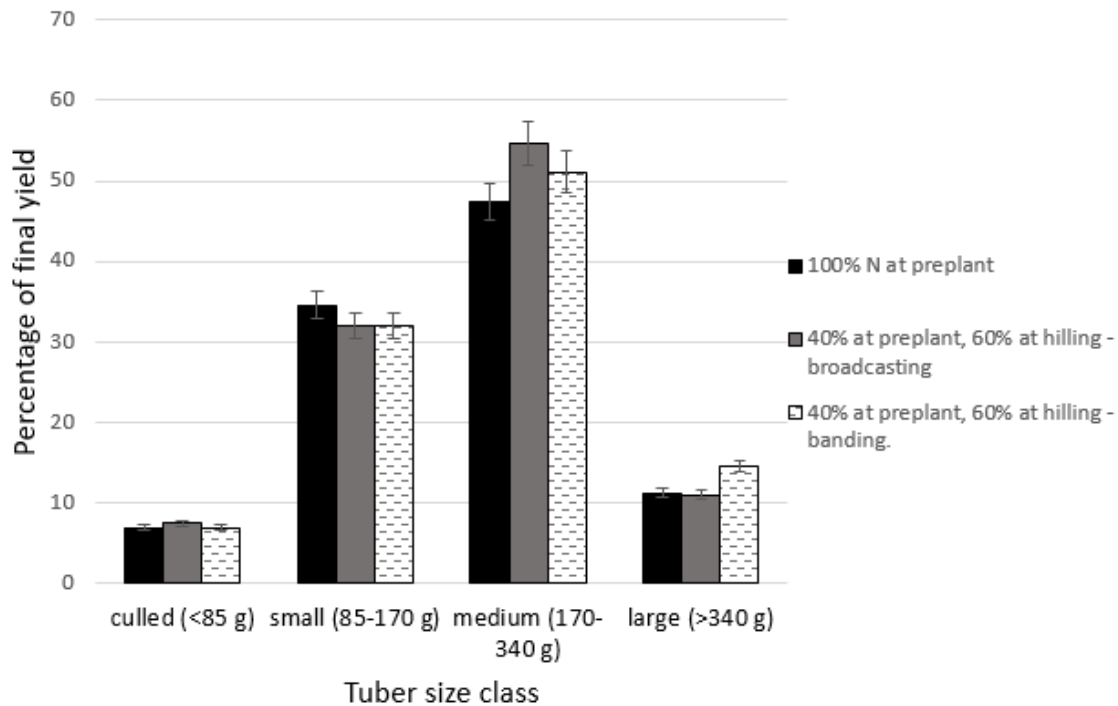


Figure 8: Effect of split nitrogen application on the percentage of culled, small, medium and large potato tubers in the final yield. Adapted from Gao et al. (2018).

2.4.2.2 Effect of Potassium and Sulphur Fertilization on TSD

The influence of K fertilization on potato yield and TSD is widely studied and soil K replacement based on crop removal is generally accepted as a management strategy in commercial production systems. These recommendations are mainly based on early findings from Dickins et al. (1962) and Birch et al. (1967) and more recently by Allison et al. (2001) who recommends the use of no more than 210 K kg/ha for yield optimization. In TSD studies, Simpson et al. (1973) applied incremental quantities of K (0-240 kg/ha) and Mg (0-54 kg/ha) in a factorial design to evaluate the main effect of the two nutrients and their interaction on yield and TSD. K application had no significant effect on final tuber yield except in 1 site where application of K in excess of 70 kg/ha showed an increase in total tuber yield. This site was found to have a historical record of low K concentrations. The authors however found that application of K in excess of 70 kg/ha generally increased the yield of *ware-sized* tubers (> 57 mm diameter) by a mean of 1.3 t/ha while the yield of *seed-sized* potatoes (32-57 mm) was reduced by margins ranging from 0.25 t/ha to 6 t/ha. These results are consistent with the authors' previous works (Simpson, 1962; Simpson & Crooks, 1961) as well as that of Henderson (1965), Dickins et al. (1962) and Arora (1987). In order to

describe the elasticity of the tuber size distribution, Simpson et al. (1973) calculated the *ware-sized* to *seed-sized* ratio on all their data points and report a range of 0.1 to 2.0 which suggests a highly elastic distribution, finding that the treatments with higher concentrations of K tended to cluster on the higher end of the range. More recently, Panique et al. (1997) also found that the yield proportion of US No 1 size tubers (> 51 mm diameter) in the total yield increased with K rate up to 332 K kg/ha in 5 of 11 experiments conducted over 11 years, with the remaining sites not responding due to a high soil K test. Similar observations were made by Haase et al. (2007) and Li et al. (2015), providing recent evidence to the historical observations of a positive influence of K on TSD and justification for its continued use in agronomic management recommendations.

Henderson (1965) and Dickins et al. (1962) found that the composition of K fertilizer also has an effect on TSD. In both studies, the effects of KCl and K₂SO₄ on TSD were compared, with consistent results in both experiments showing that incremental concentrations of KCl significantly ($P < 0.05$) favoured the production of ware grade (>57 mm) tubers (Figure 9) while K₂SO₄ favoured the production of seed-grade (31-57 mm) potatoes. These results were corroborated by Nabi et al. (2000) and form the basis for the widespread recommendation of KCl for tuber size maximization.

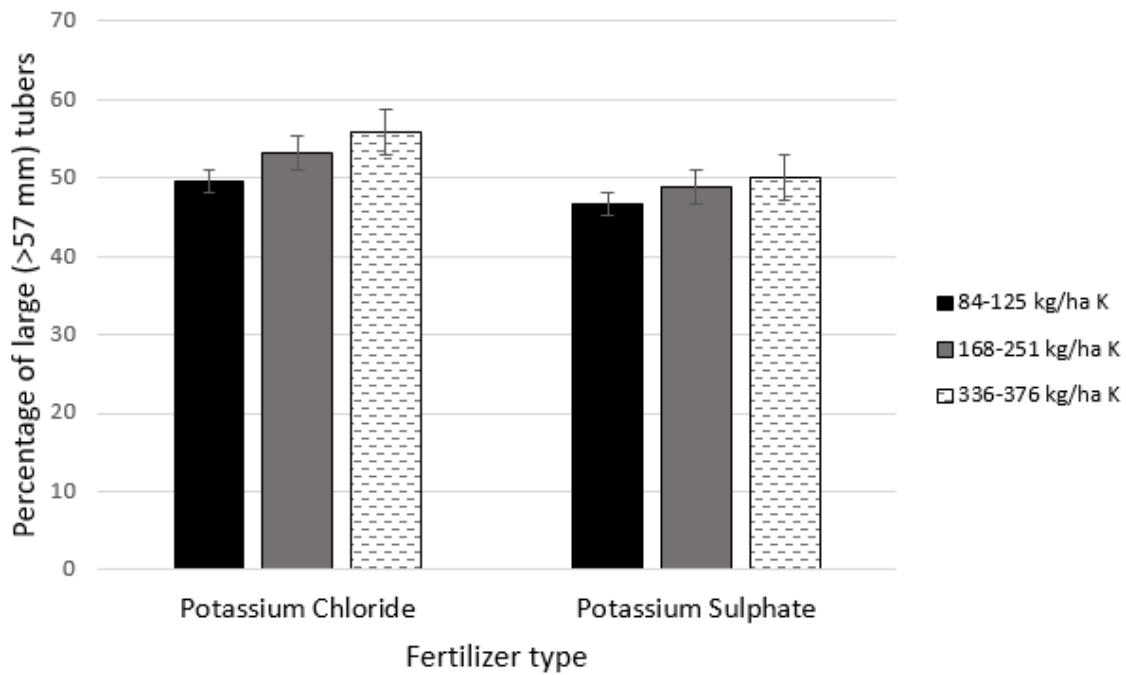


Figure 9: Effect of Potassium (K) fertilizer type and rate on the percentage of large potato tubers in the final yield. Adapted from Dickins et al. (1962).

In an attempt to explain the mechanisms behind the contrasting effects of KCl and K₂SO₄ on TSD, Beringer et al. (1990) carried out plant tissue analysis of plants treated with KCl and K₂SO₄, focusing on the effect of each fertilizer on osmotic potential in leaf cells as a proxy to cell expansion potential. Plants treated with K₂SO₄ were found to have significantly higher osmotic potential and less water content than KCl treated plants (P<0.05). Consequently the K₂SO₄ treated plants had higher dry matter content owing to a larger pool of K from the dissolution of K₂SO₄, which is in agreement with findings from Panique et al. (1997) that potatoes from KCl treated plots had significantly lower specific gravity than K₂SO₄ when the treatments were compared at equivalent rates. Additionally, cell sap from KCl treated plants had less K content than those from K₂SO₄ plants, which Beringer et al. (1990) suggests may be a driver of phloem loading and transportation of photosynthetic products to the tubers, explaining the higher dry matter content in the K₂SO₄ treatment.

As noted from the Henderson (1965) experiment, the larger pool of K after the dissolution of K₂SO₄ and the subsequent high dry matter content does not always result in the large tuber sizes observed by Simpson et al. (1973) study, which may point to a secondary effect caused by the anion SO₄²⁻. Beringer et al. (1990) reported that cell sap from K₂SO₄ treated

plants had significantly larger concentrations of organic anions than the KCl treatment. Panique et al. (1997) reported that K_2SO_4 treated plots produced more large-size tubers (> 170 g) than KCl, up to 280 K kg/ha applied. However, beyond the optimum rate, tuber yield decreased for K_2SO_4 but remained stable for KCl. While the composition of the organic anions was not analysed in the Beringer et al. (1990) study, it may be hypothesized that the reconstitution of SO_4 into protein structures in the K_2SO_4 treatment may have been responsible for the large concentrations of organic anions, which may potentially explain the higher dry matter content as suggested by Barczak et al. (2013). Meanwhile, the KCl treatment's lower osmotic potential favours the exertion of turgor pressure which may be responsible for faster cell expansion with higher water content (Laboski & Kelling, 2007). These results therefore point to a potential influence of sulphur on potato TSD, which has not been extensively studied.

2.4.2.3 Effect of Phosphorus on TSD

Potato tubers are known to be the primary sink of absorbed P, containing up to 83% of all P in plant biomass (Houghland, 1960). The number of stolons produced by a potato plant is positively related to the concentration of phosphorus in its growth media, which has a direct impact on the tuberization potential of the plant and subsequently yield and TSD (Houghland, 1960; O'Brien et al., 1998). Potato yields respond positively to P fertilizer application even in soils known to have high residual levels of P. This is due to the high concentration of readily available forms of P in fertilizers compared to soil residual P, which is often found in highly stabilized precipitates of aluminium or iron in the acidic soils where most farmers grow potatoes strategically to control scab (Hawkins, 1954; Houghland, 1960). Freeman et al. (1998) applied a range of P rates to Russet Burbank (0 to 475 P kg/ha) and Kennebec (0 and 120 P kg/ha) potatoes to evaluate the yield response curves in relation to P fertilization. They reported that Russet Burbank showed significant ($P < 0.05$) increases in processing-quality yield (tubers weighing > 75 g) in response to applied P at 11 out of 12 experimental sites while similar responses were noticed at 6 of the 9 sites for Kennebec. Additionally, a varietal effect was noted with yield responses curves reaching an asymptote at 27 mg/kg for Kennebec while no asymptote was reached for Russet Burbank. Freeman et al. (1998) also noted that P application skewed TSD in favour of large tubers when the TSD was measured as the percentage of large tubers (> 280 g) per plant. Recently, the influence

of soil inherent resin-extractable P on TSD was observed by Fernandes and Soratto (2016), who found that soils with a P analysis of 36 mg/dm³ produced a significantly higher percentage of marketable tubers (>45 mm diameter) than those with inherent low P (14 mg/dm³) as illustrated in Figure 10. In contrast, Rosen and Bierman (2008) found that incremental rates of P fertilizer between 0 and 74 kg/ha did not affect the percentage of *marketable* (>85 g) Russet Burbank yield in loamy sand soil with medium to high soil test phosphorus concentrations (25 to 33 mg/kg Bray P1). This was attributed to an increase in the number of small tubers happening concurrently with a reduction in the percentage of large tubers (>285 g) as P rate increased (Figure 11). Quoting Westermann & Kleinkopf (1985), Rosen and Bierman (2008) attribute this response to a shift in dry matter partitioning from tubers to vegetative growth as leaf P increased. This is strengthened by the further observation that increasing P rates resulted in an increase in the number of stems per plant though the response was not consistent across sites due to many uncontrolled confounding variables, of which the authors single out Ca content as a dominant player due to its ability to fix phosphorus in the soil

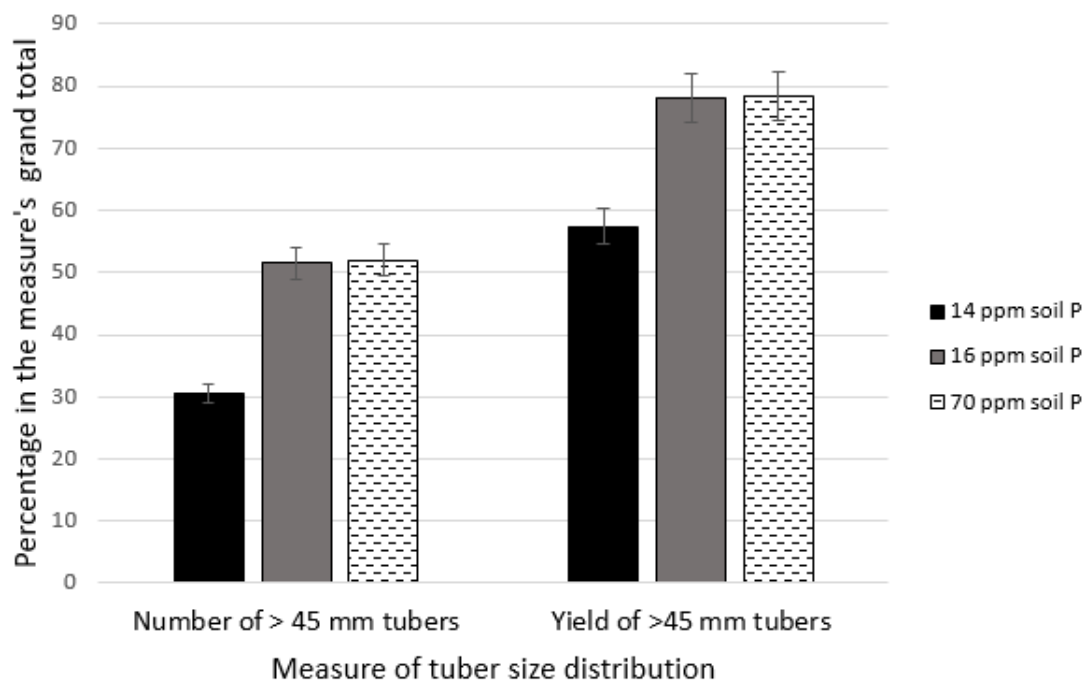


Figure 10: Effect of inherent soil phosphorus (P) concentration on potato tuber size distribution. Adapted from Fernandes et al. (2016).

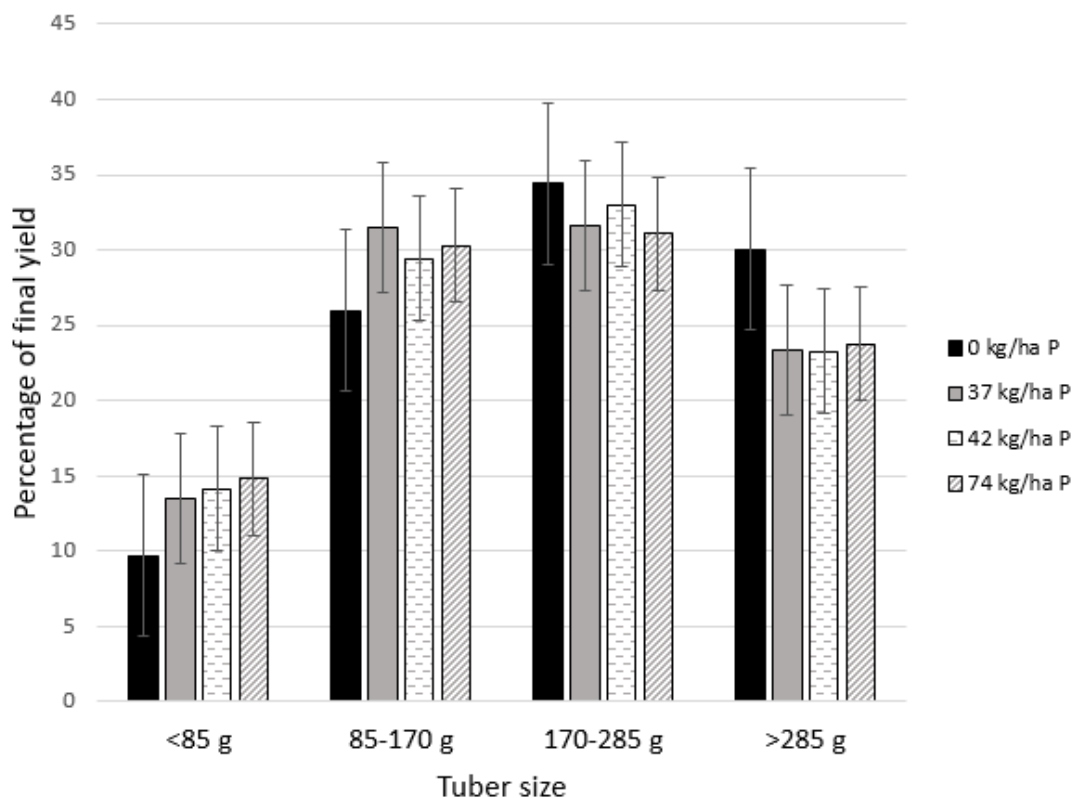


Figure 11: Effect of Phosphorus (P) rates (0-74 kg/ha) on the percentage of various tuber weight classes in the final yield. Adapted from Rosen and Bierman (2008).

. Arora (1987) also found that increasing P rate also increased the proportion of small tubers per square metre by the 90th day after planting at the expense of medium and large tubers, which is further corroborated by Birch et al. (1967) and Prummel and Von Barnau-Sijthoff (1984). The response of TSD to P levels can be affected by interactions with other elements in the soil. P is known to exhibit antagonistic interrelationships with zinc (Zn) and magnesium (Mg) under alkaline conditions and Fe and Al under strongly acidic conditions (Rietra et al., 2017). These four elements precipitate P in soil solution and render it unavailable for plant uptake, hence confound the effect of P fertilization on agronomic parameters. Boawn and Leggett (1964) first reported the antagonistic effect of excess P fertilization on Zn availability which induced Zn deficiency, with subsequent studies by Soltanpour (1969), Jackson and Carter (1976) supporting the results. The antagonistic relationship between Zn and P has since become a well-studied subject in literature. Barben et al. (2010) tested the effect of incremental concentrations of available Zn in growth solution on the P uptake of Russet Burbank potato plants. Their findings show that increase

in concentrations of Zn led to an accumulation of P in potato shoots and a decline of P in potato roots. Since potatoes tend to accumulate most of their P in the tubers rather than the shoots (Houghland, 1960), future research should incorporate the antagonistic effects of Zn on P uptake and sink partitioning and how this affects the tuber size and bulking rates. These results highlight the limited availability of often conflicting published research on the complex interactions between P and other nutrients in relation to TSD. The effect of P on TSD and any usefulness in its targeted soil amendment in production management is therefore still an area that requires further studies to eventually generate consensus.

2.4.2.4 Secondary Macronutrients

Ca is a divalent cation which is predominantly concentrated in plant apoplasts while its water soluble form is predominantly stored in the vacuoles where it plays a role in maintenance of plant vigour and stiffness and delays maturity (Hirschi, 2004). Calcium is also known to ameliorate soil salinity by replacing Na from exchange surfaces to make it available for leaching thereby lowering the soil CEC (Hadi & Karimi, 2012). Additionally, calcium precipitates phosphorus into poorly soluble forms which become unavailable for plant uptake in calcareous soils (Naeem et al., 2013) and alkaline soils (Tunesi et al., 1999) which may therefore be expected to influence TSD.

Ozgen and Palta (2005) found a significant negative effect of Ca fertilization on tuber number by treating Russet Burbank potatoes with Ca in a calcium ammonium nitrate (CAN) form and a calcium chloride form (CaCl) in comparison with non-treated controls. Both the CaCl and CAN had significantly ($P < 0.05$) fewer tubers than the non-treated controls but there was no significant difference between them, proving direct causation of the tuberization inhibitory effect by Ca rather than the activity of the counter-ions in the fertilizers (e.g. Cl). Additionally, Ozgen and Palta (2005) reported no significant difference in total tuber yield between Ca treatments and the controls. This suggests that Ca fertilization can be used to improve TSD toward larger grades since the total tuber biomass is partitioned among fewer tubers, which is in agreement with Ozgen et al. (2003). Indeed, Ozgen and Palta (2005) report a significant positive advantage in mean tuber weight and the proportion of tubers > 56 g in Ca-treated plots over the controls, in agreement with Simmons and Kelling (1987) who found up to 16% increase in the marketable tuber grade (> 51 mm) with a 336 kg/ha calcium addition at the expense of small tubers. However, a similar study

using CAN, CaCl and Gypsum by Kleinhenz et al. (1999) reported that Ca application did not alter tuber grade in comparison with non-treated controls although the concentration of Ca in tubers was higher in the Ca-treated plots. Most studies on Ca fertilization focus on understanding the Ca uptake pathway from the soil and the mechanisms controlling its accumulation in tubers or lack thereof. It is mainly accepted that Ca is co-assimilated into the plant through the roots following the transpiration stream (Busse & Palta, 2006; Kratzke & Palta, 1985; Wiersum, 1966), though there is also evidence of direct Ca uptake by tubers in experiments with radioactively labelled Ca (Habib & Donnelly, 2002). Busse and Palta (2006) and Habib and Donnelly (2002) both further determined that radioactively labelled Ca accumulates in above-ground biomass in a Ca gradient that is sustained regardless of the entry pathway of the Ca. A proposition by Ozgen and Palta (2005), supported by Gilroy and Jones (1993) and Bush et al. (1993), is that Ca uptake is stimulated by GA3 which controls the production of α -amylase enzyme which contains at least one Ca molecule to maintain its activity. With GA being associated with delayed tuberization, this may explain the negative effect of Ca on tuber numbers as observed by Ozgen and Palta (2005). In conclusion, Ca is expected to affect TSD either directly by its effect on GA activity or indirectly through its influence on P availability on the exchange surface in calcareous and alkaline soil. However, more studies are required to add to the evidence from Ozgen and Palta (2005).

Birch et al. (1967) analysed the effect of magnesium on potato tuber size and observed no general response in the yield of each size grade and the *ware-sized to seed-sized* ratio, which was consistent with findings by Holmes (1962) and Birch et al. (1967). Since K was a second treatment in the experiment (discussed earlier), the authors report that an increase in Mg concentration generally depressed the effect of increasing K concentration on TSD, particularly the yield of ware-grade potatoes. K fertilization over 70 kg/ha resulted in fewer tubers, which the authors attribute to stolon damage caused by the excessive K fertilization. The stolon damage was speculated to depress the number of tuber-bearing stolons thereby encouraging the oversized growth of tubers on the remaining stolons, but more Mg was associated with a reduction in this effect. There is very little evidence from research on the advancement of this hypothesis and the effect size of Mg on TSD is comparatively much smaller than can be expected from the primary macronutrients. This is reflected in the limited availability of studies with Mg as a treatment since the Birch et al. (1967) study.

As discussed earlier, the role of sulphur in the reduced efficacy of K_2SO_4 compared to KCl in maximizing tuber sizes is a rarely studied and often discounted (Simmons & Kelling, 1987) subject of speculation. However, Caldiz et al. (2018) tested effect of three levels of S (0, 10 and 20 kg/ha) on TSD and found that 61% of the variation in the proportion of small tubers (<50 mm) was explained by the variation in S content of the soil ($P < 0.05$). Increase in sulphur concentration in the soil had a positive correlation with the percentage of small tubers in the final yield. With limited application of S in potato fields, its in-field variation may ultimately be correlated to in-field variations in TSD and the evidence from Caldiz et al. (2018) supports the hypothesis of an increase in small-sized tubers observed in K_2SO_4 applications by Henderson (1965).

2.4.3 The Influence of Soil Physical Properties on TSD.

Soil physical properties like structure, texture and porosity can be reasonably expected to affect potato tuber development and size distribution, however, there is a limited supply of peer-reviewed literature on experiments that examine this relationship. Soil compaction is usually used as a one-size-fits-all proxy for describing the soil physical variations in commercial fields as impacted by heavy machinery traffic.

Oijen et al. (1995) examined the effect of increasing soil penetration resistance on the root growth of potatoes and reported a high rate of root senescence with increased compaction due to limited aeration, without a significant effect on root length. Additionally a net reduction in nutrient (N, P and K) uptake was observed due to limited soil water movement as a consequence of reduced aeration. Observations by Ross (1986) also suggest that potatoes compensate for hard sub-surface pans by increasing the horizontal spread of their root system. Copas et al. (2009) tested the effect of heavy traffic compaction and subsoil tillage on TSD in Russet Burbank potatoes in a 3 year experiment. There was no effect of both compaction and subsoil tillage on the proportion of *U.S. Number 1* potato yield observed over the three year period, mainly attributed to inconsistencies in the proportions of discarded and lower-grade tubers. An overall reduction in mid-sized tubers (113-170 g) was noticed across all three years but the reduction was not significant ($P = 0.074$).

A similar study by Pierce & Burpee (1995), investigated the effect of compaction on TSD by comparing zone tillage and in-row subsoiling against conventional tillage. In line with

findings by Mundy et al. (1999), no significant advantage in TSD was observed in the altered tillage treatments over conventional tillage, however, a total yield advantage was recorded with zone tillage when in-row spacing was reduced from 36 cm to 25 cm. Multi-year experiments by (Sojka, Westermann, Brown, et al., 1993; Sojka, Westermann, Kincaid, et al., 1993) however report an overall 7% increase in Grade-A tuber yield with zone subsoiling treatments, showing the possibility of optimizing tuber size with compaction control and soil texture improvements.

Redulla et al. (2002) found inconsistent weak relationships between soil texture and tuber yield as well as tuber number. Overall, positive correlations between Clay content and tuber yield and number were observed while negative correlations were observed for Sand content. The authors concede that the models explained relatively low proportions (30%-41%) of the variation in their data. As noted by Redulla et al. (2002), studies on the effect of soil texture on potato yield TSD are rare and the previously discussed limited influence on soil structure on potato TSD makes it an unlikely hypothesis to pursue. In conclusion, the evidence in the literature shows that soil physical properties do not have as much impact on TSD as the soil mineralogical properties and plant phenotypic characteristics, however, the quantification of the extent to which compaction alters would help to reduce Gaussian noise in the spatial datasets and improve any TSD statistical models developed for TSD.

2.4.4 Apparent Electrical Conductivity (ECa)

ECa refers to the bulk electrical conductivity of the solid and liquid phases of the soil and is popular in precision farming as a quick method of non-destructive assessment of soil variability (A. N. Cambouris et al., 2006; Corwin & Lesch, 2003; Perron et al., 2018). Additionally, ECa is preferred over the determination of EC from soil solution extracts because of the large variability in soil solution concentrations over short distances within the field, which require intensive sampling and processing of undiluted soil solutions through labourious and costly pressurized extraction methods (Corwin & Lesch, 2003). ECa can be determined as the inverse of electrical current resistivity between a source electrode and receiver electrode in the field, which has been the preferred method of electrical resistivity measurement for determining soil salinity and ECa since the early 1990s (Corwin & Lesch, 2003). An array of four electrodes (two current sources and two receivers) are placed into the soil surface to measure differential current flow as influenced by the

subtending soil's constituents, producing accurate measurements of resistivity and ECa in homogeneous soils. An alternative method that assures accuracy in non-homogeneous soils is the non-contact electromagnetic (EM) induction method where the loss in eddy currents between a transmitter and receiver are detected and converted to ECa readings (Corwin & Lesch, 2005). The most common EM meter is the EM-38 from *Geonics*TM which can detect magnetic signals up to a depth of 1.5 m (Cambouris et al., 2006; Corwin & Lesch, 2003; Perron et al., 2018).

Since ECa instruments measure the bulk electrical conductivity of all the phases of the soil, there are no deterministic models in use that infer the prevalence of a specific soil property, though highly accurate statistical models have been developed for measuring volumetric water content and salinity (Bouksila et al., 2008). In both the resistivity and EM methods, ECa values are additively influenced by the dissolved solute concentration of the soil solution as well as the water content, as a result, different factors control ECa at every measurement site, making it a necessity to calibrate ECa data with soil property data before making inferences (Perron *et al.*, 2018). A typical ECa survey in precision agriculture therefore involves an initial intensive ECa data collection followed by stratified soil sample collection across the field based on the ECa map and the determination of soil factors that influence the ECa measurements through ordinary or partial least square regression or principal component analysis. Corwin and Lesch (2003) conducted ECa experiments to correlate the ECa values measured using the *Geonics* EM-38 sensor with soil physicochemical characteristics at 6 soil sampling locations. The results were site dependent, whereby volumetric water content had the highest correlation with ECa at one site while sodium adsorption ratio (0.89) and the concentration of boron (0.91) were dominant at another site.

Valente et al. (2012) studied the effect of ECa on the soil properties of Typic Hapludox soils in a 20 ha field in Brazil using the resistivity method at electrode spacing of 20 cm and 40 cm. This was followed by an intensive soil sampling of 141 points in an irregular mesh from which soil texture and chemical properties were determined. The results showed a relatively low range and mean of ECa values at both electrode spacings, with an average of 1.8 mS/m and a range of 0.4 to 5.24 mS/m. While the ECa values at the two electrode spacings were strongly correlated ($r = 0.90$), there was weak but significant correlation between ECa and

all the soil parameters measured including pH, P, K, Ca, Mg, Al, CEC and organic matter (*Table 2*). The highest correlation was found between ECa and available phosphorus with a coefficient of 0.43 which is close to the values reported by several other authors (A. N. Cambouris et al., 2006; De Caires et al., 2015). Valente et al. (2012) evaluated the soil property-ECa relationships using only Pearson's correlations, however, observed insensitivity of ECa to variations in soil properties showed why deterministic models for soil properties cannot be developed with high confidence from ECa data.

Perron *et al.* (2018), in an experiment involving field-scale potato production, evaluated the efficiency of georeferenced ECa data collected at 30 cm and 1 m depths for the purpose of delineating management zones in two fields using unsupervised k-means clustering. The ECa data was analysed for correlation to spatially referenced soil physiochemical properties including texture, N, P, K, Mg Ca, Al and potato tuber yield. There was high contrast between the correlation of soil properties to ECa at the two study sites, revealing again the highly contextual nature of ECa data interpretation; for example, there was strong correlation between ECa and the percentages of clay (0.81), silt (0.61) sand (-0.71) and gravel (0.61) in *field 1*, while none of the particle sizes had a strong correlation with ECa in *field 2*. Clay content seems to correlate highly to ECa data due to its high electric charge capacity as noted in several studies (Carroll & Oliver, 2005; Medeiros et al., 2018; Rodríguez-Pérez et al., 2011). The highest correlation coefficient in *field 2* of the Perron *et al.* (2018) study was also between ECa and clay content at a non-significant -0.19 coefficient. Meanwhile, there was no relationship between particle size distribution (clay and sand) and ECa in studies by Singh et al. (2016) and Valente *et al.* (2012) as illustrated in *Table 2*. These findings point to the contextual nature of ECa data and the need to develop contextual models to understand the underlying determinants at each location.

Table 2: Correlation coefficients between ECa and a selection of edaphic factors from 3 different studies.

Soil Property	R _{ECa} Valente <i>et al.</i> (2012)	R _{ECa} Singh <i>et al.</i> (2016)	R _{ECa} Perron <i>et al.</i> (2018)	R _{ECa} Perron <i>et al.</i> (2018)
Available P	0.465	0.228	-0.48	-0.31
Mn	0.457	NS	N/A	N/A
CEC	0.393	0.448	N/A	N/A
Ca	0.386	0.292	0.48	0.7
pH	0.286	NS	0.36	0.29
Mg	0.23	0.616	0.53	NS
OM	-0.178	0.121	N/A	N/A
Al	NS	-0.121	-0.66	-0.73
Cu	NS	0.371	N/A	N/A
Clay	NS	NS	0.81	NS
Coarse Sand	NS	NS	-0.71	NS

Cambouris *et al.* (2006) used the Geonics EM-38 sensor to create an ECa map of a 13 ha commercial potato field and to delineate two management zones (MZs) using K-means clustering. The delineated MZs were found to show relative homogeneity in soil water regime and physicochemical properties, additionally, there was significant but weak positive correlation between potato tuber yield and ECa data with r values ranging between 0.25 and 0.47 depending on the month of ECa data collection. This level of correlation was also observed by Whelan and Mulcahy (2017) who report a significant but weak correlation ($r = 0.22$) between georeferenced ECa values and potato yield.

Perron *et al.* (2018) also utilized K-means clustering to define management zones based on ECa and then compared differences in potato yields between the clusters using ANOVA to test the efficacy of ECa in maximizing the differences between zones. The delineation of MZs was effective in elucidating the spatial variability in tuber yield *field 1* while no effect was observed in *field 2* due to low within-field ECa variability, however, it can be noted that *Field 2* had 36% more Ca with a highly significant ($P < 0.001$) correlation to ECa (0.72). Ca was

the dominant contributor to variability of ECa in *field 2* and the geospatial analysis reported a lower nugget ratio (15%) than field 1 (25%) which shows a higher spatial dependence. Ca activity is known to precipitate P at high pH (Naeem et al., 2013), as well as competing with equal and lower valence ions at clay surface complexes, thereby affecting their availability (Singh & Dahiya, 1976). It can be expected that weighting ECa values with Ca data may achieve a better correlation with soil available nutrients, hence improving delineation of management zones. The significant influence of soil mineral components on ECa provides an opportunity for using ECa as a unified proxy for understanding how soil variability affects TSD, however, no such studies have been identified in literature.

To summarize the effect of edaphic factors on TSD, literature review shows that nitrogen, potassium, sulphur and calcium have probable effects that may be masked by interactions and confounding factors from other soil nutrients and the plant itself (e.g. plant density). As discussed above, P has been previously shown to affect TSD, however, there are also studies that have reported contrary results and there are significant antagonistic relationships between P and other minerals which need to be modelled in order to elucidate the P effect adequately. In the above review, one notices that TSD has been defined differently by different authors, with most describing it as a ratio of a desired category of yield to the total yield. This comes from the lack of global standardization of what TSD is. When probability distribution functions like the Weibull function are fitted onto tuber size data, a research question therefore exists whether the edaphic factors N, P, K, S, and Ca have any predictable effect on the distributions which can be controlled by farmers. Finally, the data for all these nutrients are usually collected at low sampling intensity due to cost limitations, therefore, to make use of the data in a precision agriculture context, near-continuous spatial data surface of these nutrients need to be generated by geospatial modelling or regression modelling with ECa data.

2.5 Remote Sensing in Precision Agriculture

Plant leaves are known to exhibit unique, species-dependent, responses to incident radiation, generally showing high absorption in the ultraviolet and blue spectra, high reflectance in the green spectrum, high absorption in the red spectrum and high reflectance in the near-infrared portion (Gates et al., 1965). Chlorophylls and carotenoids account for 99% of the reflectance attributed to leaf pigmentation (Tucker & Garratt, 1977). Variability

in the chlorophyll content, water content and cell-to-air space ratio in the leaves directly influences spectral reflectance of plants in the visible (400-700 nm) spectrum (Cochrane, 2000). Advances in digital image analysis technology have enabled the exploitation of this spectral sensitivity in the development of techniques for proximal and remote sensing of plant health from canopies.

Physiological differences between plants cause different species to exhibit distinct spectral signatures which can be used to remotely detect or distinguish specific plants in the field. (Smith & Blackshaw, 2003) found evidence that plant species exhibit distinct spectral reflectance properties beyond the red-edge zone (>700 nm), enabling a species detection accuracy of up to 90%. Distinct spectral signatures in different grass species have also been widely reported and is partially responsible for the proliferation of computer vision based precision weed management applications (Singh et al., 2020). Such results strengthen the case for using spectral reflectance properties to distinguish plants at the cultivar level.

The variation in reflectance of electromagnetic radiation by plants based on species and physiological condition has enabled the development of remote sensing applications for crop monitoring and precision agriculture. Soon after the launch of the Landsat Satellite in 1972, Bauer (1973) used visible and NIR reflectance properties of crop canopies at 80 m resolution to classify crop species coverage in mid-western US with 83% accuracy. Since that time, the spatial resolution of satellites has improved from 80 m per pixel to sub-metre resolution, complemented by wider spectral resolution, which has enabled the development of an array of spectral indices for soil and canopy classification for use in precision agriculture applications (Mulla, 2013).

Seelan et al. (2003) recorded the progress achieved in the use of remote sensing techniques in precision agriculture since the launch of the Landsat satellite in 1972. They identified the biggest limitation for the adoption of remote sensing in precision agriculture to be the lack of knowledge on the amount of remotely sensed data available and how it can be used for management decision support at the farm level. However, they also point to the need for improved spatial and temporal resolution to accompany the improvements in spectral resolution as well as improved integration with meteorological and agronomic data. This section therefore reviews current techniques in acquisition of spectral data, popular vegetation indices reported in literature as well as their applications in potato yield

prediction. The goal of the review was to identify current research questions within the field of remote sensing for determination of potato plant density, stem density and yield prediction, which are pertinent to the modelling of TSD.

2.5.1 Data Acquisition and Spectral Analysis Techniques

Satellite image data is available in the public domain at a global scale with frequent temporal coverage through the repositories of Landsat-8 (up to 30 m resolution, 16 day revisit time) since 1972 (Bauer & Cipra, 1973) and the Sentinel (up to 10 m resolution, 5 days revisit time) satellites since 2015 (Szantoi & Strobl, 2019). Due to the coarse spatial resolution of satellite imagery, pixels of crop canopy data are often composites of reflected light from soil and the canopy which confounds interpretation of reflectance data, necessitating the use of spectral un-mixing algorithms and soil adjusted vegetation indices to improve data quality (Mulla, 2013). Additionally, the data quality of spectral data is often affected by cloud cover and may need correction to account for the dispersing effects of the atmosphere on reflected radiation as well as interpolative smoothing to generate data at non-sampled spectral positions if the spectral resolution of the deployed sensor does not cover exact desired wavelengths (Moran et al., 1997). The proliferation of consumer-grade unmanned aerial vehicles (UAVs) solves the problems of spatial resolution, cloud cover and atmospheric dispersion as well as providing a degree of autonomy for spatial analysts in acquisition of aerial images when required (G. Yang et al., 2017). However this comes at the expense of spectral resolution due to the limited spectral range of consumer-grade sensors mounted on UAVs (Sankaran et al., 2017; Yang et al., 2017).

A typical UAV unit for field-based crop phenotyping and precision agriculture consists of an unmanned aircraft equipped with electromagnetic radiation sensors and GPS technology which enables georeferenced acquisition of aerial imagery at user-defined spatial resolution (G. Yang et al., 2017). UAVs hold an advantage over manned aircraft and satellite imagery due to their lightweight nature, however their low payload currently limits the type of sensors that can be deployed (Chapman et al., 2014). Consequently, visible light and 4-band multispectral sensors are most commonly used for field based phenotyping and precision agriculture Yang *et al.* (2017). High spatial resolutions achieved by low flight altitudes enable a high degree of separation of features in UAV images (Sankaran *et al.*, 2015) allowing accurate ground-level feature classification which is not possible with low-resolution

satellite images. Digital orthorectification is mostly achieved using commercial image analysis software like *Pix4dtm* and *Ag-Photoscantm* which deploy feature matching and structure-from-motion algorithms to stitch images in space and correct for some pixel distortion (Brenner et al., 2018; Yang et al., 2017), enabling the creation of high-resolution complete surfaces of the UAVs flight path hence covering the whole field-of-interest (Brenner et al., 2018; Holman et al., 2016; Yang et al., 2017).

Apart from spectral index based image analysis, UAVs have been used in phenotyping of structural canopy metrics like plant height and leaf area index (LAI) (Holman et al., 2016; Xiong et al., 2017). These metrics are derived from the calculation of normalized digital surface models, defined as the difference between the digital elevation model of the canopy and the elevation model of the underlying ground (Holman *et al.*, 2016). The elevation of the underlying ground is either estimated from extrapolated models of bare patches of soil within the canopy orthoimage or from a separate orthomosaic of imagery acquired before crop emergence (Holman *et al.*, 2016).

While above-ground canopy data are relatively easy to collect with UAVs and process with GIS software like arcGIS, correlation between above-ground variation and potato tuber yield and size distribution within a field would need to be established first before such UAV-based phenotyping can be useful. For example, temporal plant height evaluation can be important in assessment of growth rates and biomass accumulation, which can be potentially linked to branching and hence secondary stem development (Domagalska & Leyser, 2011), which are important in the development and final TSD of a crop (Harris, 1992). Various spectral analysis techniques have been developed to extract useful information from radiometric canopy data in the form of vegetation indices with wide-ranging applicability in the description of spatial variability of vegetative health for decision support in precision farming. A review of these vegetation indices is therefore warranted to identify high potential indices for use in prediction of potato yield and size distribution.

2.5.2 Vegetation Indices and their Applications in Potato Production

One of the main areas of interest for satellite imagery after the launch of the Landsat satellite in 1972 was in the field of vegetation monitoring for agricultural management decision support, particularly in fertilizer management and cattle ranch management. With

this in mind, (Pearson & Miller, 1972) developed the first vegetation indices to enhance the contrast between vegetation and soil in satellite imagery using the Ratio Vegetation Index (*Equation 1*) and the Vegetation Index Number (*Equation 2*) abbreviated as RVI and VIN respectively. Being based on simple ratio, it was however noticed early on that the two indices are less sensitive in non-dense vegetation which may cause misclassification in early season crops and unhealthy canopies.

$$RVI = \frac{R}{NIR} \dots\dots\dots (1)$$

$$VIN = \frac{NIR}{R} \dots\dots\dots (2)$$

(Rouse et al., 1973) developed a band ratio parameter (BRP) using the difference in reflectance between blue and NIR wavelengths detected by the Landsat satellite divided by their sum (*Equation 3*). Regression analysis was used to test this BRP with ground-truth values for canopy greenness, and vegetation moisture content, with results showing R² values of 93% and up to 89% of the variation explained by canopy greenness alone. Their study was based on 8 sampling points of 7 km² each and their data was corrected for sun angle and atmospheric attenuation through square root transformation. The high effectiveness of this BRP has led to wide adoption as the most commonly used vegetation index in agricultural remote sensing, now referred to as the normalized difference vegetation index (NDVI) calculated using *Equation 3*.

$$NDVI = \frac{NIR-R}{NIR+R} \dots\dots\dots (3)$$

NDVI has been applied in a wide range of analyses as a proxy for global precipitation, agricultural crops presence, temporal analysis of land use patterns (Rokni & Musa, 2019), yield prediction in cereals (Sultana et al., 2014) and crop yield in simulation models (Doraiswamy et al., 2004). Most studies typically establish the relationship between NDVI and dependent variables of interest through linear regression models. However, the efficacy of NDVI as a proxy for understanding the major parameters of interest in agriculture (i.e. yield, heat and precipitation) is highly contextual with mixed results from different studies

(Turvey & McLaurin, 2012). Leblois and Quirion (2013) report that NDVI was more correlated to crop biomass but was a poor indicator of yield, a finding that hinders wide scale adoption of NDVI in yield prediction (Turvey & McLaurin, 2012). Consequently, more studies are required to establish context-specific thresholds for correlating NDVI to harvest indices in statistical models.

The NIR band used in NDVI calculation is strongly correlated to leaf area index since NIR light is largely reflected by canopies as a function of mesophyll layer development and green vegetation density (Tucker, 1979). This means the NDVI may be more correlated to canopy metrics that quantify leaf development and plant population, which is more relevant to potato stem number studies. Statistical modelling of such a relationship would enable remote evaluation of potato plant population and its spatial variation.

2.5.3 Application of the NDVI in Potato Studies

Sankaran *et al.* (2017) used NDVI to segment emerging potato plant clusters from images taken at 15 metres above ground using a UAV at 32 days after planting. Thresholding was used to segment 8-bit NDVI images into binary images of plant clusters and non-plant clusters, the plant clusters were then counted to give a computer-generated plant count which had r values of up to 0.82 when correlated to manual plant counts. The ability to assess plant counts using aerial imagery is important as it can be used to check the efficiency of planting operations and refine yield expectations, however, estimations of crop emergence are less accurate when potato canopies consolidate and gaps are covered by sideways growth of the canopy (Sankaran *et al.*, 2017). Apart from object-based plant counts, Sankaran *et al.* (2017) used the sum of NDVI values in all the pixels (sum-NDVI) per plot to generate consolidated NDVI values for an entire plot and correlated them with manual plant counts. The authors report a highly significant correlation ($P < 0.0001$) for the 2 potato varieties under the study with r values of 0.62 and 0.73 using UAV images collected at 32 days after planting. The correlation coefficients diminished with subsequent imagery collected at 37 and 43 days after planting but remained significant up to the 43rd day with albeit r value of 0.38. It must be noted that the computation of sum-NDVI essentially reduced the spatial resolution of each plot in the study to 1 pixel (the plot size was ~6 m by 1 row). These findings therefore suggest the possibility of phenotyping plant emergence rates remotely using consolidated 5 m resolution satellite data. With public domain data

from visible and NIR bands available from the Sentinel 2A and 2B satellite at 10 m resolution (Revel et al., 2019), there is a possibility of phenotyping plant counts using satellite imagery. The temporal deterioration of the correlation between sum-NDVI and plant counts would be a cause of concern, however the maintained significance of the correlation over a 10 day period gives an opportunity for optimizing image acquisition time for maximum NDVI expression and cloud free satellite days.

With a goal to achieve a level of potato yield prediction, Bala and Islam (2009) extracted temporal mean NDVI values from low resolution (500 m) TERRA MODIS imagery and regressed them with potato yields from area production estimates of 0.5 ha farms, finding a highly significant relationship with an R^2 value of 0.84 and an average error of 15% when the study was repeated in the subsequent year. While this is a promising result, its repeatability can be subject to debate due to the large discrepancy between the sizes of the farms (0.5 ha) and the resolution of the TERRA MODIS from which the NDVI was computed (25 ha). It can be hypothesized that the average NDVI of the region (which may be related to precipitation and overall suitability of the location for crop growth) has a significant effect on potato yield. Preceding to Bala and Islam (2009), a similar study was conducted by Groten (1993) on regional millet yield in Burkina Faso where multiple regression models between temporal NDVI increments from the NOAA-AVHRR satellite and yield showed high predictability ($R^2 = 0.87$), results corroborated by Rasmussen (1992). For precision farming applications at the farm level, there is need to develop similar models for potatoes with high spatial resolution.

Al-Gaadi et al. (2016) developed predictive models of potato yield based on NDVI and the Soil Adjusted Vegetation Index (SAVI) from Landsat-8 and resolution Sentinel satellite data in simple linear regressions with farm-level potato yield samples, achieving predictive accuracies (R^2) ranging from 0.39 to 0.65. The positive correlation of NDVI and potato yield has also been established with NDVI computed from handheld active sensors like the GreenSeeker™ with R^2 values of up to 0.90 (Gómez et al., 2019), however the proximal nature of the sensing method is most suitable for small fields and lacks scalability for large-scale farms. Such significant R^2 values reported by multiple authors make a case for the inclusion of NDVI or SAVI as covariates in yield prediction models, however, no studies have linked NDVI to tuber size distribution. Testing this hypothesis would be highly dependent on

the ability to establish adequate spatial autocorrelation in field-observed variation in the phenological parameters, independent of planting-date manipulation.

2.5.4 Other vegetation indices

Apart from the NDVI, other vegetation indices have been developed for classification of spectral variability on vegetated surfaces at a spatial scale. Xue & Su (2017) and Bannari et al. (1995) reviewed a compendium of spectral indices which are most frequently used in remote sensing applications that deploy satellite imagery. It can be noted that most of the indices are developed to improve the classification of surfaces into vegetation, soil, water and man-made structures. Bannari *et al.* (1995) reviewed 24 indices for vegetation classification, with particular emphasis on indices that improve upon the NDVI by using visible and NIR frequencies to enable the accounting of non-vegetation effects in the coarse resolution of satellite imagery, however, except for a few deterministically established indices, most of the indices make use of statistically derived constants for telemetric correction which were developed from multispectral satellite imagery. As a result, NDVI-based applications still dominate the body peer-reviewed literature.

The high spatial resolution made possible by UAVs means an appropriate flight height can be chosen to remove the need for spectral un-mixing for separation of soil effects in vegetation pixels, which is important for accurate description of in-field variability in a precision farming context Sankaran *et al.* (2017). This can be seen in the proliferation of the use of NDVI in UAV studies without soil adjustment. Table 3 shows some of the most commonly reported vegetation indices used in crop health monitoring, with special emphasis to indices that make use of visible and near infrared wavelengths which are most commonly found on UAV sensors (Yang *et al.*, 2017).

Table 3: A summary of the most popular vegetation indices based on R, G, B and NIR in the units of remote-sensing reflectance ratio.

Index Name	Main Uses	Formula	Reference
Normalized Difference Vegetation Index	Detection of green vegetation and variability in canopy health	$\frac{NIR - R}{NIR + R}$	Rouse et al. (1973)
Soil Adjusted Vegetation Index	Detection of green vegetation variability in canopy health	$\frac{NIR - R}{NIR + R + L} * (1 + L)$	Huete (1988)
Difference Vegetation Index	Detection of vegetation	$NIR - R$	Clevers (1986)
Redness Index	Correction of soil colour effects on vegetation indices	$\frac{R - G}{R + G}$	Huete and Escadafal (1991)
Ratio Vegetation Index	Detection of vegetation	$\frac{R}{NIR}$	Pearson and Miller (1972)
Vegetation Index Number	Detection of vegetation	$\frac{NIR}{R}$	Pearson and Miller (1972)
Excess Green Index	Detection of green vegetation	$2G - R - B$	Woebbecke et al. (1995)

2.5.5 Practical Use of Imagery in UAV-based Remote Sensing in Potatoes

The most widely used vegetation index for green plant segmentation from near-sensing images collected with UAVs and digital cameras is the excess green Index. The index was first proposed by Woebbecke *et al.* (1995) utilizing the red, green and blue bands only to achieve a near-binary distinction of green colour from soil background in canopy images.

The index has been widely used and reported in remote sensing work for enumerating plant stands in potatoes (B. Li et al., 2019), wheat (Jin et al., 2017) and rapeseed (Zhao et al., 2018). No literature was identified that develops this technique further to produce plant density variability maps across the field, rather than just a whole-field aggregated plant number. Such a technique would be important in precision farming because such a map can be incorporated in variable rate fertilizer and pesticide application regimes to optimize management. Li *et al.* (2019) noticed and reported the general loss of accuracy in potato plant stand models developed using green vegetation threshold techniques once the potato canopy consolidates. The models are highly sensitive to the stage of crop development. Early imaging runs a risk of under-classification of vegetation due to late emerging plants while late acquisition may lead to under-estimation of plant numbers due to merged canopies where individual plants cannot be separated.

Additionally, the vegetation indices only take a truecolor or multispectral image as input and produce a greyscale image as output. To produce a plant detecting model, traditional image analysis is employed to define rules for assigning individual pixels to predetermined classes of objects within the image scene. Clustering techniques like Otsu segmentation and semantic segmentation have been used to generate binary masks where objects of interest (i.e. potato plants) are in the foreground and all other objects are in the background (B. Li et al., 2019; Machefer et al., 2020). While approaches like the Otsu segmentation algorithm often return satisfactory binary masks, they suffer from a lack of robustness in sub-optimal images with non-Gaussian greyscale histograms (Yang et al., 2012). Subsequent feature extraction and regression or classification modelling therefore becomes dependent on the non-robust data pre-processing methods deployed to clean the binary mask, which reduces the reliability of the models in deployment.

Recent advances in deep learning approaches for object detection from images offers the potential for producing deterministic models for potato plant or stem detection with relative robustness to sub-optimal timing of image acquisition or image quality. Machefer et al. (2020) used a region-based Convolutional Neural Network (RCNN), specifically the Mask R-CNN to produce a model for potato plant detection from UAV imagery with a mean average precision on 0.41. The Mask-RCNN is an image classification CNN wrapped with an object detection and localization framework. For example, Machefer et al (2020) utilized the

ResNet-101 (He et al., 2016), a residual CNN with 101 layers. Detecting the exact location of a desired object in a CNN-classified image is achieved by object detection frameworks like the Faster R-CNN (Ren et al., 2015) or the “You Only Look Once” (YOLO) framework (Redmon et al., 2016). In the case of Mask R-CNN, the Faster R-CNN (FRCNN) is used as the object detection framework to produce bounding boxes around a single or multiple desired objects of interest in an image (e.g. potato stems), with the addition of a semantic segmentation framework to produce accurate masks of the regular or irregular extent of each object (He et al., 2017).

For practical potato stem or plant counting purposes, accurate object enumeration is more important than generating pixel-level masks of the extent of each object, therefore the FRCNN most likely suffices without the need for semantic segmentation. The FRCNN is a unified framework that learns rough regions within an image which are likely to contain objects of interest (termed as region proposals), classifies these regions using the backbone CNN (e.g. the ResNet-101) then localizes classified object with a bounding box (Ren et al., 2015). In Machefer et al. (2020), the FRCNN model was shown to have performed satisfactorily in counting the number of potato plants from a UAV in slightly merged canopies but accuracy was lost once the canopy was completely merged. In a different approach, (Dijkstra et al. (2019) developed an object detection framework based on a convolutional neural network to count potato plants in merged canopies by tracking the centroid pixels of plant clusters, assuming that the leaf architecture of a plant cluster as viewed from a UAV permits the learning of vectors pointing to the centroid origin of the leaves which is the location of the mother tuber. While this framework shows a lot of potential, there is a potential shortcoming in the assumption since potato stems often grow independently of their mother tuber and therefore the derived vectors are more likely to point to the centroid of stems rather than plants.

In summary, there appears to be a gap in research on the efficacy of remote sensing data in potato yield prediction at the farm level. This is mainly because of the general use of low-resolution satellite data which makes sub-pixel prediction complicated. Plot-level studies like Li *et al.* (2019) show a great potential for the use of vegetation indices for plant-population evaluation, however, pertinent research questions remain over the robustness of the model, whether plant population prediction can be done at the stem-level within the

season and whether an algorithm can be developed to reliably express the plant population as a 2D density plot so that spatial autocorrelation can be tested or continuous maps developed. It is therefore pertinent to investigate the potential for the development of custom vegetation indices for potato stem identification using the spectral properties of plants and the potential for leveraging public domain transfer learning models to produce robust stem and plant detecting models. These models can in turn be used to predict tuber number and size distribution variation across 2D density plots of an entire field's orthomosaic.

2.6 Geospatial Modelling for Precision Agriculture

The term precision agriculture is used to describe the optimization of agricultural production inputs based on intensive assessment of soil and crop requirements (Nawar et al., 2017). Apart from maximization of investment returns through adequate fertilization, interest in optimized input management at a spatial scale is driven by deeper understanding of the deleterious role of excessive nutrient application on nutrient cycles and downstream ecosystems (Rodriguez et al., 2011). Precision agriculture therefore involves the modelling of spatial variability across the field using soil, topography, remote sensing data and other spatially supported information (Mulla, 2016; Nawar et al., 2017). Within-field spatial variation has historically been described and managed using soil analysis as a proxy, however, the availability of large volumes of spatial data due to advances in proximal and remote sensors and accurate GPS systems has enabled the use of other sources of variation for more optimized spatial modelling (Mullar, 2015). Geospatial statistical techniques can be used to overlay multiple sources of data on spatial variability and decompose seemingly unrelated layers of variables into 2D variability, which can generate homogeneous clusters referred to as management zones in precision agriculture (Mulla, 2016; Nawar et al., 2017; Perron et al., 2018).

This section reviews the typical cycle of precision agricultural management comprising of the collection and processing of variability data, geospatial overlaying and analysis and the spatial modelling involved to enable delineation of management zones. The goal was to evaluate the general tools that have been used for modelling spatial information to ultimately guide the selection of techniques for interpolating low-intensity point estimates

of soil and above-ground variables to produce continuous surfaces for spatially modelling TSD.

2.6.1 Collection of Geospatial Data

Precision farming starts with the mapping of spatial properties of interest which entails the collection of soil data using traditional soil analysis methods and more rapid proximal or remote sensing approaches (Nawar *et al.*, 2017). Soil samples are typically collected at an intensity of 1 (Mulla, 2015) to 3 (Nawar *et al.*, 2017) samples per hectare for traditional nutrient analysis purposes, however, the sampling approach may be altered due to the level of spatial variability within the field of interest. The choice of a soil sampling method will depend on prior assessment of the nature of soil variability which can be based on historical soil and yield maps, subjective visual assessment of soil colour and topographical gradients or an exploratory sparse initial sampling (Swyngedouw & Crépin, 2008). An initial conceptual model of soil variation can then be developed from which a sampling plan can be drawn. To avoid subjectivity, the availability of temporal satellite images at high resolution can help to establish objective conceptual models based on variables such as soil brightness.

Soil sampling strategies are classified into design-based and model-based methods based on whether prior assumptions about variation are taken into account or not (Brus & DeGrujter, 1993). Design-based methods treat within-field variation as a random process without assumptions on the gradient of variation, thereby confining variation into a completely stochastic realm (Brus & Grujter, 1993). Typically, sampling strategies under this approach will fall under the simple random sampling or stratified simple random sampling (Swngedouw & Crepin, 2008). The designed-based approach induces stochasticity through the randomization process, therefore the efficiency of the sampling design is confined to the procedure used to generate the sampling points, rather than the natural stochasticity at the sampling points themselves (Swyngedouw & Crepin, 2008). Any iteration of a sample drawing process will draw a unique sample with a unique estimate for making inferences to the population (Brus & Grujter, 1993; Swyngedouw & Crepin, 2008). Brus and Grujter. (1993) give an example of the simple random sampling design as a completely probabilistic approach where each sampling location has an equal probability of being drawn based on any randomization procedure deployed.

In the model-based approach, the probability of a sampling outcome at a given sampling location is not fixed by the design process but modelled based on a stochastic but natural process (Brus & Guijter, 1993). A continuous probability density is imposed on assumed variation across the field therefore the population (i.e. the whole field being sampled) is considered as a single realization of the random process, from which a model can be used to select optimum sampling locations (Brus & DeGrujter, 1993; Castro-Franco et al., 2015). The accuracy of a model-based design therefore largely depends on the chosen model. The availability of temporal proximal and remote sensing data like yield maps, soil electrical conductivity and vegetation index data enables the creation of a model whose continuous distribution can be used for determination of sampling locations (Castro-Franco *et al.*, 2015). This is typically achieved by overlaying the digital variation maps of all the chosen predictors and running classification algorithms to partition the field into homogeneous clusters. Castro-Franco *et al.* (2015) recommend the use of Fuzzy C-Means Clustering (FCMS) or a conditioned Latin Hypercube Sampling (cLHS) for sample size determination. FCMS analyses and partitions the data space into homogeneous clusters whose centroids represent ideal sampling locations which maximize the prediction of the combined variation, therefore the sample size is equal to the number of clusters. cLHS imposes a grid hypercube with the rows and columns representing the spatial scale of the field while the third dimension represents the layers of prior variability maps (Minasny & McBratney, 2006). cLHS is a stratified random sampling procedure that uses the concept of the Latin square to fit sampling points in the data in such a way to satisfy the conditions of a Latin hypercube (Castro-Franco et al., 2015). The cLHS and FCMS are the most widely reported model-based approaches for geo-location of soil sampling points in geo-statistical work (Boettinger et al., 2010; Castro-Franco et al., 2015; de Grujter et al., 2010; Minasny & McBratney, 2006; Roudier et al., 2012). Castro-Franco. (2015) ran FCMS, cLHS and simple random sampling on a spatial dataset containing Slope, NDVI and land use as predictors, then re-extracted all predictor-data (Slope, NDVI, Land Use) from a the determined sampling locations to compare the results. It was found that the cLHS iteration was the most accurate at mimicking the original distribution while the other methods slightly over- and under-sampled some areas in the distribution.

Model-based sampling approaches generally use more data to generate sampling locations, however, the choice of a design-based or model-based approach will ultimately depend on whether model variables can be determined which have predictive value for the response that a researcher wishes to detect in their soil analysis. Brus and Gruijter (1993) report improvements of sampling efficiency between 0 and 60% when a model-based approach is adopted over a design-based approach, adjusting for experimental bias which led to fivefold improvements in sampling efficiency using the same data. This shows the importance of the underlying model assumptions and statistical analysis procedure in the usefulness of any model-based approach. The adoption of any model-based approach for predicting TSD in potatoes needs to first focus on the determination of spatial variables that independently affect TSD, it therefore requires independent regressions of a compendium of soil and other environmental variables to TSD and elimination of nuisance variables, after the most pertinent variables are determined, proximal and remote sensing data for estimating these variables can be chosen to create a useful model.

2.6.2 Geospatial Analysis Techniques

2.6.2.1 Spatial Interpolation

Variable rate management of inputs largely depends on the establishment of variability maps from which fertilizer, herbicides and other inputs demands can be calculated and relayed into GPS-controlled applicators (Nawar *et al.*, 2017). spatial interpolation therefore plays a critical role in precision farming. The first step to geospatial analysis is making a determination whether the data expresses a spatial pattern (Scott, 2015). Descriptive statistics can be potentially used as simple evidence of spatial arrangement. For example the weighted mean centre, where the mean central coordinate of a variable is determined using the values at each coordinate as weights (Scott, 2015), can be used to trace epicentres of spatial distribution in the variable. Advanced geostatistical analysis of spatial structure however commonly involves the determination of spatial autocorrelation, a measure of the relationship between the values of a single variable at two spatial locations (Getis, 2015). Haining (2015) describes autocorrelation as positive when closely located points have converging values and negative when the opposite occurs, however, a note is made that continuously distributed data almost exclusively exhibits positive autocorrelation. The

occurrence of autocorrelation is proof that a variable in space is a realization of a spatially dependent model with an infinite number of possible realizations (Haining, 2015). The null hypothesis for testing for spatial autocorrelation is therefore that the variable follows a random process (Scott, 2015). Apart from diffusion or transfer processes, autocorrelation may also result from dependence, where one variable inherits the spatial autocorrelation of another due to their relationship (Haining, 2015), this can be expected in highly correlated variables like ECa and soil nutrients since ECa is partly governed by the cations present in a soil (Corwin & Lesch, 2003). Consequently, singular value decomposition of such highly correlated variables may be useful to avoid redundancies in data when building variability for purposes of management zone delineation in precision agriculture. This also gives a strong case for the use of ECa as a singular description of variability in some cations, as long as the effect of the cations on ECa can be quantified. Spatial autocorrelation is tested using Joint-count test for nominal data (Iyer, 1949) or the Geary's Contiguity ratio (Geary, 1954) and Moran's correlation coefficient (Moran, 1950) tests for interval data of which the Moran test (denoted as I) is most popular (Scott, 2015; Haining, 2015).

In the interval data methods which are most pertinent to agricultural data, the Geary test (Denoted as C) takes a collective summation of the sum of squared differences between each spatially referenced datum and all other data. The squared differences are weighted with a "zero" if the datum are adjacent to each other or as a "one" if they are far from each other (*Equation 4*).

$$C = (N - 1) \sum_i \sum_j \delta_{i,j} (y(i) - y(j))^2 / 2W (\sum_i^n y(i) - \bar{y})^2 \dots \dots \dots (4)$$

Where δ represents the weighting decision based on the distance between i and j , N represents the number of data locations, W represents the sum of all δ and \bar{y} is the mean of all the data for the variable.

The Moran test (*Equation 5*) also takes a collective summation, however instead of the squared difference, the deviation of each datum from the variable mean is taken then a summation of the cross products of each pair of deviations in the data is calculated.

$$I = \frac{N}{W} \sum_i^n \sum_j^n (\delta_{i,j} (y(i) - \bar{y})(y(j) - \bar{y})) / \sum_i^n (y(i) - \bar{y})^2 \dots \dots \dots (5)$$

The Geary and Moran tests describe the level of spatial autocorrelation of the whole field of study, however, to adequately evaluate the increase or decrease in autocorrelation with distance, an iterative process has to be done where any of the two tests are done at an increasing distance each then the results plotted as distance against the resultant statistic. This is done by replacing the weight variable in the Geary or Moran test with the search radius at each iteration (Getis, 2001; Haining, 2015). The resultant graphs from a Moran test are called correlograms and those from a Geary test are known as semivariograms (Haining, 2015). In summary, the global Moran's I statistic is commonly used and compared to an expected value generated from the null hypothesis that the data occurs from a random process. A Z-score is used to determine whether the two indices are significantly difference from zero, from which an inference can be made about the spatial autocorrelation (Scott, 2015). If a significant autocorrelation is discovered, interpolation can be done by fitting a gaussian process model (e.g. Kriging), otherwise inverse distance weighting is used for data without evidence of spatial autocorrelation (Nawar *et al.*, 2017).

2.6.2.2 Inverse Distance Weighting (IDW)

IDW is a deterministic interpolation method which assumes a linearly incremental dissociation between data points with increasing distance between each other (Nawar *et al.*, 2017; Singh & Verma, 2019). IDW is the most commonly used interpolation method when the number of data points is too low to evaluate spatial autocorrelation (Webster Oliver, 2007). To estimate the value for a given point using IDW, a neighbourhood or sphere of influence is chosen then a weighted average of all data points within the neighbourhood is used to determine the missing value (Pramasivam & Venkatramanan, 2019) using *Equation 6*.

$$f(x, y) = \frac{\sum_{i=1}^N w(d_i)z_i}{\sum_{i=1}^N w(d_i)} \dots\dots\dots(6)$$

Where $w(d)$ is the weighting function which can be distance or any other defined function, Z is the data value at point i and d_i is the distance from point i to (x,y) . In large datasets, the natural neighbour inverse distance interpolation can be used, which triangulates the closest points to a missing points for the calculation. However it must be noted that IDW interpolation maps can have spikes around data values (Singh & Verma, 2019), to minimize

this, a tension spline mathematical function can be applied to the IDW to obtain results that approximate natural variation (Wahba, 1991).

2.6.2.3 Kriging and Covariance Structures

Kriging follows a similar estimation procedure to IDW, however, apart from deterministic distance weighting, kriging incorporates a geostatistical model based on a distribution function fitted onto a semivariogram of the data (Mulla, 2016; Singh & Verma, 2019) with the assumption of steady covariance across the geographical space (Miller, 2017; Nawar et al., 2017). The use of a geostatistical model means that prediction error terms (uncertainty) can be calculated (Nawar *et al.*, 2017) which is useful in decision making and gives kriging its edge over IDW. To maintain positive parameters for a fitted semivariogram model during kriging, a limited number of models are widely accepted of which the most common are spherical, exponential, linear and Gaussian models (Mulla, 2016). These models ensure a positive “nugget” (y-intercept), Sill (asymptotic y-maxima) and range (Miller, 2017; Mulla, 2016) from which the strength of the autocorrelation can be evaluated using the partial sill (difference between range and nugget) and the nugget to sill ratio (Miller, 2017) as illustrated in Figure 12.

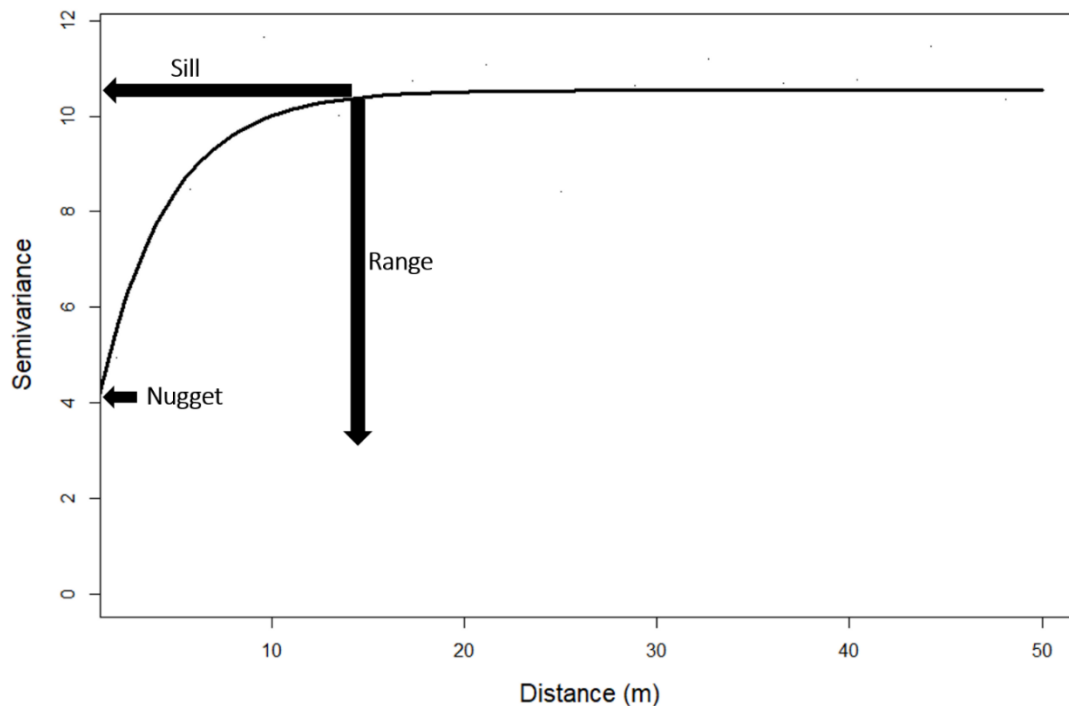


Figure 12: Schematic diagram of a semivariogram of a soil phosphorus test in ppm (Mulla, 2015).

Modelling agricultural phenomena using the standard variogram models has recently come under scrutiny as previous research has shown that agricultural yield processes follow a rough autocorrelation structure that decreases at a slower rate than provided for in the exponential model (McCullagh & Clifford, 2006; Minasny & McBratney, 2005), a consequence of the homogenization of monocropped fields. In this case, the assumptions of Gaussian, exponential, spherical or linear variogram models become inappropriate. The Matérn covariance function (Stein, 1999) has been proposed and used for modelling autocorrelation in agricultural yield components without assuming a theoretical variogram (Cho et al., 2021; McCullagh & Clifford, 2006; Minasny & McBratney, 2005). Cho et al. (2021) found that kriging with an underlying Matérn covariance structure produced the most accurate yield maps in Maize compared to Nearest Neighbour interpolation, Inverse Distance Weighting and traditional kriging methods. Kriging is considered a better linear unbiased estimator over spatial regression since spatial surface model produced by kriging always passes through measured data points because it uses a form of Bayesian inference to make a deterministic prediction while at the same time calculating a statistical uncertainty, unlike regression models where this is not guaranteed (Miller, 2017; Mulla, 2016). There are many kriging techniques, most of which differ in the level of assumption of a stationary mean, covariance and resultant residuals (Paramasivam & Venkatramanan, 2019). Simple kriging is the most direct kriging method which assumes a stationary mean and covariance across the whole field of study, ignoring any potential local deviations in variance and mean values within a search window (Miller, 2017), while more complicated co-kriging techniques involve incorporation of multivariate data for more efficient prediction, which may be useful in precision farming. Ordinary kriging is the most commonly used interpolation method as it re-calculates non-stationary local trends in mean and covariance within a kriging search window to avoid the generalization of global means on local predictions. However, the need for accurate estimation of means at a local level means ordinary kriging needs a high sampling intensity within the search window to achieve good accuracy, which impedes its adoption (Nawar *et al.*, 2017).

Most reported spatial interpolation studies for potatoes were conducted at large-scale regional level and the potato crop was used as a proxy to understand a secondary parameter of interest like the regional spread of potato cyst nematode (Contina et al.,

2018). The importance of within-field soil variability on yield and TSD has already been discussed, however, the prohibitive cost of soil analysis means most farmers still only collect 1-3 samples per hectare, which does not provide the level of resolution needed to map spatial variation in TSD on small farms. Tuber formation processes also operate in a spatio-temporal dimension which increases uncertainty on predictions based on spatial inferences only. This is particularly pertinent to prediction of tuber formation and bulking in potatoes as it is affected by the spatial effects of plant density and soil factors as well as the temporal effects of photoperiod and radiation intensity (Knowles & Knowles, 2006; O'Brien et al., 1998). Practical methods for the interpolation of variables that affect tuber formation in space and time is therefore important for the further development of precision agriculture tools. Where many sources of variation are available for spatial analysis, spatial modelling needs to incorporate dimensionality reduction to select the most relevant variables for describing the particular independent variable. Prior knowledge plays a critical role. For example, prior knowledge of any deterministic effect of stem density on TSD can be incorporated into spatial models (Miller, 2017). This helps in the decomposition of multivariate data into global trends so that the trend effect can be removed and kriging done on the residual to improve the interpolation result.

Statistical procedures can also be used to de-trend spatial data, in a study aimed at producing a regression model for predicting above ground biomass using NDVI in potatoes, Heuvelink & van Egmond (2010) fitted a double logistic function on temporal data (days between planting and temporal NDVI) to define a general trend in NDVI development towards a critical tuber maturation stage. The residuals from this general trend were then used to build an experimental variogram which was able to map crop development for prediction of a critical vine desiccation day when kriged. Heuvelink and Egmond (2010) admit that space-time kriging techniques need further research and maturation, however for the spatial dimension, the basic concepts of de-trending data and predicting the overall effect of production inputs on TSD at harvest still have validity which has not been tested and reported yet in literature.

Geospatial statistics offer the tools necessary for intensive analysis of spatial data to isolate and model variation for predicting TSD, however, the performance of the models will depend on the strength of the relationship between TSD parameters and available data.

Remotely sensed data is widely available at high sampling intensity which may even remove a need for geospatial interpolation (Nawar *et al.*, 2017). It is therefore important to review and identify remote sensing data that has the highest potential for describing in-field variability which has pertinence to tuber yield and size distribution for building predictive geospatial models.

2.7 Literature Review Conclusion

The literature review has shown that the tuber yield and TSD in any sample of potatoes is a realization of a complex model with variables that are related to soil nutrient availability, hormonal activity within the plant, competition due to plant population dynamics and solar radiation through its effects on photoperiod. All these variables have been shown to vary with time, adding a temporal tier to the array of variability that affects TSD. Additionally, there is a lot of covariance within the variables, whereby hormonal activity affects apical dominance, while being controlled by the changes in photoperiod, and plant nutrition. These complex interactions mean experiments on any one variable's effect on TSD are bound to have significant latent spatial and temporal patterns of unexplained variation. A wide range of variables have been identified to affect TSD, however, comparison between papers is difficult as there seems to be no standardized and universally accepted unit for describing it. It is however noted that most studies measure TSD in relation to the maximization of yield in a desired grade, though the size range in the chosen grade is understandably unstandardized. The most important gap that exists in the literature is a standard measure of TSD that can be used to compare results from different studies and can be related mechanistically to the variables that are known to TSD.

Another gap is the general lack of testing of some of the conclusions from controlled experiments at a spatial scale in uncontrolled environment. All of the experiments that attribute TSD-alteration to differences in edaphic factors rely on the establishment of a large range of concentrations, which increase the chances of observing an effect. Whether these large variations are observable in the highly homogenized monocropping environments to a level that can explain TSD is debatable. It was therefore important to generate observations of some edaphic variables in a spatial field survey scenario to evaluate whether they contribute to TSD. The Central Research Question of the research project is whether it is possible to predict and control TSD by adopting variable

management based on in-field variability in soil and crop growth. The following research questions have been generated from the literature review:

1. Defining a unit for TSD: What is the difference in accuracy of TSD models based on the Normal and Weibull distributions at predicting yield at a particular finite size grade?
2. Use of ECa for producing high resolution density plots of soil variation nutrients: Can ECa be used to create spatial models with edaphic factors as covariates to predict tuber yield and size distribution?
3. Vegetation Indices: Can vegetation indices and satellite image time series be combined with other covariates to predict yield and/or biomass accumulation?
4. Plant Density Algorithms: Can the principles of meristematic light interactions established by Gates et al., (1965) be used to develop a vegetation index to enumerate the number of stems and number of plants in a potato field at full canopy?

CHAPTER 3 – Relationships between Soil Variability and Tuber Size Distribution

3.1 Comparison of Potato Tuber Size Distribution Fitting Methods and Evaluation of the Relationship between Soil Properties and Estimated Distribution Parameters

Abstract

Accurate estimation of tuber size distribution (TSD) parameters in discretely categorized potato (*Solanum tuberosum L*) yield samples is desired for estimating modal tuber sizes that are fundamental to yield prediction. In the current work, systematic yield digs were conducted on five commercial fields (N=119) to compare the Weibull, Gamma and Gaussian distribution functions for relative-likelihood-based goodness-of-fit to the observed discrete distributions. Parameters were estimated using maximum likelihood estimation (MLE) for the three distributions but were also derived using the percentiles approach for the Weibull distribution to compare the accuracy of this closed-form approach to MLE. The relationship between TSD and soil nutrient variability was examined using the best-fitting model's parameters. The percentiles approach had lower overall relative likelihood than the MLE approaches across five locations, but had consistently lower Root Mean Square Error in the marketable tuber size range. Negative relationships were observed between the percentile approach's shape parameter and the concentrations of phosphorus and nitrogen, with significant ($P < 0.05$) regression coefficients for P (-0.74 ± 0.33 for distribution of proportional tuber numbers and -1.3 ± 0.62 for tuber weights). Stem density was negatively associated with the scale and mode of the tuber number (regression coefficients -0.98 ± 0.63 and -1.08 ± 0.78 respectively) and tuber weight (regression coefficients -0.99 ± 0.78 and -1.04 ± 0.69 respectively) distributions. Phosphorus negatively related to the scale of the tuber number based distribution while positively associating with the tuber weight distribution. The results suggest that excess P application was associated with the increase in small tubers that did not contribute significant weight to the final yield.

3.1.1 Introduction

Potato (*Solanum tuberosum* L.) production is a high input, high output operation driven by well-developed, technologically advanced markets which depend on the consistent supply of high-quality potato raw materials. Nevertheless, high output does not necessarily translate into high returns for growers due to the selectivity of processing factories for tuber size grades (Machakaire et al., 2016). This occurs especially in the pre-fried potato processing sector which accounts for 62% of the global processed potato market (Keijbets, 2008). Agronomic techniques for optimizing tuber size distribution (TSD) are therefore an important consideration for potato growers and researchers.

Several methods of quantifying potato TSD have been proposed in the literature. Travis (1987) described TSD using the spread of tuber sizes around the modal grade assuming a Gaussian distribution, allowing the determination of a coefficient of variation (CV) as an index for TSD. Ideally, farmers can use this to conduct mid-season TSD assessments, which can then support management decisions on vine desiccation timing. Struik et al. (1990) and others subsequently supported the Travis (1987) method. However, the probability densities plotted by Struik et al. (1991) revealed that the TSD by weight skews to the right and the Gaussian distribution may not necessarily capture the spread of the data.

Several alternatives have been suggested like the Weibull (Bussan et al., 2007; Nemecek et al., 1996) Log-normal (Marshall et al., 1993) and the Gamma (Aliche et al., 2019) functions. Whilst these alternative functions fit TSD more accurately, their parameters are often determined using maximum likelihood estimation, which makes it non-ideal for quick field assessments by non-statisticians. A Gaussian distribution is therefore often assumed due to the simplicity of determining its parameters (i.e. mean and standard deviation) from yield digs. Currently, TSD is mostly evaluated using the percentage of marketable tuber weight in the total tuber yield.

A positive association between soil nitrogen concentration and TSD has been consistently reported by several authors over the past 5 decades, mostly when TSD is measured as the proportion or absolute quantity of yield above a weight or transversal diameter threshold (Arsenault et al., 2001; Gao et al., 2018; Porter & Sisson, 1991; Schippers, 1968b). The overall effect of N on the shape, location and scale of the TSD has

not been consistently demonstrated partly due to the lack of standardized and generally accepted parameters for measurement (Wurr et al., 1993).

Potato growers, and subsequently researchers, target different tuber sizes at harvest depending on localized outlet market demands (Taylor et al., 2018; Wurr et al., 1993), making it difficult to standardize the size classes and objectively compare TSD from different studies. The influence of potassium fertilization on potato yield and TSD is also widely studied (Allison et al., 2001; Birch et al., 1967; Dickins et al., 1962) and soil K replacement based on crop removal is generally accepted as a management strategy in commercial production systems. For phosphorus, Rosen & Bierman (2008) found that incremental rates between 0 and 74 kg/ha did not affect the percentage of marketable (>85 g) Russet Burbank yield in loamy sand soil with medium to high P concentrations (25 to 33 mg/kg Bray P1). This was attributed to an increase in the number of small tubers happening concurrently with a reduction in the percentage of large tubers as P rate increased. Quoting Westermann and Kleinkopf (1985), Rosen and Bierman (2008) attribute this response to a shift in dry matter partitioning from tubers to vegetative growth as leaf P increased. The response of TSD to P can be affected by P interactions with other elements in the soil.

Phosphorus is known to exhibit antagonistic relationships with zinc (Zn) and magnesium (Mg) under alkaline conditions and iron (Fe) and aluminium (Al) under strongly acidic conditions (Rietra et al., 2017). These four elements precipitate P out of the soil solution and render it unavailable for plant uptake, hence confounding the effect of P fertilization on agronomic parameters. The influence of Mg is worth consideration because it is often applied in potato fields as Epsom salt to control Mg-deficiency-related leaf chlorosis. Finally, the role of the Sulphate counter ion in $MgSO_4$ salts and K_2SO_4 , as well as the inherent soil variability in sulphur is rarely studied and is an often discounted subject of speculation (Simmons & Kelling, 1987). However, Caldiz et al. (2018) found that 61% of the variation in the proportion of small tubers (<50 mm) was explained by the variation in soil S content ($P < 0.05$). Increase in S concentration in the soil had a positive correlation with the percentage of small tubers in the final yield. Within-field variation in S may ultimately be correlated to variation in TSD and evidence from Caldiz et al. (2018) supports the hypothesis of an increase in small-sized tubers observed in K_2SO_4 applications by Henderson (1965).

The objective of the current study was to compare Gaussian, Gamma and Weibull distributions for fitting potato TSD and evaluate their predictive performance. For the

Weibull distribution, the current study particularly deployed a direct estimation of the scale and shape parameter from the cumulative distribution function using probabilities of different tuber size grades from sample yield digs, which has not been reported in previous studies. Additionally, the study considered various soil nutrients for their relationships to TSD in a multivariable regression environment, selecting plausible models based on theoretical considerations and conditional information criteria.

3.1.2 Methodology

3.1.2.1 Site Characterisation

The study was conducted at four sites as summarized in Table 4. Deaton 6 and HF7 sites were located in the East of England (Lincolnshire) on reclaimed marsh land with a shallow water table and high organic matter content. There was variation in soil physical and chemical properties across the field due to the presence of Roddons, historical features in drained marshland soils where silty clay soils follow the course of historical streams and waterways. Horse Foxhole and Buttery Hill were located in the West of England (Shropshire) on well-drained slightly stony, sandy loam soil subtended by weathered sandstone with low variation in soil nutrients across the field. Additional tuber sampling for TSD modelling (without soil analysis) was conducted at Crabtree Leasow, also located in the West of England with similar soil and weather conditions to Buttery Hill and Horse Foxhole. Planting and field management was carried out by the respective farmer at each field. Consequently, land preparation was conducted similarly in all fields by ploughing at 30 cm depth followed by bed-forming at 90 cm between rows and destoning. Fertilizer was applied uniformly by broadcasting macro and micronutrients based on soil analysis as summarized in Table 4. Deaton 6 and HF7 were irrigated by drip irrigation while a hose reel irrigator was used at Horse Foxhole and Buttery Hill. All management practices were conducted uniformly across the field throughout the growing period.

Table 4: Summarized information of the study sites

Field Name	Year	Coordinates	Variety	N ¹	Fertilizer	Nutrient Rate (kg/ha)
HF7	2020	53°12'40.71"N 0°24'49.76"W	Maris Piper	30	Nitrogen	107
					Phosphorus	94
					Potassium	290
B.Hill ²	2020	52°46'22.05"N 2°25'40.46"W	Amora	30	Nitrogen	173
					Potassium	94
Deaton 6	2019	53°12'20.97"N 0°21'55.06"W	Maris Piper	12	Nitrogen	100
					Phosphorus	150
					Potassium	307
C.Leasow ³	2020	52°46'15.21"N 2°21'37.57"W	P.Dell ⁴	18	Nitrogen	167
					Potassium	89
H.Fxhole ⁵	2019	52°46'26.94"N 2°25'49.38"W	Amora	29	Nitrogen	125
					Phosphorus	140
					Potassium	238
					Magnesium	40
					Sulphur	75

1 = Number of samples collected. 2 = Buttery Hill. 3 = Crabtree Leasow. 4 = Pentland Dell. 45= Horse Foxhole.

3.1.2.2 Sampling Design

A field survey was designed at each of the five fields using a model-based sampling approach to determine representative soil sampling locations that captured the variability in the field. The number of samples collected at all locations are as provided in Table 4. Soil sampling was done at all sites except Crabtree Leasow, which was hence not included in the soil analysis. The soil samples were collected at Buttery Hill (N=23), HF7 (N=24), Deaton 6 (N=12) and Horse Foxhole (N=23). Soil macronutrient quantities are known to correlate with organic matter content (Y. Yang et al., 2011), which in turn influences soil colour (Costa et al., 2020). The Soil Brightness Index (SBI) as described by Mponela et al. (2020), was chosen as a substitute for spatially modelling the soil colour differences at each field and generating

strata for a stratified random sampling design (equation 7). At each field, the SBI was calculated at least one day per month for three months prior to crop emergence and then the average SBI was calculated. The SBI at each site was calculated using atmospherically corrected (Level-2A) satellite imagery of 10 m resolution acquired by the Sentinel-2 satellite, on manually inspected cloud-free days. Each field was delineated into 3 clusters by k-means clustering (k=3) based on SBI to generate zones of relative homogeneity which formed the sampling strata. A sampling unit of 6 m by 6 m (36m²) was chosen to cover the accuracy specification of the Garmin™ eTrex 20 GPS receiver that was used for soil sampling. A grid of 36m² quadrats was imposed across a rasterized SBI surface then random quadrats were drawn from each stratum. A mapped example of the SBI-model-based sampling is provided in appendix A. The equation for SBI was:

$$SBI = \left(\frac{R^2 + G^2 + B^2}{3} \right)^{0.5} \dots \dots \dots (7)$$

Where R, G and B were the pixel-level remote sensing reflectance values of B04, B03 and B02 bands of the Sentinel-2 satellite reflectance data, respectively.

Power analysis to determine sample size for the survey was calculated to resolve SBI variability with a statistical power of 0.8 as recommended by Cohen (1988). The effect size was estimated based on the expected within-field contrast between the k-means cluster with the lowest SBI value (dark soil) and the one with the highest SBI value (bright soil) in the sample. The effect size was therefore calculated as the difference between the mean SBI of dark soils and the combined mean of the medium and light clusters divided by the standard deviation of the entire dataset. R v4.0.2 (R Core Team, 2019) was used to calculate the sample size using the “pwr.t.test” function from the “pwr” package (Champely et al., 2018). Once the sample size of each cluster was determined, sampling locations were selected by randomly selecting quadrats from the grid imposed on the SBI raster. The quadrats were georeferenced and assigned with unique identifier codes then exported as a GPx file into the GPS receiver for tracking during soil and yield sampling. All raster analysis steps were performed using ArcGIS (ESRI, 2020).

3.1.2.3 Soil and Nutrient Analysis

Soil sampling was conducted before planting, but after fertilizer incorporation. Soils were sampled using a 30 cm auger. Samples were collected in triplicate from each quadrat and mixed to form a composite sample. The soil samples were then air dried at 30°C for 72 hours. After air drying, the soils were ground and sieved (< 2 mm) prior to analysis. The percentages of sand, silt and clay in each soil sample were determined using the sedimentation method (Jackson et al., 1986). Hydrogen peroxide was used to oxidize organic matter, after which the particle size distribution was determined through sieving and sedimentation.

Soil samples were analysed for N, C and S using the Dumas method (Kirsten & Hesselius, 1983). Air dried soil (0.25 g for N and 0.15 g for C and S) was passed through a furnace at 1000°C in the presence of oxygen. The oxidized gases were then detected and measured using a thermal conductivity cell. The Olsen method (Page, 1982) was used to estimate available P in the soil. Sodium bicarbonate was used to extract P from the soil into solution and form phosphomolybdate after reaction with ammonium molybdate. The phosphomolybdate was reduced by ascorbic acid to form a blue complex whose concentration was measured spectrophotometrically at 880 nm. Concentrations of K and Mg were determined by flame photometry using ammonium nitrate as an extractant as described in (Jackson et al., 1986).

3.1.2.4 Yield Data Collection

At every sampling location, the number of plants within a one metre row was counted and recorded as a measure of plant density. At harvest, all the plants in the one metre length were carefully uprooted with a spade and the number of main stems was counted as a measure of stem density. Excavation was carried out carefully to minimise any loss of tubers. All tubers were separated from their stolon and stored for further processing.

The number of tubers at each sampling point was counted. At all locations except for Horse Foxhole, all tubers with a transversal diameter greater than or equal to 25 mm were graded using potato sizing squares into 10 mm size grades up to 65 mm, with all tubers over

65 mm in diameter placed in one bin. All tubers under 25 mm diameter were binned into one grade. After grading, the tuber number in each category was counted and its weight was determined at 0.01 g accuracy. For Horse Foxhole, the tubers were separated into typical commercial grading of 0-25 mm, 25 mm-45 mm, 45-65 mm and greater than 65 mm.

3.1.2.5 Data Analysis

Tuber Size Distribution was modelled using the Gaussian (Aliche et al., 2019; Travis et al., 1987), Gamma (Aliche et al., 2019) and Weibull (Bussan et al., 2007, Nemececk et al., 1996) distributions. The Gaussian distribution is the most widely adopted of the three distributions, with the mode equalling the mean of the distribution and its parameter estimation is simple and intuitive as described in Travis et al. (1987). For the Gamma distribution, the probability density is as described in Aliche et al. (2019), with respect to TSD in potatoes. The Weibull distribution's density function was described by Nemececk et al. (1996). The Gamma and Weibull distribution are considered flexible to oft-observed right-skewed potato TSD (Bussan et al., 2007; Nemececk et al., 1996; Aliche et al., 2019), hence they can potentially give better estimates of the modal tuber size than the Gaussian distribution. Love & Thompson-Johns (1999) also demonstrated that agronomic practices such as wider plant spacing can also lead to left-skewed TSD, making the Weibull distribution an ideal candidate for modelling the shape of the distribution flexibly. Figure 13 illustrates the effect of changing the shape parameter on a conceptual Weibull probability density curve. Generally, the distribution resolves to an approximately symmetrical distribution with a shape values of 3.6 and approaches right-skewness or left-skewness above or below that respectively (Lai et al., 2006). This makes the Weibull distribution more appropriate for its flexibility to model both left and right skewed data.

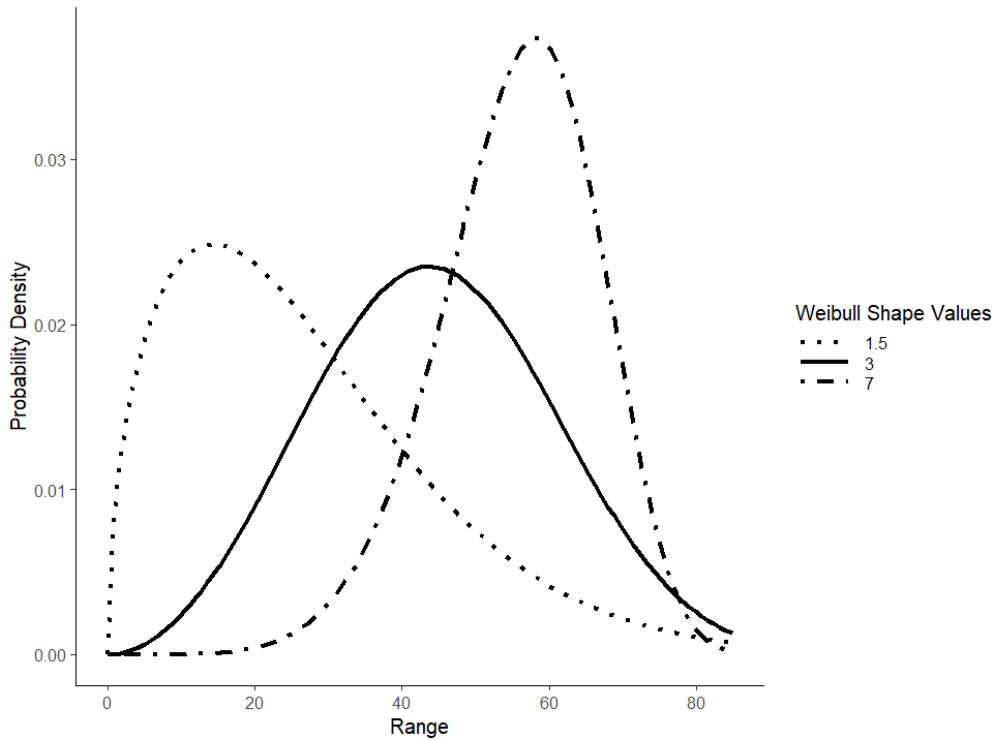


Figure 13: The effect of changing the shape parameter on a conceptual Weibull probability density curve

Maximum likelihood estimation approach was used to obtain estimates for the mean and standard deviation of the Gaussian distribution, and the scale and shape parameters for the Weibull and Gamma distributions. The “fitdstrplus” package (Delignette-Muller & Dutang, 2015) was used to obtain the parameter estimations for all three distributions from the right-censored interval potato TSD data of the current study. Accordingly, the likelihood of each parameter θ in each distribution was fitted as follows:

$$L(\theta) = \prod_{j=1}^{N_{leftC}} F(x_j^{upper}|\theta) \times \prod_{k=1}^{N_{rightC}} 1 - F(x_k^{lower}|\theta) \times \prod_{m=1}^{N_{intC}} (F(x_m^{upper}|\theta) - F(x_m^{lower}|\theta)) \dots\dots\dots (7)$$

Using the cumulative distributions (F), where x_j^{upper} represented the upper values defining the N^{leftC} left-censored observations, x_k^{lower} represented the lower values defining the N^{rightC} right-censored observations, x_m^{lower} and x_m^{upper} represented the intervals defining the N^{intC} interval-censored observations (Delignette-Muller & Dutang, 2015).

The Weibull distribution parameters were also estimated using the percentiles method (Dubey, 1967). Accordingly, the shape parameter ($\beta_{Weibull}$) of the Weibull distribution was estimated by linearizing the cumulative distribution function at two different discrete diameters (e.g. 45 mm and 65 mm) then combining the two equations to solve for $\beta_{Weibull}$ as follows:

$$\hat{\beta}_{Weibull} = (\ln x_i - \ln x_j)^{-1} \times \left\{ \ln \left[\frac{\ln(1-f(x_j))}{\ln(1-f(x_i))} \right] \right\} \dots\dots\dots(8)$$

The scale parameter $\hat{\alpha}_{Weibull}$ was then calculated using $\hat{\beta}_{Weibull}$ and the cumulative density at one known quantile as follows:

$$\hat{\alpha}_{Weibull} = \frac{x_i}{[-\ln(1-f(x_i))]^{\frac{1}{\hat{\beta}_{Weibull}}}} \dots\dots\dots(9)$$

Where $f(x_{i..j})$ represented the cumulative probability of tuber number or weight at x_i or x_j tuber diameter and $x_{i..j}$ where the chosen i^{th} or j^{th} discrete diameter of a tuber

In each sample, the estimated parameters of the four distribution-fitting approaches (Gaussian, Gamma, Weibull with MLE and Weibull with percentiles approach) were used to predict the tuber numbers in each original discrete size grade, creating fully-specified ordered discrete distributions. The Weibull percentiles approach was fitted at the percentiles corresponding to 45 mm and 65 mm tuber sizes, selected because this represents the marketable range for main crop potatoes. In this case, the percentiles were the cumulative proportions of the tuber number or weight at 45 mm or 65 mm, and were therefore different for every sample. The logarithm of the relative likelihood (hereinafter referred to as log relative likelihood) of the predicted discrete distribution (relative to the actual discrete distribution) was then calculated as illustrated in Lindsey (1974). The likelihood of the discrete distribution was calculated as the likelihood of a fully specified multinomial distribution follows:

$$L(P) = \prod_j P_j^{n_j} \dots\dots\dots(10)$$

Where P is the probability of the j^{th} category and n is the frequency of the j^{th} category.

The log relative likelihood was then used as a ranking index of the plausibility of the models, with the most plausible model having the highest likelihood. The log relative likelihood was calculated as follows:

$$L_{RR} = \sum n_j [\ln(\hat{L}_j) - \ln(L_j)] \dots\dots\dots(11)$$

Where n_j is the observed frequency of a category, \hat{L}_j is the probability of the predicted distribution and L_j is the likelihood of the observed distribution.

Uncertainty in the log relative likelihood was assessed using 95% confidence intervals. Fisher’s information was used to estimate the variability of the estimate. The Fisher’s information was derived by negating the expected value of the second derivative of the log likelihood equation (Ly et al., 2017), which for the multinomial distribution used was defined as follows:

$$I(\theta) = -E\left(-\frac{n}{P_i^2}\right) \dots\dots\dots (12)$$

Where n is the frequency of a category and P_i is the likelihood of the category. The reciprocal of the square of the fisher’s information was used as the standard error component of the confidence interval formula.

The main purpose of fitting the theoretical continuous distributions to the discretely measured tuber size fractions is to maximize the accuracy of the estimate of the modal tuber size of the distribution, which is the marketable component of the production. This falls within the 45 mm to 65 mm size bands. Therefore, the most suitable distribution was considered to be the one that maximized the likelihood of this tuber size fraction. The log relative likelihood estimates of the 45 mm to 65 mm size band were therefore also compared for the four models. Additionally, the Root Mean Square Error (RMSE) of prediction for the frequencies of the 45 mm to 65 mm size fraction were compared. The RMSE was calculated as follows:

$$RMSE = \sqrt{\frac{1}{N} \sum_{i=1}^n (y_i - \hat{y}_i)^2} \dots\dots\dots (13)$$

Where N is the number of observations, y_i is the predicted value and \hat{y}_i is the observed value. The modal tuber size of the most plausible model within the 45 to 65 mm size fraction was considered to be the best estimate of the distribution's model. For comparison purposes, the most plausible distribution fitted using the benchmark maximum likelihood approach was used to compare the modal tuber size predictions of the other models using RMSE. The mode of the Gaussian distribution was considered to equal the mean. For the Gamma and Weibull distributions, the modes were calculated as follows:

$$Mode_{Gamma} = \hat{\gamma}_{Gamma} \times (\hat{\alpha}_{Gamma} - 1) \dots\dots\dots (14)$$

$$Mode_{Weibull} = \hat{\alpha}_{Weibull} \times \left(1 - \frac{1}{\hat{\beta}_{Weibull}}\right)^{\frac{1}{\hat{\beta}_{Weibull}}} \dots\dots\dots (15)$$

Where γ_{Gamma} is the scale parameter of the Gamma distribution, α_{Gamma} is the shape parameter of the Gamma distribution, $\hat{\alpha}_{Weibull}$ is the scale of the Weibull distribution and $\hat{\beta}_{Weibull}$ is the shape parameter of the Weibull distribution.

To assess the significance of the responses of TSD to soil nutrients, mixed effect regression models were computed for the primary macronutrients. The outcome variables of the linear models were the shape and scale parameters of the best-fitting models, treated as new observations, with all estimates receiving the same weight in any further data analysis. The study locations were used as the source of random variation. Cognisant of the spatial non-independence of the observations within each location, the mixed effect models included a Matern covariance structure to account for spatial autocorrelation (Minasny & McBratney, 2005; Stein, 1999). The Matern covariance was fitted by restricted maximum likelihood. Statistical analysis was conducted in R v4.0.2 (R Core Team, 2019) and the spatial regression model was fitted using the SpaMM package (Rousset & Ferdy, 2014). Statistical significance was evaluated using confidence intervals and the goodness of fit for multivariable regressions was evaluated using the nRMSE, which was computed by dividing the RMSE by the mean of the observed variable.

3.1.3 Results

3.1.3.1 Summary Statistics

Summary statistics for the soil and plant variables measured in the study are presented in Table 5. Soil texture ranged from predominantly sandy silt loams at HF7, through sandy loams at Buttery Hill and Horse Foxhole to predominantly Silty Clays at Deaton 6.

Table 5: Summary statistics of key soil and plant variables measured at each study site

Soil.Prop¹	Deaton 6	HF7	Buttery Hill	Horse Foxhole
	Mean (CV²)	Mean (CV)	Mean (CV)	Mean (CV)
Clay (%)	38.5 (0.19)	18.3 (0.58)	9.3 (0.15)	14.3 (0.29)
Silt (%)	55.4 (0.12)	38.1 (0.20)	24.6 (0.21)	17.4 (0.30)
Sand (%)	6.1 (0.31)	43.5 (0.30)	66.1 (0.09)	68.3 (0.10)
N (g/kg)	9.4 (0.29)	8.4 (0.45)	1.3 (0.12)	1.7 (0.14)
C (g/kg)	124.2 (0.36)	101.8 (0.46)	12.9 (0.12)	16.3 (0.09)
S (g/kg)	3.3 (0.47)	2.2 (0.51)	0.3 (0.12)	0.3 (0.19)
P (mg/kg)	41.2 (0.15)	42.4 (0.17)	100.0 (0.13)	91.1 (0.12)
pH	7.5 (0.08)	6.6 (0.05)	7 (0.03)	6.6 (0.03)
K (mg/kg)	291.3 (0.27)	272.7 (0.24)	276.8 (0.18)	202.4 (0.19)
Mg (mg/kg)	185.0 (0.29)	80.1 (0.25)	87.4 (0.12)	88.4 (0.14)
Plants/m²	2.5 (0.12)	2.5 (0.24)	2.8 (0.26)	5.2 (0.30)
Stems/m²	9.8 (0.17)	12.4 (0.34)	13.9 (0.28)	17.0 (0.16)
Tubers/m²	38.7 (0.10)	41.1 (0.28)	35.4 (0.29)	48.3 (0.14)
Yield (kg/m²)	4.2 (0.12)	5.2 (0.19)	3.4 (0.27)	5.5 (0.11)

1 = Soil Property. 2 = Coefficient of variation.

Mean total C was highest at Deaton 6 (124.15 g/kg) and HF7 (101.77 g/kg), a reflection of the high organic matter content, while the carbon content of Buttery Hill, and Horse Foxhole were lower. Deaton 6 and HF7 soils also contained higher concentrations of N and S but had lower concentrations of P than the sandy loams. Plant spacing was consistent at approximately 2.5 plants/m² across locations except Horse Foxhole where inconsistent

planting spacing led to an average of 5 plants/m². Horse Foxhole also recorded the highest number of stems, tubers and yield per square metre.

Table 6 shows the summary statistics of the TSD parameters at the five study sites where the TSD modelling was conducted. Parameter Mu, which was the tuber size with the largest probability (modal tuber size with respect to the probability densities of tuber number as determined using the best-fitting TSD model) ranged from 37 mm at Buttery Hill to 51 mm at Horse Foxhole. The same pattern was also reflected in the Mu with respect to tuber weight (49 mm at Buttery Hill and 61 mm at Horse Foxhole). Similarly, the scale of the tuber size distribution with respect to tuber numbers, ranged from 41 mm at Buttery Hill to 56 mm at Horse Foxhole and with respect to tuber weight, the scale was largest at Horse Foxhole (62.44 mm) and lowest at Buttery Hill (50.42 mm). This large variation between fields was not replicated within field with CVs for the distribution scale ranging from 0.07 at Buttery hill to 0.03 or less at Horse Foxhole for both tuber size and weight. Within-field variation in TSD with respect to tuber number was higher when quantified as the shape of the distribution.

The average shape of Weibull curves fitted on within-field TSD with respect to size ranged from 3.36 at Buttery Hill to 5.04 at Deaton 6. With respect to weight, higher shape values were observed, with the minimum at Buttery Hill (6.46) and maximum at HF7 (8.52). The higher shape values suggested that TSD with respect to tuber weight was more left skewed than with respect to tuber number. Overall, more within-field variability was captured in the shape parameter than scale parameter. The CV ranged from 0.12 at Deaton 6 and Horse Foxhole to 0.23 at Buttery Hill with respect to tuber number and up to 0.27 at Buttery hill with respect to tuber weight. The CV of the scale parameter was consistently under 0.1 for both tuber number and weight, suggesting low variability in the modal tuber size or weight class despite large variability in the shape of the tail that influence the shape parameter.

Table 6: summary statistics of the tuber size distribution (TSD) parameters at five different sites

Parameter	Deaton 6	HF7	B.Hill	H.Foxhole	C.Leasow
	Mean (CV ¹)	Mean (CV)	Mean (CV)	Mean (CV)	Mean (CV)
Mu² (mm)	49.46 (0.03)	44.50 (0.07)	36.50 (0.08)	51.10 (0.03)	43.70 (0.05)
Mu_{wt}³ (mm)	56.71 (0.05)	53.57 (0.06)	48.45 (0.07)	61.09 (0.03)	49.49 (0.05)
W.Shape⁴	5.0 (0.12)	4.5 (0.16)	3.4 (0.23)	4.7 (0.12)	5.15 (0.28)
W.Scale⁵	51.8 (0.03)	48.8 (0.07)	40.6 (0.07)	55.8 (0.03)	45.93 (0.06)
W.Shape_{wt}⁶	7.59 (0.20)	8.52 (0.26)	6.46 (0.27)	7.38 (0.14)	7.09 (0.12)
W.Scale_{wt}⁷	57.88 (0.04)	54.35 (0.07)	50.42 (0.07)	62.44 (0.02)	50.53 (0.08)

1= Coefficient of variation. 2 = modal tuber size with respect to proportional tuber weight. 3 = modal tuber size with respect to proportional tuber weight. 4:5 = Weibull or scale shape of proportional tuber numbers. 6:7 = Weibull shape or scale parameter of proportional tuber weight

3.1.3.2 Comparison of TSD functions

Figure 14 shows the distribution functions fitted to the average proportional tuber weights at each location. The visual variations in the distributions' locations of central tendency were apparent. The Gaussian and Gamma distributions predicted relatively lower probability densities at the modal tuber size than the two Weibull distribution. As illustrated through the example in Figure 14, the Weibull distributions tended to predict higher probability densities between 50 mm and 60 mm but the probability density quickly fell off towards the right tail, predicting low tuber yield in the oversized tuber size fractions (>65 mm). The Gaussian and Gamma distributions maintain a gentle descent of probability densities towards the right tail and predict higher yields in the oversized fractions.

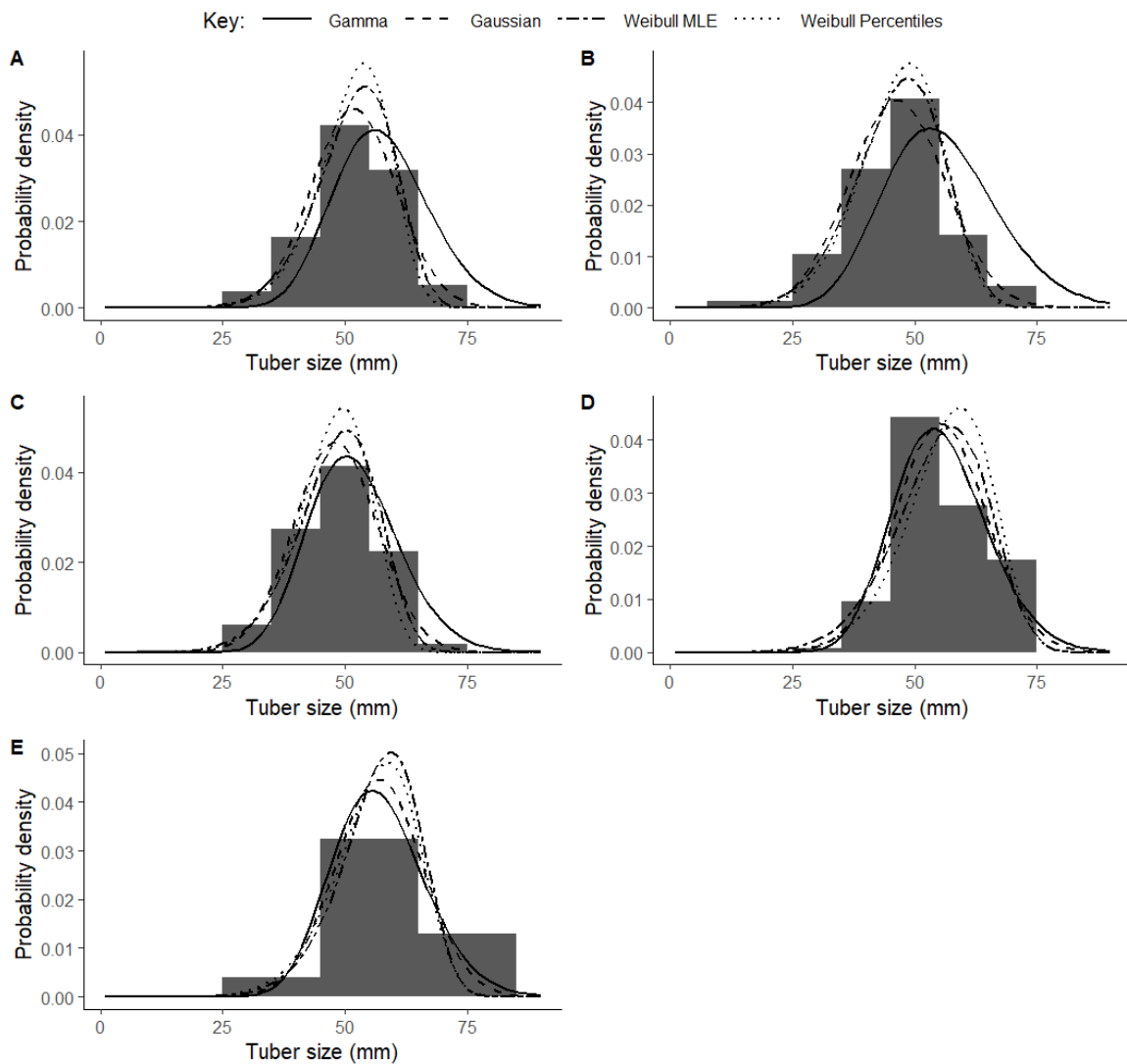


Figure 14: The Gaussian, Gamma and Weibull distribution functions fitted to the average proportional tuber weights at HF7 (A), Buttery Hill (B), Crabtree Leasow (C), Deaton 6 (D) and Horse Foxhole (E) .

Figure 15 shows the distribution functions fitted to the proportional tuber numbers at all 5 locations. As illustrated, all the distributions estimated the modal tuber size accurately, including in the right-skewed Buttery Hill crop. The Gamma distribution tended to underestimate the TSD relative to the other three fitting-methods.

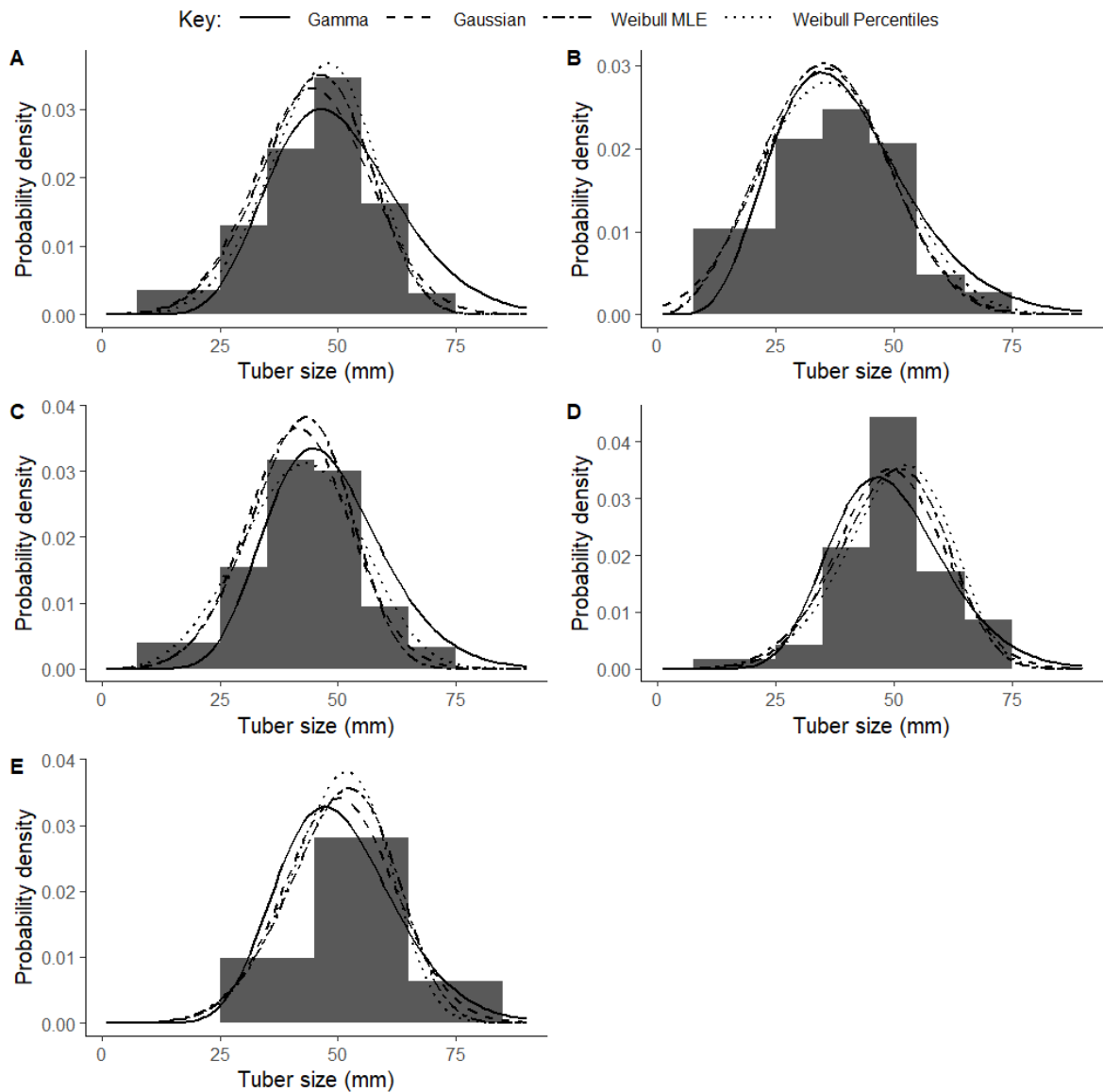


Figure 15: The Gaussian, Gamma and Weibull distribution functions fitted to the average proportional tuber numbers at HF7 (A), Buttery Hill (B), Crabtree Leasow (C), Deaton 6 (D) and Horse Foxhole (E)

Apart from the right-skew at Buttery Hill, the TSD with respect to tuber number was roughly symmetric and the difference between the Gaussian and the two Weibull methods was not readily discernible, visually. As shown in Table 6, the Weibull shape at Crabtree Leasow, Buttery Hill, Horse Foxhole and Deaton 6 ranged from 4.7 to 5.0, suggesting left-skewed distribution.

Table 7 shows the log relative likelihood estimates of the overall distributions of the four tested models, relative to the overall distribution of the observed tuber numbers and tuber

weights in each size fraction. The confidence intervals of the estimates are also shown. With respect to tuber number, the Gaussian distribution was found to be the most plausible model at one out of the five locations (Crabtree Leasow) while the Weibull distribution was the most plausible at Branston Booths, Buttery Hill and Deaton 6. The Weibull distribution with percentiles approach to parameter estimation was found to be most plausible at Horse Foxhole, where the tubers were sized in commercially-practiced main crop size fractions. The log relative likelihood estimates of all the distributions at all locations were significantly different such that their confidence intervals did not overlap has shown in Table 7.

Table 7: Average log relative likelihood estimate and confidence intervals of fitted Gaussian, Weibull, Gamma and Weibull Percentiles curves to potato tuber size distributions at five, relative to the likelihood of the observed discrete distribution

Distr.¹	HF7	B.Hill²	C.Leasow³	Deaton 6	H. Foxhole⁴
Tuber Number					
Gaussian	-3.10±0.03	-3.02±0.02	-2.15±0.03	-4.52±0.03	-2.31±0.01
W.MLE ⁵	-2.75±0.03	-2.95±0.02	-2.83±0.02	-3.73±0.02	-1.53±0.02
Gamma	-5.27±0.03	-3.47±0.03	-2.74±0.03	-8.71±0.02	-2.48±0.01
W.Perc ⁶	-3.68±0.03	-3.86±0.03	-2.42±0.04	-5.38±0.01	-0.03±0.01
Tuber weight					
Gaussian	-345.31±0.01	-272.14±0.04	-160.71±0.01	-249.75±0.01	-3.87±0.01
W.MLE	-197.33±0.01	-196.74±0.04	-110.32±0.03	-222.35±0.02	-2.70±0.01
Gamma	-538.54±0.01	-398.75±0.01	-247.98±0.01	-431.97±0.02	-4.79±0.03
W.Perc	-392.47±0.01	-322.85±0.03	-272.79±0.02	-309.53±0.02	-0.33±0.01

1= Distribution. 2 = Buttery Hill. 3 = Crabtree Leasow. 4 = Horse Foxhole. 5 = Weibull distribution with parameters estimated by maximum likelihood estimation. 6 = Weibull distribution with parameters estimated by the percentiles approach

With respect to tuber weight, the Weibull distribution with maximum likelihood estimation was the most plausible model at Branston Booths, Buttery Hill, Crabtree Leasow and Deaton 6, with the highest relative likelihood to the observed discrete distribution as shown in Table 6, with the highest relative likelihood to the observed discrete distribution as shown in Table 7. Similar to the distributions of the tuber numbers, the Weibull distribution with percentile-based parameter estimation was the most plausible model at Horse Foxhole with no overlapping confidence intervals at all five locations. Overall, the Gamma distribution was found to be the least plausible of the four tested models with respect to both tuber number and weight while the Gaussian distribution ranked second to the Weibull maximum likelihood estimates. The maximum likelihood estimates, particularly the Gamma and Weibull distributions, performed better than the Weibull percentiles approach in generalizing the predicted theoretical curve to the observed discrete distribution, on account of the fitting procedure which took full advantage of the discrete bins in the maximum likelihood estimation. On the other hand, when less information (i.e. wider bins) was available as was the case at Horse Foxhole, the Weibull percentiles approach was more plausible than the maximum likelihood approach.

While the overall generalization of the distribution to the observed discrete distribution is important, it is more crucial to maximize the log relative likelihood within the marketable tuber size fraction of the main crop (45 mm to 65 mm), where the mode of the distribution occurs. This is because the primary goal of modelling tuber size distribution is to estimate the tuber size fraction with the highest probability density, which is then used to predict tuber yield at harvest using the Travis et al (1987) procedure. Table 8 shows the log relative likelihood of marketable tuber number and weight proportions. With respect to tuber number, the results show that the Weibull percentiles approach generalizes better than all the three other approaches, on account of its high relative likelihood. The closed form of the percentiles approach meant that the differences between the estimated proportions and the actual proportions was very small, with log relative likelihood approaching zero. For the maximum likelihood approaches, better generalization to the overall distribution meant less goodness of fit in the marketable tuber portion where the mode of the distribution occurs. The same result was observed with respect to tuber weight, where the Weibull percentiles approach performed better than all three other approaches on account of its high log relative likelihood.

Table 8: Average log relative likelihood estimate and confidence intervals of fitted Gaussian, Weibull, Gamma and Weibull Percentiles curves to the 45 mm to 65 mm size band of potato tuber size distributions at five, relative to the likelihood of the observed discrete distribution

Distr.¹	HF7	B.Hill²	C.Leasow³	Deaton 6	H. Foxhole⁴
Marketable Tuber Numbers					
Gaussian	-4.05±0.19	-2.10±0.13	-1.45±0.2	-6.81±0.14	-13.97±0.12
W.MLE ⁵	-2.64±0.2	-2.23±0.14	-0.79±0.2	-4.50±0.15	-11.49±0.11
Gamma	-6.83±0.17	-3.62±0.12	-2.82±0.18	-11.89±0.13	-22.18±0.1
W.Perc ⁶	0.00±0.02	-0.17±-0.11	-0.12±-0.02	0.00±0.02	0.00±0.49
Marketable Tuber Weight					
Gaussian	-223.53±0.03	-171.91±0.03	-88.92±0.03	-186.17±0.02	0.53±1.25
W.MLE	-29.73±0.02	-66.03±0.02	31.75±0.03	-85.66±0.02	0.53±1.28
Gamma	-405.03±0.02	-318.12±0.02	-212.83±0.02	-382.95±0.02	0.53±1.31
W.Perc	0.00±0.02	-0.03±0.01	-0.08±0.02	0.00±0.02	0.00±0.05

1= Distribution. 2 = Buttery Hill. 3 = Crabtree Leasow. 4 = Horse Foxhole. 5 = Weibull distribution with parameters estimated by maximum likelihood estimation. 6 = Weibull distribution with parameters estimated by the percentiles approach

With respect to both tuber number and weight, the Weibull distribution was also the most plausible of the three models fitted by maximum likelihood estimation. This analysis showed that the Weibull distribution with the percentiles approach had the highest log relative likelihood of the observed marketable tuber profile, making it the best candidate for describing the TSD for the purposes of predicting the modal tuber size. However, the maximum likelihood estimate of the Weibull distribution proved to be a better model for generalizing the overall distribution outside the marketable component.

Using the Weibull distribution with maximum likelihood estimation as a benchmark, the deviation of the other models from the benchmark in the prediction of the modal tuber size was as shown in Table 9.

Table 9: Root Mean Square Error (RMSE) of estimates from the Gaussian, Gamma and Weibull (Percentiles approach) benchmarked against the Weibull model with Maximum Likelihood Estimation (MLE)

Tuber Number						
Location	gauRMSE¹	gamRMSE²	weiRMSE³	shapeRMSE⁴	scaleRMSE⁵	
HF7	1.63	5.08	2.57	0.77	1.83	
B.Hill ⁶	2.21	3.91	5.49	0.78	3.05	
C. Leasow ⁷	1.55	4.36	2.53	1.21	1.82	
Deaton 6	1.63	5.06	2.04	0.76	1.17	
H.Foxhole ⁸	0.85	6.71	2.99	1.21	1.75	
Tuber Weight						
HF7	2.24	3.85	1.36	1.19	1.51	
B.Hill	1.94	4.25	1.57	1.25	1.47	
C. Leasow	2.17	3.84	1.35	1.07	1.70	
Deaton 6	2.28	3.82	1.16	0.76	1.03	
H.Foxhole	2.48	3.63	2.63	3.06	2.15	

1= RMSE of the mode of Gaussian model vs Weibull MLE, 2 = RMSE of the mode of the Gamma model vs Weibull MLE. 3 = RMSE of mode of the Weibull percentiles model vs Weibull MLE. 4 = RMSE of Weibull percentiles shape vs Weibull MLE. 5 = RMSE of Weibull percentiles scale vs Weibull MLE. 6 = Buttery Hill. 7 = Crabtree Leasow. 8 = Horse Foxhole.

With respect to tuber weight, the Weibull percentiles approach yielded the lowest RMSE to the Weibull maximum likelihood approach's mode estimation at all locations except Horse Foxhole. However, as seen in Table 7, the percentiles approach was the most plausible model at Horse Foxhole, therefore its low RMSE was considered to be due to the lesser accuracy of the Weibull maximum likelihood approach at this location. These results were mirrored in the RMSEs of the modal tuber weight as shown in Table 9. Apart from Horse foxhole, the RMSE of the shape parameter between the maximum likelihood and percentiles approaches at all locations was within 1.5 units, showing that the percentiles approach approximated the shape of the distribution comparably to the benchmark. Similar observations were made for the scale parameter. At Horse Foxhole, higher RMSEs were

observed, partially attributable to the lesser accuracy of the maximum likelihood approach. The analysis showed that the percentiles approach was comparable to the maximum likelihood approach in the estimation of the modal tuber size and yielded the highest log relative likelihood of the observed marketable yield. Therefore the distribution shape, scale and modal tuber size as estimated using the percentiles approach were tested for their predictability using within-field soil nutrient variation.

3.1.3.3 Linear Modelling

Table 10: Linear modelling results for the relationships between soil nutrients (and stem density) and TSD parameters with respect to tuber number

Response	Predictors	Estimate	nRMSE_{fixed}¹	delta AICc²	D.F.³	ICC1⁴
Shape	Intercept	4.35±0.63				
	Stem	-0.04±0.17				
	Density		0.18	7.15	75.66	0.37
	Phosphorus	-0.74±0.33				
	Nitrogen	-0.29±0.25				
Scale	Intercept	49.15±7.22				
	Stem	-0.98±0.63				
	Density		0.13	14.77	72.19	0.87
	Phosphorus	0.92±0.27				
	Nitrogen	1.44±1.16				
Mode	Intercept	45.71±8.05				
	Stem	-1.08±0.78				
	Density		0.14	11.41	72.66	0.83
	Phosphorus	-2.37±1.99				
	Nitrogen	0.85±1.40				

1= Normalized Root Mean Square Error of the fixed effects model, with random effects set to zero. 2 = change in the conditional Akaike Information Criteria between the current model and the random intercept model. 3 = effective degrees of freedom. 4 = Intraclass correlation of the random effects.

Table 10 shows the linear modelling results for the relationships between soil nutrients and TSD parameters with respect to tuber number. Stem density was also included as a fixed effect. For the shape parameter, no significant relationship was observed with the stem density, with a very low regression coefficient (-0.04) as shown in Table 10. The coefficients suggested that the proportional number of tubers falling into the pre-defined size bands was not affected by the stem density. However, P and N were observed to negatively associate with the shape parameter with statistical significance through the confidence intervals as shown in Table 10. The strongest negative relationship with the shape parameter was observed with P, suggesting that P increased the proportional numbers of small-sized tubers. The overall effect of P on the tuber size distribution at the four sites were as shown in Figure 16, where the average shape and scale parameter from low-P samples (P concentration less than the location’s mean) and high-P samples (P concentration higher than the location mean) were plotted to visualize the relationship.

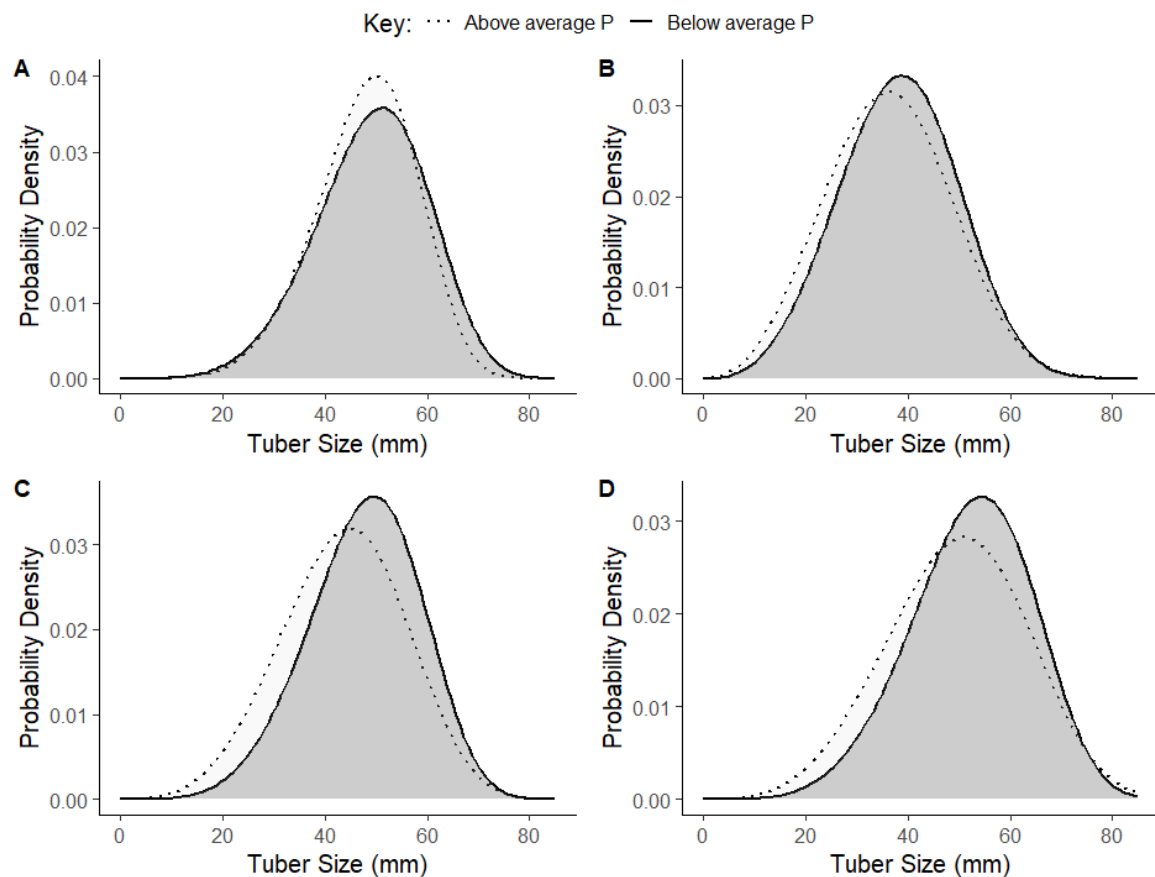


Figure 16: Illustration of the effect of Phosphorus concentration on the tuber size distribution at Deaton 6 (A), Buttery Hill (B), HF7 (C), and Horse Foxhole (D).

For the scale parameter, a significant negative relationship was observed with stem density, with a standardized regression coefficient of -0.98 , suggesting that increased stem densities led to a decrease in the overall range of the distribution. Positive relationships with the scale parameter were observed for P and N, suggesting that the two nutrients increased the overall range of the distribution, though only P was observed to hold a statistically significant relationship. Overall, increase in P at all four locations was associated with a shift of the TSD towards a right skew, leading to a lower probability density of the modal tuber size. As shown in Table 8, the mode of the distribution with respect to tuber number was also significantly related to the stem density and P, with a statistically significant regression coefficient of -2.37 for P. Setting the random effects to zero, the fixed-effects-only model had an nRMSE of 0.14 for the mode, suggesting that the expected modal tuber size across the field can be predicted to acceptable accuracy using stem density and soil nutrient information, with a Matern covariance structure fitted across the surface.

Table 11 shows the regression coefficients of the shape, scale and mode variables of the TSD (with respect to tuber weight) as a function of stem density and the concentrations of soil nutrients. The shape parameter was negatively related to stem density with a regression coefficient of -0.31 , showing that increasing stem numbers moderately associated with a shift of the TSD towards a right skew. The same association was also observed with nutrients P and N, suggesting that increased soil nutrient concentrations in these soils were associated with an increase in the proportion of low-weight tubers. The relationships between the three variables and the shape parameter were all significant as evaluated through their non-zero confidence intervals. The fixed-effects-only model fitted the data with an nRMSE of 0.22 . Stem density also had a significant negative association with the scale parameter, which suggested that observations with relatively high stem densities had a smaller range of tuber sizes with a higher concentration of small tubers. Phosphorus and nitrogen had significant positive relationships with the scale parameter, suggesting that the overall range of the distribution was increased with the increase of these soil nutrients. Potassium was also negatively related to the scale parameter. The fixed effects explained the variation in the scale parameter with an nRMSE of 0.09 . The model fitted for the modal tuber size showed significant negative relationships between stem density and tuber size. Phosphorus and nitrogen both had positive relationships with the mode as shown by the

positive regression coefficients in Table 11. However, the P relationship was not significant as evaluated the zero-coverage of the confidence interval. The fixed effect coefficients fitted the observed data with an nRMSE of 0.21.

Table 11: Linear modelling results for the relationships between soil nutrients (and stem density) and TSD parameters with respect to tuber weight

Response	Predictors	Estimate	nRMSE_{fixed}¹	delta AICc²	D.F.³	ICC1⁴
Shape	Intercept	7.46±0.36				
	Stem Density	-0.31±0.59	0.22	5.01	77	0.37
	Phosphorus	-1.3±0.62				
	Nitrogen	-0.89±0.63				
Scale	Intercept	56.26±5.79				
	Stem Density	-0.99±0.78	0.09	12.69	74.23	0.72
	Phosphorus	2.6±1.83				
	Nitrogen	2.1±1.17				
	Potassium	-0.75±0.8				
Mode	Intercept	54.79±6.28				
	Stem Density	-1.04±0.69				
	Phosphorus	1.27±1.57	0.21	11.94	75.14	0.79
	Nitrogen	1.35±1.07				

1= Normalized Root Mean Square Error of the fixed effects model, with random effects set to zero. 2 = change in the conditional Akaike Information Criteria between the current model and the random intercept model. 3 = effective degrees of freedom. 4 = Intraclass correlation of the random effects

3.1.4 Discussion

3.1.4.1 Tuber Size Distribution Model

The findings of the study showed that potato TSD was more consistent with the Weibull distribution than the Gamma and Gaussian distributions, in agreement with Nemecek et al.

(1996) and Bussan et al. (2007). The log relative likelihood analysis of the overall distribution showed that the maximum likelihood approaches generalized to the observed discrete proportions better than the percentiles approach and the Weibull distribution maximum likelihood approach was the best method for generalizing the shape and scale of the distribution. However, in the context of this study, the percentiles approach performed better at maximizing the likelihood of the tuber size fraction of interest (45 mm to 65 mm) because its closed form offered the opportunity to maintain the likelihood of this desired size fraction accurately. Ultimately, the main goal of TSD modelling is to maximize the likelihood of modelling the correct modal tuber size, which will fall within a pre-defined tuber size interval. The log relative likelihood analysis demonstrated empirically for the first time that the percentiles approach for parameter estimation performs comparably to the maximum likelihood approach in the estimation of the marketable tuber size fraction. Additionally, the Weibull percentiles approach had the lowest RMSE for the prediction of the modal tuber size, in comparison with the benchmark best-performing Weibull distribution with maximum likelihood estimation, while maintaining the highest relative likelihood for the frequency of the marketable 45 mm to 65 mm size fraction.

Large variation in the Weibull shape parameter for TSD modelled against both tuber number and weight proportions further shows the merit of adopting a flexible distribution function, in contrast to Nemecek et al. (1996) who suggested an average Weibull shape parameter of 2.3 as a general solution to simulate a right-skewed distribution. However, Nemecek et al. (1996) used tuber samples from potatoes grown for a seed market, which are desiccated early with less time allowed for tuber bulking. In the current study, some visually right-skewed distribution was observed at BATTERY Hill, which also had the smallest average tuber size. The Weibull distribution best modelled the BATTERY Hill crop as evidenced by the log relative likelihoods of both the overall distribution and the marketable portion. However, the average shape parameter was 3.4 for TSD modelled after proportional tuber numbers and 6.46 for TSD modelled after proportional weight. This showed that proportional tuber numbers were roughly symmetrically distributed around the modal tuber size, but the proportional weights were slightly left-skewed because of a higher weight per tuber of the larger tubers. Similarly across all locations, the predicted modal tuber size with respect to tuber weight was larger than the modal tuber size with respect to tuber numbers. This is in line with principles of scaling whereby the weight of an object is proportional to its volume,

which is in turn proportional to the cubic power of its linear dimensions, the principle behind the use of the modal tuber size for predicting yield in Travis et al (1987). Therefore, in an assumed Gaussian distribution of tuber numbers, the distribution of tuber weights can be expected to be slightly left-skewed with a higher modal size with respect to proportional tuber weights on account of an exponential increase of weight per tuber with increasing tuber size. These findings provide further evidence that the assumption of a Gaussian distribution as adopted by Travis (1987) does not universally hold true.

Struik et al. (1991) observed an initial right skewed TSD with a modal tuber size gradually shifting to the right as more time was allowed for tuber bulking by shifting the harvest date. There is good evidence therefore that the overall shape of the distribution is influenced by the average tuber size, which depends on the time of observation, tuber bulking rate and the timing of harvest. It can be argued that the Gaussian (Sands & Regel, 1983), Log-normal (Marshall et al., 1993) and Gamma (Aliche et al., 2019) distributions, as well as the Weibull distribution with a fixed shape parameter, are all instance-specific realizations of an underlying dynamic distribution that is a function of the tuber bulking status at the time of observation. In turn, tuber bulking rates are controlled in part by the efficiency of source-sink transportation of photosynthates which depends on the plant nutrition status of the crop (Struik et al., 1991). Allowing for a flexible shape parameter, the current results suggest that the Weibull distribution is the best estimator of the TSD curve at any stage of tuber development for the most representative prediction of the modal tuber size, which is the main purpose for modelling TSD.

A method for non-destructively modelling TSD is desirable for temporal monitoring of the changes in TSD. To achieve this, one of the parameters in the Weibull distribution needs to be modelled as a function of a non-destructively measurable variable. Both Nemecek et al. (1996) and Bussan et al. (2007) chose to model the scale parameter from empirical data, however they did so for different reasons. Nemecek et al. (1996) suggested a fixed Weibull shape parameter, as they empirically observed that distribution fit was relatively invariant in their dataset. However, Bussan et al. (2007) explicitly modelled the scale parameter because it had a high correlation to measured stem and tuber density. In the current study, the shape parameter had higher within-field variability than the scale at all study sites as measured by the CV, regardless of the method by which TSD was measured (i.e. as a function of proportional tuber number or weight).

3.1.4.2 Effect of Soil Factors on Tuber Size Distribution

Literature on TSD is dominated by plant population studies, with the number of stems per unit area being reported to have a negative effect on indicators of TSD and tuber number (Aliche et al., 2019; Bussan et al., 2007; N. R. Knowles & Knowles, 2006). These past findings all support the hypothesis that higher stem numbers per unit area increase the tuber number per unit area at the expense of tuber size, leading to more uniform but smaller-sized tubers. The results of the multivariable regression are in general agreement with these findings as stem number per unit area had the most consistent negative regression coefficients with the modal tuber size and the scale parameter of TSD, regardless of whether TSD was modelled with respect to proportional tuber numbers or weight. A lower scale parameter associated with increased stem number means that there was a smaller probability density of large tubers, supporting the previous findings. The standardized regression coefficients for stem number suggest a large effect size of stem number on the modal tuber size and scale, to provide further support to the hypothesis that stem density increase significantly affects tuber size. Stem density also had consistently negative relationships to the shape of the distribution but the effect size was low, This may be interpreted to mean that bulking rates of large tubers are reduced in the presence of high stem numbers but the tuber filling is not altered to particularly favour any one of the other predefined size classes significantly.

The results suggest that the effects of soil macronutrients on TSD may be important, considering the negative associations between P and the shape parameter with a high effect size for TSD measured with respect to tuber number or weight. This is consistent with findings that high P tests (25 to 33 mg/kg) may be associated with an increase in the proportion of small tubers in the TSD, attributed to increased vegetative growth at the expense of tuber bulking (see Birch et al., 1967; Prummel & Barnau-Sijthoff, 1984; Rosen & Bierman, 2008; Sharma & Arora, 1987).

In the current study, the lowest concentration of available P was observed at Deaton 6 (41 mg/kg), with up to 100 mg/kg at Buttery Hill, which were much greater than the soil P tests at which negative effects were observed in the Rosen & Bierman (2008) study. While positive effects of P on tuber yield components have been reported from replicated experiments by Freeman et al. (1998), the responses were in low P soils and an asymptote was reached at 27 mg/kg for the Kennebec variety. The results give evidence of a significant

negative relationship between P concentrations and the modal tuber size with respect to tuber numbers, meaning that the proportional number of smaller tubers increases as P concentration increases. However, the scale of the distribution with respect to both tuber number and weight was increased with increase in P concentration. This suggests that P did not affect the tuber filling hierarchy but led to induction of more tubers that remained within the small size fraction. The smaller tubers are expected to have a relatively low contribution to the overall yield therefore the positive effect of P on the scale of the distribution can be expected to positively affect the modal tuber size as observed in the study.

As a possible explanatory mechanism, potatoes are known to maintain P uptake even at high soil P tests like the ones observed in the current study (Jasim et al., 2020), thereby accumulating inorganic P in the cytosol. Inorganic phosphate accumulation is inhibitory to the activity of ADP-glucose pyrophosphorylase and subsequently inhibit starch synthesis and accumulation in sink organs (Crafts-Brandner, 1992; Kleczkowski, 1999; Tiessen et al., 2002). A tuber-filling hierarchy has been previously shown whereby larger tubers grow the fastest and increase the spread of the TSD (Mackerron et al., 1988), therefore high P concentrations can be expected to contribute to increased proportions of small tuber numbers without penalizing the scale of the distribution as shown in the study.

There have been a few previous studies where the effect of soil nutrients on TSD was systematically studied. Wurr et al. (1993) found that N had a significant effect of TSD measured as the spread (CV %) of tuber sizes (assuming a Gaussian distribution), however they found no effect of P. The findings by Wurr et al. (1993) are also reflective of the design-intrinsic large concentration gradients of the nutrient treatments in controlled experiments, where N becomes a limiting nutrient hence its effects are emphasized. In the adequately-fertilized sites of the current study where N was not a limiting factor for production, the evidence suggests that P equally contributes to the underlying model that explains within-field variation in TSD. Nitrogen was largely found to have the same effects on TSD parameters as P, with high standardized regression coefficients on the scale and mode with respect to tuber weight suggesting that N increases the variability in tuber size, in alignment with Wurr et al (1993). High N was associated with a lower shape parameter, showing a particularly high effect size with respect to tuber weight. However, wide confidence intervals call for a more precise estimation of the relationship.

These findings mean that field variation in expected TSD can be constructed from soil data by modelling the shape parameter and scale parameter for the field. The scale and shape parameter can also be calibrated by mid-season yield digs. The beneficial properties of N and P on tuber yield are well documented in the literature and formulate the basis of crop fertilization modelling with the assumption of a Mitscherlich exponential growing process with a horizontal asymptote. The current findings suggest the existence of an inflection point after which over-fertilization results in a linear reduction in the shape of the TSD.

3.1.5 Conclusion

In conclusion, the study has shown that the shape parameter of the Weibull distribution determined using a linearized cumulative probability function provides an adequate index for describing the overall shape of TSD and performs better than the Gaussian and Gamma distributions in simulating observed TSD. The linearized formulae for the Weibull shape and scale presented in the current paper can be easily implemented in spreadsheet software at the farm level. Using the shape parameter, agronomists can improve the monitoring methods of the temporal shift in TSD from yield digs and (where large tubers are preferred) aim for symmetrical (shape ~ 3) or left skewed (shape > 3) TSD. With the availability of Weibull cumulative probability functions in popular spreadsheet software, tuber numbers in any discrete size grades can be calculated from the modelled shape and scale parameter. From the current study, the shape parameter had larger within field variability than the scale parameter and was significantly affected by excess P and N. Ultimately, high intensity soil maps of these elements can enable high-resolution modelling of spatial TSD variation. While requirements for high intensity soil sampling remain prohibitive, modelling of soil variability using co-kriging proxies like apparent electrical conductivity becomes important and relevant for generating high resolution field variation for decision-support. Subsequent studies to validate these findings in more environments are recommended, as well as controlled studies to investigate the general point of inflection at which additional fertilization becomes detrimental to TSD.

3.2 Examination of the Relationship between Apparent Electrical Conductivity and Soil Physical and Chemical Properties

Abstract

The costs of high intensity soil sampling are high and alternative approaches where soil properties can be inferred from easily collected measurements are increasingly being sought after in commercial crop production. In particular, the relationship between Apparent Electrical Conductivity (ECa) and its relation to variability in soil water content and salinity have led to increased interest in its use as an index for delineation of management zones for precision agriculture. ECa has also been suggested as a proxy to the variability of soil mineral constituents but the reproducibility of correlations between ECa and soil mineral concentrations have not been consistent. In this study, ECa was determined at Buttery Hill and Deaton 6 Fields with the purpose of relating it to measured soil mineral constituents. The aim of this study was to examine the suitability of ECa as a proxy to soil macronutrient concentrations and texture in typical potato fields. Accordingly, soil particle distribution was measured using the sedimentation method and mineral constituents were measured using various methods including the Dumas method for N, C and S, the Olsen method for P and flame photometry using ammonium nitrate as an extractant for K and Mg. The results showed no strong correlations between ECa and all the soil macronutrients at both sites. For soil particle distribution, no correlations with ECa were observed at Deaton 6 while significant correlations were observed at Buttery Hill for Sand ($P < 0.001$), Silt ($P < 0.001$) and Clay ($P = 0.01$). These results showed the contextual nature of ECa and why understanding the locally contributing edaphic factors is important before it can be used for agronomic recommendations on soil management.

3.2.1 Introduction

Potato production is predominantly based on uniform management of the crop through predetermined seed rates, uniform irrigation and fertilisation throughout the season. Cambouris et al. (2006) report that variability of tuber sizes in this system can be addressed through delineation of field management zones based on the Electromagnetic Induction (EMI) properties of the soil, particularly the Apparent Electrical Conductivity (ECa) of the soil. The ECa is a proxy to understanding soil composition because it is an expression of the

collective effect of the soils mineralogical and hydrological composition (Castro-Franco et al., 2015). In experiments by Cambouris et al. (2006), ECa-based delineated zones were subjected to variable nitrogen application, leading to a more uniform tuber yield. There are extensive similar studies where ECa has been successfully used to predict field variability in salinity (Li et al., 2011), soil organic matter (SOM), cation exchange capacity (CEC) and soil gravimetric water content (Castro-Franco et al., 2015). High resolution georeferenced ECa maps have gained interest as a precision agriculture tool for delineation of management zones, however, their value as proxies to important soil nutrients has not been established to justify large scale adoption in commercial potato production.

Based on this background, field surveys were conducted to evaluate the relationship between, ECa and other edaphic factors

3.2.2 Data and Methods

3.2.2.1 Site Characterisation

The study was conducted at Buttery Hill and Deaton 6 as described in Section 3.1.2.1. Deaton 6 was located in the East of England (Lincolnshire) on reclaimed marsh land with a shallow water table and high organic matter content. There was variation in soil physical and chemical properties across the field due to the presence of Roddons, historical features in drained marshland soils where silty clay soils follow the course of historical streams and waterways. Buttery Hill was located in the West of England (Shropshire) on well-drained slightly stony, sandy loam soil subtended by weathered sandstone with low variation in soil nutrients across the field.

3.2.2.2 Soil Sampling and Analysis.

A field survey was designed at each of the four fields using a model-based sampling approach to determine representative soil sampling locations that captured the variability in the field. Accordingly, the soil sampling and analysis were conducted as described in 3.1.2.2 and 3.1.2.3 respectively.

3.2.2.3 Apparent Electrical Conductivity

E_{Ca} data was collected through a third party service (Precision Decisions™) at 3 m swath width across the field using the Geonics™ EM-38 E_{Ca} scanner, giving a sampling intensity of 1 sampling point per 13.6 m². At each sampling point, E_{Ca} was measured at *Shallow* depth (0-75 cm) and *Deep* depth (75-150 cm) and georeferenced with DGPS coordinates with 5 cm accuracy. E_{Ca} data was measured in milli Siemens per meter (mS/m).

3.2.2.4 Geostatistical Interpolation and Data Analysis

The Matern covariance structure was fitted to model the spatial autocorrelation of E_{Ca} data and interpolate to the locations where soil sampling was done. After some iterative curve fitting, a kappa parameter fixed at 0.5 was chosen to construct the theoretical variogram to fit onto the experimental variograms constructed from the shallow and deep E_{Ca} data at both Buttery Hill and Deaton 6. The spatial autocorrelation was assumed to be omnidirectional and the presence of drift was accounted for by fitting a first order polynomial at Buttery Hill. The fitted variograms were then used to predict the E_{Ca} values at the soil sampling locations at both sites using ordinary kriging. The interpolated E_{Ca} values at the positions where soil sampling was done were extracted and appended to soil analysis results. Pearson's Product Moment Correlation Coefficient analysis was used to create a correlation matrix of all variables under consideration to examine the presence of any relationships.

3.2.3 Results

3.2.3.1 General Ranges of Data

Table 12 shows the summary statistics for the variation in a selected set of variables. A relatively high C content of 124.6 g/kg was observed at Deaton 6, reflective of the high organic matter content of the marsh reclaimed soils. In comparison, 12.9 g/kg of C was observed at Buttery Hill. Deaton 6 also had a higher content of N (9.4 g/kg) than Buttery Hill (1.3 g/kg). The two soils had similar levels of K, however, Buttery Hill had a very high content of P (100 mg/kg) compared to Deaton 6 (41 mg/kg). Deaton 6 contained silty clay soils with an average 55% Silt and 39% Clay while Buttery Hill was a sandy loam soil with 66% sand. As

shown in Table 12, substantial differences were observed between ECa₇₅ and ECa₁₅₀ at both sites, with ECa readings increasing with depth at both sites consistently.

Table 12: Summary statistics of major variables considered for analysis

Soil Property	Deaton 6		Buttery Hill	
	Mean	CV ¹	Mean	CV ¹
Clay (%)	38.5	0.19	9.3	0.15
Silt (%)	55.4	0.12	24.6	0.21
Sand (%)	6.1	0.31	66.1	0.09
N (g/kg)	9.4	0.29	1.3	0.12
C (g/kg)	124.2	0.36	12.9	0.12
S (g/kg)	3.3	0.47	0.3	0.12
P (mg/kg)	41.2	0.15	100.0	0.13
K (mg/kg)	291.3	0.27	276.8	0.18
Mg (mg/kg)	185.0	0.29	87.4	0.12
ECa Shallow (mS/m)	17.80	0.23	3.18	0.48
ECa Deep (mS/m)	41.43	0.25	11.23	0.34

1 = Coefficient of variation

3.2.3.2 Variography

Figure 17 and Figure 18 show the fitted variograms at Buttery Hill for ECa₇₅ and ECa₁₅₀ respectively. While an exponential variogram best fitted both ECa₇₅ and ECa₁₅₀ semivariance, ECa₇₅ showed a rougher autocorrelation structure (practical range = 8 m) compared to ECa₁₅₀ (practical range = 180 m). This entailed rapid deterioration in spatial autocorrelation at the surface, as evidenced by the steep increase in semivariance with respect to distance in Figure 17, compared to a slower increase at ECa₁₅₀ (Figure 18). Similar observations were made at Deaton 6, where ECa₇₅ had a lower practical range (125 m) than ECa₁₅₀ (182 m). However, the deterioration in horizontal autocorrelation at Deaton 6 with respect to depth was less obvious, as evidenced by the similar fitted variogram trends in Figure 19 and Figure 20. This suggested that Deaton 6 had more vertically homogeneous soil

than Buttery Hill and the higher practical ranges show a smoother horizontal process governing the properties of the soil compared to Buttery Hill.

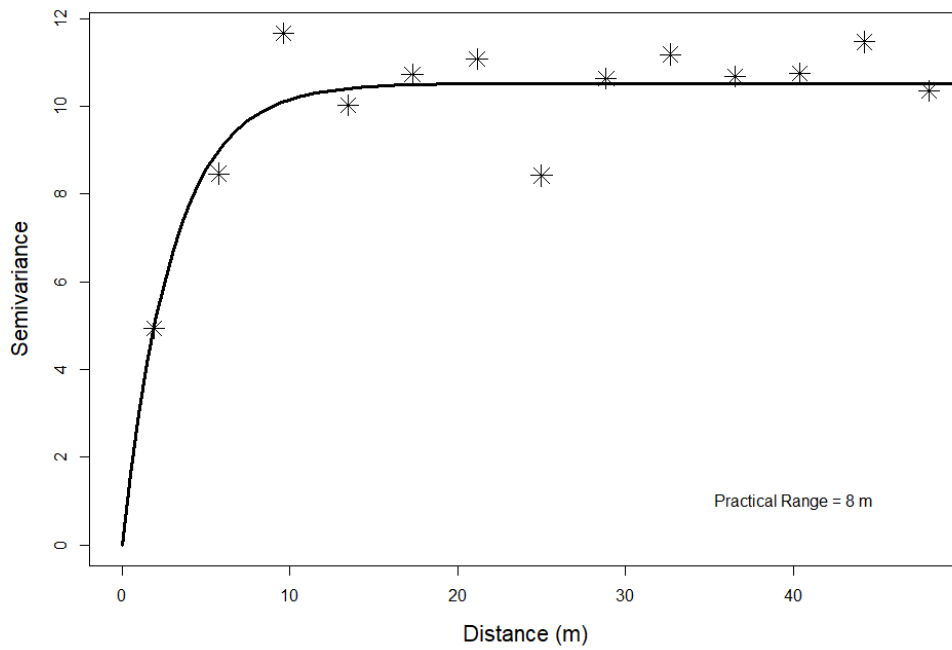


Figure 17: Experimental variogram of apparent electrical conductivity of soil at Buttery Hill in the first 75 cm depth

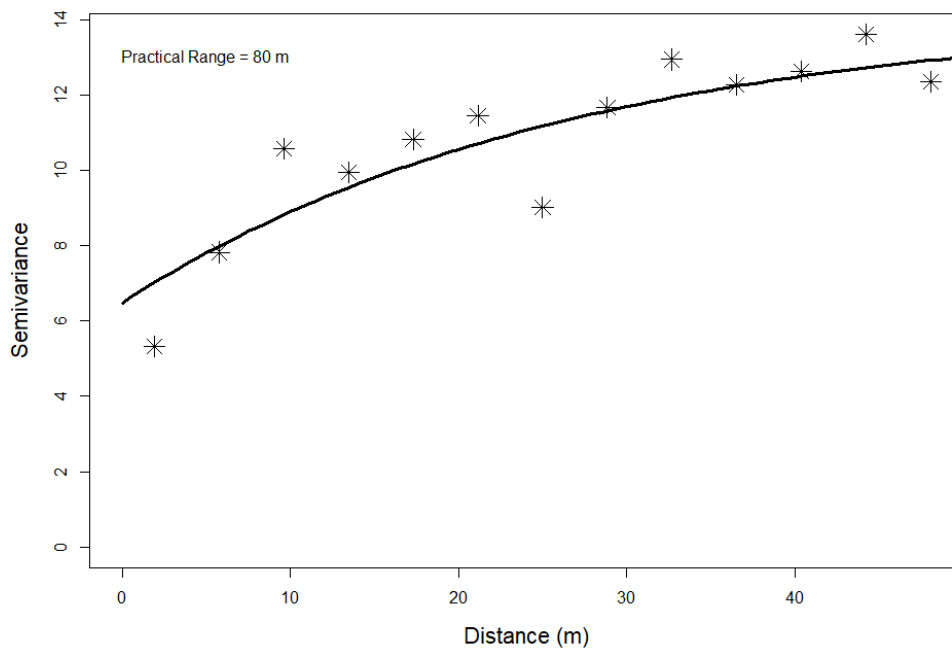


Figure 18: Experimental variogram of apparent electrical conductivity of soil at Buttery Hill between 75 cm and 150 cm depth

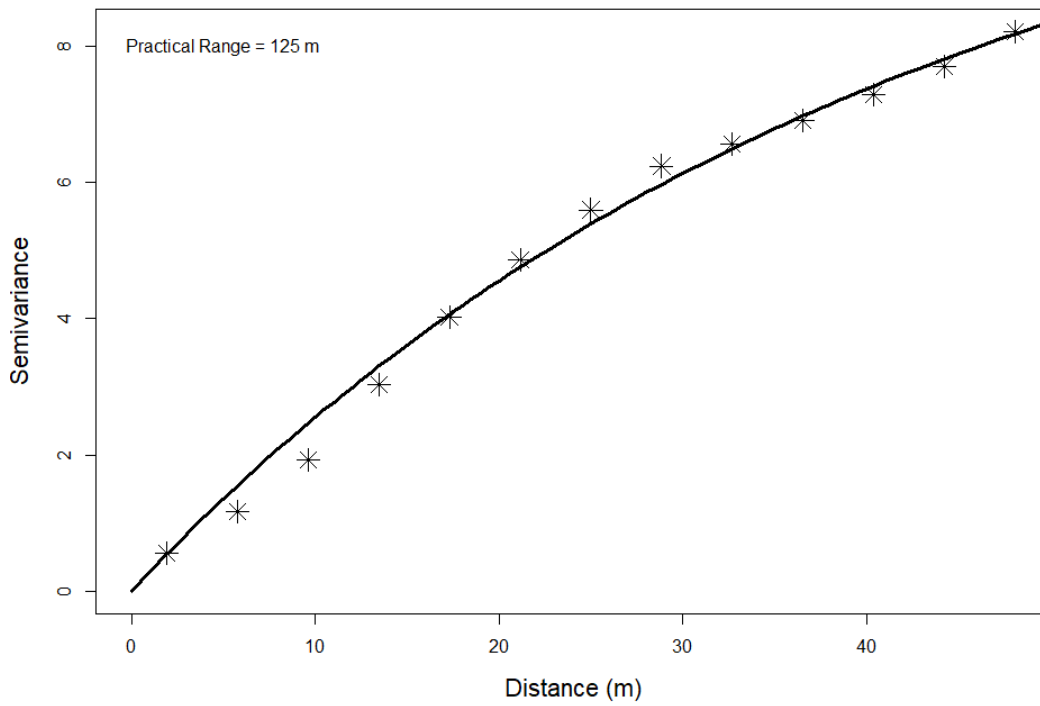


Figure 19: Experimental variogram of apparent electrical conductivity of soil at Deaton 6 in the first 75 cm depth

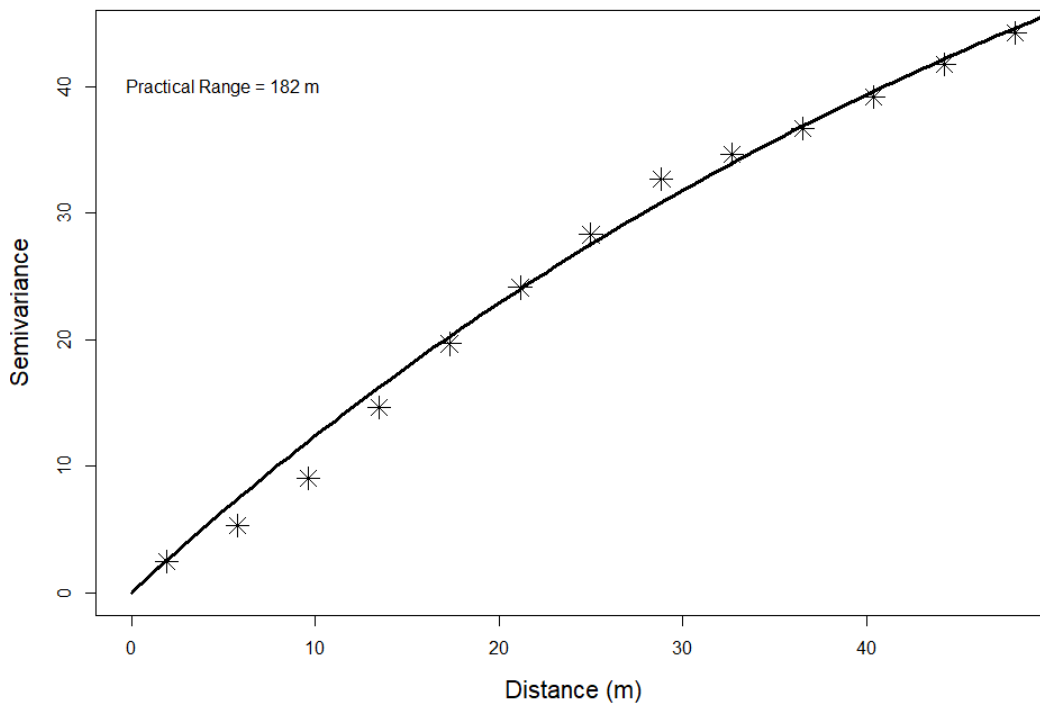


Figure 20: Experimental variogram of apparent electrical conductivity of soil at Deaton 6 between 75 cm and 150 cm depth

3.2.3.3 Correlation between ECa and Soil Properties

At Buttery Hill, strong correlations were observed between ECa and the proportions of sand and silt. ECa₇₅ and ECa₁₅₀ had $r = 0.76$ correlation with silt proportion and $r = -0.73$ with sand proportion (Table 13). This suggested that electrical conductivity reduced with increasing sand proportion and increased with silt proportion. Weak positive correlations were observed between clay proportions and ECa₇₅ ($r = 0.47$) and ECa₁₅₀ ($r = 0.45$). No strong correlations were observed between all measured soil nutrients and ECa at both depths at Buttery Hill. The highest correlation was observed between ECa₇₅ and Mg ($r = 0.33$) but this was a weak and non-significant correlation. No strong correlations were observed between ECa at the two depths and all the soil properties at Deaton 6. Soil nutrients N, C, and S had consistently negative correlations with ECa at both sites but none of the correlations were significant, suggesting against the use of ECa as a proxy to soil nutrient concentrations at these two sites.

Table 13: Correlation coefficients between Apparent Electrical Conductivity and edaphic factors at Buttery Hill and Deaton 6

Soil Property	Buttery		Deaton 6	
	ECaShallow	ECaDeep	ECaShallow	ECaDeep
N	-0.01	-0.05	-0.31	-0.26
Clay	0.47*	0.45*	0.23	0.30
Silt	0.76***	0.76***	-0.21	-0.27
Sand	-0.73***	-0.73***	-0.12	-0.19
C	-0.03	-0.05	-0.26	-0.21
S	-0.07	-0.10	-0.29	-0.24
Ph	-0.18	-0.14	0.22	0.17
P	-0.23	-0.33	0.06	-0.02
K	0.14	-0.01	-0.19	-0.25
Mg	0.33	0.28	-0.20	-0.19

3.2.4 Discussion

The results of the variography show that at ECa_{150} depths where interference from non-edaphic factors is relatively limited, a smoother Gaussian process relative to ECa_{75} depths governs the variation in ECa. This suggests that ECa at this depth is likely governed by soil-forming processes which act on a spatial scale larger than the typical size of the field.

Delbari et al. (2019) equally suggested that spatial variability in soil within a field is partially governed by large scale soil forming processes. Within ECa_{75} , where the potato root zone is likely to be, ECa variability is relatively rougher with a shorter practical range, which may be due to the influence of agricultural activity on soil porosity in the plough layer that alters the water holding and aeration properties of the soil, the main drivers of ECa (Corwin & Lesch, 2005). This is in line with findings by (Minasny & McBratney, 2005), who observed rough spatial autocorrelation in soil, reasonably estimated by the exponential model ($\kappa = 0.5$). However, Minasny and McBratney also observed a smooth process governing ECa ($\kappa = 3$), though they attribute this finding as an artefact of their data collection process where measurements overlapped and the depth of the ECa scan was not apparent from their report. The implications of a rough autocorrelation are that a high sampling intensity is required to produce credible maps of spatial variation. Higher ECa scanning intensities are likely to come with cost, therefore the potential utility of ECa depends on whether useful correlations can be established with soil nutrients.

In line with widely reported observations (Cambouris et al., 2006; Perron et al., 2018; Valente et al., 2012), no strong correlations were observed between ECa and any soil Macronutrients at either site. Perron et al. (2018) found that ECa was more influenced by physical properties (texture and water content) than nutrient concentrations, in agreement with the findings at Buttery Hill. However, despite the large variation in the particle size distribution at Deaton 6 (Sand CV = 0.31), the textural classes showed no significant correlation to ECa. These results are similar with observations by Perron et al. (2018) where ECa was strongly related to soil texture properties in one field and not correlated in another field. These results show the contextual nature of ECa and why understanding the locally contributing edaphic factors is important before it can be used for agronomic recommendations on soil management.

The correlations between ECa, and sand as well as clay observed at BATTERY Hill agree with the findings of Cambouris et al. (2006) and Perron et al. (2018). In both studies, sand concentrations were generally negatively correlated to ECa, with Perron et al. (2018) finding similar correlations to observations in the current study. In line with both Cambouris et al (2006) and Perron et al. (2018), clay concentrations were positively correlated to both ECa₇₅ and ECa₁₅₀, at both current sites. Additionally, although Deaton 6 had very high C content with very high variability (CV = 0.36), no significant correlation with ECa at any depth was observed. Cambouris et al. (2006) also report no significant effect of organic carbon on ECa. In agreement with Cambouris et al. (2006), Perron et al. (2018) found that ECa was more influenced by physical properties (texture and water content) than nutrient concentrations. It must be noted that the Cambouris et al. (2006) experiment was done in soils with a mean of 2.4% organic C and 80% sand, while in the Perron et al. (2018) study, the total C percentage was 2.1 ppm and 3.41% sand. These low C and high sand values partly explain the differences in the significance of C from this study and further strengthen the case for interpreting ECa data side-by-side with soil nutrient data.

3.2.5 Conclusion

The observations showed that ECa is a poor predictor of soil nutrients, suggesting that the premise of using ECa as a proxy to soil nutrient variation is likely only plausible in some contexts and cannot be generalized. ECa was shown to be a spatially rough process at the top soil but the autocorrelation becomes smoother with a longer practical range as depth into the soil is increased. This entails the need for high intensity sampling in precision agriculture (up to 8 metre swath widths to cover the range of autocorrelation observed in this study) in order to produce accurate maps. However, the low correlations between ECa and soil Macronutrients show that this approach only has limited applicability in the production of high-resolution soil nutrient maps without case-by-case data analysis. Adoption of this approach in a typical commercial precision agriculture would therefore require bespoke investigations on the nature of the relationship between ECa and soil nutrients at each location.

CHAPTER 4 - Applying Colour-Based Feature Extraction and Transfer Learning to Develop a High Throughput System for detecting Potato (*Solanum tuberosum L.*) Stems with Images from Unmanned Aerial Vehicles after Canopy Consolidation.

Abstract

Potato (*Solanum tuberosum*) stem density variation in the field can be used to inform harvest timing to improve tuber size distribution. Current methods for quantifying stem density are manual with low throughput. This study examined the use of Unmanned Aerial Vehicle imagery as a high-throughput alternative. A colour-based feature extraction technique and a deep convolutional neural network (CNN) were compared for their effectiveness in enumerating apical meristems as a proxy to subtending stems. Two novel colour indices, named the Cumulative Blue Differences Index and Blue Difference Normalized Index, showed significant differences ($P < 0.001$) between meristematic leaves and mature leaves in comparison to other indices. The two indices were used to generate 500 pseudo-labelled human-corrected images as training data for the CNN. Benchmarked against a human labelled test dataset, the CNN performed better with a normalized Root Mean Square Error (nRMSE) of 0.09 than the sole use of the image analysis algorithm (nRMSE = 0.3) in predicting the number of meristems in a canopy at 52 days after planting. Furthermore, the CNN had better precision (Intersection over Union [IOU]: 0.49 and 0.56, respectively) than the image analysis algorithm (IOU: 0.33 and 0.13, respectively). Meristem counts in both approaches showed a linear relationship with actual subtending stem counts ($P < 0.001$). This study demonstrates the validity of using traditional image analysis and CNNs to generate meristem detectors with acceptable nRMSE. Transfer learning with CNN is proposed for developing meristem detectors for evaluating stem density variation from UAV images in the field.

4.1 Introduction

At emergence, Potato (*Solanum tuberosum* L.) seed tubers produce variable sprout numbers depending on the physiological status of the seed, which results in variable stem numbers per potato plant (Knowles & Knowles, 2006). Estimation of spatial variation in plant density is important in potato production, with several studies linking it to tuber size and total yield variations at harvest (Bleasdale, 1965; Gray, 1972; Knowles & Knowles, 2006; Love & Thompson-Johns, 1999; Wurr, 1974). Potato growers normally have a market-determined target range of optimum tuber size, outside of which the value of the produce declines. Therefore it is in the interest of growers to determine the factors that cause tuber size variation in the field and tailor management practices to mitigate the effects.

At the stem level, a negative correlation between potato stem density and mean tuber size has been widely recognized (Goesser et al., 2012; Shayanowako et al., 2015) and predictive models have been produced to describe potato tuber size distribution using stem density as a covariate (Bussan et al., 2007). To counteract the negative effect of stem density on average tuber size, several studies propose delayed harvesting to prolong tuber bulking period as a strategy to increase tuber size (O'Brien & Allen, 1992; Rejbarz et al., 2015; Waterer, 2007).

With this background, there is interest in techniques for quantifying stem density within an actively growing crop to enable spatially and temporally variable downstream crop management like vine desiccation, in order to maximize yield within desired tuber size classes. Manual stem counting in randomly or systematically selected quadrants around the field give approximations of stem densities which can be geospatially interpolated to the whole field, however this is a laborious, sometimes destructive, and a low throughput method. The validity of data interpolation relies on assumption of a random distribution of stem numbers or the unpredictable chance of establishing enough spatial autocorrelation in stem numbers to model the variation with minimal error, which is not always possible.

Using the spectral reflectance of potato plants to determine stem numbers from canopies is a potential approach for estimating accurate stem density from RGB or multispectral sensors mounted on Unmanned Aerial Vehicles (UAVs). This approach offers a high-throughput solution to estimate variation in stem population across the entire field without interpolation. Potato stems terminate with leaf primordia forming the growing tip of the

stem, which sometimes convert to floral primordia depending on the variety (Firman et al., 1995). The leaf primordia therefore represents a distinct unit which can be used to estimate the total number of stems in a closed canopy. Plant canopies exhibit unique, species-dependent, responses to incident radiation, generally showing high absorption in the ultraviolet and Blue (490–450 nm), high reflectance in the Green (560–520 nm), high absorption in the Red (700–635 nm) and high reflectance in the near-infrared portions of the electromagnetic spectrum (800-2500 nm) (Gates et al., 1965). Variability in chlorophyll content, water content and cell-to-air space ratio in the leaves directly influences spectral reflectance of plants in the visible (400-700 nm) range (Cochrane, 2000), which can enable the use of computer vision and image analysis techniques to decompose consolidated crop canopies and enumerate features of interest based on their spectral reflectance.

Multispectral sensors with the near-Infrared band operating around 750 - 850 nm, enable the use of well-defined vegetation indices like the Normalized Difference Vegetation Index (NDVI) to assess and classify crop canopy components. Sankaran et al. (2017) used NDVI to extract and count emerging potato plant clusters from images taken at 15 metres above ground using a UAV at 32 days after planting with R^2 values of up to 0.82 when regressed to manual plant counts. However, predictive power was lost as the canopy gradually consolidated at 43 days after planting. The most widely used colour index for individual green plant segmentation from canopy remote sensing data is the Excess Green Index (ExG), first proposed by (Woebbecke et al., 1995). The index has been used, in combination with other indices, for enumerating plant stands in wheat (Jin et al., 2017), rapeseed (Zhao et al., 2018), and in potatoes (Li et al., 2019), where the index was used to detect potato plant clusters at emergence. These techniques provide sufficient accuracy for counting clusters of stems from the same mother tuber at emergence before canopy closure. However, individual stem enumeration after full crop establishment, which is the level of accuracy required in precision farming for variable desiccation management, has not yet been reported.

This study hypothesized that a colour index to extract clusters of leaf primordia and enumerate them as a proxy to actual stem counts would potentially offer a solution. Following the spectral properties of plants outlined in Gates et al. (1965), an ideal colour index would be one that is sensitive to the differences between Blue and Green reflectance

since the growing tips have less chlorophyll, thereby exhibiting lower reflectance in the Blue range compared to older leaves. The performance of object detectors based on image colour calculations depends on the acquisition of high quality imagery with optimum light conditions which are not always possible in the field. A deep learning approach therefore potentially presents a more robust approach with respect to variation in image quality. Ground-truth labelled data is essential in deep learning training pipelines and forms the basis of model evaluation in so called supervised learning models. Labelling a large dataset of leaf primordia from closed canopies has a large time cost as it requires expertise in identifying irregular leaf primordia. Semi-supervised learning therefore becomes a potentially important solution. Pseudo-labelling is a widely used technique to train Convolutional Neural Networks from non-labelled data with high accuracy. It involves the generation of an accurate model from a limited labelled dataset then using the model on unlabelled data and selecting all predicted labels that have high confidence as new labels, which helps to expand the labelled dataset.

The objective of this study was to use the spectral properties of plants in the visible wavelengths to develop colour indices for enhancing primordial features in canopies and use them to infer variation in actual stem number. The study also tested the use of colour indices for developing an automatic labelling algorithm for generating a training dataset for transfer learning using "Faster Regions with Convolutional Neural Network" (FRCNN) to generate a robust potato meristem detector for inferring variations in stem number.

4.2 Materials and Methods

4.2.1 Feature Engineering: Development of Colour Indices

4.2.1.1 Data Acquisition

Development and evaluation of colour indices was conducted using potato canopy imagery collected from Harper Adams University, Shropshire, England (52°46'26.8"N, 2°25'48.9"W) on a dark brown stone-less sandy loam soil. The images were collected from Amora and Maris Piper varieties at 91 and 50 days after planting respectively as shown in Table 14.

Table 14: Specifications of Unmanned Aerial Vehicle cameras and crop stage used in the study

Location	Camera Description (Alias)	Variety	DAP
Colour Index Development			
HAU, Shropshire, England	DJI™ Mavic Air UAV equipped with a 1/2.3-inch CMOS sensor producing 12 MP still images at 88° FOV (Mavic)	Amora	91
HAU, Shropshire, England	DJI™ Inspire equipped with a Zenmuse X3 Camera equipped with 1/2.3-inch CMOS sensor producing 12.4 MP still images at 90° FOV (Inspire)	Amora	91
HAU, Shropshire, England	3DR Solo UAV mounted with a Mapir™ Survey 3N Camera with a Sony Exmor™ R IMX117 sensor, f/3.0 Aperture and 41° FOV (Mapir)	Amora	91
HAU, Shropshire, England	3DR Solo UAV mounted with a GoPro™ Hero 3+ Black Edition camera equipped with a 1/2.3-inch sensor with 12 MP and a fisheye lens with a 94.4° FOV (GoPro)	Maris Piper	50
Model Training Data			
HAU, Shropshire, England	Phantom 4 pro UAV equipped with a Hasselblad L1D-20c aerial camera with a 1 inch CMOS sensor producing 20 MP still images at 70° FOV	Maris Piper	48
HAU, Shropshire, England	Phantom 4 pro UAV equipped with a Hasselblad L1D-20c aerial camera with a 1 inch CMOS sensor producing 20 MP still images at 70° FOV	Pentland Dell	48
HAU, Shropshire, England	Phantom 4 pro UAV equipped with a Hasselblad L1D-20c aerial camera with a 1 inch CMOS sensor producing 20 MP still images at 70° FOV	Amora	82
Model Testing Data			
Shawbury, Shropshire	Mavic Air UAV equipped with a 1/2.3-inch CMOS sensor producing 12 MP still images at 88° FOV at 20 m attitude.	45 different varieties (see Appendix B)	52

MP=Mega pixels. CMOS = complementary metal-oxide-semiconductor. FOV = Field of View, DJI = Dà-Jiāng Innovations™, Shenzhen, China. HAU = Harper Adams University, DAP = Days after planting.

Four different cameras, with varying sensor sizes and resolutions were used to generate variable sensor sharpness and colour resolving power. This enabled evaluation of the ability of the colour indices to distinguish meristem and old leaf pixels at different sensor

sharpness and colour resolving powers so as to select the indices with the most consistent performance across sensors. The crops were grown using standard UK commercial practices for all inputs. For the Amora variety, the aerial images were captured with 4 different visible light (Red, Green and Blue) sensors on UAV systems as outlined in Table 14. The Maris Piper crop was added to increase variation in the dataset as well as capture soil background because the canopy had not fully consolidated to cover the soil. Additionally, the Maris Piper images were collected on a day where the field was partially irrigated, providing the option of sampling pixels from both dry and wet soil. The captured images were manually evaluated to exclude pictures with distortion or blur due to UAV speed and a total of 5 images were selected from each camera, resulting in 20 images from which colour indices were evaluated.

All image processing was done using Matlab™ R2020a. From each image, pixels from Meristems, Mature Leaves, wet Soil and Dry Soil features were manually selected, and reflectance values for Red, Green and Blue were extracted. For each canopy feature, grayscale values were calculated from all selected pixels and the first 25 pixels from either side of the mean were selected to create 50 pixels per feature per camera. The final dataset for the evaluation of colour indices therefore contained 500 labelled data points of features with their Red, Green and Blue values.

4.2.1.2 Visible Light Colour Index Selection

Several colour indices were evaluated, with inclusion based on a literature search of widely used visible light spectrum indices as shown in Table 15. To provide context, Figure 21 shows an aerial view of a typical potato plant as well as how the growing tips of stems are expressed.



Figure 21: An aerial view of a typical potato plant (left) with labelled locations of stem growing tips that a vegetation index or object detection model are expected to elucidate (right)

The ExG is most widely used for segmenting vegetation against soil background, however there is no publicly available evaluation of its potential for differentiating leaf age, health or stress. Other indices included the Excess Red (ExR) Index for automatic segmentation of vegetation from soils, the difference between the Excess Green and Excess Red (xGxR), the Colour Index of Vegetation Extraction (CIVE) and the Excess Blue index (ExB), which is analogous to the ExR index. The Normalized Difference Green Redness index (NDGR), normally used for enhancing the contrast between red backgrounds and vegetation was also considered.

Following the spectral reflectance properties of meristematic leaves described by Gates et al. (1965), it was hypothesized that the difference between Blue and Red, and Blue and Green reflectance at the pixel level would have the highest potential for maximizing contrast between meristems and older leaves. It was expected that meristematic pixels would reflect more Red than Blue while mature leaves would reverse this order due to darkening of the leaf as chlorophyll accumulated. Due to the darker hue of soil, it was assumed that soil pixels would exhibit negligible differences in reflectance among the three light bands. Two novel indices were therefore derived based on these premises. The Red to Blue difference was plotted against the Green to Blue difference using all the selected pixels from section 4.2.1.1 as data points.

Table 15: Descriptions and functions of popularly cited and custom colour indices based on standard Red, Green and Blue bands.

Index Name	Formula	Source
Excess Green	$ExG = 2G - R - B$	Woebbecke et al. (1995)
Excess Red	$ExR = 1.4R - G$	Meyer and Neto (2008)
Excess Green minus Excess Red	$ExG - ExR = 3G - 2.4R - B$	Meyer and Neto (2008)
Colour Index for Vegetation Extraction	$CIVE = 0.441R - 0.811G + 0.385B + 18.78745$	Kataoka et al. (2003)
Excess Blue	$ExB = 1.4B - G$	Guijarro et al. (2011)
Normalized Difference Green Index	$NDGR = \frac{R-G}{R+G}$	Bannari et al. (1995)
Cumulative Blue Difference Index	$CBDI = R + G - 2B$	Generated in this study
Blue Difference Norm Index	$BDNI = \sqrt{(R - B)^2 + (G - B)^2}$	Generated in this study

Visual observations showed that the Manhattan Distance or Euclidian Norm of each point as a vector from the Cartesian origin would provide an index that maximizes the difference between meristems and non-meristems. These two distances were therefore simplified into linear expressions, with the Manhattan distance termed as the Cumulative Blue Difference Index (CBDI) and the Euclidian Norm termed as the Blue Difference Norm Index (BDNI).

All colour indices were calculated for all pixel features. The resulting dataset was comprised of pixels as observations, the four features as factors and the 8 colour indices as continuous independent variates. Differences in means from sensors which only contained Meristem and Leaf features were analysed using the T-Test while data from the GoPro sensor, which contained dry and wet soil features apart from the canopy vegetation features, was analysed by ANOVA using R version 4.0.2 (R Core Team, 2020) adopting a Completely Randomized Design. Means were compared using Fisher's unprotected Least Significant Difference. The colour indices with significant highest differences in index value between meristematic and other features were selected for further analysis.

Following selection of colour indices, an algorithm was designed to estimate the number of stems in an image using Matlab™ R2020a. Briefly, the model consisted of (1) K-means clustering for segmenting the image into foreground pixels of interest and background pixels and (2) establishing an objective process for consolidating fragmented pixels of leaflets into single meristem units. These two components were used to create and test a feature-extraction and object detection process as illustrated in Figure 22.

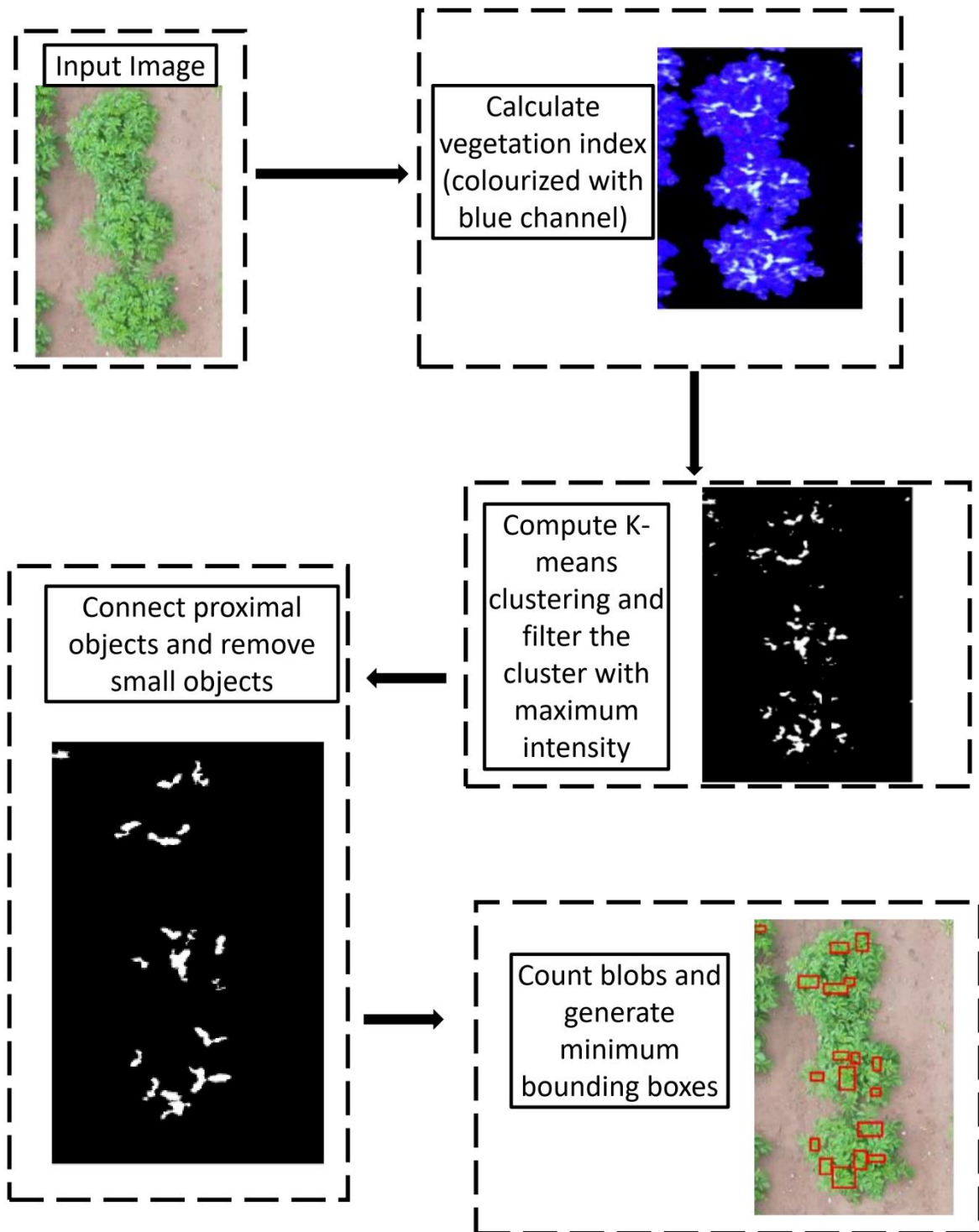


Figure 22: Flow chart of the image analysis algorithm for generating meristem objects and inferring stem number

4.2.2 Image Segmentation using k-Means Clustering

Both Otsu-based and adaptive threshold methods have been extensively reported in literature for green vegetation segmentation, but they perform poorly in images where the frequency of target and non-target pixels does not result in a bi-modal distribution of intensities (Yang et al., 2012). The growing tips constitute a small percentage of the image area in comparison to the rest of the canopy and non-canopy features. Consequently, intensity histograms from indices that maximize the reflectance of meristems against all other features like the CBDI and BDNI are expected to follow an exponential decay, which renders Otsu-based threshold selection unreliable for effective segmentation.

Since the images predominantly contained 3 object classes (i.e. Soil, and the non-meristem canopy component as background and the meristems as the foreground), k-means clustering with three means was applied as the most appropriate method for clustering the three classes and segmenting the foreground without computation of a threshold. Using k-means clustering for segmentation is effective to separate object classes by minimizing the intra-class squared distance (Hartigan & Wong, 1979), and is widely applied in foreground segmentation in canopy images collected from UAVs and remote sensing systems (Chen et al., 2019; Cinat et al., 2019; Sun et al., 2019). Accordingly, the pixel with the maximum greyscale intensity in each image was identified, then k-means clustering was performed on each image and the cluster containing the identified pixel was chosen to represent the meristems. The image was then binarized with the selected cluster as foreground and all other clusters as background.

4.2.3 Noise Reduction and Final Bounding Box Generation

Due to the compound nature of potato leaves, the k-means-based segmentation produced unconsolidated meristem objects. Therefore, it was necessary to consolidate unconnected meristem pixels that belonged to the same stem to minimize the chances of double-counting, while ensuring that meristems belonging to adjacent stems were not wrongly attributed. Morphological operations like erosion or dilation have the risk of consolidating some independent but proximal objects in a binary image (Pesaresi & Benediktsson, 2001). To avoid this, a custom noise reduction technique was created by shrinking every binary object in the image to its centroid pixel, followed by a pixel-wise iterative range search to index all other pixels located within a Euclidian distance that corresponded to the average

size of a stem in the image. The average size of a stem at the plot level was estimated by calculating the average number of pixels per foreground object in each binary image. As a result, all pixels located in close proximity to each other were indexed together and considered to originate from the same primordia, then joined together. Pixels that were separated by a distance more than the estimated average stem size were not connected and constituted separate instances of a meristem. The number of connected components was then used as an approximation of the number of stems in the image and a minimum bounding box was generated to approximate the location and size of each stem, signalling the end of the algorithm. The flow chart of the algorithm was as illustrated in Figure 22.

4.2.4 Development of a Transfer Learning Model

An aerial survey with a UAV was conducted at Harper Adams University on 09th June 2020 to develop a model training dataset of images images collected at 15 m altitude using a Phantom 4 pro UAV as specified in Table 14. Varieties covered in the survey were Maris Piper (0.5 ha) and Pentland Dell (0.5 ha) at 48 days after planting and Amora (9.4 ha) at 82 days after planting. The images were then cropped into 500 images of 500 pixels wide and 1500 pixels long then processed using the developed algorithm to generate bounding boxes around proposed potato meristems. The generated bounding for each of the 500 images were inspected and corrected manually by deleting erroneous detections and adjusting the extent of each valid box to fit the extent to which a human would label the data. Wu et al. (2020) emphasize on the computational constraint of training FRCNN object detectors from large UAV images, in their case 5472 X 3648 pixels, which necessitated the cropping of their images to 1000 X 800 pixels for optimized computation. The sensor used in this study produced 5472 X 3648 pixels, which were cropped to 1500 X 500 pixels to approximate the size of each plot in a compiled test dataset. All generated bounding boxes were stored as pseudo-labels to create a training dataset for deep learning with a CNN.

Fuentes et al. (2017) tested the Visual Geometry Group's (VGG-16) CNN (Simonyan & Zisserman, 2015) against deeper residual networks in the similar task of deep feature extraction of disease-caused leaf colour changes in tomatoes and found that the VGG-16 performed better than the deeper networks with up to 83% mean average precision. To keep the number of network backbone layers minimal for producing the simplest model with faster training times, A FRCNN model (S. Ren et al., 2015) with the VGG-16 network

backbone and ImageNet weights was chosen. FRCNN is a unified framework that learns an object region proposal network from a CNN feature map, classifies each proposed region and localizes the class of the object within the region with the introduction of anchor boxes, from which object bounding boxes are learnt and refined by regression. To convert a VGG-16 CNN into a FRCNN object detector, a region proposal network was trained on the final convolutional feature map and the last max pooling layer was replaced by an ROI-max-pooling layer after which FRCNN's classification and box regression layers were added to achieve object detection and localization. The training was conducted on an Nvidia GeForce GTX 1070 GPU with 8 GB Video RAM for 11 hours. The model was trained with a fixed learning rate of 0.0001, a single image mini batch size and 48 anchor boxes. The anchor boxes used in this study were predetermined iteratively by estimating an increasing number of anchor boxes and their sizes with each iteration, then checking their IoU with the ground truth data using the *estimateAnchorBoxes* function in Matlab™ R2020a. The final number and size of anchor boxes was chosen by observing the asymptote of the scatter plot of the determined IoU against the number of anchor boxes. Loss was optimized using the stochastic gradient descent with 0.95 momentum. The model converged after 50000 iterations in 100 epochs. The flow chart of the training pipeline is as illustrated in Figure 23.

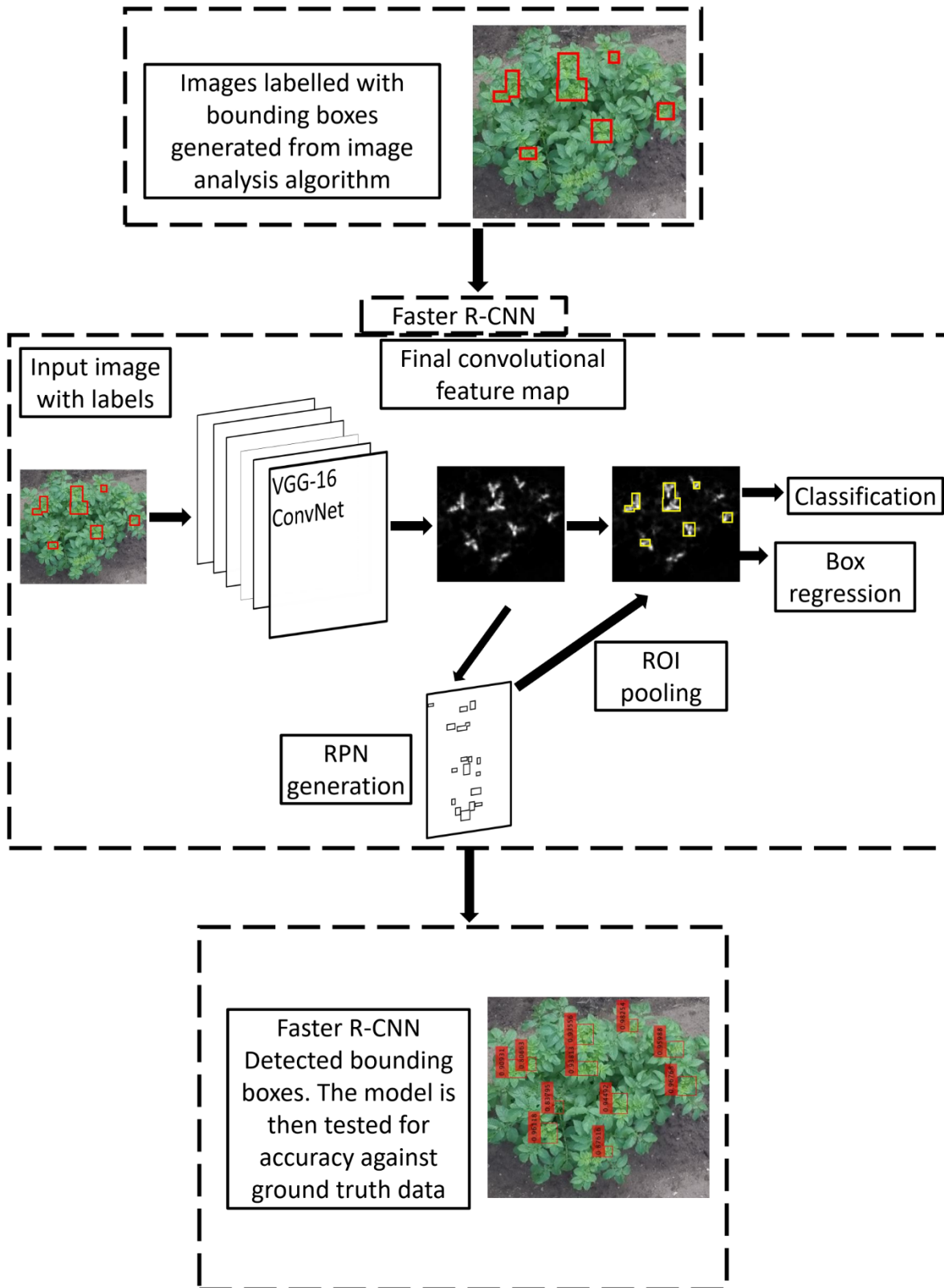


Figure 23: Flow chart of the Faster R-CNN algorithm for training a potato meristem object detector

4.2.5 Model Testing

4.2.5.1 Data Acquisition

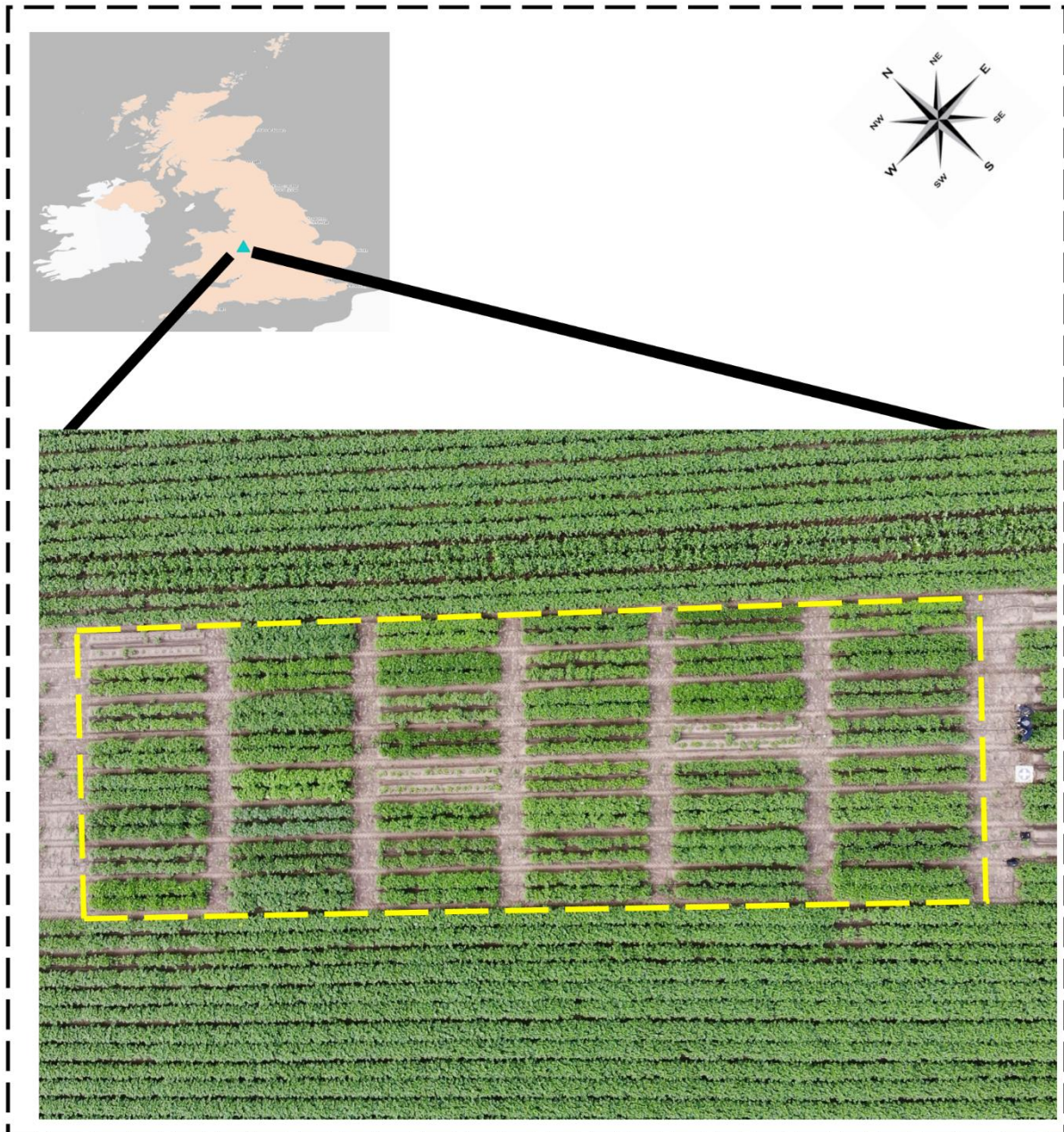


Figure 24: Aerial image of the testing site for the image analysis and convolutional neural network algorithms

The traditional image analysis algorithm and the deep learning model were tested for performance accuracy using a testing dataset of images collected from 45 potato varieties (see Appendix B for a list of the varieties) grown at Eaton Upon Tern Runway (Figure 24),

Shawbury, Shropshire, England (52°48'19.3"N, 2°30'41.8"W) on a Clayey Loam soil. The potato varieties came from the four determinacy classifications (Group one to four) and some varieties were non-classified by determinacy. Twenty Seven of the 45 varieties were drawn from the top 50 varieties grown in the UK in 2019 in terms of area planted. The varieties acted as a source of variation in stem numbers per unit area and canopy colour intensity. Differential performance between varieties was not considered in order to generalize model accuracy across varieties. The 45 varieties were planted on 29/04/2019, uniformly managed throughout the season and harvested on 10/09/2019. The ground-truth number of above ground stems was manually determined on 10/09/2019 before harvest. The number of visible meristems on top of the canopy was also manually counted. To create the model testing image dataset, two adjacent rows of 5 metres each per variety were imaged on 20/06/2019 at 52 days after planting at 20 m altitude using a Mavic Air UAV as specified in Table 14.

4.2.5.2 Image Processing and Data analysis

The aerial images were cropped manually around each of the 45 varieties plots to create an image for each plot for analysis then bounding box labels were manually defined for all meristems in each cropped image using Matlab™ R2020a's "image labeller" application. For each image in the test set, meristem counts were generated using the image analysis algorithm and the FRCNN model then compared to the manually counted number of meristems. Bounding boxes were generated from the two predictive models. For each image representing a plot, the bounding boxes for the ground truth, FRCNN detections and image analysis detections were converted into binary masks then confusion matrices were computed for the two detection models against the ground truth. The rates of true positives (TP) and false positives (FP) were computed for each of the 45 plots from confusion matrices. From these metrics, classification precision, as a measure of model performance, was computed as follows:

$$Precision = \frac{True\ Positives}{True\ Positives + False\ Positives} \dots\dots\dots (16)$$

Precision was chosen over Recall and F1-score metrics because the image analysis approach was based on the detection of minor colour aberrations at the apex of the plant. This meant that bounding boxes for the image analysis approach were expected to be smaller than the

human-verified ground truth where shape features that distinguish a meristem from older leaves were identified and the bounding boxes expanded. This was projected to cause a high rate of false negatives which would penalize Recall and subsequent F1-scores and therefore, the precision metric was used. The most important output of the model for practical decision support is the detection of the presence of a meristem for calculating stem density, while its size and extent are secondary considerations. Furthermore, the Intersection over Union (IoU) was calculated as follows:

$$\text{Intersection Over Union} = \frac{B_1 \cap B_2}{B_1 \cup B_2} \dots\dots\dots (17)$$

Where B_1 represents the ground truth and B_2 represents the predicted bounding boxes from the two models.

The final dataset contained the variety, breeder, the number of manually counted above ground stems, number of manually counted meristems, and the number of meristems predicted by the image analysis and FRCNN approaches. Observed vs Predicted plots were plotted for each prediction against the ground truth data to examine the residuals then the Root Mean Square Error (RMSE) was calculated for each model as follows:

$$RMSE = \sqrt{\sum_{i=1}^n \frac{(\text{Predicted} - \text{Observed})^2}{n}} \dots\dots\dots (18)$$

The RMSE was divided by the mean of the observed stem or meristem counts to calculate the normalized RMSE (nRMSE).

4.3 Results

4.3.1 Feature Engineering and Selection of Appropriate Indices

When the difference between Green and Blue light was plotted against the difference between Red and Blue light, grouped by the pixel source, four distinct clusters were visually discernible in Cartesian space. The data points of the meristems clustered in the first quadrant, the mature leaf data points clustered in the second quadrant while the two soil sources clustered near the origin (Figure 25). Upon visual assessment (Figure 25), the meristem data points were clustered at the largest Euclidian distance from the origin, followed by mature leaves. From this assessment, the CBDI and BDNI were considered to have potential to represent the overall variation linearly and guaranteeing that the

meristematic pixels would be at the maxima of this variation's range, therefore enabling a predictable threshold selection. The CBDI and BDNI were calculated and compared with established RGB-based colour indices.

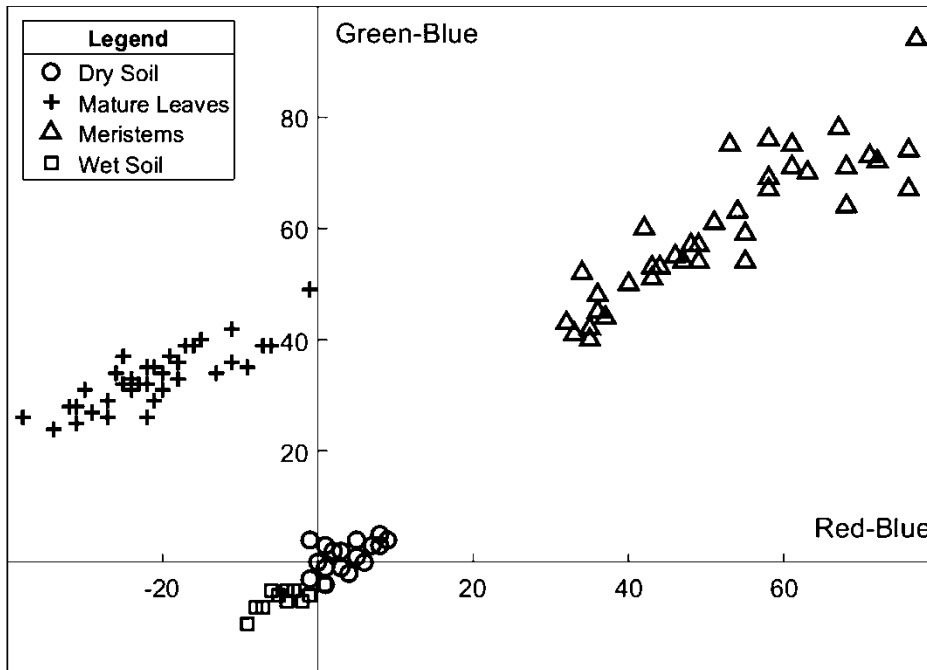


Figure 25: The difference between Green and Blue colour plotted against the difference between Red and Blue colour in pixels selected from four prevalent features in a potato canopy

All the colour indices exhibited significant statistical differences between pixels from meristems and older leaves in mean intensity values ($P < 0.05$), a trend sustained across all sensor types except for the ExR in the Mapir camera (Table 16). This suggests that the features of interest occur in exclusive quantiles of the range of each index, and therefore a k-means clustering approach would adequately segment the image into meristems and background, eliminating the need for determination of a subjective threshold. To maximize the chances of accurate segmentation, it was necessary to select colour indices that maximize the value of the meristematic pixels while maintaining a large separation with all other features. To achieve this, the separation between the maximum and minimum quantile of mature leaves and meristems was evaluated and the percentage overlap was calculated, with the aim of selecting the colour index with the largest difference between the values of meristem and non-meristem features.

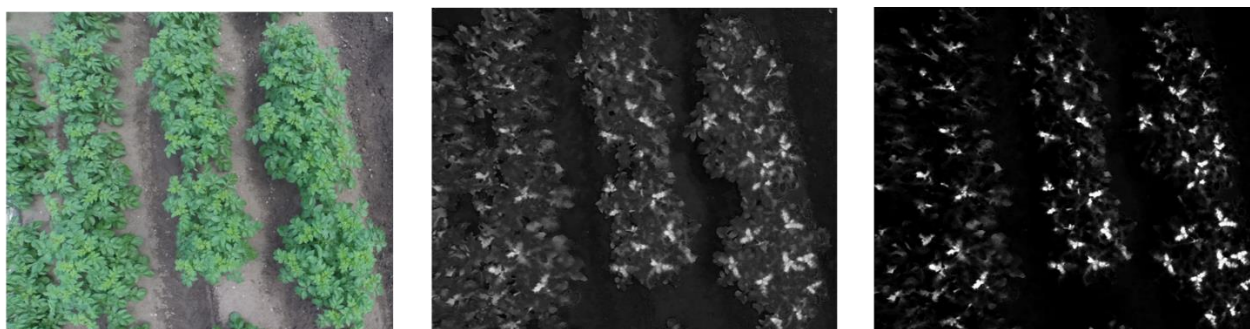


Figure 26: Examples of the blue difference normalized index (middle) and the cumulative blue difference index (right) applied to an aerial image of a growing potato crop (left)

Figure 26 shows examples of the CBDI and BDNI applied to a potato canopy image. Of all the colour indices, the BDNI (Figure 27-a) and CBDI (Figure 27-b) had the most consistent maximization of the index values for meristematic pixels, with distinct visual separation between the targeted and background features in boxplots of the indices. Boxplots of ExG, (Figure 27-c) and CIVE (Figure 27-d) showed an overlap of index values between the mature leaves and meristems. The minimum quantiles of meristematic pixels were consistently higher than the maximum quantiles of the mature leaves in only the CBDI and BDNI (Table 16). The opposite trend was consistently observed in the ExB, where the meristematic pixels had negative values due to a Blue colour deficit while the soils and mature leaves had excess Blue, resulting in a positive index, except in the Mavic and Mapir images. Unlike the EXG-ExR (Figure 27-e), NDGR (Figure 27-f) ExR (Figure 27-g), indices, the ExB index (Figure 27-h) achieved a linear positioning of features that would enable clustering. However, there were overlaps in the index values of meristem and mature leaf features from images obtained with all cameras except the GoPro, with the Inspire having a 28% overlap (Table 16).

As illustrated in Table 16, the performance of the indices was consistent across camera type used to collect the data. Index values of the features of interest overlapped in 6 out of 8 indices in images taken with the Mapir Camera. The Mavic, Inspire and GoPro cameras had overlaps in five, four and two indices respectively. The ExG index consistently showed overlapping in all the cameras while the CBDI and BDNI indices only overlapped in the Mapir camera images. Based on this analysis, the CBDI and BDNI were chosen for use in the k-means clustering.

In all further images, the two indices were calculated at each pixel and the resulting images normalized to 8-bit range then the two indices were combined into a single channel by averaging. The resultant grayscale image was then used for k-means clustering and subsequent stem count generation and bounding box approximation for both the image analysis and FRCNN approaches.

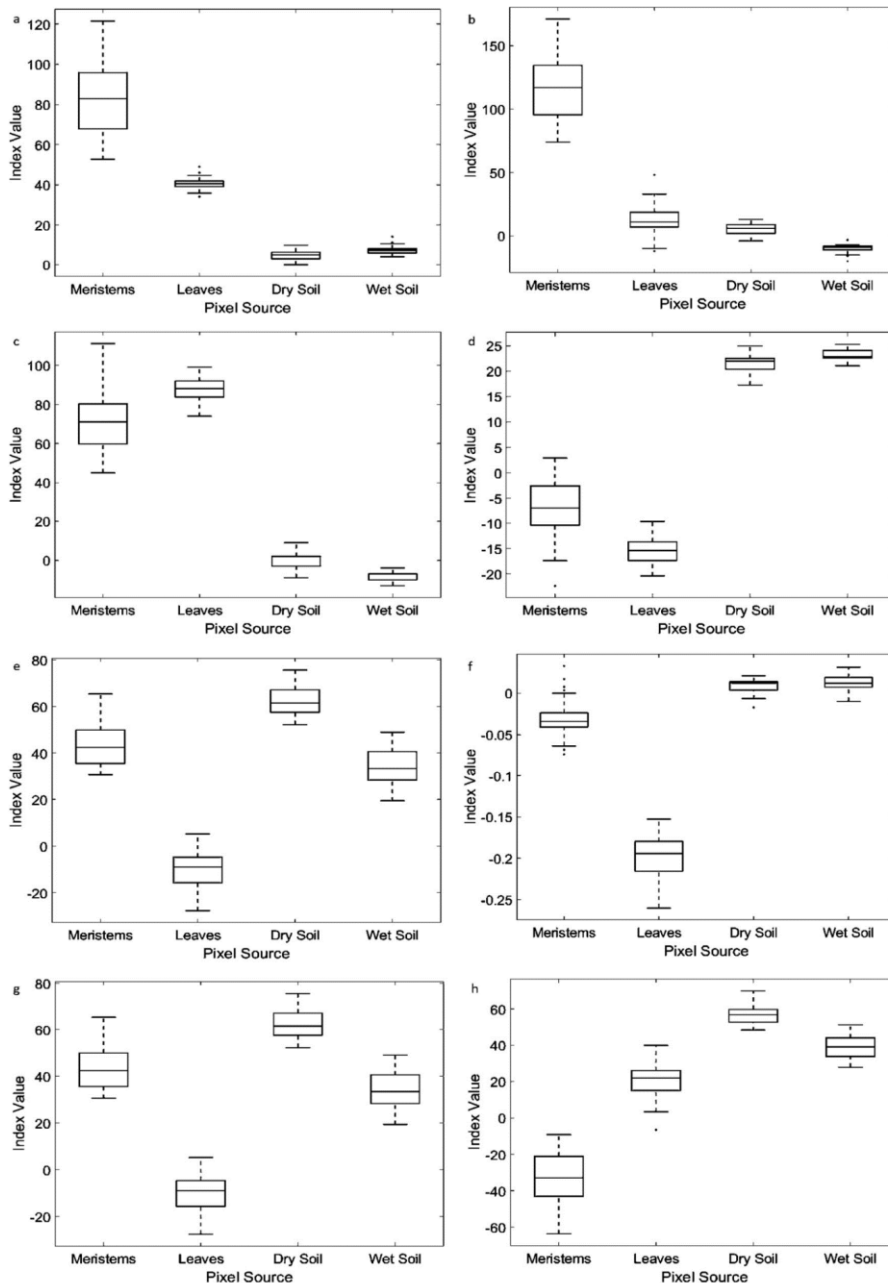


Figure 27: Index values of Meristems, Leaves, Dry soil and Wet soil using eight colour indices, from images taken before canopy consolidation of partially irrigated Sandy Loam soil. a - Blue Difference Normalized Index, b - Cumulative Blue Difference Index, c - Excess Green minus Excess Red Index, f - Normalized Difference Green Redness Index, g - Excess Red, h - Excess Blue Index

Table 16: Mean (and standard deviations) of indices calculated from the pixels of Leaves, Meristems, Wet soil and Dry soil using four cameras

Camera ^a	Feature	BDNI	CBDI	CIVE	ExB	ExG	xGxR	ExR	NDGR ^c
GoPro	Leaf	40.3 (2.7)	12.3 (11.7)	-15.6 (2.3)	19.8 (9.8)	87.8 (5.6)	97.5 (11.2)	-9.7 (7.6)	-20 (3.0)
GoPro	Meristem	82.1 (17.8)	115.6 (25.2)	-6.7 (5.6)	-32.1(13.0)	70.2 (14.6)	27.2 (15.8)	42.9 (8.9)	-3.0 (0.2)
GoPro	Wet Soil	4.9 (1.9)	-10.0 (3.2)	23.6 (1.0)	56.9 (5.9)	-8.3 (2.1)	41.1 (9.2)	33.6 (7.7)	1.0 (0.2)
GoPro	Dry Soil	7.4 (2.4)	5.2 (4.3)	21.8 (1.6)	39.1 (5.8)	-1.6 (3.8)	-64.3 (9.0)	62.7 (5.9)	1.0 (0.3)
GoPro	Gap ^b	0.3***	1.4***	-3.0***	0.1***	-3.0***	0.1***	2.5***	27***
Inspire	Leaf	33.5 (4.9)	-16.5 (4.9)	-3.1 (7.1)	19.3 (4.8)	54.0 (17.5)	75.8 (26.6)	-21.5 (10.3)	-3.0(1.0)
Inspire	Meristem	87.8 (14.7)	115.4 (22.6)	-28.7 (5.2)	-28.2 (16.4)	125.0 (13.0)	103.9 (19.8)	21.2 (11.1)	-1.0 (0.4)
Inspire	Gap ^b	1.0***	1.5***	-1.0***	-2.8***	-0.4***	-7.0***	0.1***	0.1***
Mapir	Leaf	81.2 (17.9)	114.3 (25.6)	-6.6 (5.6)	-31.7 (13.2)	69.9 (14.7)	27.5 (15.6)	42.4 (8.4) ^{NS}	-3.0 (0.02)
Mapir	Meristem	150.1 (16.1)	211.20 (22.5)	-31.9 (8.3)	-91.4 (15.9)	135.6 (21.04)	93.2 (27.7)	42.41 (9.6) ^{NS}	-0.6 (0.02)
Mapir	Gap ^b	-1.0***	-1.0***	1.9***	2.4***	-1.6***	-2.1***	-0.1	-1.0***
Mavic	Leaf	50 (5.5)	43.20 (10.9)	-23.6 (3.9)	-14.9 (14.6)	107.2 (9.5)	131.8 (17.9)	-24.6 (12.0)	-3.0 (0.7)
Mavic	Meristem	127.4 (16.6)	170.40 (24.3)	-47.5 (7.7)	-77.5 (18.8)	171.80 (17.9)	170.5 (28.3)	1.4 (13.2)	-2.0 (0.3)
Mavic	Gap ^b	1.5***	2.1***	-0.1***	-0.8***	-0.2***	-4.5***	-5.1***	28***

a = Camera alias, unless otherwise stated, there was significant difference in mean index values between meristem and non-meristem features in each camera ($P < 0.05$). Standard deviations from each mean are expressed in parentheses. b = the interval between the minimum value of meristems and the maximum value of a mature leaf, expressed as a proportion of the range $\times 10^{-1}$ ($\times 10^{-2}$ for NDGR), negative values indicate that the ranges of the two features overlap. c = $NDGR \times 10^{-2}$. NS=No significant difference between meristem and non-meristem features. CBDI = Cumulative Blue Difference Index, ExG = Excess Green Index, NDGR = Normalized Difference Green Redness, ExR = Excess Red, ExB = Excess Blue, xGxR = Excess Blue to Excess Red difference, CIVE = Colour Index of Vegetation Extraction, BDNI = Blue Difference Normalized Index.

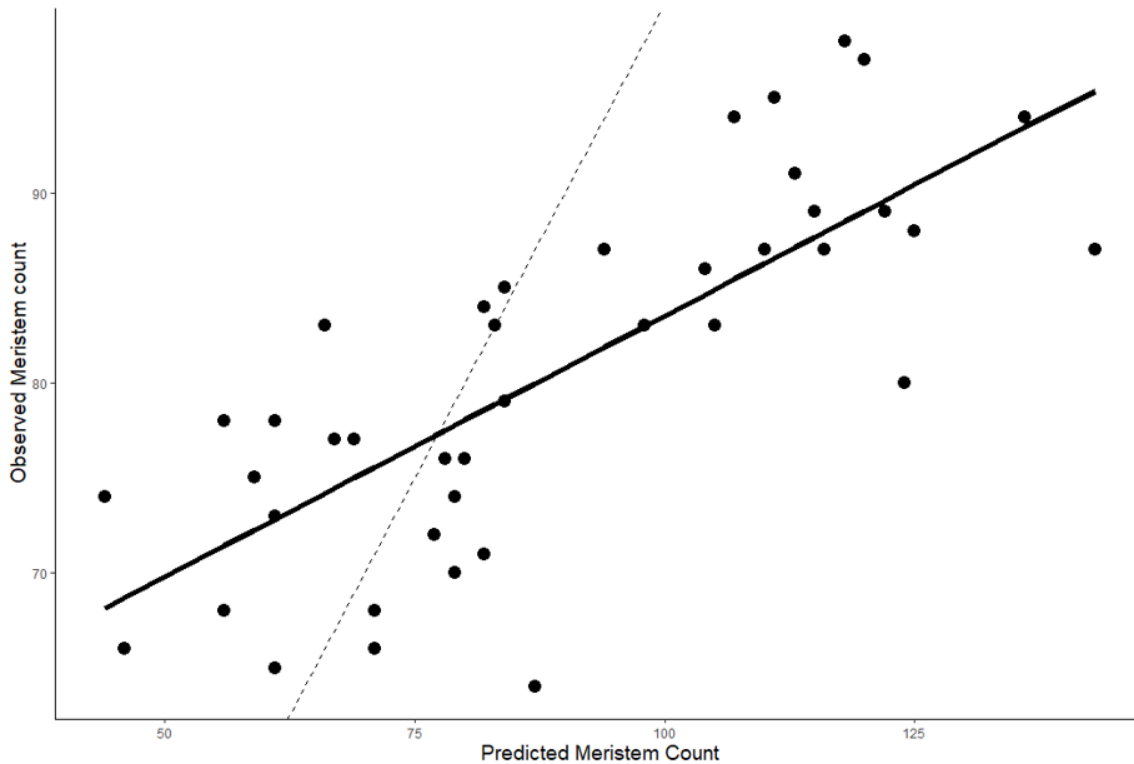
4.3.2 Model Testing

4.3.2.1 Mean Stem Counts

Table 17: Performance of image analysis and Convolutional Neural Network approaches in the enumeration of meristems in all the varieties. The varieties are grouped into determinancy types for presentation purposes and “Actual Stem Number” information is included to illustrate the difference between meristem and stem counts.

Variety Group	Actual Meristem Number	Actual Stem Number	Image Analysis Meristem Prediction	CNN Meristem Prediction
1	77.5 (2.1)	40.5 (3.5)	82.0 (2.8)	70.0 (2.8)
2	82.6 (12.2)	50.3 (13.2)	102.0 (32.1)	75.0 (8.5)
3	78.4 (7.9)	47.4 (6.7)	87.1 (22.6)	73.0 (8.0)
4	67.3 (3.1)	48.7 (5.1)	74.0 (16.1)	67.7 (1.5)
UG ^a	81.1 (9.1)	49.3 (11.5)	92.2 (28.2)	75.8 (10.0)
Grand Mean	79.8	48.7	90.6	74.5
RMSE^m^b			24.1	7.3
nRMSE^m^b	-	-	0.3	0.1
RMSE^s^c			46.9	26.8
nRMSE^s^c	0.7	-	0.9	0.6

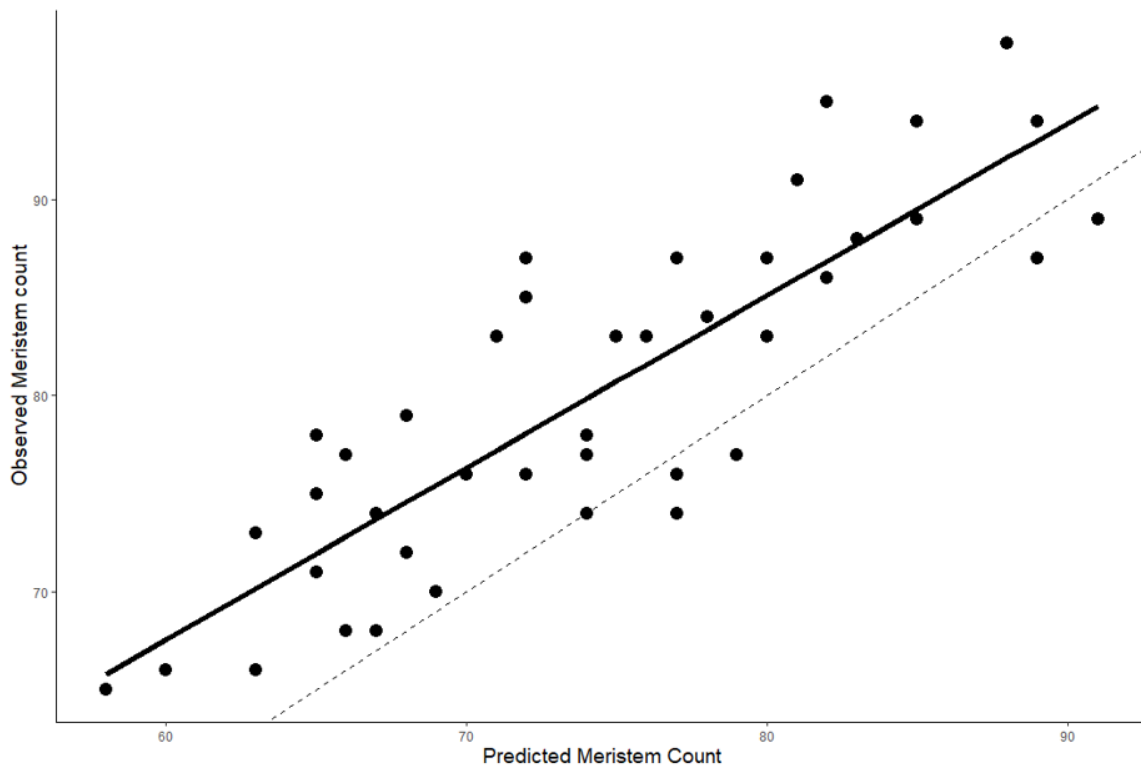
RMSE = Root Mean Square Error. nRMSE = Normalized Root Mean Square Error. a = Unknown variety group. b = RMSE or nRMSE with meristem ground truth as the observed variable. c = RMSE or nRMSE with manual stem counts as the observed variable



Legend: — = regression line ($y=56 + 0.28x$, R-squared = 0.57) -- = 1:1 line

Figure 28: Observed vs Predicted of the number of meristems in potato canopies when predictions were made using the traditional image analysis approach

Actual main stem counts from the field validation showed that the average number of above-ground stems per determinacy group had low variation ranging from 47 to 50 stems while there was more variation in the actual number of meristems counted, ranging from 67.3 in group 4 varieties to 82.6 in group 2 varieties (Table 17). FRCNN had a better predictive accuracy for the total number of meristems (nRMSE=0.09) than the image analysis method (nRMSE=0.3). Both FRCNN and image analysis algorithms had low accuracy in predicting the actual number of stems in the plot (nRMSE was 0.6 and 0.9 respectively) and the same observation was made when manually labelled meristem were compared to the manual stem counts (nRMSE = 0.7) as shown in Table 17.



Legend: — = regression line ($y=14.87 + 0.88x$, R-squared = 0.73) -- = 1:1 line

Figure 29: Observed vs Predicted number of meristems when predictions were made using a Convolutional Neural Network-based object detector

Least squares linear models of the predicted meristem counts against manual meristem counts showed an R^2 value of 0.57 (Figure 28) and 0.73 (Figure 29) for the image analysis method and FRCNN learning method respectively. Additionally, there was a significant ($P < 0.001$) relationship between manual counts of main stems and FRCNN meristem detections (Figure 30) as well as counts from the image analysis approach (Figure 31).

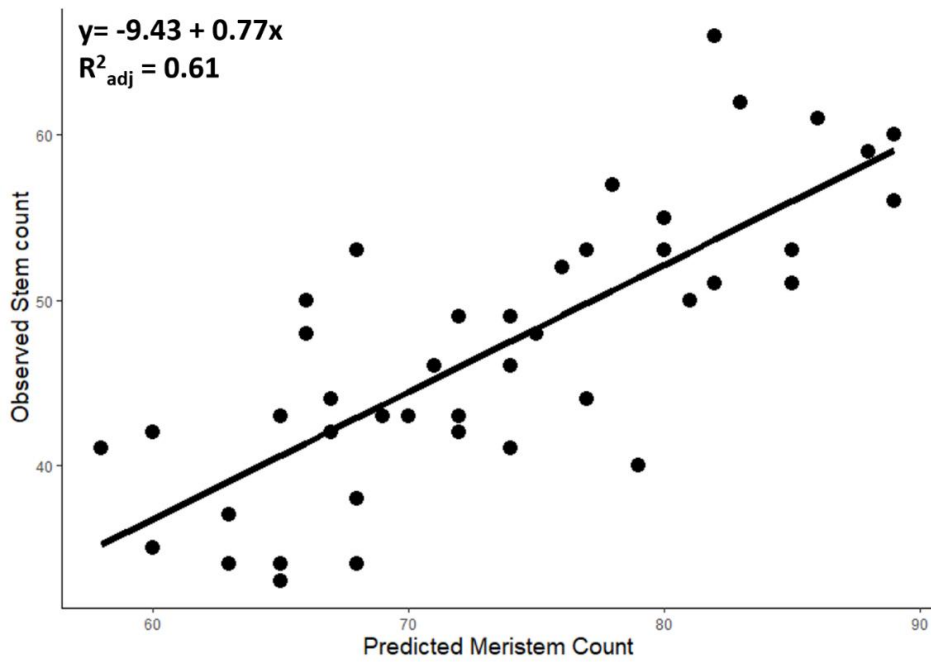


Figure 30: Observed number of stems vs Predicted number of meristems when predictions were made using a Convolutional Neural Network

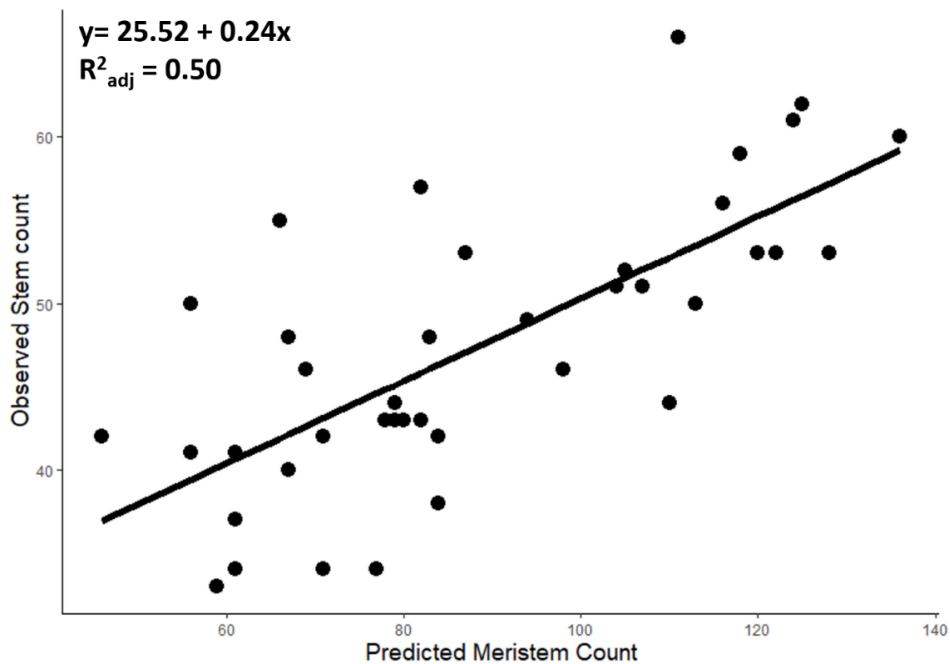


Figure 31: Observed number of stems vs Predicted number of meristems when predictions were made using the traditional image analysis approach

4.3.2.2 Localization Accuracy

Table 18: Means and standard deviations (in parentheses) of detection and localization performance metrics of the image analysis and Convolutional Neural Network against manually labelled meristem data

Group	Ground Truth	Image Analysis			Faster R-CNN		
	BB ^a Size	IoU ^b	Pr ^c	BB ^a Size	IoU ^b	Pr	BB ^a Size
1	2991.1 (657.5)	0.4 (0.3)	0.2 (0.2)	1739.8 (584.2)	0.5 (0.5)	0.6 (0.2)	3161.1 (45.2)
2	2382.7 (745.9)	0.31 (0.5)	0.1 (0.7)	1253.8 (222.2)	0.4 (0.5)	0.4 (0.1)	3168.9 (130.6)
3	2985.4 (366.9)	0.32 (0.7)	0.1 (0.6)	2468.9 (304.2)	0.5 (0.7)	0.6 (0.2)	3159.0 (111.4)
4	2851.7 (320.5)	0.3 (0.5)	0.1 (0.7)	938.8 (343.7)	0.4 (0.3)	0.6 (0.1)	3015.9 (172.2)
UG ^d	2996.3 (553.5)	0.34 (0.9)	0.4 (0.9)	2132.6 (204.9)	0.5 (0.5)	0.6 (0.1)	3125.9 (110.6)
Mean	2930.2	0.3	0.1	2009.8	0.5	0.6	3129.2
IQR^e	814.4			609.9			159.6

a = Bounding Box. b = Intersection over Union, standard deviation values are x 10⁻¹. c = Precision, standard deviation values are x 10⁻¹. d = Unknown Variety Group. e = Interquartile Range

The image analysis method had a low mean IoU (0.3) and Precision (0.1) compared to the FRCNN method (IoU = 0.5, Precision = 0.6) against the ground truth bounding boxes (Table 18). The Image Analysis algorithm had an average bounding box size that was closer to the

average size of the ground truth boxes than observed in the FRCNN model (Table 18). The Inter-quartile Range (IQR) showed that there was more spread in the bounding box predictions of the image analysis method than the FRCNN method, which predicted more equally sized bounding boxes (IQR =159.6).

4.4 Discussion

4.4.1 Feature Engineering and Development of Colour Indices

Both the CBDI and BDNI indices achieved better classification of the meristematic leaves than the other indices compared. The CBDI and BDNI indices were derived in such a way as to take advantage of the theory that plant leaves exhibit variable reflectance of the Blue wavelength based on the age of the leaves, and the maximization of index values in meristematic features is in line with the projected spectral signature of Gates et al. (1965). The Excess Blue index equally agrees with the findings of Gates et al. (1965) as it shows sensitivity to the diminished level of Blue light reflectance in meristematic structures, leading to lower index values than older leaves and soil.

In agreement with findings from Woebbecke et al. (1995), The Excess Green index adequately separated soils from canopy features. However, the index showed insensitivity to the amount of reflected green light between the meristematic structures and leaves, though the matured leaves had a higher mean reflectance than the meristems. The range of the Excess Green index and all other indices (Figure 27) in meristematic leaves overlaps with the range of the matured leaves, reflecting different levels of chlorophyll in meristematic leaves as affected by the age of the leaf. This is expected as noted by Gates et al. (1965) that a sharp drop in Red reflectance accompanies the continued increase in green reflectance with leaf age as proto-chlorophyll is converted to chlorophyll.

Though potatoes generally contain a larger concentration of the lighter shaded chlorophyll-a than chlorophyll-b (Anžlovar et al., 1996), a noticeable difference in Blue reflectance can be expected in mature leaves compared to the meristems which still have proto-chlorophyll. This is confirmed by Gates et al. (1965) who illustrates a slightly higher reflectance in the Blue range from mature leaves than younger leaves in reflectance curves. The CBDI and

BDNI achieve better classification of meristematic leaves because they take this Blue light reflectance into account in relation to green reflectance. The difference between these two wavelengths is responsible for the high Manhattan distance and Euclidian norm from the origin in the meristems (Figure 25). The results also show that the difference between Blue and Green reflectance is minimal in soils, showing more reflectance in the Green range than the Blue range in dry soils. This is in agreement with soil reflectance curves reported by (Huete, 2004) which show a linear increase in reflectance from Blue to Near Infrared. (Baumgardner et al., 1986) reported similar curves which consistently show more Red than Blue reflectance in soil. The findings for dry soils in this study concur with Baumgardner et al. (1986), however, wet soils were found to reflect more Blue light than Red. Huete (2004) and Baumgardner et al. (1986) discussed a decrease in reflected energy which makes soils appear darker, consistent with the high reflectance of Blue wavelength observed. These findings make the CBDI and BDNI ideal as they minimize the index values of soils and mature leaves in comparison to meristems. Comparison of the boxplots of the two indices additionally shows that the BDNI can be used as a general colour index as it additionally separates vegetation from soils, while the overlap between mature leaves and soils in the CBDI would make it unsuitable as a general colour index.

When targeting sparse features that do not show a peak in the feature space's histogram, Otsu-method binarization of an image is known to produce non-satisfactory segmentation. K-means segmentation adopted in this study provides an alternative that formulates clusters of features based on the variation in the feature space (Yang et al., 2012) rather than a subjective segmentation threshold. Where the feature space is defined by the Manhattan distances using the CBDI or Euclidian distances in the BDNI, automatic selection of a cluster of interest as a basis for binarizing the image is made possible since the meristems cluster is bound to occur at the upper quantiles of the histogram.

4.4.2 Model Testing

Observed vs predicted plots of the number of meristems in the image analysis and FRCNN methods had R^2 values of 0.57 and 0.73 respectively. FRCNN has an advantage over image analysis with a low nRMSE of 0.09 compared to 0.3 nRMSE observed in the image analysis.

With no previous studies on potato stem detection, these results can be benchmarked against models that detect variation in leaf colour and shape due to viral leaf yellow mottling and crinkling akin to the underdeveloped leaves of growing tips. In this respect, the FRCNN performs comparably to findings by Duarte-Carvajalino et al. (2018) where convolutional neural networks achieved a maximum of 0.82 R^2 value for the detection of incidences of Late Blight (*Phytophthora infestans*) on potato leaves when compared to manually labelled ground truth data. Comparably, (Sugiura et al., 2016) similarly developed an image analysis protocol for estimating the severity of late blight with R^2 of 0.77. The results presented here show that the FRCNN approach is as efficient as other studies that aim to detect objects of interest in potato canopies that humans identify based on colour and leaf shape. The difference between predicted counts and observed counts in the image analysis approach show the need to account for more variation within the image by improving the image segmentation and the algorithm's inclusion criteria of an independent stem. Improvements in the image segmentation can be achieved by further feature engineering to generate more robust colour indices. Furthermore, although K-means clustering and subsequent cluster segmentation overcomes the problems of Otsu-based segmentation in non-bimodal data, the hard-coding of cluster number introduces the possibility of misclassification of ambiguous pixels, a double-edged sword that caused both false positives and false negatives (Kanungo et al., 2002). More in-depth studies into possible adaptive threshold selection techniques at the image level are needed to generate robust clustering and threshold selection rules to improve accuracy. Differences between predictions and observations in the FRCNN model can partially be attributed to the limited variation in the training dataset, generated from two potato varieties, against the testing dataset which contained 45 varieties with variable canopy characteristics.

The performance of region-based CNNs is influenced by the adequate determination of the number of anchor boxes and their sizes at the training phase (Zhao et al., 2019). The irregularity of potato meristems means there needs to be a representative compendium of anchor boxes to cover the high variation in ground truth bounding box sizes. In this study, the ground truth bounding boxes had a high IQR of 814.38 pixels compared to the predicted bounding boxes of the CNN (159.61) and image analysis (609.86) on the test dataset (table

17). The CNN model produced regular (equally-sized) but larger bounding boxes than the ground truth while the image analysis approach produced smaller bounding boxes than the ground truth but were more variably sized, more naturally representing the variation in sizes of growing tips. In subsequent studies with the CNN approach, a more exhaustive method of anchor box size estimation is warranted, but equally so is the development of the model from lower resolution imagery at higher UAV altitude to reduce the ground truth IQR of the test dataset and potentially improve the model accuracy, though this comes at a cost of more errors in labelling low resolution imagery. These observations signal potential improvements to the data collection and hyper-parameter settings which may improve model accuracy in future studies. The small bounding boxes in the image analysis approach were reflective of the results of k-means clustering on the novel colour indices which were highly optimized to maximize values of meristematic pixels against mature leaves. However, the high R^2 values observed in both models show that there is a significant correlation between the predicted and actual meristem counts, as well as actual main stem counts, which shows that both models can be used in mapping this variation at field scale, a key desire for farmers who seek to vary vine desiccation dates based on stem density to manage potato tuber sizes and their distribution at harvest.

The FRCNN model achieved higher precision (0.56) and mean IoU (0.49) across the variety groups compared to the image analysis method (0.13 and 0.33 precision and IoU respectively), showing better efficiency at learning the features that a human labeller would identify with meristems, as well as the effect of the human-verification and adjustment of training labels on the final model. In the absence of potato meristem segmentation studies, precision scores were benchmarked against the Potato Virus Y (Polder et al., 2019), whose primary symptom is chlorotic foliage akin to the signal being detected by the image analysis approach to label stems. Polder et al. (2019) found precision scores between 0.23 and 0.54 when a fully convolutional network was used to achieve semantic segmentation of Potato Virus Y. This is comparable with the performance of the FRCNN approach but outperforms the image analysis method. While the image analysis approach also adequately identifies the presence or absence of a meristem, the size and centroid of its resultant bounding boxes is less consistent since the system is purely based identifying the extent of the colour

aberration at the very tip of the youngest leaves and not learning any other advanced features as in the FRCNN. As a result, the image analysis approach produces highly variable meristem sizes within an image as shown by the high IQR. However, its inclusion in the FRCNN pipeline is justified as it speeds up the labelling of a large dataset, allowing a human-labeller to only correct the computer generated labels. The image analysis method allows the generation of initial annotations to guide labellers and train non-expert labellers to identify canopy features of interest from which they can simply adjust bounding box extents and hence speed up the annotation process.

For the purposes of deriving a management or phenotyping tool for evaluating variations in stem sizes across different stem densities, the establishment of a significant linear relationship between predicted stem counts and actual counts is important despite the presence of residuals because the linear relationship can be used to model spatial variation in stem density at field scale. While Sankaran et al. (2017) reported a predictive model with R^2 values of 0.83 for modelling plant density variation at emergence using the NDVI, they observed that predictive accuracy was lost as the canopy consolidated and they were not able to successfully run the prediction after 43 days from emergence. Furthermore, the effective unit of plant density in the potatoes is the stem, which can only be evaluated when all potential stems have developed, after plant canopy consolidation (Wurr & Morris, 1979). The overall 0.73 R^2 value in this study's CNN method gives a level of accuracy that is comparable to Sankaran et al. (2017) while offering the desired ability to enumerate the preferred unit of plant density, which can be incorporated in vine desiccation decision support systems for manipulating tuber size distribution at harvest and in high throughput phenotyping. With 40 tubers planted per plot, the actual stem counts found in this study mean that the average number of above ground stems per plant (1.21) falls within the ranges (1-4.4) reported in literature (Wurr & Morris, 1979). Most plants had one or two primary stems due to physiologically young seed tubers, stored below induced dormancy-breaking temperature. While the meristems represent the termination of both primary and secondary stems as well as sympodial branches, it can be noted that the average number of meristems per plant (2.01) also falls within the range of the number of main stems per potato plant reported in literature (Wurr & Morris, 1979) and further suggests that most

plants in this study produced one or two primary stems and one secondary stem. The potato main stem always terminates with a meristem in all varieties and a sympodial branch continues growth in indeterminate varieties (Almekinders & Struik, 1996). The average number of secondary branches per stem reported in literature is minimal ranging from 0.5 to 0.9 branches per main stem (Vos & Biemond, 1992; Wurr & Morris, 1979). Therefore, while the number of meristems does not directly correspond to the number of main stems, its density variation across the field is a predictable proxy for stem density variation, which is the main desired unit of potato plant density whose determination at field-scale had so far been elusive (Wurr & Morris, 1979).

The number of main stems formed by a potato is largely variable and contingent upon the physiological age, plant population density and other agronomic and management factors (Knowles and Knowles, 2006). The number of secondary stems formed is also dependant on factors that affect apical dominance like inherent determinacy characteristics and frost events (Chang et al., 2014). Additionally, differences in growth rates between stems means some meristems are occluded from view at the top of the canopy by other leaves, hence cannot be captured by UAV. These factors all contribute to the residuals between the number of actual main stems and the number of meristems detected at the top of the canopy. The results of this study suggest that the number of meristems visible at the top of the canopy can be predicted using a CNN with low residuals ($nRMSE = 0.09$). Predicting the actual number of stems from the meristems proved to be less accurate due to the influence of secondary stems that also terminated in a meristem. However, this study established that the predicted number of meristems at the top of the canopy explains a large portion of the variation in the actual number of stems, providing a statistical route for generating 2D density maps of the variation in stem density from UAV, using meristem density as a proxy. Future studies must focus on generating methods for distinguishing a meristem originating from a main stem from those originating from branches and secondary stems. Unlike the physiologically young seed used in this study, temperature-primed physiologically old seed is mostly used in commercial production, with low apical dominance, forming multiple primary main stems at emergence and only branching late in the season after flowering (Knowles and Knowles, 2006). To partially solve the problem of secondary stems, it is

therefore suggested that the meristem detection models should be used before significant branching occurs. Future studies must also focus on determining the optimum timing of imagery for minimizing the probability of detecting secondary meristems.

4.5 Conclusion

This study represents the first attempt to enumerate potato stem number after canopy consolidation using UAV based sensors. The prospect of accurately mapping variation in stem density across a field enables the possibility of using precision agriculture techniques to manipulate potato tuber size distribution through variable harvesting dates and other in-season management practices. This study provides evidence that deep learning and image analysis approaches can be used to accurately enumerate potato meristems and estimate stem density variation in 45 UK potato varieties. Based on the spectral properties of plants, the colour indices developed in this study should also have potential applicability in mapping physiological maturity and leaf discolouration due to biotic or abiotic stress. More studies to test the wider applicability of these indices are therefore recommended. The study has also demonstrated the validity of automated labelling for generating a large dataset of pseudo-labelled ground truth data which can be more rapidly quality-checked and adjusted by a human labeller then used to train deep learning models that learn the features of interest and achieve high IoU with manually labelled test data.

CHAPTER 5 - Mapping Potato Plant Density Variation Using Deep Learning and Unmanned Aerial Vehicles for Accurate Predictions of Yield

Abstract

In Potato (*Solanum tuberosum*) production, the spatial mean and variance in the number of tubers harvested is related to the plant population. Maps of the spatial variation in plant density are therefore important for evaluating the efficiency of planting operations and predicting yield. Computer vision has been proposed to enumerate plant numbers using images from Unmanned Aerial Vehicles (UAV) but inaccurate predictions in images of merged canopies remains a challenge, for which neural network architectures with difficult annotation-requirements are increasingly proposed in the search for the “perfect” model. Some research has been done on individual potato plant bounding box prediction but there is currently no information on the spatial structure of plant density that these models may reveal and its relationship with potato yield quality attributes. In this study, the Faster Region-based Convolutional Neural Network (FRCNN) framework was used to produce a model with which to estimate plant densities across a UAV orthomosaic. Using aerial images collected from potatoes at 40 days after planting, a FRCNN model was trained to an average precision (aP) of 0.78 on unseen testing data. The model was then used to generate predictions on quadrats of a grid imposed on orthomosaic rasters captured at 14 and 18 days after emergence. After spatially interpolating the plant densities, the resultant surfaces were highly correlated to manually-determined plant density ($R^2=0.80$). Furthermore, the predicted plant densities were correlated with tuber number ($r = 0.54$ at Buttery Hill; $r = 0.53$ at Horse Foxhole) and marketable tuber weight per plant ($r = -0.57$ at Buttery Hill; $r = -0.56$ at Horse Foxhole). There was also a strong link between variation in early-season Normalized Difference Vegetation Index values to variations in plant density predicted by the FRCNN model ($r = 0.61$). These results show that accurate interpolation of the variation in plant density can be constructed from UAV imagery with high correlation to important yield components, despite the loss of accuracy of FRCNN models in images containing partially merged canopies.

5.1 Introduction

Potato (*Solanum tuberosum*) plant density is a basic measurement of the population that has been linked to significant differences in yield and tuber size distribution (Allen & Wurr, 1992; Arsenault et al., 2001; N. R. Knowles & Knowles, 2006; Love & Thompson-Johns, 1999). Increasing plant spacing significantly reduces the plant population and subsequently decreases yield (Bohl et al., 2011). Potatoes form multiple main stems per planted tuber, which are considered a more representative unit of plant population due to their established relation to tuber number at harvest (Allen & Wurr, 1992). However, the practical difficulties in accurate enumeration of potato stems make it more practical for farmers to use the weight of tubers planted per unit area as a standard of seed rate that directly relates to plant density rather than stem density (Allen & Wurr, 1992). This requires farmers to determine the effective plant density in the field in order to evaluate the efficiency of planting operations, seed germination rates, and to accordingly adjust yield expectations. Currently, farmers predominantly evaluate plant density using visual counts of emerged plants during the establishment phase of crop development (Sankaran et al., 2017), which is unreliable due to lack of reproducibility and is impractical in large fields. Reliable, efficient and reproducible methods of plant density determination are therefore an important need in precision agriculture.

A potential solution for estimation of potato plant density can be obtained by leveraging advances in computer vision and aerial image photogrammetry. Unmanned Aerial Vehicles (UAV) fitted with imaging sensors provide a platform for remote sensing of canopy development with the potential to determine variation in plant density for precision agriculture applications. A commonly cited application of UAVs in agriculture is the generation of spatial variation maps using vegetation indices derived from multispectral camera data. These maps may be used to infer vegetation health, utilizing known spectral responses of vegetation to plant health and molecular constitution (Gates et al., 1965). Classification algorithms applied at spatio-temporal scales are useful for the evaluation of vegetation cover characteristics, a proxy to crop growth rate and leaf area index that is required in most yield forecasting crop models (Mendes dos Santos et al., 2020). Apart from

pixel-level image analysis applications, there is considerable interest in using UAVs for non-destructive and non-invasive evaluation of properties of interest within crop canopies such as plant heights with light detection and ranging, instances of diseases or pests and plant population counts (Franceschini et al., 2019; S. Jin et al., 2020).

Several computer vision algorithms have been proposed for determining plant counts from aerial images of different crops using traditional image analysis and machine learning approaches. The most prevalent approach involves feature extraction using traditional image analysis followed by a machine learning approach for predicting image class labels from extracted features. Several variations of this two-step approach have been used to produce plant-counting models in wheat (Fernandez-Gallego et al., 2020), Rapeseed (Zhao et al., 2018), potatoes (B. Li et al., 2019) and other crops. In weed-free fields, images of emerged plants before canopy consolidation consist mostly of green pixels of the objects of interest against a background dominated by soil (Machefer et al., 2020). This dichotomy is utilized in the feature extraction step to classify and consolidate connected foreground pixels as objects of interest using reflectance values of the pixels. Colour indices are often used to generate two-dimensional grayscale images from truecolor (RGB) or multispectral images. Generation of a binary mask representing the dichotomy between the foreground and background often involves the selection of a threshold that is either learned from the image using the Otsu algorithm (B. Li et al., 2019) or subjectively selected (Sankaran et al., 2017). While these approaches return satisfactory binary masks in some situations, subjective selection of a threshold is clearly not expected to be robust in all environments and the Otsu algorithm becomes sub-optimal when vegetation indices produce multi-modal frequency histograms (X. Yang et al., 2012). Subsequent feature extraction and regression or classification modelling therefore becomes dependent on data pre-processing methods deployed to clean the binary mask, impacting repeatability.

Following up on the traditional computer vision approach by Li et al. (2019) Machefer et al. (2020) trained a Mask R-CNN model, predicting potato and lettuce instances using bounding boxes and sizing the extent of each instance with a mask. This overcame the need for manual feature extraction and demonstrated the superiority of deep learning over the

traditional approach. Dijkstra et al. (2019) also developed a framework based on a fully convolutional neural network to count potato plants in merged canopies. However, both the Mask R-CNN (Machefer et al., 2020) and the two-step computer vision (B. Li et al., 2019) approaches suffer from a loss of accuracy in distinguishing overlapping plants. Homogeneity in potato plants, and the difficulty of separating individual plant units in merged canopies during data annotation makes it difficult to train models that can accurately distinguish individual plants after potato canopy consolidation. A potential solution to this problem would be to conduct imaging before canopy consolidation. However, potato emergence rates vary spatially with soil temperature, disease incidence, and treatments that alter apical-dominance at the seed-lot level (Sankaran et al., 2017). Additionally, calcium deficiency at the terminal bud can induce the loss of apical dominance, which necessitates branching and determines the number of sprouts per tuber, causing a spatial variation in canopy growth rates across the field (Jefferies & Lawson, 1991). Variations in planting depth also cause variations in the number of days to emergence, with deeper planted tubers taking up to a week longer to emerge than shallower planted tubers within a field (Bohl & Love, 2005). These factors make it necessary to delay image acquisition, so as to minimize the chance of underestimating emergence.

Dijkstra et al. (2019) report accurate mapping of centroids of plants in merged canopy using a custom CentroidNet architecture supported by a fully convolutional network learning the centroid origin of leaves in overlapping potato canopies. The premise of this method is that potato leaves grow outwardly from the location of the planted tuber, and the model can therefore detect the location of a plant by learning the vectors pointing to the centroid of a plant object. In merged canopies, this assumption may be violated by the fact that potato leaves grow outward from their subtending stem and each stem eventually grows independently from its mother tuber (Allen & Wurr, 1992). Therefore, overestimation can be expected in multi-stem plants using the CentroidNet. Indeed, Dijkstra et al. (2019) report observing false positives due to oddly-shaped plants, which may be primary or secondary stems. Evidence suggests that accurate potato plant counting remains an object detection problem that is best modelled from UAV data before canopy overlap when individual plants

are discernible to data annotators. The practical need for plant counting algorithms to farmers is the generation of a plant density map across the field from the detected objects, making this primarily an object detection problem, and the accurate pixel-wise segmentation problem is secondary. Faster R-CNN (FRCNN), the detection framework on top of which Mask R-CNN is built therefore provides an adequate and simplified training protocol. Training FRCNN models also requires less hyperparameter tuning requirements than MASK-RCNN (Machefer et al., 2020).

The ultimate goal of plant counting algorithms is to replace the need for manual estimations of plant density across a field, which is done by interpolation of manually collected stem count data. The accurate production of 2D density maps that represent the spatial variation in plant density is therefore more pertinent than fine-grain plant-by-plant accuracy because the economic and practical feasibility of site-specific management is contingent upon the establishment of a practically manageable range of spatial autocorrelation (Taylor et al., 2018). Variables that respond to plant density (e.g. yield) are also likely to only be managed if they exhibit relatively long-range spatial autocorrelation. Taylor et al. (2018) reported large differences in the range of autocorrelation in potato yields from 12 m to 425 m. In commercial production, farmers aim to produce uniform plant density across the field and any variation is likely to come from factors such as a systematic fault in the planting operation, low viability of a batch of seed, or soil-borne factors that affect seed germination (Bohl et al., 2011). Such systematic sources of variation are likely to exhibit spatial autocorrelation relative to the size of the field. Therefore, plant density maps need to capture this spatial structure rather than merely capturing local variation. This provides a geostatistical solution to the problem of plant-density determination using computer vision and deep learning algorithms in fields with slightly merged canopies. In a large orthomosaic of UAV imagery, plant detection can be conducted on a sliding window as suggested by (Machefer et al., 2020) then a filtering step can be added post-detection, discarding all images containing overlapped plants. This would create a sparse matrix of detections across the field from which geostatistical interpolation can be used to re-generate a continuous representative 2D density map. The 2D density map can then be related to variation in yield

parameters or used to test the utility of other sources of variation like satellite-derived early-season NDVI. With the main potato-related papers in this field focused solely on detection (Dijkstra et al., 2019; B. Li et al., 2019; Machefer et al., 2020), this approach has not been reported in literature.

In this chapter, it is demonstrated plant counting in potatoes as a detection problem solvable by a FRCNN model without the need for instance segmentation. For the first time, a geostatistically interpolated 2D plant density plots were produced, compared to satellite-derived early-season NDVI density plots and the relationships between the density plots and potato yield attributes were evaluated.

5.2 Methods

5.2.1 Data capture and Modelling

Table 19: Summary of the locations, ground sampling distances (GSD) and crop stage of the images used in the study. In all instances, the cropped variety was Amora

Use	Field Name	Year	Coordinates	GSD (mm)	Crop Stage
Model Training	H.Foxhole ¹	2019	52°46'26.94"N 2°25'49.38"W	2 cm	10 days after emergence
Model Testing	B.Hill ²	2020	52°46'22.05"N 2°25'40.46"W	2 cm	18 days after emergence
Model Testing	H.Foxhole ¹	2019	52°46'26.94"N 2°25'49.38"W	1 cm	14 days after emergence

1 = Horse Foxhole. 2 = Buttery Hill

The study site for model development was a commercially planted potato crop (variety Amora) planted at Harper Adams University, Shropshire, United Kingdom (Table 19). The field was planted on 27th March 2019 at a targeted 25 cm between planting stations. First emergence was observed on 18th April 2019, after which a 10-day interval was allowed before imaging, allowing the emergence of a sufficient number of plants for annotating a training dataset. Consequently, aerial images were captured on 28th April 2019 at 30 m altitude using a Mavic Air UAV hosting a 2.54 cm CMOS sensor producing 12MP images with an 88° field of view (FOV).

To ensure separation between model training and testing data sources, the initial image acquisition was restricted to a designated sub-section of the field for training the model, while the remaining portion of the field was used for validating the model. Thirty images were randomly selected from the collected image set and divided into 338 x 304 pixel sub-images, creating 1000 images for annotation. The images were then manually annotated using Matlab's (MATLAB, 2020) Image Labeller application. With a ground sampling distance of 2 cm per pixel, the images contained enough perceptual detail to manually produce bounding boxes for plant objects and the earliness of the image acquisition made it possible to delineate overlapping plant clusters and place bounding boxes for each distinct plant. After a visual inspection of the 1000 training images, 172 were excluded due to blur caused by camera movement during image acquisition or if there were no potato plants present (because a section of the headland was captured by the UAV). The resulting 828 images were partitioned into a training set of 580 and a testing set of 248 images. All generated bounding boxes were stored as labels to create a training dataset for transfer learning with a CNN.

Transfer learning was conducted using FRCNN with a VGG-16 network backbone, pre-trained on the ImageNet dataset (Deng et al., 2009). VGG-16 is an image classification convolutional network that takes input of 224x224 RGB images through a sequence of convolutional layers with minimal 3 x 3 filters, a fixed 1-pixel stride and max-pooling with a stride of 2 (Simonyan and Zisserman 2015). Three fully connected layers follow the convolutional layers, with the final fully connected layer containing a number of channels

equal to the number of training classes (in this case 2, representing the potato plants and background) and followed by a soft-max layer. The FRCNN framework utilizes the VGG-16 final convolutional feature map to train a region proposal network (RPN) and spatially locate the objects within the convolutional feature map. To create a potato plant detector, the final convolutional feature map of VGG-16 was used to train a RPN and the last max-pooling layer was replaced by an ROI (region of interest) max-pooling layer as proposed by Ren et al. (2015) followed by FRCNN's classification and regression layers. The training was conducted on an Nvidia GeForce GTX 1070 GPU with CUDA version 10.1.243 and 8 GB Video RAM. The training was run for 100 epochs which completed in 6 hours. The hyperparameters used included a learning rate of 0.0001 and a mini-batch size of 4. Stochastic gradient descent was used to optimize loss with a momentum of 0.95. To minimize gradient explosion, extreme gradient values were clipped to ensure that the L2-norm equalled the threshold of 1. The flow chart of the training pipeline is as illustrated in Figure 32.

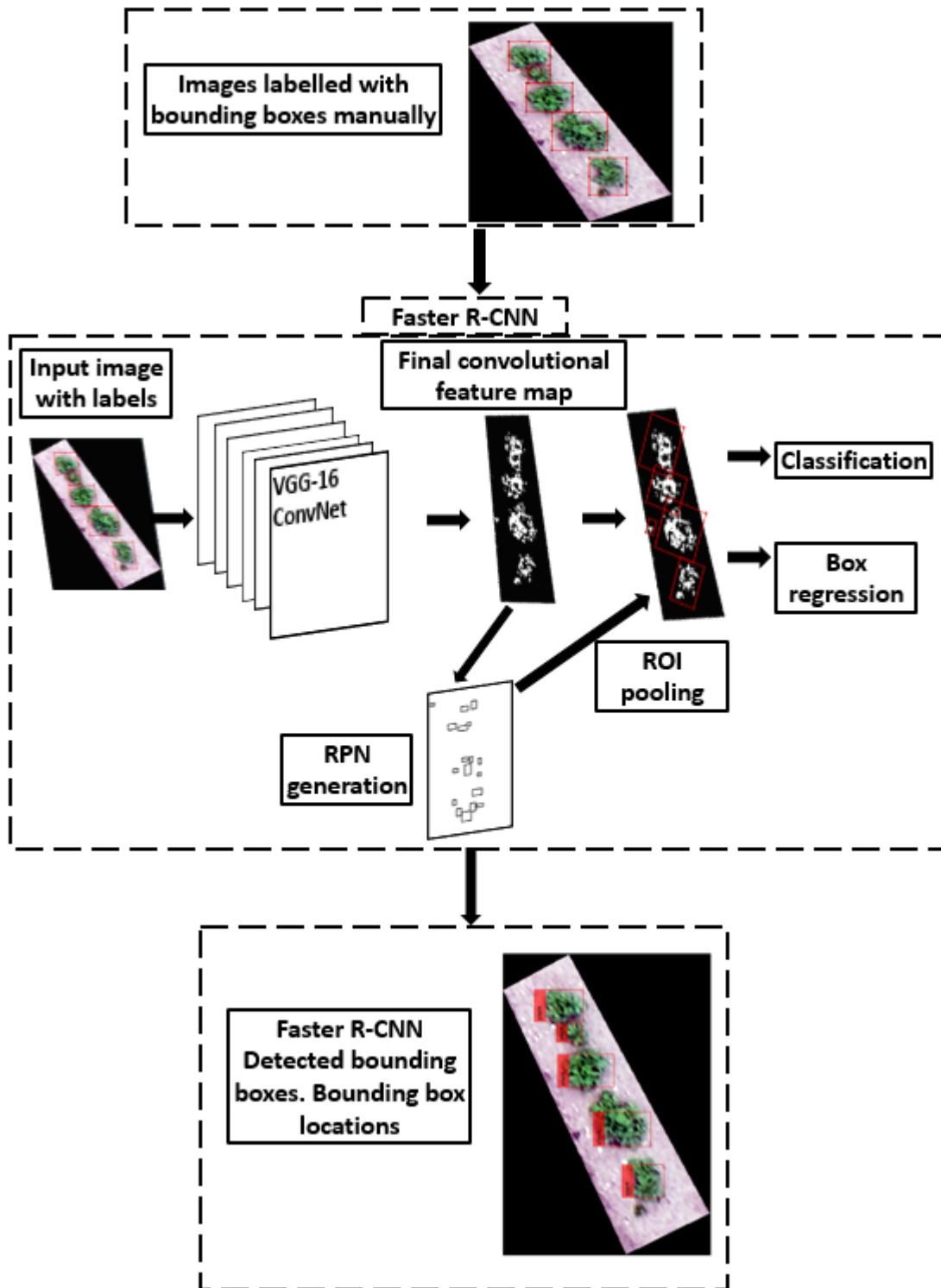


Figure 32: Flow chart of the Faster-RCNN-based transfer learning process for producing a Potato plant detection model

5.2.2 Model Testing

FRCNN model performance was evaluated as follows. Firstly, model performance diagnostics on unseen data were conducted using the test dataset. Accordingly, the bounding boxes of the FRCNN detections were compared with the ground truth. The Intersection over Union (IoU) of all bounding boxes with ground truth data were computed then all predicted bounding boxes with more than 0.5 IoU were classified as true positives (TP) while those with less than 0.5 were classified as false positives (FP). The TP and FP instances were computed for each image and the precision of the detection was evaluated as follows:

$$Precision = \frac{TP}{TP+FP} \dots\dots\dots (19)$$

At the standard IoU threshold of 0.5, a high rate of FP was expected, resulting from random bias in the ground truth bounding boxes, as opposed to the refined bounding boxes generated by the FRCNN model. A high FN rate was expected to penalize Recall and F1-scores, therefore, the precision metric was used. From an end-product standpoint, it was considered more important to accurately detect the presence of a plant while its accurate sizing is not as important, prompting the choice of Precision over Recall. The aP of the model was computed averaging across all bounding boxes in all the test dataset images.

The model was also evaluated for the accurate generation of an observed plant count at 30 different sites across the Horse Foxhole Farm collected 14 days after emergence.

Accordingly, an aerial imagery survey covering the entire field was conducted on 2nd May 2019 at 30 m altitude using a DJI Phantom 4 pro UAV with a global positioning device for geo-referencing images. The UAV was equipped with a Hasselblad L1D-20c aerial camera with a 2.54 cm CMOS sensor producing 20 MP still images with a 70° field of view (FOV). The UAV and image acquisition interval ensured an 80% overlap in adjacent images at a ground sampling distance of 1 cm. A second field named Buttery Hill (Table 19) was also evaluated using the model. Images at Buttery Hill were acquired using the DJI phantom 4 at an increased altitude of 80 m with a ground sampling distance of 2 cm per pixel on 1st May

2020, 43 days after planting and 18 days after emergence. At each of the two fields, a single geo-referenced raster for the entire field was produced by stitching all the images together with structure-from-motion techniques using Pix4D (Pix4D, 2016).

To predict a plant density map at the two fields, a grid of 1 m² sized quadrats was imposed on the raster for each field in order to run the FRCNN model. Quadrats of less than 1 m² at the edge of the field were also processed. After detection, it was necessary to determine the presence of merged stems which could not be reliably counted. To do this, each detected bounding-box was converted to a binary mask and the length of its major axis was calculated and converted to centimetres using the ground sampling distance of the image. Twenty-five centimetres was chosen as a threshold to represent the length of the major axis (diagonal) of a bounding box at which it would be considered to represent a merged group of plants. All quadrats where a merged plant was discovered were removed from the analysis and the quadrat was replaced by an equally-sized null matrix. For all valid detections, a null matrix equal to the size of the quadrat was also produced but the centroid pixel of the matrix was assigned a value equal to the number of plants that was detected in the quadrat, creating a sparse matrix with only the centroid pixel containing a non-zero value. The series of sparse and null matrices were then stitched together to re-constitute a grayscale image of the same dimensions as the original raster. The grayscale image was saved as a Tagged Image File Format (TIFF) file and associated with the “world file” of the original geo-referenced raster. This processing created a georeferenced grayscale image predominated by zeros, with a series of non-zero pixels representing estimated plant densities from the FRCNN model at the non-zero pixel locations. The raster was then vectorised into spatial sampling points in arcGIS (ESRI, 2020) and all null-valued points were discarded, leaving a point sampling dataset of estimated plant densities across the field. The points dataset was then interpolated across the entire field to produce a continuous 2-D plant density plot of the field using a Gaussian variogram in ArcGIS (ESRI, 2020). The flow chart of the process to generate of 2D density plots from UAV orthomosaics was as illustrated in Figure 33.

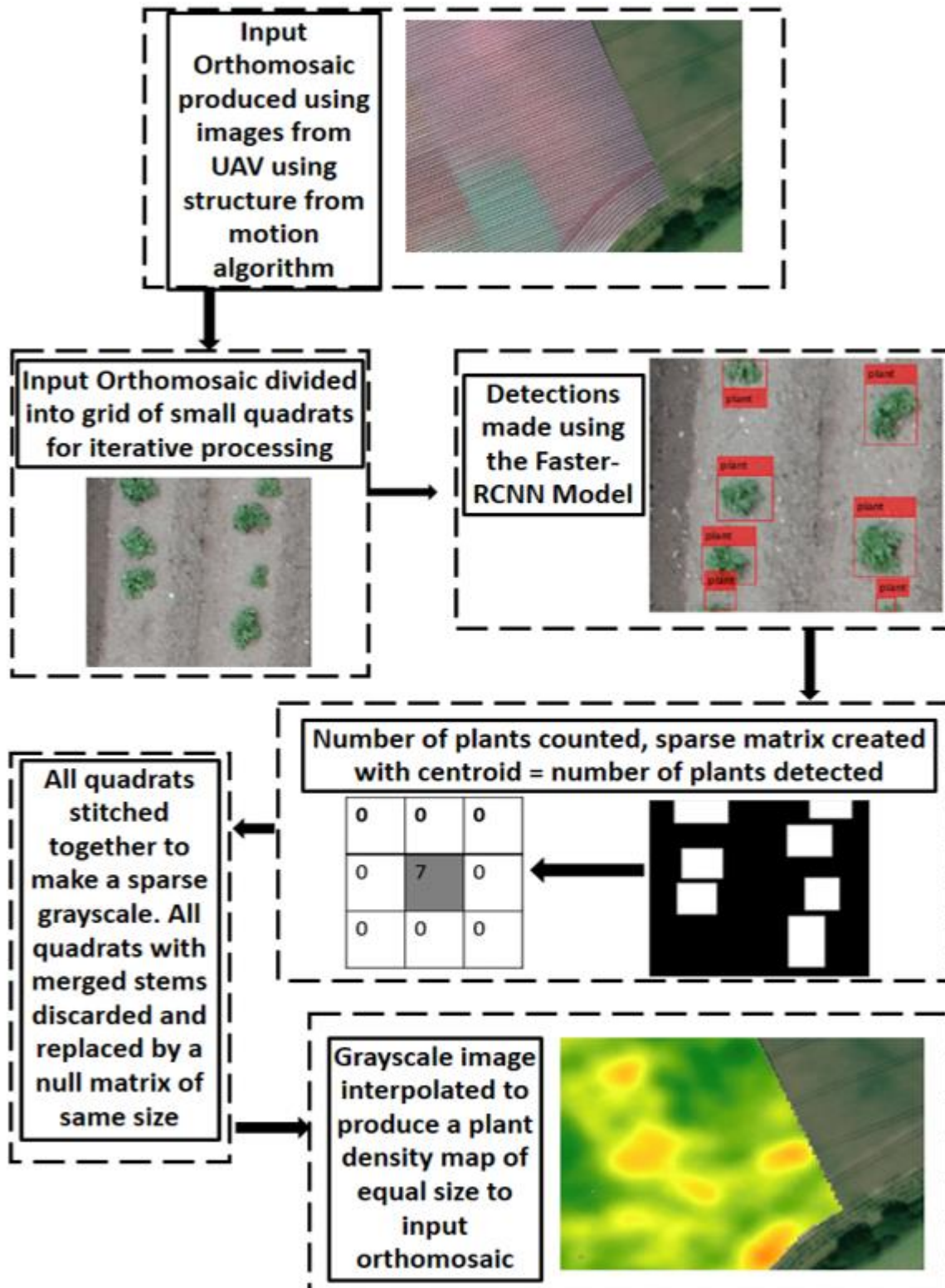


Figure 33: Flow chart for the production of a plant density plot from a transfer-learning model

At Horse Foxhole, atmospherically corrected (Level – 2A) Sentinel-2 satellite imagery was acquired from the Copernicus Open Access Hub on 12th May 2019. The date was chosen due to the absence of clouds in the satellite imagery after manual inspection. Additionally, this was the date on which the first discernible green vegetation spanning all of Horse foxhole was visible in the satellite images. Manual inspection was also conducted to ensure that there was spectral mixing with soil features in the images, indicating the lack of canopy closure. The satellite imagery of 10 m spatial resolution was clipped to the field boundaries of Horse Foxhole then processed in ArcGIS to calculate the NDVI of Horse Foxhole. The pixel values of the NDVI at 10 m spatial resolution were extracted then an interpolated surface of the whole field at 1 m spatial resolution was created by kriging with a Gaussian variogram model. Kriging was chosen after the inspection of significant spatial autocorrelation in the NDVI (Moran’s test P-value <0.001). Similarly, a manual inspection was conducted on the Sentinel-2 satellite imagery at Buttery Hill for cloud-free images. However, no further analysis of satellite imagery was conducted at Buttery Hill because all available cloud-free images met the exclusion criteria of having either bare soil (before emergence) or merged canopies without visual spectral mixing between vegetation and soil.

In both fields, 30 sampling sites were randomly selected and plant densities determined at each point using a 1 m row of plants. At harvest, the potato yield components were determined including marketable yield per square metre, average tuber weight, number of total and marketable tubers (per plant and square metre) and number of stems per square metre. The utility of plant density predictions from the interpolated surfaces of the FRCNN model and the NDVI in inferring the yield components was evaluated using the Pearson’s Product Moment Correlation (PPMC). The accuracy of the interpolated FRCNN surfaces in predicting the actual plant densities were evaluated using the root mean squared error (RMSE).

5.3 Results

Using the test dataset of 248 images from Horse Foxhole, the FRCNN model achieved an aP score of 0.78. Figure 34 shows the actual vs predicted number of plant objects in the test dataset drawn from the same pool as the training data. Overall, the model predicted the

actual number of plants in an image to within 2 stems error as illustrated in Figure 34 (RMSE = 1.59). The model had a nRMSE of 0.19 and R^2 of 0.80, though the scatter plot revealed relatively larger variation between observations and model predictions at higher plant densities, elucidating the decrease in model accuracy in closely spaced and potentially merged plants. Manual assessments showed that the model under-predicted the ground-truth bounding boxes in images with merged plants.

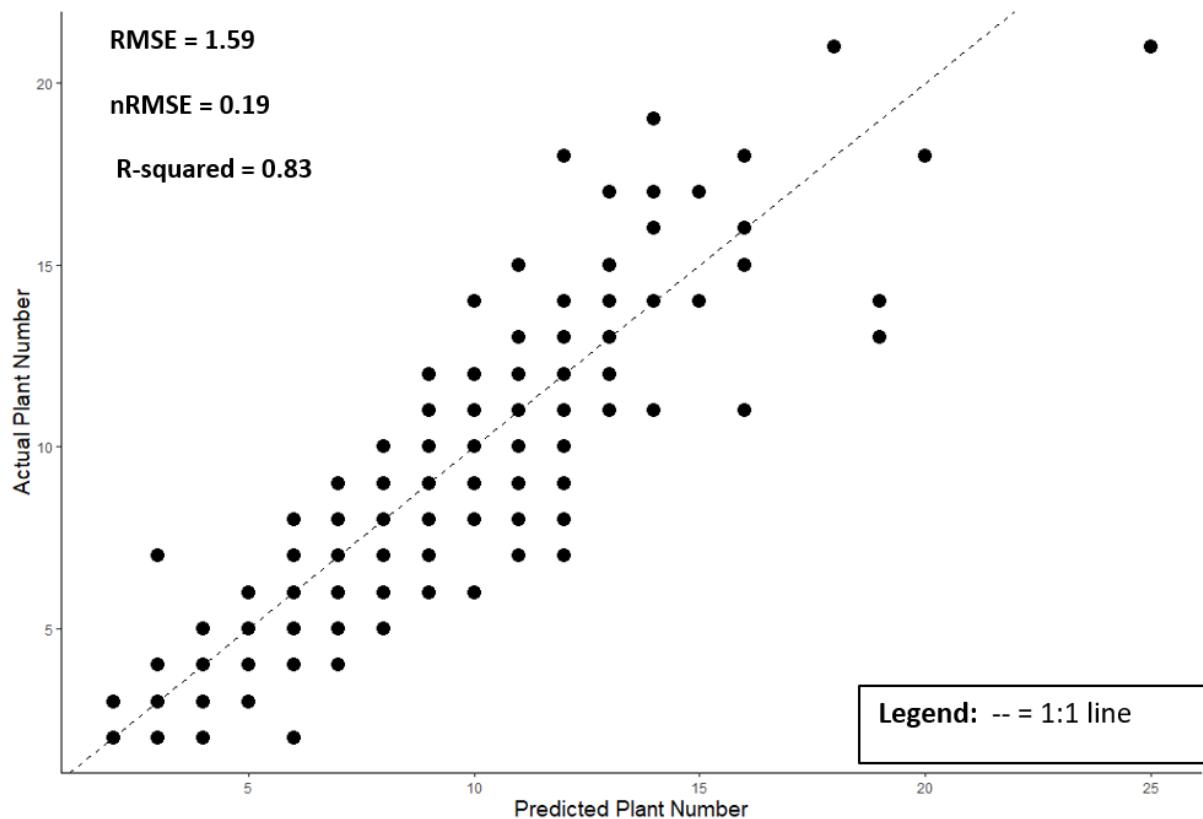


Figure 34: Actual vs Predicted potato plant numbers in a test dataset of potato plants using predictions from a Faster-RCNN transfer learning model

Some images contained potato plants that were emerging from the ground but had not formed enough above-ground foliage to be confidently annotated. The model learned and labelled these as potato plants, leading to over-prediction in a small number of instances. An illustration of this is in Figure 35, where the model predicted one more plant than the originally annotated ground truth on account of a single planting station that had delayed emergence and was not annotated in the ground truth but predicted by the model. In

practical terms, the model predictions were closer to the actual plant density than the ground truth labels in this instance. Due to the clear linear relationship between the predicted and actual plant counts, reliable plant density maps of the whole field could be constructed from the model and compared to observed densities.



Figure 35: Visualisation of the bounding-box predictions from a Faster-RCNN transfer-learning model (red colour) against manually labelled bounding boxes (yellow colour) at Horse Foxhole Field (image width = 1.5 m)

The plant density map of Horse Foxhole (Figure 36) revealed considerable systematic spatial variation in the plant stand, showing higher plant densities in the edges of the field compared to the middle. This was determined to result from an inconsistent seed metering mechanism during planting at the edges, resulting in very high plant densities. This was rectified when the middle section of the field was planted, culminating in the observed

differences. The variation in predicted plant density coincided with the variation observed in NDVI (Figure 37), showing that early-season NDVI sensed by the sentinel-2 is partially influenced by the plant density on the ground. NDVI was not measured at Buttery Hill due to the lack of cloud-free images before significant canopy consolidation in the Sentinel-2 repository, therefore the NDVI map and plant density map are not shown.

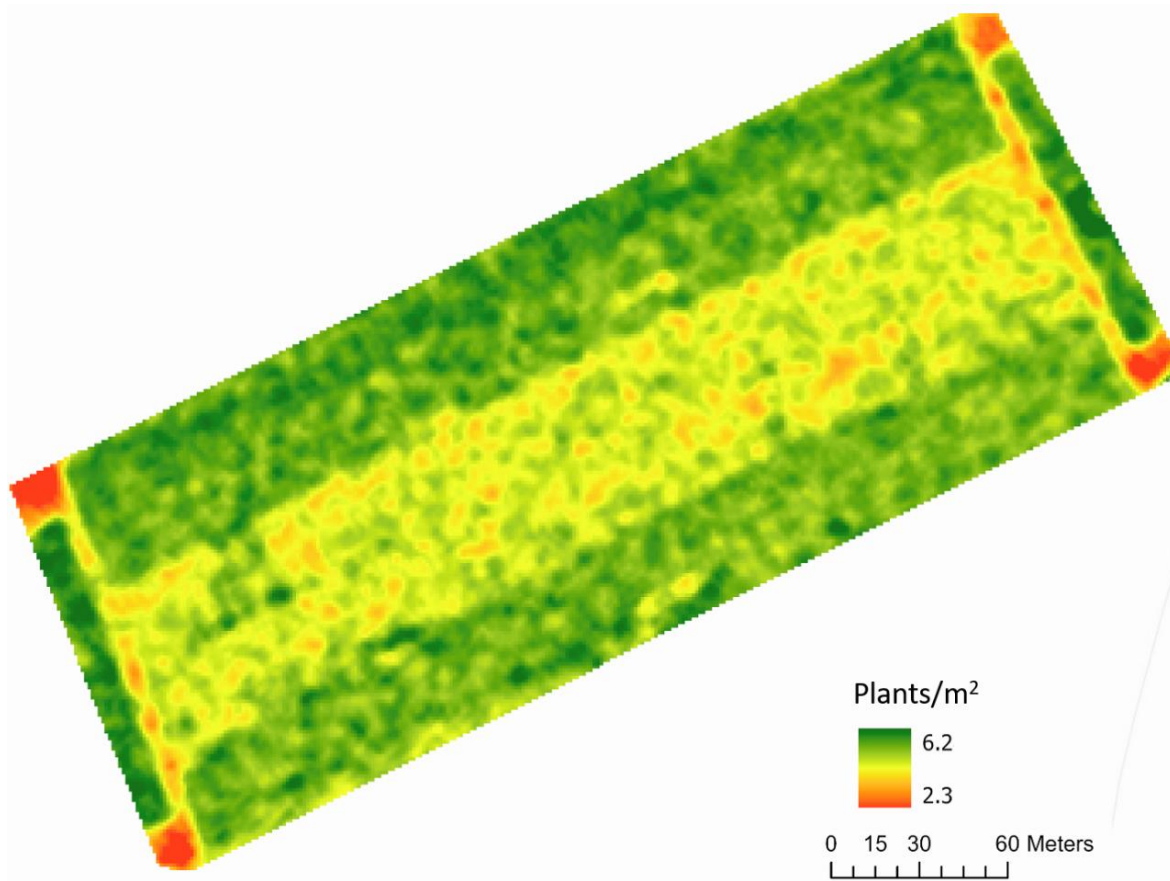


Figure 36: An interpolated predicted plant density plot of Horse Foxhole field, predicted using the Faster-RCNN transfer learning model

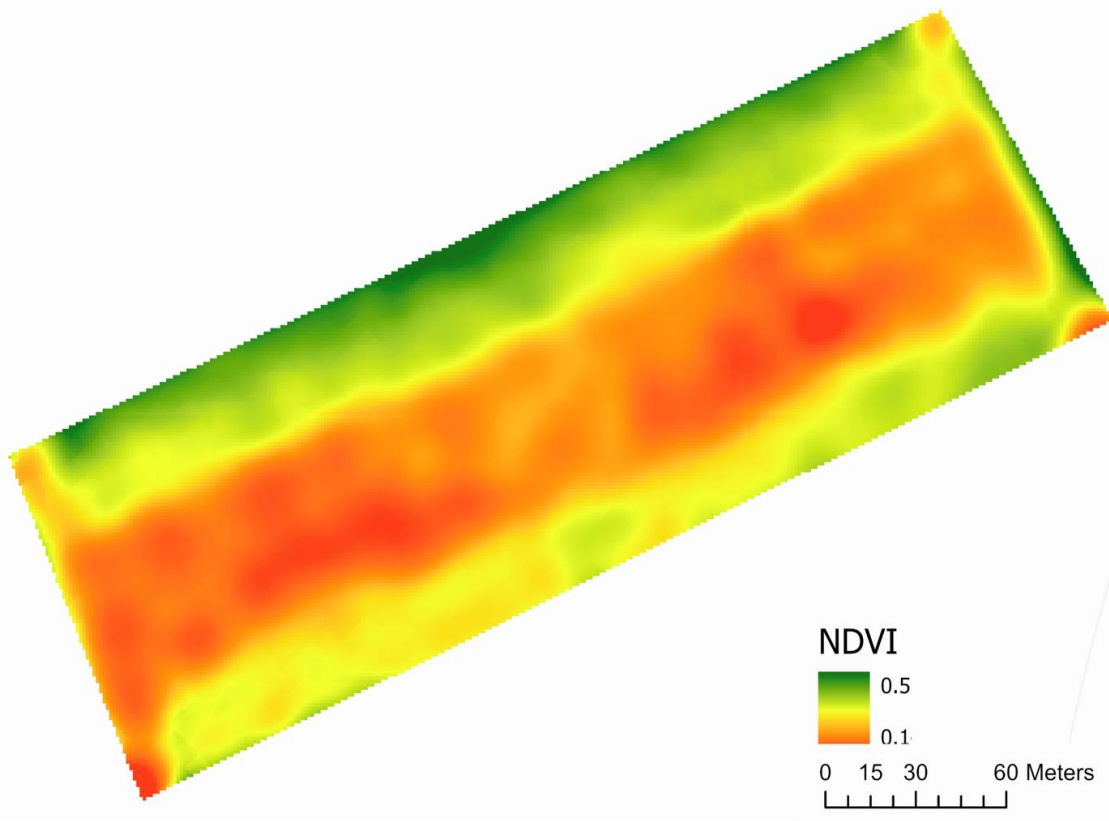


Figure 37: An interpolated plot of early-season NDVI in the Horse Foxhole field constructed from a Sentinel-2 (10 m spatial resolution) satellite image

Comparison of the actual plant populations at Horse Foxhole and Buttery Hill against the predictions from the FRCNN model (Figure 38) showed that the model performed comparably with the test dataset, with a RMSE of ~ 1 plant, nRMSE of 0.24, showing good accuracy at low plant densities but largely under-predicted at the high plant densities at Horse Foxhole. Overall, there was less variation in planting density at Buttery Hill compared to Horse Foxhole where high actual plant densities of up to 8 plants per square metre were observed, corresponding to approximately 12 cm spacing between plants. There was a large degree of overlap between plants at these plant densities, causing the model to miss some detections and subsequently return lower plant densities than expected. However, the model still highly captured the variation in plant densities ($R^2 = 0.80$) and therefore the density map produced was a reflectance of observed variation.

Table 20: Summary statistics of the plant density and Potato yield components at Buttery Hill and Horse Foxhole fields

Measure	Buttery Hill	Horse Foxhole
	Mean (STD)	Mean (STD)
SN/m ²	13.45 (3.79)	17.03 (2.7)
PPN/m ²	2.69 (0.77)	5.19 (1.58)
Mark.TN/m ²	34.03 (8.21)	48.26 (6.75)
Mark.TN/plant	17.83 (6.12)	11.3 (3.28)
Mark.TN/stem	3.5 (0.86)	3.22 (0.37)
Mark.Y/m ²	3.19 (0.78)	5.49 (0.61)
Mark.TW/plant	1.31 (0.5)	1.18 (0.4)
Avg.TW (g)	73.45 (9.72)	103.18 (9.82)
TTN/m ²	44.97 (12.24)	108.59 (14.83)

SN=Stem number, PN = Plant number, Mark.TN = Marketable tuber number, Mark.Y = Marketable yield in kilograms, Mark.TW = Marketable tuber weight in grams, Avg.TW = average tuber weight in grams, TTN = Total tuber number, NDVI = Normalized Difference Vegetation Index, PPN = Predicted plant number, STD = Standard deviation

Correlation analysis showed a highly significant correlation between the FRCNN plant density predictions and the actual plant densities as shown in Table 21. At both sites, there was a correlation of exactly 0.87 between predicted and measured plant density.

Furthermore, there was a strong correlation ($r = 0.61$) between plant density predicted by the FRCNN model and the NDVI derived from the Sentinel-2 satellite, quantitatively buttressing the visual similarity between the FRCNN plant density map (Figure 36) and the

NDVI map (Figure 37). The FRCNN-predicted plant density, actual plant density and NDVI all showed a similar pattern in their correlation coefficients with potato yield components.

Table 21: Correlation coefficients showing the relationship between actual plant density, potato yield components and plant density predicted from the Faster-RCNN transfer learning model at Buttery Hill and Horse Foxhole fields

Measure	Buttery Hill			Horse Foxhole			NDVI
	SN/m ²	PN/m ²	PPN/m ²	SN/m ²	PN/m ²	PPN/m ²	
SN/m ²	1	0.53*	0.66**	1	0.47*	0.48*	0.58*
PN/m ²	0.53*	1	0.87***	0.47*	1	0.87***	0.65**
Mark.TN /m ²	0.55*	0.46*	0.36	0.78***	0.29	0.33	0.36
Mark.TN /plant	-0.16	-0.6*	-0.61*	-0.28	-0.88***	-0.78***	-0.5*
Mark.TN /stem	-0.50*	-0.22	-0.40	-0.56*	-0.09	-0.18	-0.22
Mark.Y/ m ²	0.43	0.48*	0.35	0.58**	-0.08	-0.07	0.07
Mark.T W/plant	-0.20	-0.60*	-0.57*	-0.35	-0.94***	-0.82***	-0.56*
Avg.TW	-0.046	0.17	0.20	-0.42	-0.71***	-0.62**	-0.55*
TTN/m ²	0.46*	0.71**	0.54*	0.78***	0.48*	0.41*	0.53*
NDVI				0.58*	0.65**	0.61*	

* P < 0.05, ** P < 0.01, *** P < 0.001. SN=Stem number, PN = Plant number, Mark.TN = Marketable tuber number, Mark.Y = Marketable yield in kilograms, Mark.TW = Marketable tuber weight in grams, Avg.TW = average tuber weight in grams, TTN = Total tuber number, NDVI = Normalized Difference Vegetation Index, PPN = Predicted plant number.

Increasing plant density was associated with decreasing tuber number per plant ($r = -0.61$ at Buttery Hill and $r = -0.78$ at Horse Foxhole). Similarly, a negative significant correlation was

observed between NDVI and the number of tubers per plant at Horse Foxhole. The weight of tubers per plant was also negatively associated with plant density at both sites and a similar negative relationship was observed with NDVI at Horse Foxhole. Despite the significant relationships between plant population and the weight per plant, no strong correlation with yield per square metre was observed at both sites. Similarly, no correlation between marketable yield and NDVI was observed at Horse Foxhole. The negative correlation between predicted plant density and tuber weight per plant at Horse Foxhole ($r = -0.82$, $P < 0.001$) coincided with a positive correlation between predicted plant density and total tuber number ($r = 0.41$, $P = 0.01$). However, while the tuber number per unit area was positively related to the predicted plant density ($r = 0.41$ at Horse Foxhole and $r = 0.54$ at Buttery Hill), the overall yield per unit area was not significantly different. As observed in Table 21, high PPN at Horse Foxhole were negatively correlated with tuber weight ($r = -0.62$). The tuber weight per square metre at Buttery Hill was only weakly correlated to predicted and actual plant density although the tuber weight per plant was negatively correlated ($r = -0.57$) and the total tuber number was positively correlated ($r = 0.54$).

5.4 Discussion

The predictive precision obtained by the FRCNN model (0.78) is much higher than previously reported 0.41 mean average precision by Machefer et al. (2020), who used a Mask-RCNN architecture on overlapped plants. Though utilizing Mask-RCNN offers the prospective advantage of filtering individual plant masks from overlapping potato plants over ordinary FRCNN, Machefer et al. (2020) concede that accurate annotation of individual plants from canopy images of overlapped plants is difficult for domain experts and subsequently the trained models struggle to make accurate detections. Additionally, Mask-RCNN's detection framework is based on FRCNN, however, Machefer et al. (2020) conducted their study using images taken later than four weeks after emergence, while the image acquisition in this study was restricted to less than three weeks days after emergence. Therefore, large improvements in precision observed in this study are partially due to less overlapping plants in the images, on account of earlier image acquisition. While Dijkstra et al. (2019) report accurate mapping of individual plant centroids in merged canopies, they did not report the

average precision of their models. However, the inherent assumptions of the CentroidNet model in relation to potato plants reveal an underlying limitation that at least needs to be acknowledged; the radial expansion of a cluster of potato leaves from a centroid location is only likely to be valid in non-overlapping single-stem plants. Each planted potato tuber produces multiple competing stems that eventually function as independent plants, complicating the unit of plant density (Allen & Wurr, 1992). The direction of vectors learned from canopy leaf images are therefore expected to point towards the centroid of individual stems and not the overall plant object. Similarly, it is not practical for data annotation to be conducted in potatoes after a large degree of canopy consolidation because of the difficulty in assigning perceived individual main stems and leaves to individual plant units accurately. Machefer et al. (2020) also acknowledge this limitation in their data annotation and Li et al. (2019) acknowledge it as a source of error in their random-forest-based classification of potato plant numbers in an image from extracted plant object features. Because of these limitations, it can be considered impractical to conduct plant detection on images containing overlapped plants. While earlier image acquisition can solve the limitations, asynchrony in potato emergence days makes it difficult to determine an optimum day for obtaining a representative plant population. Beyond the scope of this study, striking a balance between premature and late imaging provides one potential solution to these challenges, which can be studied for each variety by evaluating model accuracy as a function of the number of days after planting. However, this would entail variety-specific recommendations for imaging time, which also need further calibration against factors that affect emergence rate like planting depth and average soil temperature. In this study, a geostatistical approach was chosen to create a sparse matrix of accurate plant density predictions at locations where no overlapping plants were observed.

In the two-stage (FRCNN detection then geostatistical interpolation) approach used in this study, it was demonstrated that an accurate 2D surface of the variation in plant population density can be created from partially merged canopies, by conducting detections on non-overlapping plants and interpolating across the whole surface. Except for soil temperature and disease incidence, the factors that have been reported to contribute to asynchrony in potato emergence like variety, seed-tuber physiological age and apical-dominance-altering

seed treatments vary at the seed-lot level (Sankaran et al., 2017). It is therefore reasonable to assume that spatial variation in plant emergence early in the season is attributable to systematic inefficiencies in planting operations. With an nRMSE of 0.19 for the determination of actual plant numbers per image as well as a high R^2 value (0.83), the current FRCNN model exhibits the robustness required to produce reliable field maps of spatial variation in plant density to inform precision agriculture decisions. Comparably, the image-analysis-based algorithm by Li et al. (2019) reported a high R^2 value of 0.96. However, as noted by both Li et al. (2019) and Machefer et al. (2020), the algorithm is heavily dependent on the accurate production of a noise-free binary mask based on the Excess Green vegetation index, which is not always guaranteed and cannot distinguish between weeds and potato plants. The current FRCNN model therefore provides a robust modelling pipeline free of the complexity of generating potato image masks from vegetation indices deployed in the Mask-RCNN and random-forest-based image analysis algorithm.

The high correlation between satellite-imagery-derived NDVI and the FRCNN model results reported represents novel evidence of a link between early-season NDVI and potato plant density. Before canopy consolidation, NDVI is influenced by soil brightness in coarse-resolution imagery, which is normally corrected using the Soil-Adjusted Vegetation Index (Huete, 1988a) when evaluating vegetation health. In the present study, non-adjusted NDVI was used with the premise that the level of interference from soil is dependent on the number of plants in the pixel. The high correlation value ($r = 0.61$) between the FRCNN modelled plant densities and the NDVI values substantiates this premise. A limitation to the use of satellite data for this purpose is the uncertain availability of cloud-free images after emergence before canopy consolidation (highlighted in this study by the lack of available cloud-free images within this window at BATTERY Hill). Nevertheless, early-season NDVI can be calculated from UAVs hosting Red and NIR sensors, down-sampled to reproduce the spectral mixing observed in satellite imagery.

The findings agree with Knowles and Knowles (2006) that there is a significant negative effect of plant density on the number of tubers per plant. Additionally, they found a negative correlation between tuber size (measured as average tuber fresh weight in g) and

plant density, in line with the results. In controlled-treatment studies, the effects of plant density on yield are largely inevitable due to large fixed differences in plant density between treatments, which may not be observed within a typical commercial production field. Previous studies (Arsenault et al., 2001; Bohl et al., 2011; N. R. Knowles & Knowles, 2006; Love & Thompson-Johns, 1999) report significant positive association between plant density and yield, in line with the observations at BATTERY Hill. However, the relationship was not observed at Horse Foxhole, with yield more related to stem number than plant number. Bussan et al. (2007) also found that yield was more related to stem number than plant number, with the latter explaining a negligible portion of the variation ($R^2=0.06$).

Ultimately, the association between plant density and yield appears to be complicated. While the findings suggest that areas of high plant density within a field produced more tubers per unit area, the number of marketable tubers at harvest was smaller. Assuming exponential growth in dry matter production over time (Goudriaan & Monteith, 1990; Kooman & Haverkort, 1995), marketable tuber numbers can potentially be increased by delaying harvest timing in high density areas to allow for more tuber bulking. One utility of the main findings is that plant density maps produced from UAVs can be used as a basis for management and harvest decisions, such as variable in-season nitrogen management to delay senescence for tuber bulking purposes and subsequently incorporate variable vine desiccation and harvest timing.

5.5 Conclusion

This study demonstrated the feasibility of FRCNN-based models in the prediction of potato plant population and the subsequent production of representative 2D-density maps which can inform decisions on precision agriculture. FRCNN models for potato plant detection are known to be less accurate in predicting yield when canopies merge and the asynchrony in potato emergence makes the trade-off between early and late image acquisition especially difficult and most likely impractical for commercial application. Nevertheless, the goal of these models is the accurate estimation of variation at the field-relevant spatial scale rather than per-plant pin-point accuracy. Therefore, the filtering and subsequent interpolation of reliable non-merged FRCNN predictions provides a work-around to the problems of

overlapping plants. It is demonstrated that plant density maps produced from this approach are consistent with early-season satellite-imagery-derived NDVI scores. Plant counting algorithms for potatoes have captured the interest of several computer vision and deep learning researchers, and therefore improvements in the CNN architecture and object detection frameworks can be reasonably expected, especially in the direction of the CentroidNet architecture. Finally, it was shown that simple frameworks like FRCNN are adequate for predicting potato yield components while avoiding the problems associated with other estimation methods.

CHAPTER 6 - Use of Spatio-Temporal Variation in Sentinel-2 Data to Develop Indices of Fine Scale Canopy Variations for Potato Yield and Stem Density

Abstract

Satellite Image Time Series (SITS) have been used to predict potato yields (*Solanum tuberosum* L.), at regional scales, but extension of such models to local field scale for practical use in precision agriculture is lacking. In this study, multispectral data from the Sentinel-2 satellite were used to extrapolate continuous spectral signatures of potato plants and generate vegetation indices and the red edge inflection point (REIP) to relate to marketable yield and stem density. The SITS data were collected from 94 sampling locations across five commercially planted potato fields in England, United Kingdom. The sampling locations were georeferenced and the number of stems per square metre, as well as marketable yield, were determined at harvest. The first principal components of the temporal variation of each SITS wavelength were extracted and used to generate 54 canopy growth indices to relate to marketable yield and stem population. Marketable yield was negatively correlated to the overall seasonal reflectance (first principal component) at 559 nm with a beta coefficient of -0.53 ± 0.18 (margin of error at 95% confidence interval). Early-season normalized difference vegetation index, manually counted Stem Density and the overall reflectance at 703 nm had a positive significant relationship with Marketable yield, suggesting that integration of satellite imagery and manually collected estimates of stem density can be used to predict yield. Marketable yield, with respect to the four covariates, was modelled with a normalized root mean square error (nRMSE) of 0.16. On the other hand, Stem density was significantly related to the Specific Leaf Area Vegetation Index ($\beta = 1.66 \pm 1.59$) but the REIP's farthest position during the season was reached later in dense canopies ($\beta = 1.18 \pm 0.79$) and the reflectance at the REIP was higher ($\beta = 3.43 \pm 1.9$). This suggested that denser canopies took longer to reach their maximum chlorophyll intensity and the intensity was lower than in sparse canopies. Potato stem density, with respect to remote sensing estimates of vegetation, leaf area and chlorophyll absorption indices was modelled with a nRMSE of 0.24. These results reinforce the importance of SITS analysis as opposed to the use of single-instance intrinsic indices. Our results highlight the relationship

between yield and 559 nm reflectance, often ignored due to the ubiquity of intrinsic indices based on the Near Infrared and Red difference.

6.1. Introduction

The variation in reflectance of electromagnetic radiation between plants of different species and physiological health conditions has enabled the development of remote sensing applications for crop health monitoring, high throughput phenotyping, and precision agriculture. Satellite-acquired multispectral image data is globally available in the public domain at various temporal intervals from the Landsat series of satellites (up to 30 m resolution, 16 day revisit time) since 1972 (Bauer, 1973; Dev Acharya & Yang, 2015) and the Sentinel satellites (up to 10 m resolution, 5 days revisit time) since 2015 (Szantoi & Strobl, 2019). Satellite image data are often used to derive vegetation indices, most notably the Normalized Difference Vegetation Index (NDVI) developed by (Rouse et al., 1973), which has been widely used for vegetation surface classification and crop health assessments. Since the launch of the Landsat satellite, a highly active research area has emerged to attempting the use of spectral reflectance values of canopies to predict or infer plant-level dependent variables of interest through traditional linear regression models or machine learning approaches. However, while remotely sensed vegetation indices are often well correlated to crop biomass, they often constitute poor indicators of crop yield, which hinders their adoption in yield prediction (Turvey & McLaurin, 2012). Consequently, very little crop-specific published literature exists on the successful use of vegetation indices from satellite image data to model yield attributes. More studies are required to establish methods for robust transformation of remotely sensed spectral reflectance measurements or the different vegetation indices derived from them in order to provide reliable explanatory variables for the crop biomass or yield variables of interest.

The potato is the world's third most important crop primarily grown for human consumption after wheat and rice (De Jong, 2016). This is partially due to its high ratio of economic biomass to total biomass (harvest index) (Bradshaw & Ramsay, 2009), which is higher than that of all the world's major cereals (*Zea mays*, *Triticum aestivum*, and *Oryza*

sativa) and grain crops (Unkovich et al., 2010). In precision potato agronomy, establishing an accurate estimate of plant density for downstream decision-support is an important open research area due to the complex physiology of the crop. Although planted seed-tuber populations and plant spacing are closely controlled by farmers, potatoes produce highly variable stem numbers per planted tuber and each stem eventually develops its own independent tuber set and acts as an independent plant unit (Knowles & Knowles, 2006). This makes the number of emerged stems a more representative unit of plant density than using the number of tubers that were planted or the number of plant clusters that emerge from the total planted tuber population. Using the spectral properties of plants, aerial image analysis has been used to predict potato plant density in potatoes (Li et al., 2019; Mhango, Harris, et al., 2021), however, the unit of plant density used in the studies (the number of emerged independent plant clusters per unit area) is not the ideal representative unit of plant population (stem density). While machine learning methods have been used to enumerate potato stems from images collected using unmanned aerial vehicles (Mhango, Grove, et al., 2021), no previous research has attempted to predict stem density from satellite images. Development of estimation techniques for stem density remains pertinent in potato production, with several studies linking it to tuber size and total yield variations at harvest (Bleasdale, 1965; Gray, 1972; Knowles & Knowles, 2006; Love & Thompson-Johns, 1999; Wurr, 1974).

Studies using satellite imagery for overall yield prediction in advance of harvest are mainly motivated by the need for objective crop production estimates in areas where ground-level records are logistically difficult to acquire (Salvador et al., 2020). Such predictive models have potentially wide applicability in region-level resource planning and early-warning systems for famine in resource-constrained environments. Therefore, several studies on agricultural yield prediction from satellite imagery have been conducted in semi-arid locations. For example, low resolution (500 m pixel dimensions) satellite imagery from the TERRA MODIS satellite has been used to calculate NDVI and demonstrated ability to explain up to 84% of the variation in potato yield (Bala & Islam, 2009). Predictive models were also developed by (Al-Gaadi et al., 2016) based on NDVI and the Soil Adjusted Vegetation Index

(SAVI) from 30 m Landsat-8 and 10 m resolution Sentinel-2 satellite images, explaining between 39% and 65% of the variation in potato yield. Additionally, machine learning models have been used to leverage NDVI for the prediction of potato yield, with a large proportion of the variation in yield (up to 86%), accounted for by the empirical models (Salvador et al., 2020). While these are promising results, the models are based on region-level studies with limited applicability at the farm level and the machine-learning-based models do not provide coefficients that are relatable to biophysical processes. Therefore, opportunity is lost to understand the underpinning phenomena behind the observed relationships for informing future studies. Models designed to infer farm-level phenomena require higher spatial resolution than provided by the MODIS satellite, and there is a general consensus that higher spatial resolution results in better model accuracy (Kharel et al., 2020). With up to 10 m spatial resolution, the Sentinel-2 satellite, therefore, provides enough detail to model within-field spatial variation in reflectance and potentially infer the processes that affect it. However, In-situ measurements for developing models or validating remotely-sensed reflectance can come at spatial resolutions that are disparate to the satellite product (Ali et al., 2016; Kharel et al., 2020). The use of coarse-scale sensors or cropping data to simulate yield neglects fine-scale variability, which raises questions over the usability of such models at finer-resolution than provided by the remote sensor (Kharel et al., 2020). To resolve this, every pixel of the remote sensing product is typically mapped to a single value of in-situ measurements, which can be determined by appropriate random sampling, or aggregation (resampling) of the in-situ measurements to the resolution of the remote sensing product (See [19,22,23]). While aggregation or collection of a single representative value per pixel allows the combination of in-situ and remotely sensed data, the establishment of relationship coefficients between the two data sources is often biased by the violation of the independence assumption in linear regression modeling, due to spatial autocorrelation (McCullagh & Clifford, 2006; Minasny & McBratney, 2005, 2006). This remains a significant issue that is often ignored when regression models are produced from remote sensing data, leading to biased coefficient estimates (Ali et al., 2016; Kharel et al., 2020). Various statistical modeling techniques including Geographically Weighted Regression (O'sullivan, 2003) have been suggested for unbiased estimation of regression

coefficients (Kharel et al., 2020). Spatial mixed effect modeling techniques (Rousset & Ferdy, 2014) provide effective ways of dealing with sample non-independence and they provide for a non-biased integration of clustered data from different study locations to estimate more robust global coefficients. While variations of such approaches are not novel and have been used in remote sensing work (see (Unnithan & Gnanappazham, 2020)), evidence of the application of these methods in the context of field-level vegetation cover modeling cannot be readily found in the literature.

The timing of image acquisition and the pre-analysis transformations required of satellite image data are important for the generation of appropriate data from which inferences can be made about the relationship between canopy reflectance and variables of interest. From a physiological standpoint, the final dry matter production in potatoes, from which final marketable yield is derived, is a function of cumulative absorbed radiation throughout the season (Kooman & Haverkort, 1995; Silva-Díaz et al., 2020). The final proportion of the daily dry matter that gets allocated to further above-ground vegetative development and/or tuber yield is dependent on a time-varying harvest index (Haverkort et al., 2015; Kooman & Haverkort, 1995). Therefore, the temporal rates at which a potato canopy develops, represented by changes in reflectance, are potential indicators of end-of-season yield. Several studies have established the occurrence of an exponential increase towards an asymptotic maximum ground cover and leaf area index in potatoes, followed by an exponential decrease at senescence (Haverkort et al., 2015; Kooman & Haverkort, 1995; Silva-Díaz et al., 2020). The rate and peak of the exponential functions that describe canopy development are affected by genetic factors (sown variety) (Geremew et al., 2007) and environmental factors such as plant abiotic or biotic stress and plant population (Li et al., 2019; Machefer et al., 2020), which all contribute to the final yield. Where the genetic factor is fixed, the rate and asymptotic peak parameters that define the exponential development of the canopy are therefore location-specific and dependent on spatially-variant biotic and abiotic stress factors. Potato crop growth models largely rely on the estimation of temporal absorption of photosynthetically active radiation which exponentially increases to a maxima at full canopy (Kooman & Haverkort, 1995), akin to the typical temporal development of

NDVI [20]. The subsequent evolution of the harvest index (ratio of economic to total biomass) follows a similar pattern while the total dry matter production follows an exponential growth curve (Goudriaan & Monteith, 1990; Kooman & Haverkort, 1995). As an implication, a cropping area that maximizes light interception earlier than other parts of the field can be expected to yield more due to relatively more time provided for maximal biomass accumulation in tubers. Therefore, the temporal rate of development of vegetation indices like NDVI can potentially be utilized to predict tuber yield but no studies have empirically evaluated this relationship. Accurate estimation of the peak and rate parameters governing the temporal development of SITS-derived indices is dependent on the regularity of the SITS. Evaluation of the relationship between temporal resolution and model accuracy would require systematic resampling of SITS and different time intervals, which is difficult in cloud-dependent irregular SITS such as those provided by the Sentinel-2 satellite. Several previous studies have used smoothed time series of vegetation indices to extract the index values at each day and correlate to crop yield variables (Aparicio et al., 2000; Thapa et al., 2019). In these previous studies, Pearson's product-moment correlation was calculated between vegetation indices and yield variables at each day for which valid (cloud-free) satellite imagery was available, then the evolution of the correlation coefficient over time was studied. The day at which the correlation coefficient was maximized was chosen as the optimal day of satellite image collection for the maximum predictive value of yield (Aparicio et al., 2000; Thapa et al., 2019). The main drawback with such methods is that they work best with a high temporal resolution of the satellite imagery over the cropping season, which is not guaranteed in satellite imagery due to erratic cloud cover. Collation of images for the whole season enables better retrospective modeling and good model performance has been reported in previous studies (Al-Gaadi et al., 2016; Bala & Islam, 2009). In a time-series study of the relationship between satellite-image-derived NDVI and potato yield, (Johnson, 2016) found that the correlation coefficient was highest when NDVI was at its peak, estimated to be at the middle of a typical growing season. Such models offer limited utility for mid-season prediction due to their requirement for full-season data, though the relationship coefficients derived from these studies are important for understanding and deriving hypotheses for the underpinning mechanistic models governing the phenological

development of plants with respect to solar radiation absorption. The discovery of effective methods for the extraction of temporal features from irregular SITS and relating them to crop phenology is therefore an open research area for which novelty is required.

The goal of this study was to contribute to the knowledge on the transformations required of Sentinel-2 satellite data to engineer features that can be related to biophysical processes of interest in potatoes. Specifically, the objective of this study was to derive simple temporal peak and rate parameters describing the development of reflectance for selected Sentinel-2 bands and relate them to potato response variables—yield and stem density. The overall temporal development of each band was also encoded as the first principal component and related to the response variables, to infer how end-of-season yield relates to this temporally accumulated variation.

6.2. Materials and Methods

6.2.1. Site Characterisation

The study was conducted at five sites as summarized in Table 22. Deaton 6 and HF7 sites were located in marsh-reclaimed land with a shallow water table and high organic matter content. Horse Foxhole, Crabtree Leasow, and Buttery Hill were located in well-drained, slightly stony, sandy loam soil subtended by weathered sandstone. At all the fields, the plow depth during land preparation was 30 cm and beds were formed with 90 cm between rows after destoning. The locations of the fields were as mapped in Figure 39. Within each site, management practices were conducted uniformly across the field throughout the growing period.

Table 22: Summary of the location and key production information of the study sites

Field Name	Location	Variety	Number of Samples	Planting Date	Harvest Date
Deaton 6	53°12'20.97" N 0°21'55.06" W	Maris Piper	12	10 April 2019	05 August 2019
HF7	53°12'40.71" N 0°24'49.76" W	Maris Piper	23	12 April 2020	18 August 2020
Buttery Hill	52°46'22.05" N 2°25'40.46" W	Amora	30	20 March 2020	24 July 2020
Horse Foxhole	52°46'26.94" N 2°25'49.38" W	Amora	23	27 March 2019	11 July 2019
Crabtree Leasow	52°46'15.73" N 2°25'35.51" W	Pentland Dell	6	16 April 2020	21 August 2020

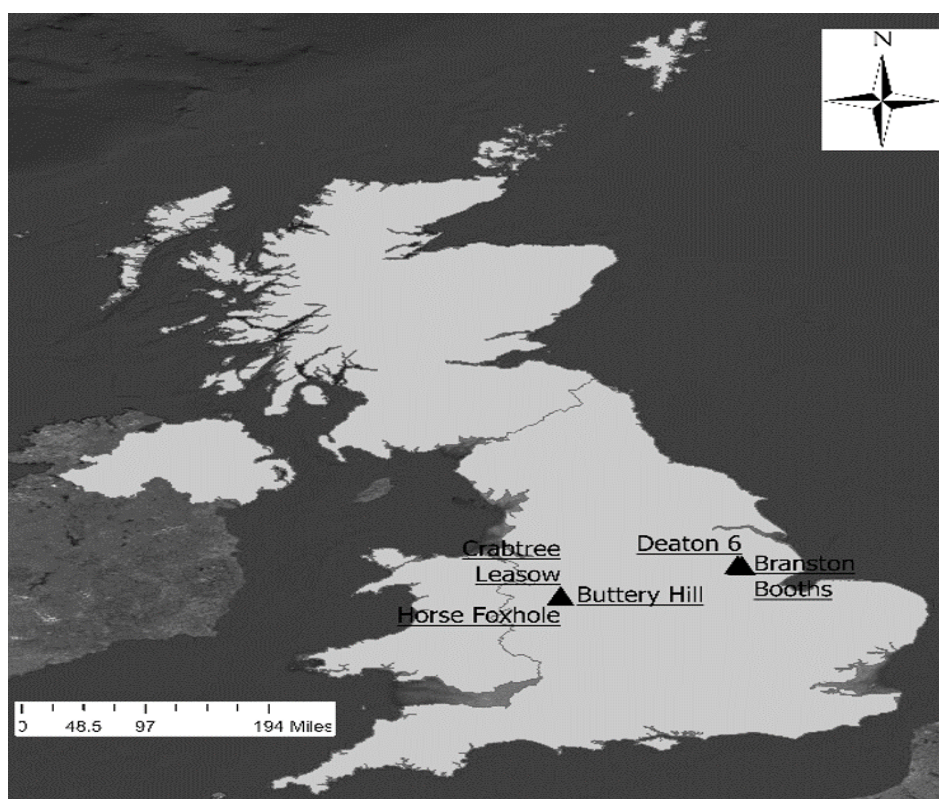


Figure 39: Map of the United Kingdom territory showing the locations of the 5 study sites (Crabtree Leasow, Horse Foxhole, Buttery Hill, Deaton 6, and Branston Booths).

6.2.2. Sampling Design

To determine representative locations for subsequent yield sampling in each field, a model-based sampling approach was taken. Our sampling was informed using soil color variation as a proxy for the variation of organic matter and by extension soil macronutrient quantities (Costa et al., 2020; Yang et al., 2011) that affect yield. The Soil Brightness Index (SBI) as described by (Mponela et al., 2020) was chosen to spatially model the soil color differences at each field. The average SBI for three months prior to crop emergence was calculated using atmospherically corrected (Level-2A) Sentinel-2 satellite imagery of 10 m resolution on manually inspected cloud-free days. From the normalized SBI choropleth map, three zones of relative homogeneity were defined by k-means clustering ($k = 3$) to define dark-colored soils (k-means cluster centroid ranging from 0.31–0.39), light-colored soils (k-means cluster centroid ranging from 0.78–0.87), and medium hue soils (k-means cluster centroid ranging from 0.56–0.61).

In commercial potato production, the variables of interest of this study (stem density and marketable yield) are likely to only be managed if they exhibit relatively long-range spatial autocorrelation to enable practical mechanized control (Taylor et al., 2018). It was therefore necessary to define a practical spatial scale for in-situ measurements. In the most recent related large-scale study of the spatial structure of potato stem density and marketable yield in the UK, (Taylor et al., 2018) reported relatively long-range spatial autocorrelation for both stem density (48 m) and marketable yield (114 m). Agricultural yield processes are known to be spatially rough but the decay in spatial autocorrelation is controlled by latent field-scale limiting factors (e.g., variety and soil type) which maintain a long-range logarithmic decay (de Wijs process) rather than an exponential decay process (McCullagh & Clifford, 2006; Minasny & McBratney, 2005). In commercial production, farmers aim to produce uniform plant density across the field and any variation is likely to come from factors such as a systematic fault in the planting operation, low viability of a batch of seed, or soil-borne factors that affect seed germination (Bohl et al., 2011), which have a long-range of autocorrelation relative to the size of the field as observed by (Taylor et al., 2018). This large-scale autocorrelation in comparison to Sentinel-2 satellite data resolution means

that fine-scale in situ data on stem number and yield can be resampled to 10 m or 20 m resolution while maintaining the structure of the spatial variability.

Resampling of sub-pixel-scale in situ data to align with the pixel size of Sentinel-2 data is a common technique deployed previously to model potato yield (Al-Gaadi et al., 2016) and other crops (Escolà et al., 2017; Hunt et al., 2019). During resampling, it is crucial to ensure that the assigned in-situ data are collected with enough locational accuracy such that their true location aligns with a single pixel of the Sentinel-2 data. In-situ sampling resolution must therefore take GPS instrument error into account, in relation to the targeted resampling resolution. In this study, a *Garmin™ eTrex 20* with 3 m accuracy specification was used to navigate to the yield sampling locations. The aim was to randomly select a sampling point within any 10 m pixel of the SBI map, therefore, a sub-pixel sampling unit of 6 m by 6 m was chosen to ensure that the sampling location was within a single 10 m pixel. A grid of 36 m² quadrats was imposed across a rasterized SBI surface then random quadrats were then drawn from each stratum as sampling points. An intersection of each drawn sampling point with the 10 m resolution SBI surface was done to check that the drawn sampling point was spatially contained within a single pixel SBI pixel. Statistical power analysis (Cohen, 1988) was used to determine the number of sampling points to draw from each stratum to maintain a statistical power of 0.8. The effect size was calculated as the standardized difference between the expected SBI of *dark* soils and the combined expected SBI of the *medium and light* clusters. Power analysis was conducted using R (R Core Team, 2019). Using ArcGIS (ESRI, 2020), the determined sample size was drawn from the grid of 36 m² quadrats, extracting the centroid pixel from every 6 m by 6 m quadrat. The extracted coordinates were exported into the *Garmin™ etrex 20* GPS receiver for tracking during yield sampling. Since the GPS receiver had a locational accuracy of 3 m, navigating to the centroid of the 36 m² quadrat with the maximum possible 3 m offset ensured that the located point was within the intended quadrat.

6.2.3. Collection and Processing of Satellite Imagery

At each site, all cloud-free dates on which the Sentinel-2 satellite captured data during the growing period were manually inspected. In total, four post-emergence cloud-free images were collected each of five locations (Buttery Hill, Crabtree Leasow, Deaton 6, HF7, and Horse Foxhole). A Keyhole Markup Language (KML) file was created for the spatial extent of each site then the `sen2r` (Ranghetti et al., 2020) package in R (R Core Team, 2019) was used to download 20 m resolution level-2A (atmospherically corrected) tiles covering the spatial extent from the Sentinel-2 image repository at all the determined cloud-free dates, forming SITS. For each retrieved image representing an individual Sentinel-2 band, bicubic interpolation was used to down-sample the raster to 6 m then the sampling points at its corresponding site were superimposed, and the pixel value at which each sampling point fell was extracted and stored. The final raw extracted dataset comprised of a time series of the pixel values of each Sentinel-2 band for each sampling point at the five study sites.

6.2.4. Principal Component Analysis

For each observation point, each of the nine Sentinel-2 bands (resampled from 20 m to 6 m resolution) had four reflectance measurements taken at four different times during the course of the season. This captured the change in reflectance during the course of the season for each band. In order to create an overall representation of the SITS for the whole season for the observation point, principal component analysis was chosen. Accordingly, at each sampling point, the data was processed by re-arranging the nine bands as observations and the four imaging dates as variables, creating a 9×4 matrix. The principal components of the four dates were then computed and the standardized first principal component was determined as a nine-element vector representing the overall temporal variation of the observation. The column vector was then transposed into a row vector with nine variables representing the values of the nine Sentinel-2 bands for the observation. This analysis, therefore, encoded the overall reflectance of each wavelength throughout the season, giving an index for its temporal expression. The percentage of variance explained by the

principal component at each observation point was also recorded in order to assess the amount of variation encoded in each component.

6.2.5. Rates of Change in Reflectance

The daily vegetative growth of a potato plant is a function of intercepted radiation and the radiation use efficiency mediated by the genotype and environment (Wolf, 2002). The intercepted radiation can be estimated as an exponential function of the crop leaf area index (LAI), plateauing at full canopy cover before exponentially decreasing towards senescence [30,38,49]. Previous reports on the temporal profile of spectral reflectance in potatoes, particularly using the Normalized Difference Vegetation Index (NDVI), suggest a similar curve of exponential increase in spectral reflectance towards a maxima followed by an exponential decrease (Islam & Bala, 2008; Shamal & Weatherhead, 2014). Extracting temporal features of interest in multispectral reflectance like the maximal value and the rate at which the maxima is reached therefore provides proxies for crop growth rates (Velichkova & Krezhova, 2019). In this study, at every sampling point, the reflectance at each wavelength was plotted against the days after planting (DAP) on which the satellite imagery was obtained (Figure 40). A second-order polynomial equation was then fitted to the data to model the exponential growth curve towards a peak. The turning point of the polynomial was maximal for wavelengths that are reflected by vegetation (e.g., Near Infrared) as shown in Figure 40, or minimal for wavelengths that are absorbed by vegetation (e.g., water absorption bands).

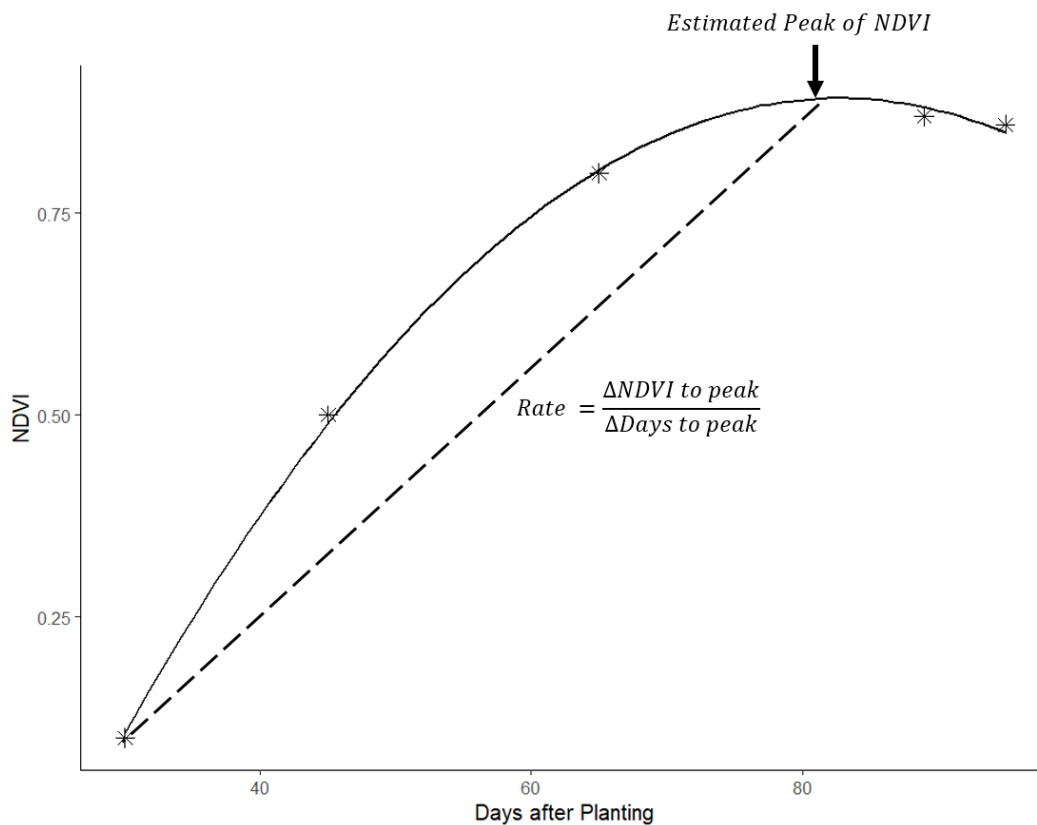


Figure 40: An illustrative graph showing how spectral index values like the Normalized Difference Vegetation Index (NDVI) were plotted in time and their peak and rate parameters derived.

The reflectance at the turning point of the polynomial was therefore determined as the peak (or trough for absorbed wavelengths) reflectance of the particular wavelength relative to DAP. The rate of growth to maximal reflectance or absorption was calculated by dividing the DAP at the turning point by the reflectance value. Apart from the single wavelengths, several ratio-based vegetation indices were also calculated, as summarized in Table 23. NDVI at tuber initiation was approximated as the NDVI value at 7 weeks after planting.

Table 23: Summary of the vegetation indices used in the study.

Index Name	Main Reported Use	Formula	Reference
Normalized Difference Vegetation Index (NDVI)	Classification of vegetation against non-vegetation background	$\frac{\rho_{865} - \rho_{664}}{\rho_{865} + \rho_{664}}$	(Rouse et al., 1973)
Specific Leaf Area Vegetation Index (SLAVI)	Approximating leaf area index	$\frac{\rho_{865}}{\rho_{664} + \rho_{2186}}$	(Lymburner et al., 2000)
Chlorophyll Index Green (CIG)	Approximating vegetation chlorophyll variations	$\left(\frac{\rho_{783}}{\rho_{560}}\right) - 1$	(Gitelson et al., 2003)
Normalized Difference Moisture Index (NDMI)	Approximating vegetation moisture variation	$\frac{\rho_{865} - \rho_{1610}}{\rho_{865} + \rho_{1610}}$	(Wilson & Sader, 2002)

6.2.6. Estimation of Red-Edge Inflection Points

A basic feature of chloroplast biology, photosystems I and II have their maximum absorption efficiency at 700 nm and 680 nm respectively, beyond which plants exhibit high reflectance of Near Infra-Red (NIR) (Hallik et al., 2019). This zone of the abrupt shift from absorption to reflection is referred to as the Red Edge (Horler et al., 1983). Several studies have shown that reflectance at the red edge inflection point becomes lower and its specific wavelength position shifts higher in vegetation with more chlorophyll-associated absorption of light. Therefore the position of the inflection point and its reflectance is used to model chlorophyll content and hence photosynthetic efficiency as proxies to dry matter accumulation and yield [56,58,59]. The red-edge inflection point can be found by identifying the first derivative of a smoothed spectral profile and finding the position of the peak in the red-edge region (Horler et al., 1983; Smith et al., 2004).

In this study, the visible and NIR spectral values derived at each date of sampling were plotted and the Savitzky-Golay filter (Savitzky & Golay, 1964) was used to estimate a smooth spectral signature (Ishikawa et al., 2015; Velichkova & Krezhova, 2019). At each location, the

reflectance values of each Sentinel-2 band were extracted, then each cloud-free date's spectral reflectance signature was plotted as an irregular series. The "sgolay" function from the "Signal" package in the R signal package (v0.7–6) was then used to construct a second-order Savitzky-Golay filter of length 3. The filtered values were used as predictor variables in a linear model to predict the original spectral signature. Prior to fitting the linear model, the filtered and original values were resampled using linear interpolation to produce a value for each wavelength between 492 nm and 864 nm ($n = 372$). Linear interpolation of Savitzky-Golay filter results to generate continuous series is a common method used in mathematics and computer science (Pan et al., 2017). The linear interpolation permitted the fitting of a fifth-order polynomial to allow inflection points at all observed wavelengths and generate smooth curves. The polynomial was fitted as a linear model and the fitted values were used to approximate the continuous spectral signature. The estimated continuous spectral signatures at different time points in the season could then be used to visually evaluate the temporal evolution of the spectral signature.

The first derivative of each smoothed spectral signature was also derived and the wavelength position of the maxima in the red edge was determined and extracted as the red-edge inflection point following (Gitelson et al., 1996). The estimated reflectance at the inflection point was extracted from the smoothed reflectance spectra and this process was repeated for all the dates of cloud-free image availability, then the change in the position of the inflection point during the course of the growing season was examined by plotting the extracted inflection points against DAP. A second-order polynomial was then fitted to the plot and the peak was calculated to extract the most advanced wavelength position of the Red-Edge inflection point (REIP), the DAP of its observation, and the rate of change. The value of the reflectance at the REIP was also extracted ($REIP_r$).

6.2.7. Yield Data Collection

At every sampling location, a representative one-meter row was randomly demarcated as a yield sampling area. At harvest, the number of plants and main stems within the row was counted and recorded as units of plant density. The number of stems was counted after

careful excavation of the one-meter demarcation with a spade to prevent any loss of stems or tubers. In a plant laboratory at Harper Adams University, the number of tubers with a transversal diameter greater than 25 mm at each sampling point was counted then the total weight of tubers was measured to 0.01 g accuracy.

6.2.8. Statistical Analysis

All tuber yield components were regressed against remotely sensed canopy data to find statistically significant relationships. By design, there were two levels of non-independence in the study. Firstly environmental and management differences between locations meant that observations within a location were more related to each other than those from different locations. Secondly, spatial autocorrelation was expected within a location. Therefore, a spatial mixed-effect model was appropriate for taking the two non-independence factors into account. To minimize assumptions on the autocorrelation structure, a Matérn covariance structure was chosen due to its flexibility in modeling different spatial covariance structures (Minasny & McBratney, 2005; Stein, 1999). All statistical analyses were conducted in R (R Core Team, 2019) and the spatial regression modeling was conducted using the SpaMM package (Rousset & Ferdy, 2014). Statistical significance was evaluated using 95% confidence intervals and the goodness of fit for multivariable regressions was evaluated using the Normalized Root Mean Square Error (nRMSE). To calculate the nRMSE, first, the RMSE was calculated as follows:

$$RMSE = \sqrt{\frac{1}{N} \sum_{i=1}^n (y_i - \hat{y}_i)^2}$$

where N is the number of observations, y_i is the predicted value and \hat{y}_i is the observed value. Then nRMSE was calculated by dividing the RMSE by the mean of the observed value. The coefficient of determination (R^2) was computed following (Nakagawa et al., 2017).

6.3. Results

6.3.1. Summary of Spectral Reflectance and Intrinsic Indices

Using a boxplot overlaid with a dot plot, Figure 41 shows the spread of the peak reflectance values of the nine Sentinel-2 wavelengths observed during the growing period at all five study sites. The reflectance pattern of individual wavelengths was typical of the spectral signature of vegetation, showing low reflectance in λ_{492} and λ_{665} with higher reflectance in the NIR bands of λ_{703} , λ_{740} , λ_{780} , and λ_{864} . Characteristically, there was higher reflectance of λ_{559} than λ_{492} and λ_{665} . At all sites, there was lower variation in the reflectance values of the absorption wavelengths λ_{492} , λ_{665} , λ_{1610} , and λ_{2186} than the reflected wavelengths. The strong absorption in the photosynthetically active region, coupled with high NIR reflectance confirms that vegetated pixels were effectively sampled in the sampling approach. Furthermore, very little variation was observed in the absorption bands in every field, suggesting relative spatial homogeneity in the absorption of photosynthetically active radiation at the peak of the season in every field. This is expected since only a single variety was planted at every location. However, a larger variation in the NIR band suggested that the slope and location of the red edge varied across a field, a potential indicator of spatially variable vegetation density.

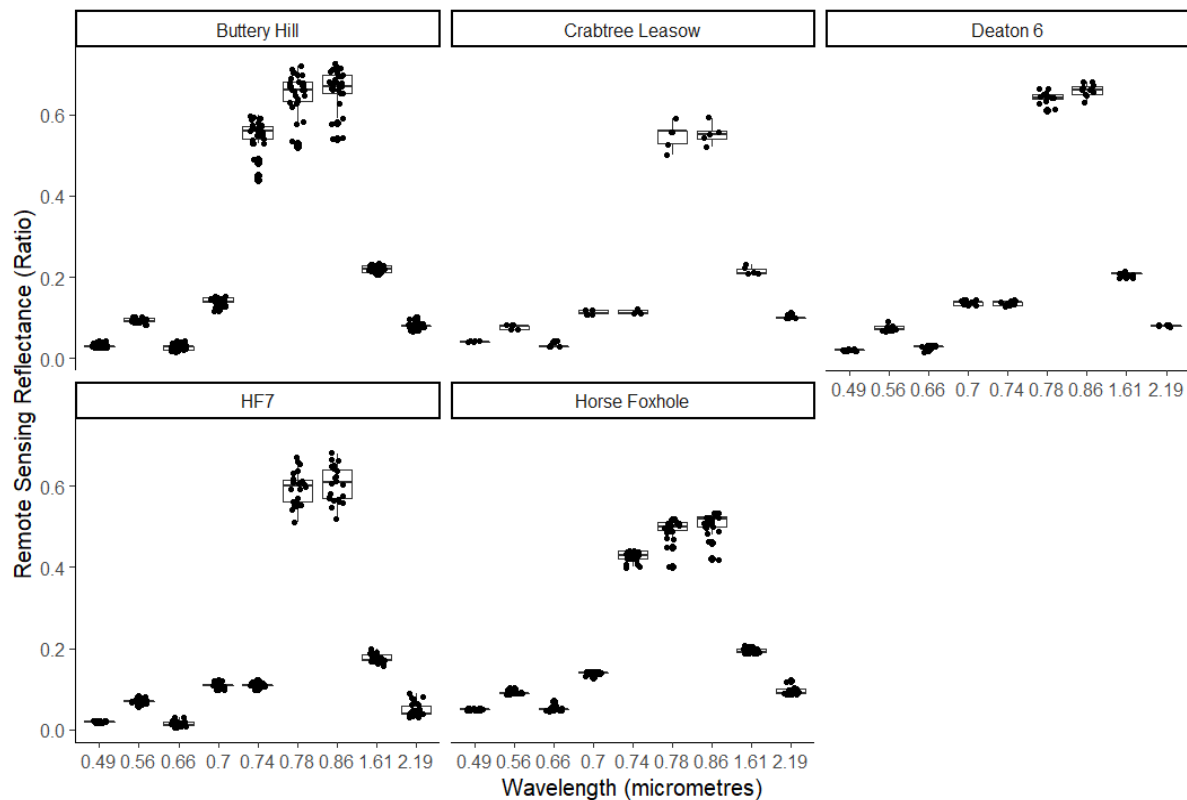


Figure 41: Illustration of the observed spread of the peak reflectance values of the nine Sentinel-2 wavelengths observed during the growing period at five study sites.

The overall performance of the intrinsic vegetation indices derived from these spectral measurements was as presented in Table 24. The peak NDVI values were close to saturation as is expected for vegetation, the lowest average NDVI being observed at Horse Foxhole (0.81). The gradual temporal increase in NDVI was also apparent, with NDVI at tuber initiation consistently lower than the peak NDVI at all sites. The estimated inflection point ranged from 711 nm at Horse Foxhole to 724 nm at Deaton 6. The peak SLAVI ranged from 3.38 at Horse Foxhole to 5.88 at Deaton 6, suggesting that latent location-specific variables control peak achievable the leaf area index. The standard deviation of the peak NDVI was low, suggesting that late-season NDVI was relatively invariable and a non-ideal indicator of spatial variation at the field scale. More variation was observed in $NDVI_{init}$, compared to peak NDVI at all fields, suggesting that the rate of vegetation development was different in a field but the seasonal peak values eventually converge. For modeling yield and stem density as a function of these variables, these results imply that more information about field

variability was contained in the temporal rate of growth than the peak values of the intrinsic vegetation indices. Similarly, there was relatively low variation in the furthest reached wavelength of the REIP across the five sites, which suggested a structural constraint to absorption beyond ~725 nm at the maximum canopy. There was however a higher standard deviation in the REIPr, suggesting that the amount of light absorbed at the inflection point—and hence the chlorophyll intensity—was highly variable in a field. These multi-level sources of variation justified the use of a multi-level analysis approach to derive insights on how they related to the final yield and stem density. Indeed, there were location-specific sources of genotypic (variety) and environmental (planting date, season) variation, necessitating a mixed-effects modeling approach to cluster the data by location.

Table 24: Means and standard deviations (in parentheses) of the peak values of vegetation indices during the potato production season.

Site *	NDVI ¹	SLAVI ²	CIG ³	NDMI ⁴	REIP ⁵ (nm)	REIPr ⁶	NDVI _{init} ⁷
D6	0.93 (0.01)	5.88 (0.12)	4.17 (0.48)	0.53 (0.01)	723.66 (0.51)	170 (9)	0.62 (0.09)
HF7	0.94 (0.03)	5.56 (0.91)	5.21 (1.00)	0.58 (0.04)	711.68 (21.23)	153 (18)	0.53 (0.03)
BH	0.94 (0.03)	5.18 (0.71)	3.32 (0.83)	0.51 (0.03)	723.39 (0.42)	268 (28)	0.14 (0.14)
CT	0.87 (0.02)	3.85 (0.31)	4.10 (1.63)	0.44 (0.02)	719.01 (2.20)	305 (19)	0.51 (0.11)
HFx	0.81 (0.03)	3.38 (0.35)	5.51 (0.61)	0.44 (0.03)	722.56 (0.49)	457 (7)	0.35 (0.06)

1 = Normalized Difference Vegetation Index 2 = Specific Leaf Area Vegetation Index. 3 = Chlorophyll Index Green. 4 = Normalized Difference Moisture Index. 5 = Red-edge inflection

point in nanometres. 6 = pixel value at REIP. 7 = NDVI at tuber initiation * : D6 = Deaton 6, BH = BATTERY Hill, CT = Crabtree Leasow, HFx = Horse Foxhole. Std = Standard Deviation.

As shown in Figure 42, the observed number of days between planting day and the peak value of each intrinsic index was also variable within and between fields. The indices peaked between 90 and 110 days. NDVI peak was observed between 89 days at HF7 and 109 days and BATTERY Hill. The farthest wavelength position of the REIP had high variation at BATTERY Hill, Crabtree Leasow, and HF7, suggesting considerable spatial variation in the evolution of chlorophyll-related reflectance. Across all sites except BATTERY Hill, the highest within-field variation in the number of days to the peak of an index was observed in the REIP, followed by the SLAVI, which are both related to leaf and chlorophyll density.

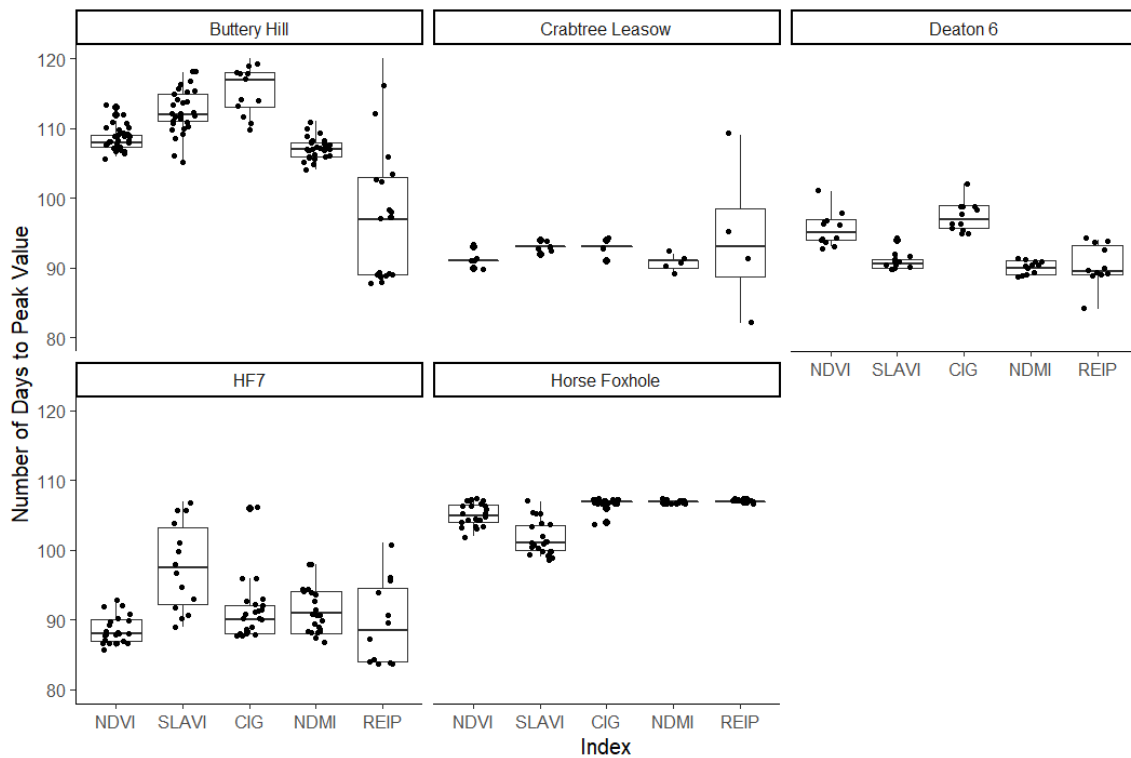


Figure 42: Illustration of the spread of the observed number of days between planting day and the peak value of Normalized Difference Vegetation Index, Specific Leaf Area Vegetation Index, Normalized Difference Moisture Index, and the Red Edge Inflection Point.

As shown in Figure 43, there was also high within-field variation in the number of days to the maxima (or minima for absorbed wavelengths) of each individual wavelength, ranging from 82 for λ_{2186} at Horse Foxhole to 130 for λ_{492} at Buttery Hill. However, there was no discernible and consistent pattern between different wavelengths when either grouped into reflected vs. absorbed wavelengths or sorted in order of wavelength position.

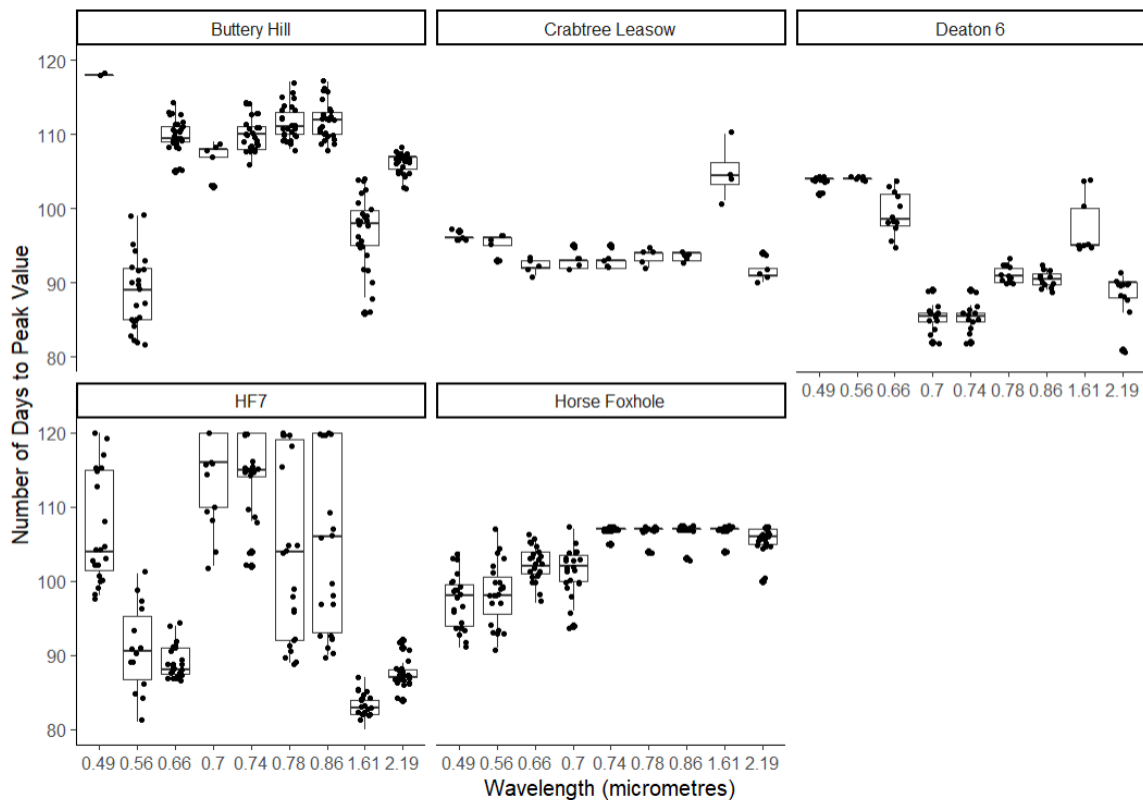


Figure 43: Illustration of the spread of the observed number of days between planting day and the peak value of each of the Sentinel-2 satellite wavebands.

6.3.2. Summary of Temporal Variables

6.3.2.1. Principal Components of Reflectance at Different Time Points

At all five sites, the percentage of variance explained by each of the derived principal components at each observation point were aggregated to assess the amount of total temporal variation encoded in each component. Table 25 shows the percentage of variance explained by the first three principal components averaged at each location. The majority of

the variation (>80%) at all locations was explained by the first principal component, with less than 20% of the variance explained by the second component and less than a percentage point by the third component. Since the principal components were fitted on the temporal information at each data point, the consistency of the percentage variation contained in the first principle component shows—as shown by the low standard deviations—that it is a stable index for encoding the temporal variation of each wavelength in a Sentinel-2 pixel.

Table 25: The mean and standard deviations (in parentheses) of the percentage of variance are explained by the first three principal components of the satellite imagery time series at each sampling point at five locations.

Location	Principal Component 1	Principal Component 2	Principal Component 3
Deaton 6	81.44 (0.24)	18.49 (0.23)	0.06 (0.01)
HF7	82.73 (10.34)	16.87 (10.51)	0.32 (0.41)
Buttery Hill	88.96 (5.67)	10.71 (5.64)	0.26 (0.06)
Crabtree Leasow	90.54 (6.58)	9.34 (6.55)	0.08 (0.03)
Horse Foxhole	87.57 (5.13)	12.24 (1.07)	0.14 (0.06)

Figure 44 shows the line plot of the standardized first principal component, overlaid with a dot plot of the actual values of the component at all the spectral wavelengths and all locations. The spectral signature of the first principal component was typical of the expected response of vegetation, with strong reflection in the NIR range above 700 nm and strong absorption at λ_{492} and λ_{665} , including a sharp inflection point around 700 nm. An intermediate level of absorption was observed at λ_{1610} and λ_{2186} at Deaton 6, Buttery Hill, Horse Foxhole, and Crabtree Leasow. High reflectance in the SWIR was observed at HF7, suggesting overall less moisture available in the canopy throughout the season at this location. This plot shows that the first principle component preserved the information of the spectral signature expected in the crop. Linear modeling of yield and stem density from the first principle component values would therefore have a theoretically relatable interpretation of coefficients.

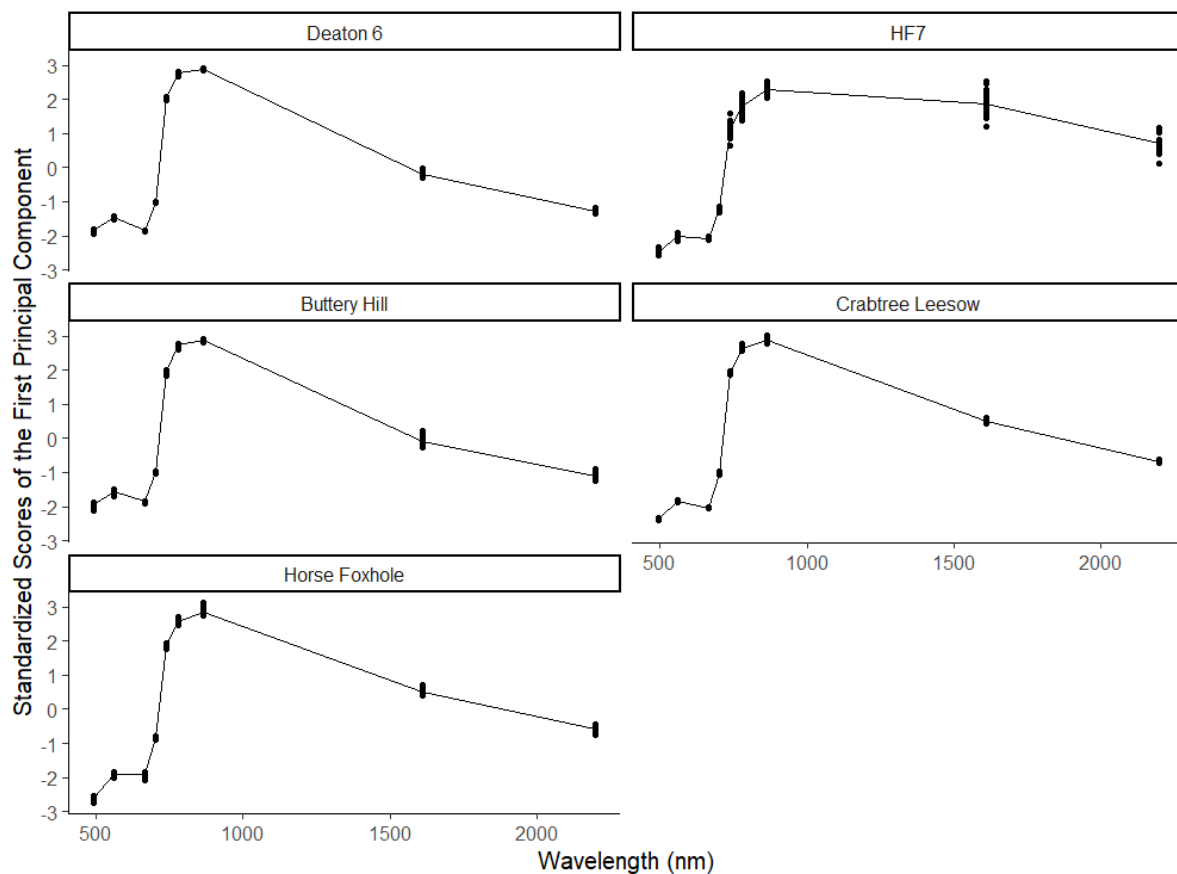


Figure 44: The spectral signature of the standardized first principal components of each Sentinel-2 waveband's temporal variation in the potato canopies at 5 different study sites

6.3.2.2. Temporal Change in the Spectral Signature and Position of the Red-Edge Inflection Point

Figure 45 shows the monthly change in the average spectral signature for each study site over a three-month period, smoothed using a Savitsky-Golay filter. At all the sites, there was a visual decrease in the reflectance near the Red-edge inflection point with time, most visually discernible at Deaton 6, Horse Foxhole, and Buttery Hill, where the reflectance at ~700 nm was consistently higher in May than June and July. The transition between low reflection ~650 nm and high reflection >700 nm was also sharper in June and July than in May, signifying the development of a sharper red-edge as the crop developed more mature vegetation, reaching full canopy and masking any bare-ground signal. The implication of this

was that the position of the inflection point also shifted towards longer wavelengths between the first and second months at all sites, consequent of reduced reflection in the Far-Red region and increased reflection in the NIR region. In the third month, reflection in the NIR decreased at four of five sites (Buttery Hill, Deaton 6, Horse Foxhole, and Crabtree Leasow), possibly due to the onset of canopy senescence. At HF7, the reflectance at the inflection point decreased in the third month coupled with a large increase in NIR reflectance.

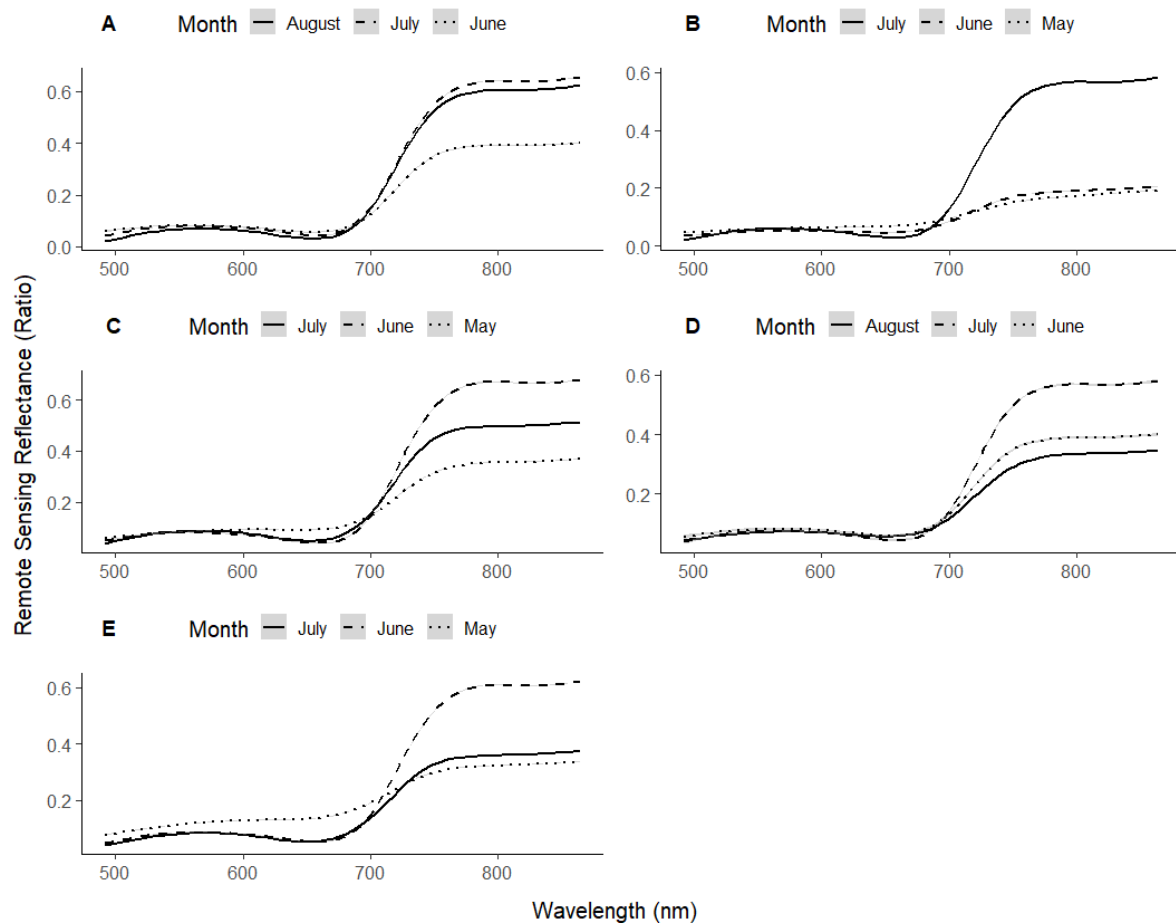


Figure 45: Smoothed (using the Savitzky-Golay filter) spectral signatures of the potato canopy at the 3 different times of the season at Buttery Hill (A), HF7 (B), Deaton 6 (C), Horse Foxhole (D), and Crabtree Leasow (E).

6.3.3. Summary Statistics of In-Situ Potato data

Table 26 shows the means and standard deviations of the potato yield components at the five study sites. The marketable yield ranged from 3.32 kg/m² at Buttery Hill to 5.49 kg/m² at Horse Foxhole showing large inter-site variation. Within the site, there was also significant variation as evidenced by the large differences in coefficients of variation for each site. Considerable variations were also observed in the number of stems per square meter within a field, ranging from 0.17 Coefficient of Variation (standard deviation divided by the mean) at Deaton 6 and 0.28 Coefficient of Variation at Buttery hill. Overall, Horse Foxhole had the highest stem and plant number due to frequent double-tuber-placement and subsequently recorded the highest yield. The lowest yield was observed at Buttery Hill, which also had very low tuber size and weight compared to the other sites. The between-sites and within-site variations necessitated the use of a mixed model approach with a spatial component to account for spatial autocorrelation when modeling the combinations of satellite-sensed variables in relation to the tuber yield components.

Table 26: Summary statistics (mean with standard deviation in parentheses) of the potato yield sampling results at five different study sites.

Yield Component	Deato n 6	HF7	Buttery Hill	Crabtree Leasow	Horse Foxhole
Marketable yield (kg/m ²)	4.17 (0.48)	5.21 (1.00)	3.32 (0.83)	4.10 (1.63)	5.49 (0.61)
Number of Plants/m ²	2.50 (0.29)	2.51 (0.60)	2.78 (0.70)	2.67 (0.61)	5.19 (1.58)
Number of Stems/m ²	9.77 (1.67)	12.37 (4.17)	13.52 (3.83)	12.22 (2.83)	17.03 (2.70)

6.3.4. Linear Model for Marketable Yield

Marketable yield was modeled as a function of the fixed effects λ_{559} , λ_{703} , and CIGpeak, using a spatial mixed-effects structure with the site as a random effect. The fixed effects

were chosen based on the theoretical expectation of causation. Table 27 shows the standardized coefficient estimates of the fixed effects as well as their confidence intervals and spatial autocorrelation estimates. Marketable yield significantly decreased with increasing overall reflectance at λ_{559} ($\beta = -0.53$) but increased with increasing overall reflectance at λ_{703} ($\beta = 0.22$).

Table 27: Estimated coefficients for explanatory variables of marketable yield and the estimated spatial autocorrelation structure.

Explanatory Variables	Estimate¹
Intercept	4.47 ± 0.18
NDVI _{init} ²	0.55 ± 0.19
Stem Density	0.48 ± 0.18
λ_{559}	-0.53 ± 0.18
λ_{703}	0.22 ± 0.19
Model Properties	
nRMSE _{fixed} ³	0.16
delta AICc ⁴	18.56
R ²	0.65
D.F. ⁵	87.99
ICC1 ⁶	0.21

1 = beta coefficient ± margin of error based on 95% confidence interval, coefficients with margins of error that don't overlap zero are statistically significant ($p = 0.05$). 2 = Normalized Difference Vegetation Index at tuber initiation. 3 = Normalized Root Mean Square Error of the fixed effects model, with random effects set to zero. 4 = change in the conditional Akaike Information Criteria between the current model and the random intercept model. 5 = effective degrees of freedom. 6 = Intraclass correlation of the random effects.

Higher $NDVI_{init}$ was associated with higher marketable yield, suggesting that higher early-season canopy coverage rates are associated with increased yield. An increase in stem density was also positively associated with marketable yield ($\beta = 0.48$). The location random effect structure with a Matérn covariance structure explained 0.27 of the total variance as shown by the intraclass correlation coefficient (ICC1) value, showing that most of the variation in the data was explained by factors other than the random effect structure. As shown in Table 27, the fixed-effect coefficients fitted the data with an nRMSE of 0.16 and the model had an R^2 of 0.65.

6.3.5. Modelling Stem Density

Table 28 shows the standardized coefficient estimates of the fixed effects that best-modeled stem density as well as their confidence intervals and spatial autocorrelation estimates. Stem density was modeled as a function of the peak SLAVI and the rate at which SLAVI was gained before the peak, assuming that areas with lower stem density would gain SLAVI at a higher rate to compensate for the sparse canopy but end up with comparatively lower final SLAVI. It was hypothesized that the shift towards the farthest possible wavelength of the Red Edge inflection point would be slower in higher stem densities due to potentially faster development of leaf area at the expense of chlorophyll intensity. Non-adjusted NDVI before canopy consolidation ($NDVI_{init}$) was also used to represent early-season differences in vegetation intensity, which are partly used to model stem and plant density. The Matérn covariance structure was used to account for the spatial autocorrelation at each site. As shown in Table 28, significant positive relationships were observed between stem density and all the variables. Field sections with higher stem densities took longer to reach their maximum possible inflection point and had a higher reflectance at the inflection point. Higher stem density was significantly associated with higher NDVI at tuber initiation ($\beta = 1.19$) and a higher $SLAVI_{peak}$ ($\beta = 1.66$), however, the rate of change towards the peak SLAVI was slower at higher stem density data points. These results suggested that dense canopies achieved a higher leaf area index and had higher early-season NDVI but were associated with a delayed date of maximum light absorption per leaf. At the farthest inflection point, denser canopies also absorbed less light (higher

reflection). The random effect structure explained 0.28 of the total variance in the stem density. The fixed effect coefficients fitted observed stem densities with nRMSE of 0.34 and the model had an R2 of 0.51.

Table 28: Estimated coefficients for explanatory variables of potato stem density and the estimated spatial autocorrelation structure.

Explanatory Variables	Estimate¹
Intercept	13.5 ± 1.42
REIP _{DAP} ²	1.18 ± 0.79
REIP _r ³	3.43 ± 1.9
SLAVI _{peak} ⁴	1.66 ± 1.59
NDVI _{init} ⁵	1.19 ± 1.01
Model Properties	
nRMSE _{fixed} ⁶	0.24
delta AICc ⁷	18.92
R ²	0.51
D.F. ⁸	74.17
ICC1 ⁹	0.28

1 = beta coefficient ± margin of error based on 95% confidence interval, coefficients with margins of error that don't overlap zero are statistically significant ($p = 0.05$). 2 = days to farthest Red-edge inflection point position. 3 = Reflectance at the farthest REIP. 4 = peak Specific Leaf Area Vegetation Index. 5 = Normalized Difference Vegetation Index at tuber initiation. 6 = Normalized Root Mean Square Error of the fixed effects model, with random effects set to zero. 7 = change in the conditional Akaike Information Criteria between the current model and the random intercept model. 8 = effective degrees of freedom. 9 = Intra-class correlation of the random effects.

6.4. Discussion

The average reflectance of individual Sentinel-2 bands at their peak as shown in Section 3.1 showed a spectral signature typical of vegetation, with high reflectance in the NIR and low reflectance in the visible range (Gates et al., 1965) at all five locations. The modeling of the temporal change in reflectance from Sentinel-2 SITS as described in Section 2.5, therefore, enabled the derivation of peak spectral signature that was relatable to the typical spectral properties of vegetation. Plotting the first PCA of the SITS on the spectrum space as shown in Section 3.2 also showed high standardized PCA scores in the NIR and low values in the visible range at all five locations. This shows that the dimensionality reduction of the SITS into one variable using PCA still produced variables that are spectrally relatable to the expected reflectance pattern of vegetation. This study showed that most of the temporal variation in the reflectance of individual wavelengths can be represented within the first principal component. This dimensionality reduction enabled the encoding of time information into one dimension while preserving the spectral reflectance information. The high percentage of variation contained within the first principal component compared to the second and third components showed the adequacy of single-dimension decomposition in this case. Subsequent yield modeling also showed that the information in the first principal component was significantly relatable to yield. With temporal information encoded within the principal component, this approach implies that there is potentially no need for conducting correlation analyses on several days of the season in order to find an optimal time of image acquisition for maximizing the correlation between yield and spectral reflectance as implemented in previous studies (Aparicio et al., 2000; Thapa et al., 2019). In forward use cases of this approach, Sections 2.4 and 2.5 describe the methods needed to replicate the representation of the temporal information. These approaches are replicable where enough cloud-free data is available from the Sentinel-2 repository. In this study, the first principle component was observed to contain the majority of the temporal variation at all 5 sites. While this was consistent across sites, it is still recommended to validate this assumption at any iteration instance and consider the other components, should they hold an equally significant amount of variance.

For the intrinsic indices, the mean NDVI approached saturation at all sites with very little variability within sites, which highlights the limitation of using the indices at full canopy for mapping within-field spatial variation. The observed REIPs between 719.10 nm at Crabtree Leasow and 723.66 nm at Deaton 6 were comparable to previous findings in potatoes using the linearized algebraic formula (Herrmann et al., 2011) and observation of first derivative peaks of the reflectance (Fernández et al., 2020). This adds to the evidence that the REIP falls around 720 nm in potatoes. The temporal pattern, as summarized by the number of days to peak reflectance values as well as the differences in the spectral signatures at different times of the season, shows a rapid early increase in canopy reflectance of NIR (and absorption of visible wavelengths) between May and July, followed by a slight decrease in August, mostly reaching a peak between 90 and 110 days. This implies that an exponential change in ground cover and leaf development leads to an increase in the surface area for NIR reflection towards a peak, which is the growth model expected for potatoes (Kooman & Haverkort, 1995). This observation gives credence to the use of SITS in place of manual canopy assessments for mid-season calibration of potato growth models to map within-field variations.

The multivariable modeling of yield as a function of spectral measurements revealed the significance of the λ_{559} wavelength in within-field yield modeling. Most studies on the multispectral analysis of the canopy for yield prediction focus on the NDVI, being a well-known index for differentiating vegetation from non-vegetation and quantifying its intensity. This often comes at the expense of the visible wavelengths, especially λ_{559} which is ignored in most vegetation indices. The analysis showed that high λ_{559} absorbance was significantly associated with a higher yield, with a high standardized beta coefficient. This suggests that a portion of PAR is absorbed in the green portion of the spectra and contributes significantly to yield. In line with this observation, (Gates et al., 1965) reported that although plants are highly reflective in the Green portion of the spectrum relative Red and Blue, the Green pigmentation darkens in mature leaves with maximum chlorophyll content, and absorption is observed in the green portion. Mature leaves with maximum chlorophyll content (and therefore relatively high photosynthetic capacity) have lower green

reflectance. This is supported by several authors (Datt, 1998; Lorenzen & Jensen, 1988; Sims & Gamon, 2002) who report chlorophyll-related absorption in the green wavelengths. Particularly, (Lorenzen & Jensen, 1988) links high green reflectance to low biomass accumulation in mature wetland vegetation. Furthermore, the high negative coefficients λ_{559} suggest that areas with a relatively larger reflective surface for λ_{559} (therefore higher above-ground leaf area) within a field had higher partitioning of photosynthetic products to the canopy at the expense of tubers, in line with the expected widely studied trade-off between canopy and tubers in the development of a harvest index (Bélanger et al., 2001; Mackerron & Heilbronn, 1985; Oparka, 1985; Oparka et al., 1987). While reflectance at λ_{559} is likely to be affected by soil in non-consolidated canopies early in the season, the relative soil effect can be expected to be uniform across the field, assuming relatively consistent soil color. The effect of soil gets diminished over time as potatoes reach maximum ground cover around 50 days after emergence (Connell et al., 1999). In this study, the median number of days to peak reflectance of λ_{559} ranged from 88 at BATTERY Hill to 105 at Deaton 6, showing that λ_{559} intensity continues to develop after the full canopy is reached and the effects of soil are no longer applicable. In line with previous research (Knowles & Knowles, 2006; O'Brien & Allen, 1992), a significant relationship was observed between stem density and marketable yield, showing the relevance of stem density as a unit of plant population with practical relevance for yield modeling. Denser canopies approach full ground cover faster and therefore have a relatively long time of tuber bulking at full canopy hence returning a higher yield potential, which is the basis of many potato yield models (Aliche et al., 2018; Kooman & Haverkort, 1995). In line with this, early-season NDVI—which was used as a proxy to differences in vegetation intensity (Salvador et al., 2020) early in the season at tuber initiation—was observed to positively relate to marketable yield. Reflectance at λ_{703} and the NIR spectrum portion as a whole is largely associated with the development stage of internal mesophyll leaf structures that act like reflection and refraction surfaces (Gates et al., 1965; Knipling, 1970). In this study, the significant positive beta coefficient between overall λ_{703} reflection and yield is therefore interpreted as a sign of the positive relationship between the surface area available for photosynthesis and the final yield.

The observed positive associations between stem density and the reflectance at the Red-edge inflection point are in line with theoretical expectations of a high reflectance in high stem density (and therefore LAI) canopies due to high NIR scattering (Clevers et al., 2017; Kamenova & Dimitrov, 2020). Increasing plant density is known to negatively affect chlorophyll content (Rietra et al., 2017) and subsequently higher stem densities are expected to take longer to reach their maximum chlorophyll concentration per plant though there may be higher chlorophyll content on a unit area basis due to more leaves. As observed in the modeled multivariable regression coefficients, high stem densities were significantly associated with higher $SLAVI_{peak}$, in agreement with previous research (Chapepa et al., 2020). A lower rate of chlorophyll accumulation per plant in high stem densities (Rietra et al., 2017) means the canopy takes longer to reach its maximum chlorophyll content—and subsequently $REIP_{DAP}$ —as observed in the multivariable model. Finally, Potato stem density is partially a factor of plant density, with higher plant densities resulting in higher stem densities (Allen & Wurr, 1992). In previous studies, early-season NDVI has been used to infer plant population from coarse-resolution aerial imagery. In line with our findings from the multivariable modeling, an overall positive relationship between early-season NDVI and plant population density has been reported in several studies (Arnall et al., 2006; Shafian et al., 2018). These results show that within-field variation in potato stem density can potentially be mapped using SITS, which can be used to map management zones for potential variable harvest timing to optimize tuber size distribution.

6.5. Conclusions

The temporal profiles of the spectral reflectance of individual bands were revealed to have a significant relationship with potato harvest yield that can be traced to physiological principles related to the spectral properties of plants. In this study, increasing stem density was observed to be related to increases in the position of the REIP and its reflectance value, in agreement with previous studies on the effect of vegetation density on chlorophyll intensity and the REIP. Additionally, increasing stem density was associated with higher NDVI values early in the season (at tuber initiation), showing that intrinsic vegetation indices derived from the Sentinel-2 satellite data can be related to this response variable. Some

Sentinel-2 data-based indicators of marketable yield were also discovered in this study. Early-season NDVI was significantly related to marketable yield, as were temporally aggregated reflectance at λ_{559} and λ_{703} , aggregated as the first principle components of the temporal variation. This study reinforces the validity of SITS analysis as an alternative to the use of single-instance values of vegetation indices like the peak NDVI. The λ_{559} band is seldom reported in spectral analysis, but this study shows that temporal change during the growing season can be predictive of yield. This study, therefore, draws attention to λ_{559} , an often discounted spectral band due to ubiquitous reliance on intrinsic indices like the NDVI that favor modeling the larger-scale difference between NIR reflectance and Red than Green wavelengths. The complex nature of yield processes requires the use of multivariable modeling and temporal feature engineering, which was shown in this study to yield useful models and highlight significant temporal variables. Finally, this study shows that potato main stem density variation can be modeled from temporal features engineered from SITS with a low RMSE when the spatial covariance of stem density is taken into account. In line with the objectives, emphasis must be made that the models developed in the study are inferential and meant to enhance current understanding of the relationships between reflectance signals picked up by the Sentinel-2 satellite and the observed ground-truth while controlling for within-field spatial effects and clustering of data in multiple locations. The coefficients generated in these models take into account the site-specific spatial covariance structure fitted using the Matérn function at the five sites. Therefore, the coefficients are valid within the confines of the study's data generating processes, though the significance of the coefficients in the context of the proposed physiological links point to the presence of key relationships that must inform future studies and/or feature engineering for predictive models.

CHAPTER 7 - General Discussion

This work aimed to contribute to the knowledge on the extent to which mapping of soil and crop growth variation can be used to infer or predict potato yield and TSD variation in typical potato farms. This overall goal was pursued using key specific objectives to:

1. Examine the relationships between soil properties and potato TSD at harvest, indexed using the Weibull distribution shape parameter
2. Examine if a significant relationship between soil properties and ECa exists
3. Develop algorithms for individual stem detection in potatoes at an advanced canopy development stage using UAV imagery
4. Investigate the usefulness of spatio-temporal variation of satellite imagery in the prediction of potato yield variation in a field
5. Evaluate the usefulness of plant density maps produced from UAV images in predicting potato yield components

The literature contains a lot of research on the role of genotype and plant population in determining the final tuber size distribution (TSD) of a crop, but different studies have used different methods for indexing TSD, posing a challenge for inter-study comparison and reproducibility. In Chapter 3, for the first time, TSD was described using the unit-less shape parameter of the Weibull distribution, creating an index that can be used in inter-study comparison. In line with previous research, the findings showed that TSD is better described by a Weibull distribution rather than the Gaussian distribution that is often assumed in TSD modelling. The use of the Weibull shape parameter to index TSD has not been reported in literature. Here, the potential adequacy of directly-estimated Weibull function parameters in modelling TSD is demonstrated. These findings make it possible for farmers and agronomists to evaluate TSD and predict weights in desired size classes from yield digs using simple formulae, making crop modelling more accessible to farmers. Repetition studies over a more diverse base of variation in growing environments and varieties are needed in order to verify the findings and evaluate their appropriateness for further adoption in commercial settings.

Chapter 3 also reported the negative effect of P over-fertilization on TSD, consistent with previous research in randomized experiments with sharp induced treatment differences (see Birch et al., 1967; Prummel & Barnau-Sijthoff, 1984; Rosen & Bierman, 2008; Sharma & Arora, 1987), but demonstrated on-farm for the first time. These findings provide evidence of yield penalties associated with over-fertilization, which are not elucidated in the literature. This brings a focus on the potential yield losses attached to current conventional production practices and contributes to the body of work on the need for variable rate management of soil fertilization in precision agriculture. This work therefore presents pertinent and valid on-farm research and provides a useful contribution to the body of work on potato TSD. The indexing of TSD using the linearized Weibull function provides a useful decision-support tool for agronomists and farmers to reliably model the variation that they observe in the field and alter harvest dates or practice variable harvest timing. Repetition studies are recommended to verify these findings in a wider range of sources of genetic and environmental variation before practical adoption.

For precision management of the soil nutrients that were identified in this work to affect TSD, high resolution interpolations of low intensity soil sampling points need to be created using indices such as ECa as proxies. In Chapter 3.2 it was demonstrated that ECa had very limited correlation with soil mineral nutrients at both study sites, making it a poor proxy for modelling soil nutrient variability. These findings are in general agreement with the research record (Cambouris et al, 2006; Perron et al., 2018) and highlight the need for a more reliable index for soil variability. Inconsistent correlations between ECa and soil physical properties across sites also showed the unreliability of ECa as a proxy model for soil texture, also consistent with the research record (Cambouris et al, 2006; Perron et al., 2018). There was no evidence of the usefulness of ECa in modelling soil property variability in this work, suggesting that the use of ECa data must be limited to soil water and salinity modelling where consistent relationships have been observed in previous studies (Corwin et al., 2009) and the direct relationship between ECa and tuber yield components were not explored further in this thesis.

Chapter 6 showed that tuber yield can be modelled from remotely sensed changes in canopy reflectance over time. To derive relationships between remote sensing data and tuber yield components, it was required to derive spatio-temporal indices rather than purely spectral indices like the NDVI. The results showed that modelling the stem density as a function of growth rate indicators like REIP_{DAP} provided the most plausible models. Yield was best modelled by indicators of photosynthetic efficiency such as the level of canopy development at tuber initiation (NDVI_{init}) and the overall seasonal reflectance at λ_{703} . With limited information in the literature on the use of spatio-temporal data analysis for yield modelling in potatoes, this work provides a significant contribution to the field. This work demonstrated that SITS can potentially be used as indices of crop phenology in time-step crop simulation models, which require accurate phenological data that adheres to exponential canopy growth (Kooman & Haverkort, 1995). Coarse spatial resolution and limited cloud-free days in satellite imagery remain a challenge for extending this work into practical use. Spatial interpolation of SITS to improve resolution is an area of research interest (Porwal & Katiyar, 2014) that is recommended to follow this work. Additionally, the prediction of spectral reflectance from synthetic aperture radar provides previously tested (Filgueiras et al., 2019) potential solutions to these problems that must be researched in future studies.

Spatial resolution problems in remote sensing are ultimately solved by UAVs albeit at a significance cost of spectral resolution. This work therefore limited the UAV component to object detection using RGB. The enumeration of stems from UAV imagery was proven to be possible using traditional image analysis and transfer learning approaches. As reported in previous canopy image analysis studies (Li et al, 2019, Machefer et al., 2020), the image analysis approach is non-robust to changes in light saturation in the image. The approach is also based on clustering algorithms that assume the presence of the object of interest within the data, which makes it possible for the algorithm to detect stems in images that do not contain any potato plants (Li et al., 2019). The clustering algorithms used for image segmentation also require post-clustering data cleaning to remove spurious clustering results and consolidate disjointed objects, all of which affected the accuracy of the final

model (Yang et al., 2012). While the development of custom vegetation indices for potato stems was a good outcome of the work, the practicality of this approach in production environments is hampered by these limitations. The custom vegetation indices developed were useful for tracking the area of young leaves at meristem tips with low chlorophyll content. These indices therefore have potential applicability in other phenotyping or plant protection studies where canopy chlorophyll content is pertinent.

The final models produced using the image analysis approach suggest that the approach can adequately be used to produce maps of the spatial variability in stem numbers, assuming stochastic sources of error in the models. The transfer learning approach solved most of the limitations associated with image analysis. In Chapter 4, a unique pseudo-labelling routine was developed, using manually cleaned data from the image analysis approach to create labelled datasets for transfer learning. In other pseudo-labelling approaches, the initial labelling data is generated by labelling a small subset of data then using high-confidence detections from models trained on this subset to generate labels in unlabelled data (Rhee & Cho, 2019). For potatoes, this approach is difficult due to the irregularity of the potato stem, which makes it hard to delineate accurate bounding boxes for non-experts. Utilizing an image analysis approach to create the initial set of bounding boxes automatically after an expert sense-check as conducted in this work provides a pathway for faster and repeatable pseudo-labelling.

This study demonstrated that the transfer learning model produced from pseudo-labelled datasets performed better than the image analysis based model in detection of stems in UAV imagery. In addition, standard transfer learning frameworks (FRCNN) were used for training both the plant detection and stem detection models. It was demonstrated that these basic frameworks, with the VGG-16 CNN, provided enough learning power to accurately classify potato plants and stems, in line with previous observations where the VGG-16 and FRCNN have been shown to be adequate for classification of crop canopy objects (Fuentes et al., 2017).

While deep learning is a highly active research field and improvements to object detection training frameworks continue at a rapid pace, this work demonstrated that obtaining plausible models is possible using the simple training frameworks. Additionally, the detection and mapping of potato plant objects is not likely to require real-time results in practical use. The production of maps is likely to be done as a post-processing operation either by a data scientist or automatically in a cloud computing environment. This means that the slower real-time processing times of FRCNN compared to more modern detection frameworks like the YOLO series is not likely to hamper the usability of the models.

In Chapter 5, it was shown that plant count estimations from FRCNN models provide adequate accuracy for production of 2D plant density maps that correlate to potato yield components. Previous research uncovered the problem of overlapping plants in late-acquired images which continue to hamper model accuracies (Machefer et al., 2020; Li et al., 2019). While the incidence of overlapping plants can be avoided by early imaging, asynchrony in potato emergence means that early imaging runs the risk of unrepresentative under-estimations of plant numbers. This makes it difficult to decide on an optimum imaging day that is early enough to minimize overlapping plants but late enough to have a representative germination rate.

In this study, it was considered better to collect and analyse the UAV images with the assumption of the presence of overlapping plants for a robust solution. Accordingly, post-processing operations involved deletion of all quadrats of the field containing overlapping plants from the UAV orthomosaic and making the model predictions on the remaining valid data, followed by geostatistical interpolation of the results to construct a high resolution 2D plant density map. The strategy used in this work therefore integrated machine learning for object detection, traditional image analysis for deletion of overlapping plants and geostatistical analysis for the construction of a continuous 2D map.

The resultant plant density maps developed from this work correlated with potato yield components, corroborating with established research findings of a significant negative relationship between plant density per unit area and potato tuber density per plant (Knowles

& Knowles, 2006). Similarly, areas where the models predicted high plant density also has significantly lower tuber sizes although the number of tubers per unit area was increased on account of the higher plant number, in line with Knowles and Knowles (2006).

This research has shown the potential for using these plant density maps as a tool for decision-support for variable in-season N management. Potential decisions from this include the delay of desiccation for tuber bulking purposes in denser sections of the field, giving a basis for variable harvest timing. Finally, for the first time, this research has demonstrated the correlation between early-season satellite-derived NDVI and plant population. This potentially implies that early-season satellite data can be used to model plant population density in potatoes. Further studies are required to ascertain the reproducibility of this finding.

7.1 Conclusion

In line with the stated objectives, this study successfully:-

1. Uncovered evidence of some negative relationships between soil nutrients concentrations and Potato TSD. This revealed potential for a negative influence of excess nutrients on tuber number and size, which have economic implications. The establishment of these relationships in on-farm experiments within the typical spatial variability observed in actual production showed the relevance of spatially variable management of soil nutrient concentrations or delineation of harvest timing management zones based on initial soil nutrient variation. Additionally, this work established the Weibull distribution as an optimum estimator of TSD and for the first time provided and tested the Weibull shape parameter as a unit-less index for TSD that can enable the comparison of results from different studies.
2. Examined the reliability of ECa as a proxy to soil properties. Crucially, the study found that relationships between ECa and soil mineral nutrients concentrations are weak. While some strong relationships with soil physical properties were

observed, the correlations were inconsistent and pointed to a conclusion that there was no evidence of a generalized relationship between ECa and the soil texture and mineral nutrient properties studied in this work.

3. Developed algorithms based on traditional image analysis and machine learning to detect and enumerate potato stems from UAV imagery. This work demonstrated the efficacy of a semi-supervised labelling routine integrating machine learning and traditional analysis to produce training data that was used to successfully learn and detect potato meristem tips. This work also developed custom vegetation indices that are effective in detecting chlorotic and young leaves, with applicability in other phenotyping domains.
4. Developed indices for temporal variability in potato canopy reflectance and used them to successfully model potato yield and stem density as a function of spatio-temporal variation in phenological development. This work showcased the potential of modelling potato yields from in-season satellite image reflectance patterns in advance of harvest.
5. Evaluated the usefulness of plant density maps produced from UAV images in predicting potato yield components. Statistically significant ($P < 0.05$) correlations were observed between plant density predicted from UAV images and the actual plant density, stem density and the total number of tubers harvested. This work therefore demonstrated a successful integration of machine learning, traditional image analysis, and geostatistical analysis to produce plant density maps that can provide insights into expected crop productivity.

7.2 Recommendations

As a follow-up to this work, it is recommended that replication studies be conducted on the effect of soil variability on TSD in different varieties, using the Weibull shape parameter to index TSD. Randomized experiments on the effect of plant population parameters on TSD are also recommended to evaluate if previous findings on the effects of stem number, physiological ageing and growth regulators on TSD can be confirmed using the Weibull shape parameter. For the satellite studies, this work did not cover the efficacy of spectral

unmixing algorithms in prediction of plant population early in the season. Spectral unmixing algorithms inherently give sub-pixel ground cover percentages, which can give a measurement of crop phenology if evaluated temporary. This work did not include spectral unmixing due to the difficulties in establishing objective end-member signatures for potatoes and soil. Research towards methods of data pre-processing to establish credible end-members is therefore recommended.

This work established methods for the enumeration of plants and stems in potato UAV imagery using an integration of machine learning, image analysis and geostatistical data analysis. While most computer vision works focus on improving the object detection models to obtain perfect enumerations, it can be contended that precision agriculture applications need an accurate representation of spatial variation in plant density rather than absolute values. It is therefore recommended that an integrated approach should be adopted, deleting spurious detections across a UAV orthomosaic using image analysis and taking advantage of the availability of advanced geostatistical interpolation methods to generate the high-resolution plant or stem density maps required for decision support. The vegetation indices produced for elucidating meristem tips in potatoes have the potential for use in identification of chlorosis-inducing biotic and abiotic stresses in canopies. It is therefore recommended that research into the applicability of these vegetation indices in other canopy analysis works is conducted.

8. References

- Agriculture and Horticulture Development Board. (2018). BG Potatoes Market Intelligence Report 2017-2018. (Great Britain): AHDB. Available online: https://potatoes.ahdb.org.uk/sites/default/files/publication_upload/GB%20Potatoes%20Market%20Intelligence%202017-18.pdf (Accessed on 15 April 2019)
- Agriculture and Horticulture Development Board. Nutrient Management Guide (RB209) Section 5: Potatoes. (2021). AHDB Knowledge Library. Available online: https://projectblue.blob.core.windows.net/media/Default/Imported%20Publication%20Docs/RB209%202021/RB209_Section5_2021-210208_WEB.pdf (accessed on 13 February 2022)
- Agri-food and Biosciences Institute. (2019). Potato Variety Characteristics (AFBI). Viewed 18 September 2019. <https://www.afbini.gov.uk/articles/potato-variety-characteristics>
- Al-Gaadi, K. A., Hassaballa, A. A., Tola, E., Kayad, A. G., Madugundu, R., Ablewi, B., & Assiri, F. (2016). Prediction of Potato Crop Yield Using Precision Agriculture Techniques. PLOS ONE, 11(9), e0162219. <https://doi.org/10.1371/journal.pone.0162219>
- Ali, I., Cawkwell, F., Dwyer, E., Barrett, B., & Green, S. (2016). Satellite remote sensing of grasslands: from observation to management. *Journal of Plant Ecology*, 9(6), 649–671. <https://doi.org/10.1093/jpe/rtw005>
- Aliche, E. B., Oortwijn, M., Theeuwen, T. P. J. M., Bachem, C. W. B., van Eck, H. J., Visser, R. G. F., & van der Linden, C. G. (2019). Genetic mapping of tuber size distribution and marketable tuber yield under drought stress in potatoes. *Euphytica*. <https://doi.org/10.1007/s10681-019-2508-0>
- Allen, E. J., & Wurr, D. C. E. (1992). Plant density. In *The Potato Crop* (pp. 292–333). Springer Netherlands. https://doi.org/10.1007/978-94-011-2340-2_7

- Allen, E. J., & Wurr, D. C. E. (1992). Plant density. In *The Potato Crop* (pp. 292–333). Springer Netherlands. https://doi.org/10.1007/978-94-011-2340-2_7
- Allen, E. J., Bean, J. N., Griffith, R. L., & O'Brien, P. J. (1979). Effects of length of sprouting period on growth and yield of contrasting early potato varieties. *The Journal of Agricultural Science*, 92(1), 151–163. <https://doi.org/10.1017/S0021859600060603>
- Allison, M. F., Fowler, J. H., & Allen, E. J. (2001). Responses of potato (*Solanum tuberosum*) to potassium fertilizers. *Journal of Agricultural Science*. <https://doi.org/10.1017/S0021859601008863>
- Almekinders, C. J. M., & Struik, P. C. (1996). Shoot development and flowering in potato (*Solanum tuberosum* L.). *Potato Research*, 39(4), 581–607. <https://doi.org/10.1007/BF02358477>
- Anžlovar, S., Kovač, M., & Ravnikar, M. (1996). Photosynthetic pigments in healthy and virus-infected potato plantlets (*Solanum tuberosum* L.) grown in vitro. *Phyton - Annales Rei Botanicae*.
- Aparicio, N., Villegas, D., Casadesus, J., Araus, J. L., & Royo, C. (2000). Spectral Vegetation Indices as Nondestructive Tools for Determining Durum Wheat Yield. *Agronomy Journal*, 92(1), 83–91. <https://doi.org/10.2134/agronj2000.92183x>
- Aparicio, N., Villegas, D., Casadesus, J., Araus, J. L., & Royo, C. (2000). Spectral Vegetation Indices as Nondestructive Tools for Determining Durum Wheat Yield. *Agronomy Journal*, 92(1), 83–91. <https://doi.org/10.2134/agronj2000.92183x>
- Arnall, D. B., Raun, W. R., Solie, J. B., Stone, M. L., Johnson, G. V., Girma, K., Freeman, K. W., Teal, R. K., & Martin, K. L. (2006). Relationship Between Coefficient of Variation Measured by Spectral Reflectance and Plant Density at Early Growth Stages in Winter Wheat. *Journal of Plant Nutrition*, 29(11), 1983–1997. <https://doi.org/10.1080/01904160600927997>

- Arora, B. R. (1987). Effect of nitrogen, phosphorus and potassium application on yield of potato tubers (*Solanum tuberosum* L.). *The Journal of Agricultural Science*, 108(2), 321–329. <https://doi.org/10.1017/S0021859600079326>
- Arsenault, W. J., LeBlanc, D. A., Tai, G. C. C., & Boswall, P. (2001). Effects of nitrogen application and seedpiece spacing on yield and tuber size distribution in eight potato cultivars. *American Journal of Potato Research*. <https://doi.org/10.1007/BF02875695>
- Bala, S. K., & Islam, A. S. (2009). Correlation between potato yield and MODIS-derived vegetation indices. *International Journal of Remote Sensing*, 30(10), 2491–2507. <https://doi.org/10.1080/01431160802552744>
- Bannari, A., Morin, D., Bonn, F., & Huete, A. R. (1995). A review of vegetation indices. *Remote Sensing Reviews*. <https://doi.org/10.1080/02757259509532298>
- Barben, S. A., Hopkins, B. G., Jolley, V. D., Webb, B. L., & Nichols, B. A. (2010). Phosphorus and zinc interactions in chelator-buffered solution grown russet burbank potato. *Journal of Plant Nutrition*. <https://doi.org/10.1080/01904160903506308>
- Barczak, B., Nowak, K., & Knapowski, T. (2013). Potato yield is affected by sulphur form and rate. *Agrochimica*.
- Bauer, M. E. (1973). Identification of agricultural crops by computer processing of ERTS-MSS data. LARS Technical Reports. Paper 20.
- Baumgardner, M. F., Silva, L. F., Biehl, L. L., & Stoner, E. R. (1986). Reflectance Properties of Soils (pp. 1–44). [https://doi.org/10.1016/S0065-2113\(08\)60672-0](https://doi.org/10.1016/S0065-2113(08)60672-0)
- Bélangier, G., Walsh, J. R., Richards, J. E., Milburn, P. H., & Ziadi, N. (2001). Tuber growth and biomass partitioning of two potato cultivars grown under different n fertilization rates with and without irrigation. *American Journal of Potato Research*, 78(2), 109–117. <https://doi.org/10.1007/BF02874766>

- Bélanger, G., Walsh, J. R., Richards, J. E., Milburn, P. H., & Ziadi, N. (2000). Yield response of two potato cultivars to supplemental irrigation and N fertilization in New Brunswick. *American Journal of Potato Research*, 77(1), 11–21. <https://doi.org/10.1007/bf02853657>
- Beringer, H., Koch, K., & Lindhauer, M. G. (1990). Source: sink relationships in potato (*Solanum tuberosum*) as influenced by potassium chloride or potassium sulphate nutrition. *Plant and Soil*. <https://doi.org/10.1007/BF00009274>
- Birch, J. A., Devine, J. R., Holmes, M. R. J., & Whitear, J. D. (1967). Field experiments on the fertilizer requirements of maincrop potatoes. *The Journal of Agricultural Science*. <https://doi.org/10.1017/S0021859600016427>
- Bleasdale, J. K. A. (1965). Relationships between set characters and yield in maincrop potatoes. *The Journal of Agricultural Science*. <https://doi.org/10.1017/S0021859600016683>
- Boawn, L. C., & Leggett, G. E. (1964). Phosphorus and Zinc Concentrations in Russet Burbank Potato Tissues in Relation to Development of Zinc Deficiency Symptoms. *Soil Science Society of America Journal*. <https://doi.org/10.2136/sssaj1964.03615995002800020030x>
- Boettinger, J. L., Howell, D. W., Moore, A. C., Hartemink, A. S., & Kienast-Brown, S. (2010). Digital soil mapping; bridging research, environmental application and operation. In *Progress in Soil Science*.
- Bohl, W. H., & Love, S. L. (2005). Effect of planting depth and hilling practices on total, U.S. No. 1, and field greening tuber yields. *American Journal of Potato Research*, 82(6), 441–450. <https://doi.org/10.1007/BF02872222>
- Bohl, W. H., Stark, J. C., & McIntosh, C. S. (2011). Potato Seed Piece Size, Spacing, and Seeding Rate Effects on Yield, Quality and Economic Return. *American Journal of Potato Research*, 88(6), 470–478. <https://doi.org/10.1007/s12230-011-9213-4>

- Bouksila, F., Persson, M., Berndtsson, R., & Bahri, A. (2008). Soil water content and salinity determination using different dielectric methods in saline gypsiferous soil / Détermination de la teneur en eau et de la salinité de sols salins gypseux à l'aide de différentes méthodes diélectriques. *Hydrological Sciences Journal*, 53(1), 253–265. <https://doi.org/10.1623/hysj.53.1.253>
- Boydston, R. A., Navarre, D. A., Collins, H. P., & Chaves-Cordoba, B. (2017). The Effect of Nitrogen Rate on Vine Kill, Tuber Skinning Injury, Tuber Yield and Size Distribution, and Tuber Nutrients and Phytonutrients in Two Potato Cultivars Grown for Early Potato Production. *American Journal of Potato Research*, 94(4), 425–436. <https://doi.org/10.1007/s12230-017-9579-z>
- Bradshaw, J. E., & Ramsay, G. (2009). Potato Origin and Production. In *Advances in Potato Chemistry and Technology* (pp. 1–26). Elsevier. <https://doi.org/10.1016/B978-0-12-374349-7.00001-5>
- Brenner, C., Zeeman, M., Bernhardt, M., & Schulz, K. (2018). Estimation of evapotranspiration of temperate grassland based on high-resolution thermal and visible range imagery from unmanned aerial systems. *International Journal of Remote Sensing*, 39(15–16), 5141–5174. <https://doi.org/10.1080/01431161.2018.1471550>
- Brus, D. J., & DeGrujter, J. J. (1993). Design-based versus model-based estimates of spatial means: Theory and application in environmental soil science. *Environmetrics*. <https://doi.org/10.1002/env.3170040202>
- Bush, D. S., Biswas, A. K., & Jones, R. L. (1993). Hormonal regulation of Ca²⁺ transport in the endomembrane system of the barley aleurone. *Planta*. <https://doi.org/10.1007/BF00198213>
- Bussan, A. J., Mitchell, P. D., Copas, M. E., & Drilias, M. J. (2007). Evaluation of the effect of density on potato yield and tuber size distribution. *Crop Science*. <https://doi.org/10.2135/cropsci2007.01.0026>

- Busse, J. S., & Palta, J. P. (2006). Investigating the in vivo calcium transport path to developing potato tuber using ^{45}Ca : A new concept in potato tuber calcium nutrition. *Physiologia Plantarum*. <https://doi.org/10.1111/j.1399-3054.2006.00741.x>
- Caldiz, D. O., Viani, P. G., Giletto, C. M., Zamuner, E. C., & Echeverría, H. E. (2018). Improving Yield and Quality of Processing Potato Crops Grown in the Argentinian Pampas: the Role of N, P and S and Their Impact on CO₂ Emissions. *Potato Research*. <https://doi.org/10.1007/s11540-018-9364-5>
- Caldiz, Daniel O, Fernandez, L. V, & Struik, P. C. (2001). Physiological age index: a new, simple and reliable index to assess the physiological age of seed potato tubers based on haulm killing date and length of the incubation period. *Field Crops Research*, 69(1), 69–79. [https://doi.org/10.1016/S0378-4290\(00\)00134-9](https://doi.org/10.1016/S0378-4290(00)00134-9)
- Cambouris, A. N., Nolin, M. C., Zebarth, B. J., & Laverdière, M. R. (2006). Soil management zones delineated by electrical conductivity to characterize spatial and temporal variations in potato yield and in soil properties. *American Journal of Potato Research*, 83(5), 381–395. <https://doi.org/10.1007/BF02872015>
- Cambouris, A. N., Zebarth, B. J., Nolin, M. C., & Laverdière, M. R. (2007). Response to added nitrogen of a continuous potato sequence as related to sand thickness over clay. *Canadian Journal of Plant Science*, 87(4), 829–839. <https://doi.org/10.4141/P06-126>
- Cambouris, Athyna N., Nolin, M. C., & Simard, R. R. (2015). Precision Management of Fertilizer Phosphorus and Potassium for Potato in Quebec, Canada (pp. 847–857). <https://doi.org/10.2134/1999.precisionagproc4.c81>
- Camire, M. E., Kubow, S., & Donnelly, D. J. (2009). Potatoes and Human Health. *Critical Reviews in Food Science and Nutrition*, 49(10), 823–840. <https://doi.org/10.1080/10408390903041996>

- Carroll, Z. L., & Oliver, M. A. (2005). Exploring the spatial relations between soil physical properties and apparent electrical conductivity. *Geoderma*, 128(3–4), 354–374. <https://doi.org/10.1016/j.geoderma.2005.03.008>
- Castro-Franco, M., Costa, J. L., Peralta, N., & Aparicio, V. (2015). Prediction of Soil Properties at Farm Scale Using a Model-Based Soil Sampling Scheme and Random Forest. *Soil Science*. <https://doi.org/10.1097/SS.0000000000000115>
- Champely, S., Ekstrom, C., Dalgaard, P., Gill, J., Weibelzahl, S., Anandkumar, A., Ford, C., Volcic, R., & De Rosario, H. (2018). Package “pwr”: Basic functions for power analysis. CRAN Repository.
- Chang, D. C., Sohn, H. B., Cho, J. H., Im, J. S., Jin, Y. I., Do, G. R., Kim, S. J., Cho, H. M., & Lee, Y. B. (2014). Freezing and Frost Damage of Potato Plants: a Case Study on Growth Recovery, Yield Response, and Quality Changes. *Potato Research*, 57(2), 99–110. <https://doi.org/10.1007/s11540-014-9253-5>
- Chapepa, B., Mudada, N., & Mapuranga, R. (2020). The impact of plant density and spatial arrangement on light interception on cotton crop and seed cotton yield: an overview. *Journal of Cotton Research*, 3(1), 18. <https://doi.org/10.1186/s42397-020-00059-z>
- Chapman, S., Merz, T., Chan, A., Jackway, P., Hrabar, S., Dreccer, M., Holland, E., Zheng, B., Ling, T., & Jimenez-Berni, J. (2014). Pheno-Copter: A Low-Altitude, Autonomous Remote-Sensing Robotic Helicopter for High-Throughput Field-Based Phenotyping. *Agronomy*, 4(2), 279–301. <https://doi.org/10.3390/agronomy4020279>
- Chen, G., & Wiatrak, P. (2011). Seeding Rate Effects on Soybean Maturity Group IV-VIII for the Southeastern Production System: I. Vegetation Indices. *Agronomy Journal*, 103(1), 32–37. <https://doi.org/10.2134/agronj2010.0153>
- Chen, Y., Hou, C., Tang, Y., Zhuang, J., Lin, J., He, Y., Guo, Q., Zhong, Z., Lei, H., & Luo, S. (2019). Citrus Tree Segmentation from UAV Images Based on Monocular Machine

- Vision in a Natural Orchard Environment. *Sensors*, 19(24), 5558.
<https://doi.org/10.3390/s19245558>
- Cho, J. B., Guinness, J., Kharel, T. P., Sunoj, S., Kharel, D., Oware, E. K., van Aardt, J., & Ketterings, Q. M. (2021). Spatial estimation methods for mapping corn silage and grain yield monitor data. *Precision Agriculture*. <https://doi.org/10.1007/s11119-021-09793-z>
- Cinat, P., Di Gennaro, S. F., Berton, A., & Matese, A. (2019). Comparison of Unsupervised Algorithms for Vineyard Canopy Segmentation from UAV Multispectral Images. *Remote Sensing*, 11(9), 1023. <https://doi.org/10.3390/rs11091023>
- Claassens, M. M. J., & Vreugdenhil, D. (2000). Is dormancy breaking of potato tubers the reverse of tuber initiation? *Potato Research*, 43(4), 347–369.
<https://doi.org/10.1007/BF02360540>
- Clevers, J. G. P. W. (1986). The derivation of a simplified reflectance model for the estimation of LAI. *Remote Sensing for Resources Development and Environmental Management. Proc. 7th ISPRS Commission VII Symposium, Enschede, 1986. Vol. 1.*
- Clevers, J., Kooistra, L., & van den Brande, M. (2017). Using Sentinel-2 Data for Retrieving LAI and Leaf and Canopy Chlorophyll Content of a Potato Crop. *Remote Sensing*, 9(5), 405. <https://doi.org/10.3390/rs9050405>
- Cochrane, M. A. (2000). Using vegetation reflectance variability for species level classification of hyperspectral data. *International Journal of Remote Sensing*, 21(10), 2075–2087. <https://doi.org/10.1080/01431160050021303>
- Cohen, J. (1988a). *Statistical power analysis for the behavioural sciences*. Hillsdale, NJ: Lawrence Erlbaum Associates.
- Cohen, J. (1988b). *Statistical power for the social sciences*. Hillsdale, NJ: Lawrence Erlbaum and Associates.

- Connell, T. R., Binning, L. K., & Schmitt, W. G. (1999). A canopy development model for potatoes. *American Journal of Potato Research*, 76(3), 153–159.
<https://doi.org/10.1007/BF02853580>
- Contina, J. B., Dandurand, L. M., & Knudsen, G. R. (2018). A spatial analysis of the potato cyst nematode *globoidea pallida* in Idaho. *Phytopathology*.
<https://doi.org/10.1094/PHYTO-11-17-0388-R>
- Copas, M. E., Bussan, A. J., Drilias, M. J., & Wolkowski, R. P. (2009). Potato Yield and Quality Response to Subsoil Tillage and Compaction. *Agronomy Journal*, 101(1), 82–90.
<https://doi.org/10.2134/agronj2007.0031>
- Corwin, D. L., & Lesch, S. M. (2003). Application of Soil Electrical Conductivity to Precision Agriculture. *Agronomy Journal*, 95(3), 455. <https://doi.org/10.2134/agronj2003.0455>
- Corwin, D. L., & Lesch, S. M. (2005). Apparent soil electrical conductivity measurements in agriculture. *Computers and Electronics in Agriculture*, 46(1–3), 11–43.
<https://doi.org/10.1016/j.compag.2004.10.005>
- Costa, J. J. F., Giasson, É., da Silva, E. B., Coblinski, J. A., & Tiecher, T. (2020). Use of color parameters in the grouping of soil samples produces more accurate predictions of soil texture and soil organic carbon. *Computers and Electronics in Agriculture*, 177, 105710. <https://doi.org/10.1016/j.compag.2020.105710>
- Crafts-Brandner, S. J. (1992). Phosphorus Nutrition Influence on Starch and Sucrose Accumulation, and Activities of ADP-Glucose Pyrophosphorylase and Sucrose-Phosphate Synthase during the Grain Filling Period in Soybean. *Plant Physiology*, 98(3), 1133–1138. <https://doi.org/10.1104/pp.98.3.1133>
- Datt, B. (1998). Remote Sensing of Chlorophyll a, Chlorophyll b, Chlorophyll a+b, and Total Carotenoid Content in Eucalyptus Leaves. *Remote Sensing of Environment*, 66(2), 111–121. [https://doi.org/10.1016/S0034-4257\(98\)00046-7](https://doi.org/10.1016/S0034-4257(98)00046-7)

- De Caires, S. A., Wuddivira, M. N., & Bekele, I. (2015). Spatial analysis for management zone delineation in a humid tropic cocoa plantation. *Precision Agriculture*, 16(2), 129–147. <https://doi.org/10.1007/s11119-014-9366-5>
- de Gruijter, J. J., McBratney, A. B., & Taylor, J. (2010). Sampling for High-Resolution Soil Mapping. In *Proximal Soil Sensing*. https://doi.org/10.1007/978-90-481-8859-8_1
- De Jong, H. (2016). Impact of the Potato on Society. *American Journal of Potato Research*, 93(5), 415–429. <https://doi.org/10.1007/s12230-016-9529-1>
- Dean, C. J., Knowles, L. O., & Knowles, N. R. (2018a). Efficacy of Seed Aging and Gibberellin Treatments for Manipulating Apical Dominance, Tuber Set and Size Distribution of cv. Shepody. *American Journal of Potato Research*, 95(5), 526–538. <https://doi.org/10.1007/s12230-018-9657-x>
- Dean, C. J., Knowles, L. O., & Richard Knowles, N. (2018b). Auxin Modulates Gibberellin-Induced Effects on Growth, Yield, and Raw Product Recovery for Frozen Processing in Potato (*Solanum tuberosum* L.). *American Journal of Potato Research*, 95(6), 622–641. <https://doi.org/10.1007/s12230-018-9668-7>
- Delbari, M., Afrasiab, P., Gharabaghi, B., Amiri, M., & Salehian, A. (2019). Spatial variability analysis and mapping of soil physical and chemical attributes in a salt-affected soil. *Arabian Journal of Geosciences*, 12(3), 68. <https://doi.org/10.1007/s12517-018-4207-x>
- Delignette-Muller, M. L., & Dutang, C. (2015). fitdistrplus: An R package for fitting distributions. *Journal of Statistical Software*. <https://doi.org/10.18637/jss.v064.i04>
- Deng, J., Dong, W., Socher, R., Li, L.-J., Kai Li, & Li Fei-Fei. (2009). ImageNet: A large-scale hierarchical image database. 2009 IEEE Conference on Computer Vision and Pattern Recognition, 248–255. <https://doi.org/10.1109/CVPR.2009.5206848>
- Dev Acharya, T., & Yang, I. (2015). Exploring Landsat 8. *International Journal of IT, Engineering and Applied Sciences Research*.

- Dickins, J. C., Harrap, F. E. G., & Holmes, M. R. J. (1962). Field experiments comparing the effects of muriate and sulphate of potash on potato yield and quality. *The Journal of Agricultural Science*. <https://doi.org/10.1017/S0021859600015380>
- Dijkstra, K., van de Loosdrecht, J., Schomaker, L. R. B., & Wiering, M. A. (2019). CentroidNet: A Deep Neural Network for Joint Object Localization and Counting (pp. 585–601). https://doi.org/10.1007/978-3-030-10997-4_36
- Domagalska, M. A., & Leyser, O. (2011). Signal integration in the control of shoot branching. *Nature Reviews Molecular Cell Biology*, 12(4), 211–221. <https://doi.org/10.1038/nrm3088>
- Doraiswamy, P. C., Hatfield, J. L., Jackson, T. J., Akhmedov, B., Prueger, J., & Stern, A. (2004). Crop condition and yield simulations using Landsat and MODIS. *Remote Sensing of Environment*. <https://doi.org/10.1016/j.rse.2004.05.017>
- Duarte-Carvajalino, J., Alzate, D., Ramirez, A., Santa-Sepulveda, J., Fajardo-Rojas, A., & Soto-Suárez, M. (2018). Evaluating Late Blight Severity in Potato Crops Using Unmanned Aerial Vehicles and Machine Learning Algorithms. *Remote Sensing*, 10(10), 1513. <https://doi.org/10.3390/rs10101513>
- Dubey, S. D. (1967). Some Percentile Estimators for Weibull Parameters. *Technometrics*, 9(1), 119–129. <https://doi.org/10.1080/00401706.1967.10490445>
- Escolà, A., Badia, N., Arnó, J., & Martínez-Casasnovas, J. A. (2017). Using Sentinel-2 images to implement Precision Agriculture techniques in large arable fields: First results of a case study. *Advances in Animal Biosciences*, 8(2), 377–382. <https://doi.org/10.1017/S2040470017000784>
- ESRI. (2020). ArcGIS Pro 2.5.2. Environmental Systems Research Institute.

- Ewing, E. E., & Struik, P. C. (2010). Tuber Formation in Potato: Induction, Initiation, and Growth. In *Horticultural Reviews* (pp. 89–198). John Wiley & Sons, Inc. <https://doi.org/10.1002/9780470650523.ch3>
- FAOSTAT. (2019). FAOSTAT: Statistical database. FAOSTAT: Statistical Database.
- Fernandes, A. M., & Soratto, R. P. (2016). Phosphorus Fertilizer Rate for Fresh Market Potato Cultivars Grown in Tropical Soil with Low Phosphorus Availability. *American Journal of Potato Research*, 93(4), 404–414. <https://doi.org/10.1007/s12230-016-9515-7>
- Fernández, C. I., Leblon, B., Haddadi, A., Wang, K., & Wang, J. (2020). Potato Late Blight Detection at the Leaf and Canopy Levels Based in the Red and Red-Edge Spectral Regions. *Remote Sensing*, 12(8), 1292. <https://doi.org/10.3390/rs12081292>
- Fernandez-Gallego, J. A., Lootens, P., Borra-Serrano, I., Derycke, V., Haesaert, G., Roldán-Ruiz, I., Araus, J. L., & Kefauver, S. C. (2020). Automatic wheat ear counting using machine learning based on RGB UAV imagery. *The Plant Journal*, 103(4), 1603–1613. <https://doi.org/10.1111/tpj.14799>
- Filgueiras, R., Mantovani, E. C., Althoff, D., Fernandes Filho, E. I., & Cunha, F. F. da. (2019). Crop NDVI Monitoring Based on Sentinel 1. *Remote Sensing*, 11(12), 1441. <https://doi.org/10.3390/rs11121441>
- Firman, D. M., O'Brien, P. J., & Allen, E. J. (1995). Appearance and growth of individual leaves in the canopies of several potato cultivars. *The Journal of Agricultural Science*, 125(3), 379–394. <https://doi.org/10.1017/S0021859600084884>
- Fontes, P. C. R., Braun, H., Busato, C., & Cecon, P. R. (2010). Economic Optimum Nitrogen Fertilization Rates and Nitrogen Fertilization Rate Effects on Tuber Characteristics of Potato Cultivars. *Potato Research*, 53(3), 167–179. <https://doi.org/10.1007/s11540-010-9160-3>

- Franceschini, M. H. D., Bartholomeus, H., van Apeldoorn, D. F., Suomalainen, J., & Kooistra, L. (2019). Feasibility of Unmanned Aerial Vehicle Optical Imagery for Early Detection and Severity Assessment of Late Blight in Potato. *Remote Sensing*, 11(3), 224. <https://doi.org/10.3390/rs11030224>
- Freeman, K. L., Franz, P. R., & De Jong, R. W. (1998). Effect of phosphorus on the yield, quality and petiolar phosphorus concentrations of potatoes (cvv. Russet Burbank and Kennebec) grown in the krasnozem and duplex soils of Victoria. *Australian Journal of Experimental Agriculture*, 38(1), 83–93. <https://doi.org/10.1071/EA96045>
- Fuentes, A., Yoon, S., Kim, S., & Park, D. (2017). A Robust Deep-Learning-Based Detector for Real-Time Tomato Plant Diseases and Pests Recognition. *Sensors*, 17(9), 2022. <https://doi.org/10.3390/s17092022>
- Gao, X., Shaw, W. S., Tenuta, M., & Gibson, D. (2018). Yield and Nitrogen Use of Irrigated Processing Potato in Response to Placement, Timing and Source of Nitrogen Fertilizer in Manitoba. *American Journal of Potato Research*. <https://doi.org/10.1007/s12230-018-9656-y>
- Gates, D. M., Keegan, H. J., Schleter, J. C., & Weidner, V. R. (1965). Spectral Properties of Plants. *Applied Optics*. <https://doi.org/10.1364/ao.4.000011>
- Geary, R. C. (1954). *The Contiguity Ratio and Statistical Mapping*. The Incorporated Statistician. <https://doi.org/10.2307/2986645>
- Geremew, E. B., Steyn, J. M., & Annandale, J. G. (2007). Evaluation of growth performance and dry matter partitioning of four processing potato (*Solanum tuberosum*) cultivars. *New Zealand Journal of Crop and Horticultural Science*, 35(3), 385–393. <https://doi.org/10.1080/01140670709510204>
- Getis, A. (2015). Spatial Association, Measures of. In *International Encyclopedia of the Social & Behavioral Sciences* (pp. 100–104). Elsevier. <https://doi.org/10.1016/B978-0-08-097086-8.72055-1>

- Gilroy, S., & Jones, R. L. (1993). Calmodulin stimulation of unidirectional calcium uptake by the endoplasmic reticulum of barley aleurone. *Planta*.
<https://doi.org/10.1007/BF00196956>
- Gitelson, A. A., Merzlyak, M. N., & Lichtenthaler, H. K. (1996). Detection of Red Edge Position and Chlorophyll Content by Reflectance Measurements Near 700 nm. *Journal of Plant Physiology*, 148(3–4), 501–508. [https://doi.org/10.1016/S0176-1617\(96\)80285-9](https://doi.org/10.1016/S0176-1617(96)80285-9)
- Gitelson, A. A., Viña, A., Arkebauer, T. J., Rundquist, D. C., Keydan, G., & Leavitt, B. (2003). Remote estimation of leaf area index and green leaf biomass in maize canopies. *Geophysical Research Letters*, 30(5), n/a-n/a. <https://doi.org/10.1029/2002GL016450>
- Goeser, N. J., Mitchell, P. D., Esker, P. D., Curwen, D., Weis, G., & Bussan, A. J. (2012). Modeling Long-Term Trends in Russet Burbank Potato Growth and Development in Wisconsin. *Agronomy*, 2(1), 14–27. <https://doi.org/10.3390/agronomy2010014>
- Gómez, M. I., Barragán, A., Magnitskiy, S., & Rodríguez, L. E. (2019). Normalized difference vegetation index, N- NO₃ and K⁺ in stem sap of potato plants (Group Andigenum) as affected by fertilization. *Experimental Agriculture*.
<https://doi.org/10.1017/S001447971900005X>
- Goudriaan, J., & Monteith, J. L. (1990). A Mathematical Function for Crop Growth Based on Light Interception and Leaf Area Expansion. *Annals of Botany*, 66(6), 695–701.
<https://doi.org/10.1093/oxfordjournals.aob.a088084>
- Gray, D. (1972). Spacing and harvest date experiments with Maris Peer potatoes. *The Journal of Agricultural Science*. <https://doi.org/10.1017/S0021859600032263>
- Groten, S. M. (1993). NDVI-crop monitoring and early yield assessment of burkina faso. *International Journal of Remote Sensing*.
<https://doi.org/10.1080/01431169308953983>

- Guijarro, M., Pajares, G., Riomoros, I., Herrera, P. J., Burgos-Artizzu, X. P., & Ribeiro, A. (2011). Automatic segmentation of relevant textures in agricultural images. *Computers and Electronics in Agriculture*, 75(1), 75–83. <https://doi.org/10.1016/j.compag.2010.09.013>
- Haase, T., Schüler, C., & Heß, J. (2007). The effect of different N and K sources on tuber nutrient uptake, total and graded yield of potatoes (*Solanum tuberosum* L.) for processing. *European Journal of Agronomy*. <https://doi.org/10.1016/j.eja.2006.09.008>
- Habib, A., & Donnelly, D. J. (2002). Calcium translocation and accumulation into potato tubers. *Potato Research*. <https://doi.org/10.1007/BF02732215>
- Hadi, M. R., & Karimi, N. (2012). THE ROLE OF CALCIUM IN PLANTS' SALT TOLERANCE. *Journal of Plant Nutrition*. <https://doi.org/10.1080/01904167.2012.717158>
- Haining, R. (2015). Spatial Autocorrelation. In *International Encyclopedia of the Social & Behavioral Sciences* (pp. 105–110). Elsevier. <https://doi.org/10.1016/B978-0-08-097086-8.72056-3>
- Hall, S. M., & Hillman, J. R. (1975). Correlative inhibition of lateral bud growth in *Phaseolus vulgaris* L. timing of bud growth following decapitation. *Planta*, 123(2), 137–143. <https://doi.org/10.1007/BF00383862>
- Hallik, L., Kuusk, A., Lang, M., & Kuusk, J. (2019). Reflectance Properties of Hemiboreal Mixed Forest Canopies with Focus on Red Edge and Near Infrared Spectral Regions. *Remote Sensing*, 11(14), 1717. <https://doi.org/10.3390/rs11141717>
- Harris, P. M. (Ed.). (1992). *The Potato Crop*. Springer Netherlands. <https://doi.org/10.1007/978-94-011-2340-2>
- Hartigan, J. A., & Wong, M. A. (1979). Algorithm AS 136: A K-Means Clustering Algorithm. *Applied Statistics*, 28(1), 100. <https://doi.org/10.2307/2346830>

- Haverkort, A. J., Franke, A. C., Steyn, J. M., Pronk, A. A., Caldiz, D. O., & Kooman, P. L. (2015). A Robust Potato Model: LINTUL-POTATO-DSS. *Potato Research*, 58(4), 313–327. <https://doi.org/10.1007/s11540-015-9303-7>
- Hawkins, A. (1954). Time, method of application, and placement of fertilizer for efficient production of potatoes in New England. In *American Potato Journal*. <https://doi.org/10.1007/BF02859983>
- He, K., Gkioxari, G., Dollar, P., & Girshick, R. (2017). Mask R-CNN. *Proceedings of the IEEE International Conference on Computer Vision*. <https://doi.org/10.1109/ICCV.2017.322>
- He, K., Zhang, X., Ren, S., & Sun, J. (2016). Deep Residual Learning for Image Recognition. *2016 IEEE Conference on Computer Vision and Pattern Recognition (CVPR)*, 770–778. <https://doi.org/10.1109/CVPR.2016.90>
- Henderson, R. (1965). Effects of type of potash and rates of nitrogen, phosphate and potassium in fertilisers on growth, yield and quality of potato crops. *Journal of the Science of Food and Agriculture*. <https://doi.org/10.1002/jsfa.2740160812>
- Herrmann, I., Pimstein, A., Karnieli, A., Cohen, Y., Alchanatis, V., & Bonfil, D. J. (2011). LAI assessment of wheat and potato crops by VEN μ S and Sentinel-2 bands. *Remote Sensing of Environment*, 115(8), 2141–2151. <https://doi.org/10.1016/j.rse.2011.04.018>
- Heuvelink, G. B. M., & van Egmond, F. M. (2010). Space–Time Geostatistics for Precision Agriculture: A Case Study of NDVI Mapping for a Dutch Potato Field. In *Geostatistical Applications for Precision Agriculture*. https://doi.org/10.1007/978-90-481-9133-8_5
- Hide, G. A., & Welham, S. J. (1992). Observations on the bulking and development of tuber size distribution in maincrop potatoes at Rothamsted in 1964–75. *Potato Research*, 35(3), 235–247. <https://doi.org/10.1007/BF02357704>

- Hirschi, K. D. (2004). The calcium conundrum. Both versatile nutrient and specific signal. In *Plant Physiology*. <https://doi.org/10.1104/pp.104.046490>
- Holman, F., Riche, A., Michalski, A., Castle, M., Wooster, M., & Hawkesford, M. (2016). High Throughput Field Phenotyping of Wheat Plant Height and Growth Rate in Field Plot Trials Using UAV Based Remote Sensing. *Remote Sensing*, 8(12), 1031. <https://doi.org/10.3390/rs8121031>
- Holmes, M. R. J. (1962). Field experiments on the magnesium requirement of potatoes in Great Britain. *The Journal of Agricultural Science*. <https://doi.org/10.1017/S002185960001025X>
- Horler, D. N. H., Dockray, M., & Barber, J. (1983). The red edge of plant leaf reflectance. *International Journal of Remote Sensing*, 4(2), 273–288. <https://doi.org/10.1080/01431168308948546>
- Houghland, G. V. C. (1960). The influence of phosphorus on the growth and physiology of the potato plant. *American Potato Journal*. <https://doi.org/10.1007/BF02855950>
- Huete, A. . (1988a). A soil-adjusted vegetation index (SAVI). *Remote Sensing of Environment*, 25(3), 295–309. [https://doi.org/10.1016/0034-4257\(88\)90106-X](https://doi.org/10.1016/0034-4257(88)90106-X)
- Huete, A. R. (1988b). A soil-adjusted vegetation index (SAVI). *Remote Sensing of Environment*. [https://doi.org/10.1016/0034-4257\(88\)90106-X](https://doi.org/10.1016/0034-4257(88)90106-X)
- Huete, A. R. (2004). Remote Sensing for Environmental Monitoring. In *Environmental Monitoring and Characterization* (pp. 183–206). Elsevier. <https://doi.org/10.1016/B978-012064477-3/50013-8>
- Huete, A. R., & Escadafal, R. (1991). Assessment of biophysical soil properties through spectral decomposition techniques. *Remote Sensing of Environment*. [https://doi.org/10.1016/0034-4257\(91\)90008-T](https://doi.org/10.1016/0034-4257(91)90008-T)

- Hunt, M. L., Blackburn, G. A., Carrasco, L., Redhead, J. W., & Rowland, C. S. (2019). High resolution wheat yield mapping using Sentinel-2. *Remote Sensing of Environment*, 233, 111410. <https://doi.org/10.1016/j.rse.2019.111410>
- Iritani, W. M., Weiler, L. D., & Knowles, N. R. (1983). Relationships between stem number, tuber set and yield of Russet Burbank potatoes. *American Potato Journal*, 60(6), 423–431. <https://doi.org/10.1007/BF02877248>
- Ishikawa, D., Hoogenboom, G., Hakoyama, S., & Ishiguro, E. (2015). A potential of the growth stage estimation for paddy rice by using chlorophyll absorption bands in the 400-1100 nm region. *Journal of Agricultural Meteorology*, 71(1), 24–31. <https://doi.org/10.2480/agrmet.D-13-00025>
- Islam, A. S., & Bala, S. K. (2008). Assessment of Potato Phenological Characteristics Using MODIS-Derived NDVI and LAI Information. *GIScience & Remote Sensing*, 45(4), 454–470. <https://doi.org/10.2747/1548-1603.45.4.454>
- Iyer, P. V. K. (1949). The First and Second Moments of some Probability Distributions Arising from Points on a Lattice and their Application. *Biometrika*. <https://doi.org/10.2307/2332537>
- Jackson, E., Farrington, D. S., & Henderson, K. (1986). The analysis of agricultural materials: a manual of the analytical methods used by the Agricultural Development and Advisory Service. In Reference Book, ADAS, Ministry of Agriculture, Fisheries and Food.
- Jackson, S. D. (1999). Multiple Signaling Pathways Control Tuber Induction in Potato. *Plant Physiology*, 119(1), 1–8. <https://doi.org/10.1104/pp.119.1.1>
- Jackson, S. D., James, P. E., Carrera, E., Prat, S., & Thomas, B. (2000). Regulation of Transcript Levels of a Potato Gibberellin 20-Oxidase Gene by Light and Phytochrome B. *Plant Physiology*, 124(1), 423–430. <https://doi.org/10.1104/pp.124.1.423>

- Jackson, T. L., & Carter, G. E. (1976). Nutrient Uptake by Russet Burbank Potatoes as Influenced By Fertilization 1 . *Agronomy Journal*.
<https://doi.org/10.2134/agronj1976.00021962006800010003x>
- Jasim, A., Sharma, L. K., Zaeen, A., Bali, S. K., Buzza, A., & Alyokhin, A. (2020). Potato Phosphorus Response in Soils with High Value of Phosphorus. *Agriculture*, 10(7), 264.
<https://doi.org/10.3390/agriculture10070264>
- Jefferies, R. A., & Lawson, H. M. (1991). A key for the stages of development of potato (*Solatum tuberosum*). *Annals of Applied Biology*, 119(2), 387–399.
<https://doi.org/10.1111/j.1744-7348.1991.tb04879.x>
- Jin, S., Su, Y., Song, S., Xu, K., Hu, T., Yang, Q., Wu, F., Xu, G., Ma, Q., Guan, H., Pang, S., Li, Y., & Guo, Q. (2020). Non-destructive estimation of field maize biomass using terrestrial lidar: an evaluation from plot level to individual leaf level. *Plant Methods*, 16(1), 69.
<https://doi.org/10.1186/s13007-020-00613-5>
- Jin, X., Liu, S., Baret, F., Hemerlé, M., & Comar, A. (2017). Estimates of plant density of wheat crops at emergence from very low altitude UAV imagery. *Remote Sensing of Environment*. <https://doi.org/10.1016/j.rse.2017.06.007>
- Johnson, D. M. (2016). A comprehensive assessment of the correlations between field crop yields and commonly used MODIS products. *International Journal of Applied Earth Observation and Geoinformation*, 52, 65–81.
<https://doi.org/10.1016/j.jag.2016.05.010>
- Kamenova, I., & Dimitrov, P. (2020). Evaluation of Sentinel-2 vegetation indices for prediction of LAI, fAPAR and fCover of winter wheat in Bulgaria. *European Journal of Remote Sensing*, 1–20. <https://doi.org/10.1080/22797254.2020.1839359>
- Kanungo, T., Mount, D. M., Netanyahu, N. S., Piatko, C. D., Silverman, R., & Wu, A. Y. (2002). An efficient k-means clustering algorithm: analysis and implementation. *IEEE*

Transactions on Pattern Analysis and Machine Intelligence, 24(7), 881–892.

<https://doi.org/10.1109/TPAMI.2002.1017616>

Kataoka, T., Kaneko, T., Okamoto, H., & Hata, S. (n.d.). Crop growth estimation system using machine vision. Proceedings 2003 IEEE/ASME International Conference on Advanced Intelligent Mechatronics (AIM 2003), 2, b1079–b1083.

<https://doi.org/10.1109/AIM.2003.1225492>

Kebrom, T. H. (2017). A Growing Stem Inhibits Bud Outgrowth – The Overlooked Theory of Apical Dominance. *Frontiers in Plant Science*, 8.

<https://doi.org/10.3389/fpls.2017.01874>

Keijbets, M. J. H. (2008). Potato processing for the consumer: Developments and future challenges. *Potato Research*. <https://doi.org/10.1007/s11540-008-9104-3>

Kelling, K. A., Arriaga, F. J., Lowery, B., Jordan, M. O., & Speth, P. E. (2015). Use of Hill Shape with Various Nitrogen Timing Splits to Improve Fertilizer Use Efficiency. *American Journal of Potato Research*, 92(1), 71–78. <https://doi.org/10.1007/s12230-014-9413-9>

Kharel, T. P., Ashworth, A. J., Owens, P. R., & Buser, M. (2020). Spatially and temporally disparate data in systems agriculture: Issues and prospective solutions. *Agronomy Journal*, 112(5), 4498–4510. <https://doi.org/10.1002/agj2.20285>

Kirk, W. W., & Marshall, B. (1992). The influence of temperature on leaf development and growth in potatoes in controlled environments. *Annals of Applied Biology*, 120(3), 511–525. <https://doi.org/10.1111/j.1744-7348.1992.tb04911.x>

Kirsten, W. J., & Hesselius, G. U. (1983). Rapid, automatic, high capacity dumas determination of nitrogen. *Microchemical Journal*. [https://doi.org/10.1016/0026-265X\(83\)90011-5](https://doi.org/10.1016/0026-265X(83)90011-5)

Kleczkowski, L. A. (1999). A phosphoglycerate to inorganic phosphate ratio is the major factor in controlling starch levels in chloroplasts via ADP-glucose pyrophosphorylase

regulation. *FEBS Letters*, 448(1), 153–156. [https://doi.org/10.1016/S0014-5793\(99\)00346-4](https://doi.org/10.1016/S0014-5793(99)00346-4)

Kleinhenz, M. D., Palta, J. P., Gunter, C. C., & Kelling, K. A. (1999). Impact of source and timing of calcium and nitrogen applications on “Atlantic” potato tuber calcium concentrations and internal quality. *Journal of the American Society for Horticultural Science*. <https://doi.org/10.21273/jashs.124.5.498>

Knipling, E. B. (1970). Physical and physiological basis for the reflectance of visible and near-infrared radiation from vegetation. *Remote Sensing of Environment*, 1(3), 155–159. [https://doi.org/10.1016/S0034-4257\(70\)80021-9](https://doi.org/10.1016/S0034-4257(70)80021-9)

Knowles, L. O., & Knowles, N. R. (2016). Optimizing Tuber Set and Size Distribution for Potato Seed (*Solanum tuberosum* L.) Expressing Varying Degrees of Apical Dominance. *Journal of Plant Growth Regulation*, 35(2), 574–585. <https://doi.org/10.1007/s00344-015-9562-1>

Knowles, N. R., & Knowles, L. O. (2006). Manipulating stem number, tuber set, and yield relationships for northern- and southern-grown potato seed lots. *Crop Science*. <https://doi.org/10.2135/cropsci2005.05-0078>

Kooman, P. L., & Haverkort, A. J. (1995). Modelling development and growth of the potato crop influenced by temperature and daylength: LINTUL-POTATO (pp. 41–59). https://doi.org/10.1007/978-94-011-0051-9_3

Kratzke, M. G., & Palta, J. P. (1985). Evidence for the existence of functional roots on potato tubers and stolons: Significance in water transport to the tuber. *American Potato Journal*. <https://doi.org/10.1007/BF02852802>

Kumar, D., & Wareing, P. F. (1972). FACTORS CONTROLLING STOLON DEVELOPMENT IN THE POTATO PLANT. *New Phytologist*, 71(4), 639–648. <https://doi.org/10.1111/j.1469-8137.1972.tb01274.x>

- Laboski, C. A. M., & Kelling, K. A. (2007). Influence of fertilizer management and soil fertility on tuber specific gravity: A review. In *American Journal of Potato Research*.
<https://doi.org/10.1007/BF02986240>
- Lai, C.-D., Murthy, D. N., & Xie, M. (2006). Weibull Distributions and Their Applications. In *Springer Handbook of Engineering Statistics* (pp. 63–78). Springer London.
https://doi.org/10.1007/978-1-84628-288-1_3
- Leblois, A., & Quirion, P. (2013). Agricultural insurances based on meteorological indices: realizations, methods and research challenges. *Meteorological Applications*, 20(1), 1–9. <https://doi.org/10.1002/met.303>
- Li, B., Xu, X., Han, J., Zhang, L., Bian, C., Jin, L., & Liu, J. (2019). The estimation of crop emergence in potatoes by UAV RGB imagery. *Plant Methods*, 15(1), 15.
<https://doi.org/10.1186/s13007-019-0399-7>
- Li, K.-L., Chen, J., Tan, M.-Z., Zhao, B.-Z., Mi, S.-X., & Shi, X.-Z. (2011). Spatio-Temporal Variability of Soil Salinity in Alluvial Plain of the Lower Reaches of the Yellow River—A Case Study. *Pedosphere*, 21(6), 793–801. [https://doi.org/10.1016/S1002-0160\(11\)60183-5](https://doi.org/10.1016/S1002-0160(11)60183-5)
- Li, S., Duan, Y., Guo, T., Zhang, P., He, P., Johnston, A., & Shcherbakov, A. (2015). Potassium management in potato production in Northwest region of China. *Field Crops Research*.
<https://doi.org/10.1016/j.fcr.2015.01.010>
- Lindsey, J. K. (1974). Comparison of Probability Distributions. *Journal of the Royal Statistical Society: Series B (Methodological)*, 36(1), 38–47. <https://doi.org/10.1111/j.2517-6161.1974.tb00983.x>
- Long, C. M., Snapp, S. S., Douches, D. S., & Chase, R. W. (2004). Tuber yield, storability, and quality of Michigan cultivars in response to nitrogen management and seedpiece spacing. *American Journal of Potato Research*. <https://doi.org/10.1007/BF02870181>

- Lorenzen, B., & Jensen, A. (1988). Reflectance of blue, green, red and near infrared radiation from wetland vegetation used in a model discriminating live and dead above ground biomass. *New Phytologist*, 108(3), 345–355. <https://doi.org/10.1111/j.1469-8137.1988.tb04173.x>
- Love, S. L., & Thompson-Johns, A. (1999). Seed piece spacing influences yield, tuber size distribution, stem and tuber density, and net returns of three processing potato cultivars. *HortScience*. <https://doi.org/10.21273/hortsci.34.4.629>
- Ly, A., Marsman, M., Verhagen, J., Grasman, R. P. P. P., & Wagenmakers, E.-J. (2017). A Tutorial on Fisher information. *Journal of Mathematical Psychology*, 80, 40–55. <https://doi.org/10.1016/j.jmp.2017.05.006>
- Lymburner, L., Beggs, P. J., & Jacobson, C. R. (2000). Estimation of canopy-average surface-specific leaf area using Landsat TM data. In *Photogrammetric Engineering and Remote Sensing*.
- Machakaire, A. T. B., Steyn, J. M., Caldiz, D. O., & Haverkort, A. J. (2016). Forecasting Yield and Tuber Size of Processing Potatoes in South Africa Using the LINTUL-Potato-DSS Model. *Potato Research*. <https://doi.org/10.1007/s11540-016-9321-0>
- Machefer, M., Lemarchand, F., Bonnefond, V., Hitchins, A., & Sidiropoulos, P. (2020). Mask R-CNN Refitting Strategy for Plant Counting and Sizing in UAV Imagery. *Remote Sensing*, 12(18), 3015. <https://doi.org/10.3390/rs12183015>
- Mackerron, D. K. L., & Heilbronn, T. D. (1985). A method for estimating harvest indices for use in surveys of potato crops. *Potato Research*, 28(3), 279–282. <https://doi.org/10.1007/BF02357582>
- Mackerron, D. K. L., Marshall, B., & Jefferies, R. A. (1988). The distributions of tuber sizes in droughted and irrigated crops of potato. II. Relation between size and weight of tubers and the variability of tuber-size distributions. *Potato Research*, 31(2), 279–288. <https://doi.org/10.1007/BF02365536>

- Maltas, A., Dupuis, B., & Sinaj, S. (2018). Yield and Quality Response of Two Potato Cultivars to Nitrogen Fertilization. *Potato Research*, 61(2), 97–114.
<https://doi.org/10.1007/s11540-018-9361-8>
- Marshall, B., Holwerda, H. T., & Struik, P. C. (1993). Synchronisation of tuber growth in potato (*Solanum tuberosum*): a statistical model. *Field Crops Research*.
[https://doi.org/10.1016/0378-4290\(93\)90041-K](https://doi.org/10.1016/0378-4290(93)90041-K)
- Mason, M. G., Ross, J. J., Babst, B. A., Wienclaw, B. N., & Beveridge, C. A. (2014). Sugar demand, not auxin, is the initial regulator of apical dominance. *Proceedings of the National Academy of Sciences*, 111(16), 6092–6097.
<https://doi.org/10.1073/pnas.1322045111>
- MATLAB. (2020). MATLAB (R2020a). In www.mathworks.com/products/matlab.
- McCullagh, P., & Clifford, D. (2006). Evidence for conformal invariance of crop yields. *Proceedings of the Royal Society A: Mathematical, Physical and Engineering Sciences*, 462(2071), 2119–2143. <https://doi.org/10.1098/rspa.2006.1667>
- Medeiros, W. N., Valente, D. S. M., Queiroz, D. M. de, Pinto, F. de A. de C., & Assis, I. R. de. (2018). Apparent soil electrical conductivity in two different soil types. *REVISTA CIÊNCIA AGRONÔMICA*, 49(1). <https://doi.org/10.5935/1806-6690.20180005>
- Mendes dos Santos, L., Ferraz, G. A. e S., Barbosa, B. D. de S., Diotto, A. V., Andrade, M. T., Conti, L., & Rossi, G. (2020). Determining the Leaf Area Index and Percentage of Area Covered by Coffee Crops Using UAV RGB Images. *IEEE Journal of Selected Topics in Applied Earth Observations and Remote Sensing*, 13, 6401–6409.
<https://doi.org/10.1109/JSTARS.2020.3034193>
- Meyer, G. E., & Neto, J. C. (2008). Verification of color vegetation indices for automated crop imaging applications. *Computers and Electronics in Agriculture*, 63(2), 282–293.
<https://doi.org/10.1016/j.compag.2008.03.009>

- Mhango, J. K., Grove, I. G., Hartley, W., Harris, E. W., & Monaghan, J. M. (2021). Applying colour-based feature extraction and transfer learning to develop a high throughput inference system for potato (*Solanum tuberosum* L.) stems with images from unmanned aerial vehicles after canopy consolidation. *Precision Agriculture*.
<https://doi.org/10.1007/s11119-021-09853-4>
- Mhango, J. K., Harris, E. W., Green, R., & Monaghan, J. M. (2021). Mapping Potato Plant Density Variation Using Aerial Imagery and Deep Learning Techniques for Precision Agriculture. *Remote Sensing*, 13(14), 2705. <https://doi.org/10.3390/rs13142705>
- Miller, B. A. (2017). Geographic Information Systems and Spatial Statistics Applied for Soil Mapping: A Contribution to Land Use Management. In *Soil Mapping and Process Modeling for Sustainable Land Use Management*. <https://doi.org/10.1016/B978-0-12-805200-6.00005-0>
- Minasny, B., & McBratney, A. B. (2005). The Matérn function as a general model for soil variograms. *Geoderma*, 128(3–4), 192–207.
<https://doi.org/10.1016/j.geoderma.2005.04.003>
- Minasny, B., & McBratney, A. B. (2006). A conditioned Latin hypercube method for sampling in the presence of ancillary information. *Computers and Geosciences*.
<https://doi.org/10.1016/j.cageo.2005.12.009>
- Moran, M. S., Inoue, Y., & Barnes, E. M. (1997). Opportunities and limitations for image-based remote sensing in precision crop management. *Remote Sensing of Environment*, 61(3), 319–346. [https://doi.org/10.1016/S0034-4257\(97\)00045-X](https://doi.org/10.1016/S0034-4257(97)00045-X)
- Moran, P. A. (1950). Notes on continuous stochastic phenomena. *Biometrika*.
<https://doi.org/10.1093/biomet/37.1-2.17>
- Mponela, P., Snapp, S., Villamor, G. B., Tamene, L., Le, Q. B., & Borgemeister, C. (2020). Digital soil mapping of nitrogen, phosphorus, potassium, organic carbon and their crop

- response thresholds in smallholder managed escarpments of Malawi. *Applied Geography*, 124, 102299. <https://doi.org/10.1016/j.apgeog.2020.102299>
- Mulla, D. J. (2013). Twenty five years of remote sensing in precision agriculture: Key advances and remaining knowledge gaps. *Biosystems Engineering*, 114(4), 358–371. <https://doi.org/10.1016/j.biosystemseng.2012.08.009>
- Mulla, D. J. (2016). Spatial Variability in Precision Agriculture. In *Encyclopedia of GIS* (pp. 1–8). Springer International Publishing. https://doi.org/10.1007/978-3-319-23519-6_1652-1
- Mundy, C., Creamer, N. G., Wilson, L. G., Crozier, C. R., & Morse, R. D. (1999). Soil Physical Properties and Potato Yield in No-till, Subsurface-till, and Conventional-till Systems. *HortTechnology*, 9(2), 240–247. <https://doi.org/10.21273/HORTTECH.9.2.240>
- Nabi, G., Rahman, N., Samad, A., Ali, Z., & Khan, J. (2000). The effect of sulphate of potash (SOP) versus muriate of potash (MOP) on the yield of potato (*Solanum tuberosum* L.) crop. *Pakistan Journal of Biological Sciences*, 3, 1303–1304.
- Naeem, A., Akhtar, M., & Ahmad, W. (2013). Optimizing available phosphorus in calcareous soils fertilized with diammonium phosphate and phosphoric acid using freundlich adsorption isotherm. *The Scientific World Journal*. <https://doi.org/10.1155/2013/680257>
- Nakagawa, S., Johnson, P. C. D., & Schielzeth, H. (2017). The coefficient of determination R^2 and intra-class correlation coefficient from generalized linear mixed-effects models revisited and expanded. *Journal of The Royal Society Interface*, 14(134), 20170213. <https://doi.org/10.1098/rsif.2017.0213>
- Nawar, S., Corstanje, R., Halcro, G., Mulla, D., & Mouazen, A. M. (2017). Delineation of Soil Management Zones for Variable-Rate Fertilization: A Review. In *Advances in Agronomy*. <https://doi.org/10.1016/bs.agron.2017.01.003>

- Nemecek, T., Derron, J. O., Roth, O., & Fischlin, A. (1996). Adaptation of a crop-growth model and its extension by a tuber size function for use in a seed potato forecasting system. *Agricultural Systems*. [https://doi.org/10.1016/S0308-521X\(96\)00034-0](https://doi.org/10.1016/S0308-521X(96)00034-0)
- O'Brien, P. J., & Allen, E. J. (1992). Effects of seed crop husbandry, seed source, seed tuber weight and seed rate on the growth of ware potato crops. *The Journal of Agricultural Science*, 119(3), 355–366. <https://doi.org/10.1017/S0021859600012193>
- O'Brien, P. J., Allen, E. J., & Firman, D. M. (1998). A review of some studies into tuber initiation in potato (*Solanum tuberosum*) crops. *Journal of Agricultural Science*, 130(3), 251–270. <https://doi.org/10.1017/S0021859698005280>
- O'sullivan, D. (2003). Geographically Weighted Regression: The Analysis of Spatially Varying Relationships, by A. S. Fotheringham, C. Brunsdon, and M. Charlton. *Geographical Analysis*. <https://doi.org/10.1111/j.1538-4632.2003.tb01114.x>
- Oijen, M., Ruijter, F. J., & Haren, R. J. F. (1995). Analyses of the effects of potato cyst nematodes (*Globodera pallida*) on growth, physiology and yield of potato cultivars in field plots at three levels of soil compaction. *Annals of Applied Biology*, 127(3), 499–520. <https://doi.org/10.1111/j.1744-7348.1995.tb07608.x>
- Ojala, J. C., Stark, J. C., & Kleinkopf, G. E. (1990). Influence of irrigation and nitrogen management on potato yield and quality. *American Potato Journal*. <https://doi.org/10.1007/BF02986910>
- Oparka, K. J. (1985). Changes in Partitioning of Current Assimilate During Tuber Bulking in Potato (*Solanum tuberosum* L.) cv Maris Piper. *Annals of Botany*, 55(5), 705–713. <https://doi.org/10.1093/oxfordjournals.aob.a086949>
- Oparka, K. J., Davies, H. V., & Prior, D. A. M. (1987). The Influence of Applied Nitrogen on Export and Partitioning of Current Assimilate by Field-grown Potato Plants. *Annals of Botany*, 59(3), 311–323. <https://doi.org/10.1093/oxfordjournals.aob.a087320>

- Ozgen, S., & Palta, J. P. (2005). Supplemental calcium application influences potato tuber number and size. *HortScience*. <https://doi.org/10.21273/hortsci.40.1.102>
- Ozgen, S., Palta, J. P., & Kleinhenz, M. D. (2003). Influence of supplemental calcium fertilization on potato tuber size and tuber number. *Acta Horticulturae*. <https://doi.org/10.17660/ActaHortic.2003.619.38>
- Page, A. L. (1982). *Methods of soil analysis-Part 2: Chemical and Microbiological properties*. (2nd edition). Am. Soc. Agron. Inc. Publ.Madison, USA.
- Pan, Z., Hu, Y., & Cao, B. (2017). Construction of smooth daily remote sensing time series data: a higher spatiotemporal resolution perspective. *Open Geospatial Data, Software and Standards*, 2(1), 25. <https://doi.org/10.1186/s40965-017-0038-z>
- Panique, E., Kelling, K. A., Schulte, E. E., Hero, D. E., Stevenson, W. R., & James, R. V. (1997). Potassium rate and source effects on potato yield, quality, and disease interaction. *American Potato Journal*. <https://doi.org/10.1007/BF02852777>
- Paramasivam, C. R., & Venkatramanan, S. (2019). An introduction to various spatial analysis techniques. In *GIS and Geostatistical Techniques for Groundwater Science*. <https://doi.org/10.1016/B978-0-12-815413-7.00003-1>
- Pearson, R. L., & Miller, L. D. (1972). Remote mapping of standing crop biomass for estimation of the productivity of shortgrass prairie, Pawnee National Grasslands, Colorado. *Proceedings of the 8th International Symposium on Remote Sensing of the Environment*.
- Perron, I., Cambouris, A. N., Chokmani, K., Vargas Gutierrez, M. F., Zebarth, B. J., Moreau, G., Biswas, A., & Adamchuk, V. (2018). Delineating soil management zones using a proximal soil sensing system in two commercial potato fields in New Brunswick, Canada. *Canadian Journal of Soil Science*, 98(4), 724–737. <https://doi.org/10.1139/cjss-2018-0063>

- Pesaresi, M., & Benediktsson, J. A. (2001). A new approach for the morphological segmentation of high-resolution satellite imagery. *IEEE Transactions on Geoscience and Remote Sensing*, 39(2), 309–320. <https://doi.org/10.1109/36.905239>
- Pierce, F. J., & Burpee, C. G. (1995). Zone tillage effects on soil properties and yield and quality of potatoes (*Solanum tuberosum* L.). *Soil and Tillage Research*, 35(3), 135–146. [https://doi.org/10.1016/0167-1987\(95\)00485-8](https://doi.org/10.1016/0167-1987(95)00485-8)
- Pix4D. (2016). Pix4Dcapture. Pix4Dcapture 3.5.1.
- Polder, G., Blok, P. M., de Villiers, H. A. C., van der Wolf, J. M., & Kamp, J. (2019). Potato Virus Y Detection in Seed Potatoes Using Deep Learning on Hyperspectral Images. *Frontiers in Plant Science*, 10. <https://doi.org/10.3389/fpls.2019.00209>
- Porter, G. A., & Sisson, J. A. (1991). Petiole nitrate content of Maine-grown Russet Burbank and Shepody potatoes in response to varying nitrogen rate. *American Potato Journal*. <https://doi.org/10.1007/BF02853766>
- Porwal, S., & Katiyar, S. K. (2014). Performance evaluation of various resampling techniques on IRS imagery. 2014 Seventh International Conference on Contemporary Computing (IC3), 489–494. <https://doi.org/10.1109/IC3.2014.6897222>
- Potato Council. (2012). Production and Price Trends 1960-2011. (Great Britain): Potato Council
https://potatoes.ahdb.org.uk/sites/default/files/publication_upload/Copy%20of%20Production%20%20Prices%20%28Nov%2712%29.pdf
- Prummel, J., & Barnau-Sijthoff, P. (1984). Optimum phosphate and potassium levels in potato tops. *Fertilizer Research*, 5(2), 203–211. <https://doi.org/10.1007/BF01052717>
- Prunty, L., & Greenland, R. (1997). Nitrate leaching using two potato-corn N-fertilizer plans on sandy soil. *Agriculture, Ecosystems and Environment*.
[https://doi.org/10.1016/S0167-8809\(97\)00043-1](https://doi.org/10.1016/S0167-8809(97)00043-1)

- R Core Team. (2019). R: A language and environment for statistical computing. In R Foundation for Statistical Computing.
- Railton, I. D., & Wareing, P. F. (1973). Effects of Daylength on Endogenous Gibberellins in *Solanum andigena* III. Gibberellin Production by the Leaves. *Physiologia Plantarum*, 29(3), 430–433. <https://doi.org/10.1111/j.1399-3054.1973.tb04844.x>
- Ranghetti, L., Boschetti, M., Nutini, F., & Busetto, L. (2020). “sen2r”: An R toolbox for automatically downloading and preprocessing Sentinel-2 satellite data. *Computers and Geosciences*. <https://doi.org/10.1016/j.cageo.2020.104473>
- Rasmussen, M. S. (1992). Assessment of millet yields and production in northern Burkina Faso using integrated NDVI from the AVHRR. *International Journal of Remote Sensing*. <https://doi.org/10.1080/01431169208904132>
- Rębarz, K., Borówczak, F., Gaj, R., & Frieske, T. (2015). Effects of Cover Type and Harvest Date on Yield, Quality and Cost-Effectiveness of Early Potato Cultivation. *American Journal of Potato Research*, 92(3), 359–366. <https://doi.org/10.1007/s12230-015-9441-0>
- Redmon, J., Divvala, S., Girshick, R., & Farhadi, A. (2016). You only look once: Unified, real-time object detection. *Proceedings of the IEEE Computer Society Conference on Computer Vision and Pattern Recognition*. <https://doi.org/10.1109/CVPR.2016.91>
- Redulla, C. A., Davenport, J. R., Evans, R. G., Hattendorf, M. J., Alva, A. K., & Boydston, R. A. (2002). Relating potato yield and quality to field scale variability in soil characteristics. *American Journal of Potato Research*, 79(5), 317–323. <https://doi.org/10.1007/BF02870168>
- Ren, B., Liu, W., Zhang, J., Dong, S., Liu, P., & Zhao, B. (2017). Effects of plant density on the photosynthetic and chloroplast characteristics of maize under high-yielding conditions. *The Science of Nature*, 104(3–4), 12. <https://doi.org/10.1007/s00114-017-1445-9>

- Ren, S., He, K., Girshick, R., & Sun, J. (2015). Faster R-CNN: Towards real-time object detection with region proposal networks. *Advances in Neural Information Processing Systems*.
- Reust, W., Winiger, F. A., Hebeisen, T., & Dutoit, J.-P. (2001). Assessment of the physiological vigour of new potato cultivars in Switzerland. *Potato Research*, 44(1), 11–17. <https://doi.org/10.1007/BF02360282>
- Revel, C., Lonjou, V., Marcq, S., Desjardins, C., Fougne, B., Coppolani-Delle Luche, C., Guilleminot, N., Lacamp, A. S., Lourme, E., Miquel, C., & Lenot, X. (2019). Sentinel-2A and 2B absolute calibration monitoring. In *European Journal of Remote Sensing*. <https://doi.org/10.1080/22797254.2018.1562311>
- Rhee, H., & Cho, N. I. (2019). Efficient and Robust Pseudo-Labeling for Unsupervised Domain Adaptation. *2019 Asia-Pacific Signal and Information Processing Association Annual Summit and Conference (APSIPA ASC)*, 980–985. <https://doi.org/10.1109/APSIPAASC47483.2019.9023239>
- Rietra, R. P. J. J., Heinen, M., Dimkpa, C. O., & Bindraban, P. S. (2017). Effects of Nutrient Antagonism and Synergism on Yield and Fertilizer Use Efficiency. *Communications in Soil Science and Plant Analysis*. <https://doi.org/10.1080/00103624.2017.1407429>
- Rodriguez, H. G., Popp, J., Gbur, E., & Chaubey Indrajeet, I. (2011). Environmental and economic impacts of reducing total phosphorous runoff in an agricultural watershed. *Agricultural Systems*. <https://doi.org/10.1016/j.agsy.2011.06.005>
- Rodríguez-Pérez, J. R., Plant, R. E., Lambert, J.-J., & Smart, D. R. (2011). Using apparent soil electrical conductivity (ECa) to characterize vineyard soils of high clay content. *Precision Agriculture*, 12(6), 775–794. <https://doi.org/10.1007/s11119-011-9220-y>
- Rokni, K., & Musa, T. A. (2019). Normalized difference vegetation change index: A technique for detecting vegetation changes using Landsat imagery. *Catena*. <https://doi.org/10.1016/j.catena.2019.03.007>

- Rosen, C. J., & Bierman, P. M. (2008). Potato yield and tuber set as affected by phosphorus fertilization. *American Journal of Potato Research*. <https://doi.org/10.1007/s12230-008-9001-y>
- Ross, C. W. (1986). The effect of subsoiling and irrigation on potato production. *Soil and Tillage Research*, 7(4), 315–325. [https://doi.org/10.1016/0167-1987\(86\)90019-X](https://doi.org/10.1016/0167-1987(86)90019-X)
- Roudier, P., Hewitt, A. E., & Beaudette, D. E. (2012). A conditioned Latin hypercube sampling algorithm incorporating operational constraints. *Digital Soil Assessments and Beyond - Proceedings of the Fifth Global Workshop on Digital Soil Mapping*. <https://doi.org/10.1201/b12728-46>
- Roumeliotis, E., Kloosterman, B., Oortwijn, M., Kohlen, W., Bouwmeester, H. J., Visser, R. G. F., & Bachem, C. W. B. (2012). The effects of auxin and strigolactones on tuber initiation and stolon architecture in potato. *Journal of Experimental Botany*, 63(12), 4539–4547. <https://doi.org/10.1093/jxb/ers132>
- Rouse, J. W., Haas, R. H., Schell, J. A., & Deering, D. . (1973). Monitoring vegetation systems in the Great Plains with ERTS (Earth Resources Technology Satellite). *Third Earth Resources Technology Satellite-1 Symposium*.
- Rousset, F., & Ferdy, J. B. (2014). Testing environmental and genetic effects in the presence of spatial autocorrelation. *Ecography*. <https://doi.org/10.1111/ecog.00566>
- S., L. L., & Wahba, G. (1991). *Spline Models for Observational Data*. *Mathematics of Computation*. <https://doi.org/10.2307/2938687>
- Salvador, P., Gómez, D., Sanz, J., & Casanova, J. L. (2020). Estimation of Potato Yield Using Satellite Data at a Municipal Level: A Machine Learning Approach. *ISPRS International Journal of Geo-Information*, 9(6), 343. <https://doi.org/10.3390/ijgi9060343>
- Sands, P. J., & Regel, P. A. (1983). V. A simple model for predicting graded yields. *Field Crops Research*. [https://doi.org/10.1016/0378-4290\(83\)90045-X](https://doi.org/10.1016/0378-4290(83)90045-X)

- Sankaran, S., Quirós, J. J., Knowles, N. R., & Knowles, L. O. (2017). High-Resolution Aerial Imaging Based Estimation of Crop Emergence in Potatoes. *American Journal of Potato Research*, 94(6), 658–663. <https://doi.org/10.1007/s12230-017-9604-2>
- Savitzky, A., & Golay, M. J. E. (1964). Smoothing and Differentiation of Data by Simplified Least Squares Procedures. *Analytical Chemistry*, 36(8), 1627–1639. <https://doi.org/10.1021/ac60214a047>
- Schippers, P. A. (1968a). The influence of rates of nitrogen and potassium application on the cooking quality of four potato varieties. *European Potato Journal*, 11(2), 88–99. <https://doi.org/10.1007/BF02364461>
- Schippers, P. A. (1968b). The influence of rates of nitrogen and potassium application on the yield and specific gravity of four potato varieties. *European Potato Journal*. <https://doi.org/10.1007/BF02365159>
- Scott, L. M. (2015). Spatial Pattern, Analysis of. In *International Encyclopedia of the Social & Behavioral Sciences* (pp. 178–184). Elsevier. <https://doi.org/10.1016/B978-0-08-097086-8.72064-2>
- Scott, R. K. (1980). An analysis of growth of the potato crop. *The Journal of Agricultural Science*. <https://doi.org/10.1017/S0021859600028598>
- Seelan, S. K., Laguetta, S., Casady, G. M., & Seielstad, G. A. (2003). Remote sensing applications for precision agriculture: A learning community approach. *Remote Sensing of Environment*, 88(1–2), 157–169. <https://doi.org/10.1016/j.rse.2003.04.007>
- Shafian, S., Rajan, N., Schnell, R., Bagavathiannan, M., Valasek, J., Shi, Y., & Olsenholler, J. (2018). Unmanned aerial systems-based remote sensing for monitoring sorghum growth and development. *PLOS ONE*, 13(5), e0196605. <https://doi.org/10.1371/journal.pone.0196605>

- Shamal, S. A. M., & Weatherhead, K. (2014). Assessing Spectral Similarities between Rainfed and Irrigated Croplands in a Humid Environment for Irrigated Land Mapping. *Outlook on Agriculture*, 43(2), 109–114. <https://doi.org/10.5367/oa.2014.0168>
- Sharma, U. C., & Arora, B. R. (1987). Effect of nitrogen, phosphorus and potassium application on yield of potato tubers (*Solanum tuberosum* L.). *The Journal of Agricultural Science*, 108(2), 321–329. <https://doi.org/10.1017/S0021859600079326>
- Shayanowako, A., Mangani, R., Mtaita, T., & Mazarura, U. (2015). Influence of Main Stem Density on Irish Potato Growth and Yield: A Review. *Annual Research & Review in Biology*, 5(3), 229–237. <https://doi.org/10.9734/ARRB/2015/9973>
- Silva-Díaz, C., Ramírez, D. A., Rinza, J., Ninanya, J., Loayza, H., Gómez, R., Anglin, N. L., Eyzaguirre, R., & Quiroz, R. (2020). Radiation Interception, Conversion and Partitioning Efficiency in Potato Landraces: How Far Are We from the Optimum? *Plants*, 9(6), 787. <https://doi.org/10.3390/plants9060787>
- Simmons, K. E., & Kelling, K. A. (1987). Potato responses to calcium application on several soil types. *American Potato Journal*. <https://doi.org/10.1007/BF02854208>
- Simonyan, K., & Zisserman, A. (2015). Very deep convolutional networks for large-scale image recognition. 3rd International Conference on Learning Representations, ICLR 2015 - Conference Track Proceedings.
- Simpson, K. (1962). Effects of soil-moisture tension and fertilisers on the yield, growth and phosphorus uptake of potatoes. *Journal of the Science of Food and Agriculture*. <https://doi.org/10.1002/jsfa.2740130405>
- Simpson, K., & Crooks, P. (1961). Effects of fertilisers on the yield of potatoes in S.E. Scotland. *Journal of the Science of Food and Agriculture*. <https://doi.org/10.1002/jsfa.2740120207>

- Simpson, K., Crooks, P., & McIntosh, S. (1973). Effects of potassium and magnesium fertilizers on yield and size distribution of potatoes. *The Journal of Agricultural Science*, 80(3), 369–373. <https://doi.org/10.1017/S0021859600058007>
- Sims, D. A., & Gamon, J. A. (2002). Relationships between leaf pigment content and spectral reflectance across a wide range of species, leaf structures and developmental stages. *Remote Sensing of Environment*, 81(2–3), 337–354. [https://doi.org/10.1016/S0034-4257\(02\)00010-X](https://doi.org/10.1016/S0034-4257(02)00010-X)
- Singh, G., Williard, K., & Schoonover, J. (2016). Spatial Relation of Apparent Soil Electrical Conductivity with Crop Yields and Soil Properties at Different Topographic Positions in a Small Agricultural Watershed. *Agronomy*, 6(4), 57. <https://doi.org/10.3390/agronomy6040057>
- Singh, M., & Dahiya, S. S. (1976). Effect of calcium carbonate and iron on the availability and uptake of iron, manganese, phosphorus and calcium in pea (*Pisum sativum* L.). *Plant and Soil*, 44(3), 511–520. <https://doi.org/10.1007/BF00011371>
- Singh, P., & Verma, P. (2019). A comparative study of spatial interpolation technique (IDW and Kriging) for determining groundwater quality. In *GIS and Geostatistical Techniques for Groundwater Science*. <https://doi.org/10.1016/B978-0-12-815413-7.00005-5>
- Singh, V., Rana, A., Bishop, M., Filippi, A. M., Cope, D., Rajan, N., & Bagavathiannan, M. (2020). Unmanned aircraft systems for precision weed detection and management: Prospects and challenges (pp. 93–134). <https://doi.org/10.1016/bs.agron.2019.08.004>
- Smith, A. M., & Blackshaw, R. E. (2003). Weed–Crop Discrimination Using Remote Sensing: A Detached Leaf Experiment 1. *Weed Technology*, 17(4), 811–820. <https://doi.org/10.1614/WT02-179>
- Smith, K. L., Steven, M. D., & Colls, J. J. (2004). Use of hyperspectral derivative ratios in the red-edge region to identify plant stress responses to gas leaks. *Remote Sensing of Environment*, 92(2), 207–217. <https://doi.org/10.1016/j.rse.2004.06.002>

- Sojka, R. E., Westermann, D. T., Brown, M. J., & Meek, B. D. (1993). Zone-subsoiling effects on infiltration, runoff, erosion, and yields of furrow-irrigated potatoes. *Soil and Tillage Research*, 25(4), 351–368. [https://doi.org/10.1016/0167-1987\(93\)90033-L](https://doi.org/10.1016/0167-1987(93)90033-L)
- Sojka, R. E., Westermann, D. T., Kincaid, D. C., McCann, I. R., Halderson, J. L., & Thornton, M. (1993). Zone-subsoiling effects on potato yield and grade. *American Potato Journal*, 70(6), 475–484. <https://doi.org/10.1007/BF02849066>
- Soltanpour, P. N. (1969). Effect of Nitrogen, Phosphorus and Zinc Placement on Yield and Composition of Potatoes 1 . *Agronomy Journal*.
<https://doi.org/10.2134/agronj1969.00021962006100020033x>
- Spooner, D. M., & Bamberg, J. B. (1994). Potato genetic resources: Sources of resistance and systematics. *American Potato Journal*, 71(5), 325–337.
<https://doi.org/10.1007/BF02849059>
- Stalham, M. A., Allen, E. J., Rosenfeld, A. B., & Herry, F. X. (2007). Effects of soil compaction in potato (*Solanum tuberosum*) crops. *The Journal of Agricultural Science*, 145(4), 295–312. <https://doi.org/10.1017/S0021859607006867>
- Stein, M. L. (1999). *Interpolation of Spatial Data*. Springer New York.
<https://doi.org/10.1007/978-1-4612-1494-6>
- Struik, P. C. (2007). The Canon of Potato Science: 40. Physiological Age of Seed Tubers. *Potato Research*, 50(3–4), 375–377. <https://doi.org/10.1007/s11540-008-9069-2>
- Struik, P. C., Haverkort, A. J., Vreugdenhil, D., Bus, C. B., & Dankert, R. (1990). Manipulation of tuber-size distribution of a potato crop. *Potato Research*, 33(4), 417–432.
<https://doi.org/10.1007/BF02358019>
- Struik, P. C., van der Putten, P. E. L., Caldiz, D. O., & Scholte, K. (2006). Response of Stored Potato Seed Tubers from Contrasting Cultivars to Accumulated Day-Degrees. *Crop Science*, 46(3), 1156–1168. <https://doi.org/10.2135/cropsci2005.08-0267>

- Struik, P. C., Vreugdenhil, D., Haverkort, A. J., Bus, C. B., & Dankert, R. (1991). Possible mechanisms of size hierarchy among tubers on one stem of a potato (*Solanum tuberosum* L.) plant. *Potato Research*, 34(2), 187–203.
<https://doi.org/10.1007/BF02358041>
- Sugiura, R., Tsuda, S., Tamiya, S., Itoh, A., Nishiwaki, K., Murakami, N., Shibuya, Y., Hirafuji, M., & Nuske, S. (2016). Field phenotyping system for the assessment of potato late blight resistance using RGB imagery from an unmanned aerial vehicle. *Biosystems Engineering*, 148, 1–10. <https://doi.org/10.1016/j.biosystemseng.2016.04.010>
- Sultana, S. R., Ali, A., Ahmad, A., Mubeen, M., Zia-Ul-Haq, M., Ahmad, S., Ercisli, S., & Jaafar, H. Z. E. (2014). Normalized difference vegetation index as a tool for wheat yield estimation: A case study from Faisalabad, Pakistan. *Scientific World Journal*.
<https://doi.org/10.1155/2014/725326>
- Sun, S., Song, H., He, D., & Long, Y. (2019). An adaptive segmentation method combining MSRCR and mean shift algorithm with K-means correction of green apples in natural environment. *Information Processing in Agriculture*, 6(2), 200–215.
<https://doi.org/10.1016/j.inpa.2018.08.011>
- Suttle, J. C. (2004). Physiological regulation of potato tuber dormancy. *American Journal of Potato Research*. <https://doi.org/10.1007/BF02871767>
- Swyngedouw, C., & Crépin, J. M. (2008). SAMPLING METHODS FOR SITE CHARACTERIZATION. In *Environmental Geochemistry* (pp. 13–27). Elsevier.
<https://doi.org/10.1016/B978-0-444-53159-9.00002-4>
- Szantoi, Z., & Strobl, P. (2019). Copernicus Sentinel-2 Calibration and Validation. In *European Journal of Remote Sensing*. <https://doi.org/10.1080/22797254.2019.1582840>
- Taylor, J. A., Chen, H., Smallwood, M., & Marshall, B. (2018). Investigations into the opportunity for spatial management of the quality and quantity of production in UK potato systems. *Field Crops Research*. <https://doi.org/10.1016/j.fcr.2018.10.002>

- Thapa, S., Rudd, J. C., Xue, Q., Bhandari, M., Reddy, S. K., Jessup, K. E., Liu, S., Devkota, R. N., Baker, J., & Baker, S. (2019). Use of NDVI for characterizing winter wheat response to water stress in a semi-arid environment. *Journal of Crop Improvement*, 33(5), 633–648. <https://doi.org/10.1080/15427528.2019.1648348>
- Tiessen, A., Hendriks, J. H. M., Stitt, M., Branscheid, A., Gibon, Y., Farré, E. M., & Geigenberger, P. (2002). Starch Synthesis in Potato Tubers Is Regulated by Post-Translational Redox Modification of ADP-Glucose Pyrophosphorylase. *The Plant Cell*, 14(9), 2191–2213. <https://doi.org/10.1105/tpc.003640>
- Travis, K. Z. (1987). Use of a simple model to study factors affecting the size distribution of tubers in potato crops. *The Journal of Agricultural Science*. <https://doi.org/10.1017/S0021859600081788>
- Tucker, C. J. (1979). Red and photographic infrared linear combinations for monitoring vegetation. *Remote Sensing of Environment*. [https://doi.org/10.1016/0034-4257\(79\)90013-0](https://doi.org/10.1016/0034-4257(79)90013-0)
- Tucker, C. J., & Garratt, M. W. (1977). Leaf optical system modeled as a stochastic process. *Applied Optics*, 16(3), 635. <https://doi.org/10.1364/AO.16.000635>
- Tunesi, S., Poggi, V., & Gessa, C. (1999). Phosphate adsorption and precipitation in calcareous soils: The role of calcium ions in solution and carbonate minerals. *Nutrient Cycling in Agroecosystems*. <https://doi.org/10.1023/A:1009709005147>
- Turvey, C. G., & McLaurin, M. K. (2012). Applicability of the normalized difference vegetation index (NDVI) In index-based crop insurance design. *Weather, Climate, and Society*. <https://doi.org/10.1175/WCAS-D-11-00059.1>
- Unkovich, M., Baldock, J., & Forbes, M. (2010). Variability in Harvest Index of Grain Crops and Potential Significance for Carbon Accounting: Examples from Australian Agriculture. In *Advances in Agronomy*. [https://doi.org/10.1016/S0065-2113\(10\)05005-4](https://doi.org/10.1016/S0065-2113(10)05005-4)

- Unnithan, S. L. K., & Gnanappazham, L. (2020). Spatiotemporal mixed effects modeling for the estimation of PM 2.5 from MODIS AOD over the Indian subcontinent. *GIScience & Remote Sensing*, 57(2), 159–173. <https://doi.org/10.1080/15481603.2020.1712101>
- Valente, D. S. M., Queiroz, D. M. de, Pinto, F. de A. de C., Santos, N. T., & Santos, F. L. (2012). The relationship between apparent soil electrical conductivity and soil properties. *Revista Ciência Agronômica*, 43(4), 683–690. <https://doi.org/10.1590/S1806-66902012000400009>
- Velichkova, K., & Krezhova, D. (2019). Extraction of the red edge position from hyperspectral reflectance data for plant stress monitoring. 130018. <https://doi.org/10.1063/1.5091303>
- Vos, J., & Biemond, H. (1992). Effects of Nitrogen on the Development and Growth of the Potato Plant. 1. Leaf Appearance, Expansion Growth, Life Spans of Leaves and Stem Branching. *Annals of Botany*, 70(1), 27–35. <https://doi.org/10.1093/oxfordjournals.aob.a088435>
- Waterer, D. (2007). Vine desiccation characteristics and influence of time and method of top kill on yields and quality of four cultivars of potato (*Solanum tuberosum* L.). *Canadian Journal of Plant Science*, 87(1), 129–135. <https://doi.org/10.4141/P06-074>
- Webster Oliver, M., R. (2007). *Geostatistics for Environmental Scientists Statistics in Practice*. In Wiley.
- Westermann, D. T., & Kleinkopf, G. E. (1985a). Phosphorus Relationships in Potato Plants 1. *Agronomy Journal*. <https://doi.org/10.2134/agronj1985.00021962007700030029x>
- Westermann, D. T., & Kleinkopf, G. E. (1985b). Phosphorus Relationships in Potato Plants1. *Agronomy Journal*. <https://doi.org/10.2134/agronj1985.00021962007700030029x>
- Whelan, B. M., & Mulcahy, F. (2017). A strategy to instigate SSCM in Australian potato production. *Advances in Animal Biosciences*, 8(2), 743–748. <https://doi.org/10.1017/S2040470017000401>

- White, R. P., & Sanderson, J. B. (1983). Effect of planting date, nitrogen rate, and plant spacing on potatoes grown for processing in Prince Edward Island. *American Potato Journal*. <https://doi.org/10.1007/BF02853800>
- Wiersum, L. K. (1966). CALCIUM CONTENT OF FRUITS AND STORAGE TISSUES IN RELATION TO THE MODE OF WATER SUPPLY. *Acta Botanica Neerlandica*.
<https://doi.org/10.1111/j.1438-8677.1966.tb00240.x>
- Wilson, E. H., & Sader, S. A. (2002). Detection of forest harvest type using multiple dates of Landsat TM imagery. *Remote Sensing of Environment*, 80(3), 385–396.
[https://doi.org/10.1016/S0034-4257\(01\)00318-2](https://doi.org/10.1016/S0034-4257(01)00318-2)
- Witney, B. D., & McRae, D. C. (1992). Mechanization of crop production and handling operations. In *The Potato Crop* (pp. 570–607). Springer Netherlands.
https://doi.org/10.1007/978-94-011-2340-2_13
- Woebbecke, D. M., Meyer, G. E., Von Bargaen, K., & Mortensen, D. A. (1995). Color indices for weed identification under various soil, residue, and lighting conditions. *Transactions of the American Society of Agricultural Engineers*.
<https://doi.org/10.13031/2013.27838>
- Wolf, J. (2002). Comparison of two potato simulation models under climate change. I. Model calibration and sensitivity analyses. *Climate Research*, 21, 173–186.
<https://doi.org/10.3354/cr021173>
- Wolf, J., & Oijen, M. va. (2002). Modelling the dependence of European potato yields on changes in climate and CO₂. *Agricultural and Forest Meteorology*, 112(3–4), 217–231.
[https://doi.org/10.1016/S0168-1923\(02\)00061-8](https://doi.org/10.1016/S0168-1923(02)00061-8)
- Wu, J., Yang, G., Yang, H., Zhu, Y., Li, Z., Lei, L., & Zhao, C. (2020). Extracting apple tree crown information from remote imagery using deep learning. *Computers and Electronics in Agriculture*, 174, 105504. <https://doi.org/10.1016/j.compag.2020.105504>

- Wurr, D. C. E. (1974). Some effects of seed size and spacing on the yield and grading of two maincrop potato varieties: I. Final yield and its relationship to plant population. *The Journal of Agricultural Science*. <https://doi.org/10.1017/S0021859600050206>
- Wurr, D. C. E., & Morris, G. E. L. (1979). Relationships between the number of stems produced by a potato seed tuber and its weight. *The Journal of Agricultural Science*, 93(2), 403–409. <https://doi.org/10.1017/S0021859600038089>
- Wurr, D. C. E., Fellows, J. R., Lynn, J. R., & Allen, E. J. (1993). The impact of some agronomic factors on the variability of potato tuber size distribution. *Potato Research*. <https://doi.org/10.1007/BF02360532>
- Xiong, X., Yu, L., Yang, W., Liu, M., Jiang, N., Wu, D., Chen, G., Xiong, L., Liu, K., & Liu, Q. (2017). A high-throughput stereo-imaging system for quantifying rape leaf traits during the seedling stage. *Plant Methods*, 13(1), 7. <https://doi.org/10.1186/s13007-017-0157-7>
- Xu, X., van Lammeren, A. A. M., Vermeer, E., & Vreugdenhil, D. (1998). The Role of Gibberellin, Abscisic Acid, and Sucrose in the Regulation of Potato Tuber Formation in Vitro1. *Plant Physiology*, 117(2), 575–584. <https://doi.org/10.1104/pp.117.2.575>
- Xue, J., & Su, B. (2017). Significant remote sensing vegetation indices: A review of developments and applications. In *Journal of Sensors*. <https://doi.org/10.1155/2017/1353691>
- Yang, G., Liu, J., Zhao, C., Li, Z., Huang, Y., Yu, H., Xu, B., Yang, X., Zhu, D., Zhang, X., Zhang, R., Feng, H., Zhao, X., Li, Z., Li, H., & Yang, H. (2017). Unmanned Aerial Vehicle Remote Sensing for Field-Based Crop Phenotyping: Current Status and Perspectives. *Frontiers in Plant Science*, 8. <https://doi.org/10.3389/fpls.2017.01111>
- Yang, X., Shen, X., Long, J., & Chen, H. (2012). An Improved Median-based Otsu Image Thresholding Algorithm. *AASRI Procedia*, 3, 468–473. <https://doi.org/10.1016/j.aasri.2012.11.074>

Yang, Y., Luo, Y., Lu, M., Schädel, C., & Han, W. (2011). Terrestrial C:N stoichiometry in response to elevated CO₂ and N addition: a synthesis of two meta-analyses. *Plant and Soil*, 343(1–2), 393–400. <https://doi.org/10.1007/s11104-011-0736-8>

Yara International Allmennaksjeselskap. (2019). Potato Market Requirements. Viewed 18 September 2019. <https://www.yara.co.uk/crop-nutrition/potato/potato-market-requirements/>

Zhao, B., Zhang, J., Yang, C., Zhou, G., Ding, Y., Shi, Y., Zhang, D., Xie, J., & Liao, Q. (2018). Rapeseed Seedling Stand Counting and Seeding Performance Evaluation at Two Early Growth Stages Based on Unmanned Aerial Vehicle Imagery. *Frontiers in Plant Science*, 9. <https://doi.org/10.3389/fpls.2018.01362>

9. Appendices

Appendix A: Example of Field Survey design for Field HF7

Field HF7 was commercial field, meaning that treatments in a replicated design could not be imposed without affecting field operations, however, a field survey could be adequately be used to delineate zone of relative homogeneity. Inherent variability in soil physical and chemical properties was expected due to the variability in clay content between the peat and the clay dominated rhodons. The gradients of these variables were expected to have an influence on crop growth and hence have some correlation with measured crop-performance-related variables. The Soil Brightness index (SBI) was chosen due to its wide use and availability in precision agriculture packages. The SBI data was calculated from Sentinel-2 satellite imagery, and used to delineate zones of relative homogeneity. The SBI variability of the whole field was re-scaled to range between 0 and 10 for relative interpretability, where 0 represented the darkest pixels and 10 represented the lightest pixels. After visual inspection of the variability in the SBI image, the field was delineated into 3 sampling zones of relative homogeneity as follows:

1. Dark Zone: SBI 0-3
2. Medium Zone: SBI 4-6
3. Light Zone: SBI 7-9

A sampling frame spanning the 1.4ha of the field was therefore created and a stratified random sampling method was chosen, using the sampling zones as strata and simple random sampling used within each stratum. Based on this, the SBI raster data was vectorized using arcGISpro, then a grid of 36m² quadrats was imposed across the vectorised surface. Random samples were then drawn from each stratum by assigning random numbers to each quadrat in the attribute table, sorting by the random number value then selecting the first *N* quadrats that satisfied the required sample number for the specific stratum.

The sample size for the survey was calculated by determining the minimum number of samples required to adequately represent the SBI variability with a statistical power of 0.8. The number of sampling locations of dark soils was based on the *dark* area proportion, while for the *medium* and *light* soils, the number of samples was determined by a randomization process since the two strata were consolidated during sample size determination. The randomization step was performed on the gridded SBI image in ArcGIS to select the actual quadrats for soil and yield sampling as illustrated in *Figure 46*. The selected quadrats were georeferenced and assigned with unique identifier codes then exported as a GPx file into the *Garmin™ etrex 20* GPS receiver for tracking during soil and yield sampling.



Figure 46: A Choropleth map of the field's variation in Soil Brightness and approximate soil sampling locations. Soil brightness was re-scaled to range between 0 and 10, where 0 represents a dark soil and 10 represents a light soil.

Appendix B *A list of the varieties used to test the object detection models*

Purpose	Breeder	Variety
Chipping	Agrico	Agria
Crisping	HZPC	Alcander
Chipping	HZPC	Althea
Chipping	HZPC	Alverstone
		Russet
Crisping	Agrico	Arsenal
Chipping	HZPC	Asterix
Unknown	Unknown	Babylon
Crisping	PepsiCo	Brooke
Chipping	HZPC	Challenger
Crisping	Agrico	Corsica
Prepack	Agrico	Desiree
Prepack	Agrico	Estima
Crisping	HZPC	Heraclea
Chipping	HZPC	Innovator
Chipping	HZPC	Ivory Russet
Prepack	Greenvale	Jelly
Prepack	Unknown	King Edward
Crisping	Meijer	Lady Clair
Prepack	Branston	Lanorma
Prepack	Branston	Laura
Salad	Agrico	Maris Peer
Chipping	Agrico	Maris Piper
Crisping	Agrico	Markies
Prepack	Meijer	Melody
Prepack	HZPC	Mozart
Prepack	IPM	Nectar

Prepack	HZPC	Panther
Chipping	SCRI	Pentland Dell
Chipping	Agrico	Performer
Chipping	Norika	Pirol
Chipping	Higgind Group	Ramos
Chipping	IPM	Rooster
Chipping	McCains	Royal
Chipping	Unknown	Russett Burbank
Chipping	HZPC	Sagitta
Crisping	Stet	SHC1010
Crisping	PepsiCo	Shelford
Unknown	Unknown	Sorentina
Prepack	HZPC	Sunita
Crisping	HZPC	Taurus
Unknown	Unknown	Thalassa
Crisping	Unknown	Titan
Crisping	HZPC	Triple 7
Unknown	Unknown	VDW 07-197
Crisping	Stet	VR808
